UNIVERSIDADE FEDERAL DO RIO GRANDE DO SUL
INSTITUTO DE CIÊNCIAS BÁSICAS DA SAÚDE
PROGRAMA DE PÓS-GRADUAÇÃO EM CIÊNCIAS BIOLÓGICAS:
BIOQUÍMICA

Bruna Bellaver

INVESTIGAÇÃO DOS MECANISMOS ENVOLVIDOS NA ATIVAÇÃO ASTROCITÁRIA NA SEPSE AGUDA

Porto Alegre
2019

Bruna Bellaver

INVESTIGAÇÃO DOS MECANISMOS ENVOLVIDOS NA ATIVAÇÃO ASTROCITÁRIA NA SEPSE AGUDA

Tese apresentada ao Programa de Pós-Graduação em Ciências Biológicas: Bioquímica do Instituto de Ciências Básicas da Saúde da Universidade Federal do Rio Grande do Sul como requisito parcial para a obtenção do título de doutora em Bioquímica.

Orientador: Prof. Dr. Eduardo Rigon Zimmer

Porto Alegre

2019

CIP - Catalogação na Publicação

Bellaver, Bruna
INVESTIGAÇÃO DOS MECANISMOS ENVOLVIDOS NA ATIVAÇÃO ASTROCITÁRIA NA SEPSE AGUDA / Bruna Bellaver. -- 2019.
237 f.
Orientador: Eduardo Rigon Zimmer.

Tese (Doutorado) -- Universidade Federal do Rio Grande do Sul, Instituto de Ciências Básicas da Saúde, Programa de Pós-Graduação em Ciências Biológicas: Bioquímica, Porto Alegre, BR-RS, 2019.

1. astrócitos. 2. sepse. 3. metabolismo energético cerebral. 4. biomarcadores. 5. neuroinflamação. I. Rigon Zimmer, Eduardo, orient. II. Título.

Elaborada pelo Sistema de Geração Automática de Ficha Catalográfica da UFRGS com os dados fornecidos pelo(a) autor(a).

"O poder nasce do querer. Sempre que um homem aplicar a veemência e perseverante energia da sua alma a um fim, vencerá os obstáculos, e, se não atingir o alvo fará, pelo menos, coisas admiráveis."

(Dale Carnegie)

AGRADECIMENTOS

Ao meu orientador, Eduardo Rigon Zimmer, por me guiar pelos momentos mais difíceis que um doutorado pode trazer. Mas também por me propiciar a vivência dos mais agradáveis. Obrigada por me fazer redescobrir a minha paixão pela ciência.

À minha querida amiga, colega e orientadora extraoficial Débora Guerini Souza, por compartilhar todos os momento da minha jornada acadêmica, sempre com palavras doces nos momentos certos.

Às queridas Andréia Rocha e Pâmela Lukasewicz, por todo suporte e amizade, seja dividindo o trabalho de bancada ou uma conversa agradável.

À minha amiga Gisele Hansel, por ser um porto seguro em um lugar distante.

À minha amiga e colega Priscila Machado, umas das pessoas mais doces que já conheci, por compartilhar momentos importantes de aprendizado.

Ao Professor Luis Valmor Cruz Portela, que me iniciou na caminhada científica e mesmo de longe deu o apoio necessário para que eu continuasse.

A todo pessoal do Zimmer Lab, por me receberem tão bem, pela convivência diária e por compartilharem todo o seu conhecimento.

Ao Professor Joseph Baur, por ter me recebido no seu laboratório e confiado no meu trabalho. Obrigada por me proporcionar a convivência com pessoas maravilhosas que me fizeram sentir acolhida e valorizada.

A todos os amigos e colegas que estão ou já passaram pelo laboratório 28, pela convivência e pelo aprendizado.

Ao meu namorado Douglas Leffa, um grande amigo e pesquisador que inspirou, compartilhou, compreendeu e incentivou todas as etapas dessa caminhada. Obrigada por ser meu ponto de equilíbrio em todos os momentos.

Aos meu pais, Vanderlei e Izete, e à minha irmã Gabriela, por serem a minha maior torcida e não medirem esforços para que eu chegasse até aqui. Sem dúvida o percurso foi menos difícil com vocês do meu lado.

Ao pessoal do biotério, da portaria e da secretaria do departamento, pelo apoio e eficiência.

Ao Conselho Nacional de Desenvolvimento Tecnológico (CNPq) e à Coordenação de Aperfeiçoamento de Pessoal de Nível Superior (CAPES), pelo apoio financeiro.

APRESENTAÇÃO

Essa tese está organizada em três Partes, cada uma sendo constituída dos seguintes itens:

Parte I: Resumo, Resumo em inglês (abstract), Lista de abreviaturas, Introdução e Objetivos;

Parte II: Resultados, que estão divididos em capítulos os quais contêm os artigos científicos que foram elaborados de maneira a contemplar os objetivos propostos;

Parte III: Discussão, Conclusão, Anexos e Referências bibliográficas citadas na Introdução da Parte I e Discussão da Parte III.

Na seção "anexos" estão os artigos científicos que foram elaborados durante o período de doutoramento que têm conteúdo associado ao tema da tese (Anexo I) e que não são diretamente associados com o tema da tese (Anexo II). Os trabalhos foram desenvolvidos no Departamento de Bioquímica da Universidade Federal do Rio Grande do Sul (UFRGS).

SUMÁRIO

PARTE I 1
RESUMO 2
ABSTRACT 3
LISTA DE ABREVIATURAS 4
INTRODUÇÃO 6
1. A sepse 6
1.1. Conceito e Epidemiologia 6
1.2. Fisiopatologia 6
1.3. Encefalopatia associada à sepse (EAS) 7
1.4. Biomarcadores 8
1.5. Modelos animais de indução de sepse 9
1.6. Comunicação entre periferia e sistema nervoso central (SNC) 10
1.6.1. Periferia 10
1.6.2. SNC 11
1.6.2.1. Envolvimento hipocampal 12
2. Os astrócitos 13
2.1. Funções astrocitária 14
2.1.1. Ativação astrocitária 14
2.1.2. Modulação do metabolismo energético 15
2.1.3. Reciclagem de neurotransmissores 16
2.1.4. Resposta inflamatória 17
2.2. Culturas de astrócitos 19
OBJETIVOS 21
Objetivo Geral 21
Objetivos Específicos 21
PARTE II 22
Capítulo 1 23
Cecal ligation and perforation model recapitulates acute amino acid abnormalities observed in septic patients. 23
Capítulo 2 42
Systemic Inflammation as a Driver of Brain Injury: the Astrocyte as an Emerging Player. 42
Capítulo 3 73
Activated peripheral blood mononuclear cells trigger astrocyte reactivity. 73
PARTE III 176
DISCUSSÃO 177

CONCLUSÃO 189
REFERÊNCIAS BIBLIOGRÁFICAS 191
ANEXOS 198
ANEXO I: Artigos publicados durante o período de doutoramento cujos temas se relacionam a esta tese, mas não foram incluídos no corpo principal da tese 198
ANEXO I-A: Resveratrol Protects Hippocampal Astrocytes Against LPS-Induced Neurotoxicity Through HO-1, p38 and ERK Pathways. 199
ANEXO I-B: Guanosine inhibits LPS-induced pro-inflammatory response and oxidative stress in hippocampal astrocytes through the heme oxygenase-1 pathway. 202
ANEXO II: Artigos publicados durante o período de doutoramento cujos temas não se relacionam diretamente a esta tese. 204
ANEXO II-B: Characterization of Amino Acid Profile and Enzymatic Activity in Adult Rat Astrocyte Cultures. 207
ANEXO II-C: Signaling mechanisms underlying the glioprotective effects of resveratrol against mitochondrial dysfunction. 209
ANEXO II-D: Higher Vulnerability of Menadione-Exposed Cortical Astrocytes of Glutaryl-CoA Dehydrogenase Deficient Mice to Oxidative Stress, Mitochondrial Dysfunction, and Cell Death: Implications for the Neurodegeneration in Glutaric Aciduria Type I. 211
ANEXO II-E: Anti-aging effects of guanosine in glial cells. 213
ANEXO II-F: Resveratrol modulates GSH system in C6 astroglial cells through heme oxygenase 1 pathway. 215
ANEXO II-G: Homocysteine Induces Glial Reactivity in Adult Rat Astrocyte Cultures. 217
ANEXO II-H: Cortical Bilateral Adaptations in Rats Submitted to Focal Cerebral Ischemia: Emphasis on Glial Metabolism. 219
ANEXO II-I: N-acetylcysteine Prevents Alcohol Related Neuroinflammation in Rats. 221
ANEXO II-J: In Vitro Adult Astrocytes are Derived From Mature Cells and Reproduce in Vivo Redox Profile. 223
ANEXO II-K: Increased Oxidative Parameters and Decreased Cytokine Levels in an Animal Model of Attention-Deficit/Hyperactivity Disorder. 225
ANEXO II-L: Transcranial direct current stimulation improves long-term memory deficits in an animal model of attention-deficit/hyperactivity disorder and modulates oxidative and inflammatory parameters. 227
ANEXO II-M: Combined use of alcohol and tobacco smoke change oxidative, inflammatory, and neurotrophic parameters in different brain areas of rats. 229

PARTE I

RESUMO

A sepse é caracterizada por um severo processo inflamatório, globalmente disseminado, que compromete diversas funções vitais ao organismo. O acometimento do sistema nervoso central (SNC) nessa patologia está relacionado a um aumento na sua taxa de mortalidade. Os biomarcadores utilizados atualmente na clínica não são suficientemente sensíveis para detectar essas complicações da sepse de maneira precoce, falhando em antecipar o início do tratamento e diminuir a morbimortalidade. O entendimento dos danos causados pela sepse no SNC vai muito além do simples estudo da função neuronal, sendo evidente o envolvimento das células gliais nos seus mecanismos patológicos. Nesse sentido, os astrócitos desempenham um papel crucial na resposta neuroimune e no controle da homeostasia energética cerebral, porém sua participação durante a sepse permanece negligenciada. Essa tese buscou elucidar alterações na funcionalidade dos astrócitos e identificar os eventos sistêmicos responsáveis pela reatividade astrocitária durante a fase aguda de sepse. Nossos resultados sugerem que o modelo de ligação cecal e perfuração (LCP) reproduz o perfil sorológico de aminoácidos observado em pacientes com encefalopatia associada à sepse (EAS). Adicionalmente, correlações entre o perfil de aminoácidos entre o soro e o líquido cefalorraquidiano foram observadas. Demonstramos também que a cultura de astrócitos reflete características observadas *in vivo* durante a sepse, representando um modelo adequado de estudo para essa patologia. Além disso, a análise de transcriptoma humano evidenciou um acometimento de vias associadas ao metabolismo energético em pacientes com sepse. Consistentemente, nosso modelo de LCP demonstrou uma substancial diminuição no metabolismo de glicose cerebral, acompanhado de um decréscimo no metabolismo glutamatérgico. Finalmente, observamos que mediadores liberados pelas células sanguíneas mononucleares (PBMCs) são capazes de promover uma ativação astrocitária acompanhada por déficit no metabolismo energético durante a sepse, fenômeno com envolvimento direto da via da fosfatidilinositol 3-quinase (PI3K). Com os resultados obtidos nessa tese nós avançamos na compreensão dos mecanismos pelo qual a inflamação sistêmica impacta na funcionalidade cerebral, indicando potenciais alvos para futuras intervenções terapêuticas.

ABSTRACT

Sepsis is a heterogeneous life-threatening dysfunction presenting high mortality rates caused by a dysregulated host response. When the central nervous system (CNS) is affected, sepsis promotes permanent cognitive impairment, therefore increasing mortality rates. The biomarkers currently available are not sufficient sensible in the clinical settings to be used as sepsis-associated encephalopathy (SAE) predictors. Thus, the implementation of better biomarkers of SAE is of high interest, as it would improve differential diagnose and early therapeutic intervention. Beyond sepsis-induced neuronal dysfunction, glial cells response has been gaining considerable attention with microglial activation as a key player. By contrast, astrocytes role during acute sepsis is still underexplored. Astrocytes are specialized immune-competent cells involved in the brain surveillance and energetic metabolism homeostasis. Based on that, this thesis aimed to evaluate the alterations in astrocyte functionality and the systemic triggers of astrocyte reactivity during the acute stage of sepsis. Our findings demonstrated that CLP model recapitulates serum data available from clinical studies regarding amino acid profile in the acute stage of SAE. Importantly, we also identified amino acid correlations between serum and cerebrospinal fluid (CSF). Additionally, we demonstrated that astrocyte culture reflects the characteristics observed in vivo during sepsis, being a reliable tool to study this pathology. Transcriptome analysis suggested multiple changes in energy signaling pathways in the blood of septic patients. In the CLP model, we identified widespread brain glucose hypometabolism along with reduced capacity of taking up glutamate. Also, by exposing astrocytes to mediators released by PBMCs from CLP animals, we reproduced the energetic failure observed *in vivo*. This phenomenon seems to be partially mediated by the phosphatidylinositol 3-kinase (PI3K) pathway. In summary, this thesis improves the understanding of the mechanisms by which systemic inflammation impacts on brain functionality, indicating potential targets for therapeutic intervention.

LISTA DE ABREVIATURAS

[^{18}F] FDG: fluorodeoxiglicose

AAA: aminoácidos aromáticos

AMPK: proteína cinase ativada por AMP (*AMP-activated protein kinase*)

ATP: trifosfato de adenosina

BCAA: aminoácido de cadeia lateral ramificada (*branched-chain amino acid*)

BSC: barreira sangue-cérebro

CM: meio condicionado

DEG: gene diferencialmente expresso (*differentially expressed gene*)

EAS: encefalopatia associada à sepse

GABA: ácido gama-aminobutírico *(gamma*-amino *butyric acid*)

G-CSF: fator estimulante de colônia de granulócito (*granulocyte-colony stimulating factor*)

GFAP: proteína glial fibrilar ácida (*glial fibrillary acidic protein*)

GLAST: transportador glutamato-aspartato (*glutamate-aspartate transporter*)

GLT-1: transportador de glutamato 1 (*glutamate transporter 1*)

GLUT1: transportador de glicose 1 (*glucose transporter 1*)

GSH: glutationa

IFN-ɣ: interferon gama

IL: interleucina

iNOS: óxido nítrico sintase induzível (*inducible nitric oxide synthase*)

LCP: ligação cecal e perfuração

LCR: líquido cefalorraquidiano

LPS: lipopolissacarídeo

OMS: Organização Mundial da Saúde

PBMC: células sanguíneas mononucleares (*peripheral blood mononuclear cells*)

PET: tomografia por emissão de pósitrons (*positron-emission tomography*)

PI3K: fosfatidilinositol 3-quinase (*phosphoinositide 3-kinase*)

PMAD: padrões moleculares associados a danos

PMAP: padrões moleculares associados a patógenos

RNAm: ácido ribonucleico mensageiro

SNC: sistema nervoso central

TCA: ciclo do ácido cítrico (*tricarboxylic acid cycle*)

TGF-β: fator de crescimento transformante beta (*transforming growth factor β*)

TLR: receptores do tipo Toll (*Toll-like receptors*)

TNF-α: fator de necrose tumoral alfa (*tumor necrosis factor alpha*)

VEGF: fator de crescimento endotelial vascular (*vascular endothelial growth factor*)

INTRODUÇÃO

1. A sepse

1.1. Conceito e Epidemiologia

O termo sepse deriva do grego *sêpsis*, que significa putrefação. O conceito de sepse vêm sendo atualizado ao longo da história. Hipócrates, no ano 700 a.C., descreveu esse quadro como um perigoso e odorífero comprometimento biológico que poderia ocorrer no organismo. Mais recentemente, o quadro de sepse foi redefinido como uma disfunção que lesa os órgãos vitais, difusamente, devido a uma resposta à infecção desregulada (Singer, Deutschman et al. 2016). Atualmente a Organização Mundial de Saúde (OMS) estima que a cada ano 30 milhões de pessoas sejam acometidas por essa síndrome clínica, chegando a causar 6 milhões de mortes anualmente. No Brasil, a situação é ainda mais alarmante. Com um total de 670 mil casos anuais, estima-se que a taxa de mortalidade chegue a 50%. A taxa de mortalidade elevada em decorrência do estabelecimento da sepse reflete a carência de um diagnóstico e de tratamento precoce. Esse panorama, somado ao preocupante aumento do número de bactérias resistentes aos antimicrobianos disponíveis na clínica, principalmente em países em desenvolvimento, impulsionou a OMS a incluir a sepse na lista de prioridades de saúde mundial (Reinhart, Daniels et al. 2017).

1.2. Fisiopatologia

O conjunto de eventos celulares e moleculares que causam os efeitos deletérios da sepse e, em última instância, a falência de órgãos, são bastante heterogêneos e dinâmicos, variando conforme o estágio da patologia observado. Fatores importantes

que determinam o desenvolvimento da sepse incluem, suscetibilidade genética, ativação exacerbada do sistema imune, produção de espécies reativas de oxigênio em excesso e também alterações metabólicas (Gotts and Matthay 2016). Assim, sugere-se que devido ao dano ao DNA causado pelo estresse oxidativo, há uma disfunção mitocondrial em pacientes acometidos por sepse, resultando em última instância em uma redução na produção de adenosina trifosfato (ATP) (Singer 2014). Consequentemente, observa-se uma generalizada redução do gasto energético a nível celular durante a sepse, o que provavelmente potencializa a disfunção orgânica, causando a perda de funções celulares especializadas de cada tecido (Rivers, Nguyen et al. 2001, Gotts and Matthay 2016). Nesse sentido, por não ser uma patologia com sintomas homogêneos, faz-se necessário o entendimento individual do mecanismo pelo qual cada órgão é afetado.

1.3. Encefalopatia associada à sepse (EAS)

O desenvolvimento de um quadro de encefalopatia associada à sepse (EAS) é definido como uma disfunção cerebral focal ou generalizada induzida por uma resposta a uma infecção sistêmica sem que haja qualquer foco de infecção direta no SNC (Wilson and Young 2003). EAS é uma apresentação clínica comum, com prevalência de até 71%, apresentando-se prematuramente em pacientes acometidos por essa síndrome (Cotena and Piazza 2012). Alguns estudos sugerem, inclusive, que uma disfunção cerebral associada à sepse ocorra antes que possa ser observado dano a qualquer outro órgão (Young 2010, Ziaja 2013) e que seu dano perdure após resolução do quadro crítico de inflamação, conduzindo a um declínio cognitivo e demência em longo prazo (Chou, Lee et al. 2017). Atualmente não existe uma terapia específica para EAS e o seu desfecho depende do tratamento rápido e adequado da sepse como um todo. Nesse

sentido, o entendimento dos mecanismos patológicos e a intervenção clínica na fase aguda de sepse são de grande valia para aumentar a sobrevivência de pacientes acometidos por EAS e prevenir, a longo prazo, as sequelas associadas.

1.4. Biomarcadores

O uso de biomarcadores na prática clínica é de fundamental importância para o diagnóstico precoce de diversas patologias, auxiliando na tomada de decisões e facilitando prognósticos. Sendo a sepse uma síndrome multifatorial, com características distintas e não completamente estabelecidas ao longo do seu curso de desenvolvimento, o uso de biomarcadores na clínica ainda é um desafio (Faix 2013, Biron, Ayala et al. 2015). Um dos marcadores mais utilizados para diagnóstico de sepse é a cultura bacteriológica de sangue. Esse método diagnóstico possui uma limitação bastante importante que é o tempo prolongado para obtenção dos resultados (cerca de 2-3 dias). Além disso, uma quantidade significativa de casos de sepse não apresentam culturas sanguíneas positivas para bactérias (Calandra and Cohen 2005, Biron, Ayala et al. 2015). Outro marcador amplamente utilizado como auxiliar do diagnóstico de sepse é o lactato sanguíneo (Lee and An 2016). Contudo, muitas vezes, níveis de lactato elevados são observados apenas após o início de falência de órgãos em pacientes. Além disso, atualmente não existem biomarcadores disponíveis na clínica capazes de predizer o desenvolvimento de EAS e facilitar o início de um tratamento precoce visando a melhoria do prognóstico e evitando danos a longo prazo. O desafio em identificar biomarcadores para EAS se deve, em parte, à dificuldade em correlacionar níveis periféricos de determinada molécula com seus níveis no SNC. Essa correlação em humanos é ainda mais desafiadora, visto a necessidade da utilização de técnicas

invasivas para coleta de líquido cefalorraquidiano (LCR). Assim, modelos animais que reproduzam parâmetros clínicos observados em pacientes são uma ferramenta bastante útil na busca por biomarcadores na EAS.

1.5. Modelos animais de indução de sepse

Visando elucidar o impacto da inflamação sistêmica sobre o SNC, diversos modelos experimentais vêm sendo utilizados na literatura, incluindo sepse cutânea, sepse abdominal e sepse induzida pela administração de lipopolissacarídeo (LPS), variando na literatura em relação à dose, tempo e via de administração. Contudo, o modelo de ligação cecal e perfuração (LCP) é considerado atualmente o padrão-ouro para os estudos relacionados à sepse. Nesse modelo, a sepse é cirurgicamente induzida através da ligação do ceco, imediatamente abaixo da válvula ileo-cecal, e da perfuração do ceco permitindo o extravasamento do material fecal do colo para a cavidade peritoneal, promovendo uma intensa reação inflamatória (Wichterman, Baue et al. 1980). Além disso, esse modelo induz uma isquemia mesentérica, que associada à peritonite, simula as grandes síndromes clínicas de sepse abdominal observadas na clínica. Assim, esse modelo promove uma infecção gradativa mista por bactérias Gram-positivas e Gram-negativas, e se correlaciona de forma mais fidedigna à sepse observada em humanos do que os outros modelos utilizados atualmente (Lee and Huttemann 2014, Neves, Marques et al. 2016, Comim, Freiberger et al. 2017). Além disso, devido ao rápido acometimento do SNC, esse modelo é amplamente utilizado para o estudo de EAS (Yokoo, Chiba et al. 2012, Steckert, Dominguini et al. 2017, Gasparotto, Girardi et al. 2018).

1.6. Comunicação entre periferia e sistema nervoso central (SNC)

O processo neuroinflamatório não é um evento dependente apenas de sinais provenientes do SNC. Pelo contrário, as respostas imunes inatas e adaptativas cerebrais são complexas e controladas de maneira a responder também a sinais periféricos (Failli, Kopp et al. 2012, Katafuchi, Ifuku et al. 2012, Ransohoff, Schafer et al. 2015). Dessa forma, no contexto da EAS, há um crescente interesse no entendimento dos mecanismos celulares e moleculares envolvidos na iniciação e propagação da inflamação cerebral, a fim de melhor compreender e, futuramente, prevenir os processos patológicos associados a essa síndrome clínica.

1.6.1. Periferia

A resposta imune durante a fase inicial da sepse é coordenada por receptores de padrões moleculares associados a patógenos (PMAPs) ou a danos (PMADs) que são originados dos organismos causadores da infecção, geralmente bactérias ou fungos (Cinel and Opal 2009). Assim, esses padrões moleculares se ligam aos seus receptores expressos nas células imunes sanguíneas, desencadeando a liberação de uma série de mediadores que vão aumentar a atividade fagocítica, a ativação do sistema de coagulação e a quimiotaxia de leucócitos para o sítio da infecção (Casey 2000, Cinel and Opal 2009). Nesse sentido, acredita-se que a ativação de células sanguíneas mononucleares (PBMCs, do inglês *peripheral blood mononuclear cells*) tenha um papel central na regulação dessa resposta aguda periférica. As PBMCs são células sanguíneas com núcleo arredondado, e sua população é constituída por linfócitos, monócitos e macrófagos. Quando ativadas, essas células liberam uma gama de mediadores inflamatórios, incluindo interferon gama (IFN-ɣ), fator de necrose tumoral alfa (TNF-α), interleucina (IL)-2, IL-4, IL-5 e IL-10 (Friberg, Bryant et al. 1994, Katial,

Sachanandani et al. 1998). Então, esses mediadores são enviados do plasma sanguíneo para outros sítios afetados pela inflamação, incluindo o cérebro (Tang, McLean et al. 2009, Godini and Fallahi 2018). Além disso, já foi demonstrado que alterações na atividade mitocondrial das PBMCs estão diretamente relacionadas com a desregulação da resposta imune e falência de órgãos durante a sepse (Adrie, Bachelet et al. 2001, Sjovall, Morota et al. 2013).

Os pacientes sobreviventes à essa fase inicial da sepse, considerada hiper-inflamatória, passam posteriormente por uma fase anti-inflamatória compensatória, chamada de imunoparalisia. Os mecanismos relacionados a essa segunda fase ainda não estão claros, mas eles incluem uma disfunção na resposta imune adaptativa, que consequentemente deixa o organismo mais vulnerável a infecções secundárias, apresentando uma taxa de letalidade elevada (Hotchkiss, Monneret et al. 2013, Boomer, Green et al. 2014). Contudo, Tang e colaboradores demonstraram que essa visão imunológica dual durante a sepse parece ser um pouco mais complexa (Tang, Huang et al. 2010). Analisando diferentes estudos publicados na literatura, esses autores não observaram padrões de expressão gênica que distinguissem as fases pró e anti-inflamatória, ou mesmo uma fase de transição, entre os acometidos por sepse (Tang, Huang et al. 2010). Dessa forma, hipotetiza-se que em uma grande quantidade de casos ambas as fases possam ocorrer simultaneamente.

1.6.2. SNC

Os sistemas imunes inato e adaptativo participam ativamente na vigilância do SNC, promovendo a manutenção da homeostasia cerebral e facilitando o combate a infecções, degeneração e dano tecidual (Waisman, Liblau et al. 2015). Durante a fase aguda de sepse, a resposta imune inata é a primeira linha de defesa cerebral, sendo

formada primariamente pela barreira sangue-cérebro (BSC), células gliais (microglia e astrócitos) e alguns mediadores químicos (Russo and McGavern 2015, Waisman, Liblau et al. 2015). Essa resposta, assim como na periferia, é coordenada por receptores de PMAPs e/ou PMADs, provocando modificações no microambiente tecidual, como alteração na expressão gênica, diferenciação celular e recrutamento de células imunes periféricas através da BSC (Hamby, Coppola et al. 2012).

1.6.2.1. Envolvimento hipocampal

Manifestações precoces de dano cerebral durante a sepse incluem ansiedade, perda de memória de curta duração e espacial, sendo esses sintomas normalmente consequências de dano hipocampal (Ebersoldt, Sharshar et al. 2007). De fato, o hipocampo é uma das regiões cerebrais mais vulneráveis a danos inflamatórios e isquêmicos (Lim, Alexander et al. 2004, Zhang, Wang et al. 2017). Nesse sentido, Nolan e colaboradores demonstraram que após um dano inflamatório há um recrutamento de macrófagos e células gliais para a região afetada, causando um dano hipocampal mediado majoritariamente por monócitos $CD14^+$ (Nolan, Vereker et al. 2003). Além disso, estudos demonstram que tratamentos que buscam diminuir o dano inflamatório agudo hipocampal, como anti-inflamatórios não esteroides (Monje, Toda et al. 2003), inibidores de morte celular mediados por caspases (Heo, Cho et al. 2006) e imunomodulação de células apoptóticas (Nolan, Campbell et al. 2005), são capazes de prevenir e/ou diminuir o dano cognitivo a longo prazo. Baseado nisso, o hipocampo emerge com uma potencial região-alvo para o tratamento de sepse (Annane 2009), e o melhor entendimento dos processos que medeiam o dano causado nessa região durante a fase aguda da sepse são fundamentais para o estabelecimento de um tratamento adequado e a diminuição de sequelas a longo prazo. O prejuízo da funcionalidade

hipocampal durante a sepse envolve o comprometimento de diversos tipos celulares do SNC, dentre os quais os mais investigados são os neurônios e a microglia. Porém, os astrócitos, células fundamentais na homeostase cerebral e com importante papel imune, vêm ganhando crescente destaque nesse contexto.

2. Os astrócitos

Os astrócitos são as células gliais responsáveis pela manutenção da homeostase cerebral, apresentando-se como o tipo celular cerebral com maior diversidade funcional, além de possuir uma capacidade dinâmica de alterar seu fenótipo no decorrer da vida (Shao and McCarthy 1994). Os astrócitos são classicamente divididos em dois grandes subtipos de acordo com as suas diferenças morfológicas e localização anatômica. Os protoplasmáticos representam o subtipo mais abundante, estão localizados na substância cinzenta e exibem muitas ramificações com uma morfologia globóide. Já os astrócitos fibrosos são encontrados ao longo de toda substância branca, apresentam menos ramificações e extensões cilíndricas, longas e finas (Miller and Raff 1984). Em geral, para o estudo da funcionalidade astrocitária utilizando culturas celulares, os astrócitos provenientes da substância cinzenta são os mais utilizados (Lange, Bak et al. 2012).

Dentre as principais funções desempenhadas pelos astrócitos estão: (a) modulação da plasticidade sináptica, participando da sinapse tripartite (Clarke and Barres 2013), (b) regulação extracelular de neurotransmissores, em especial na sinalização exercida por glutamato e ácido gama aminobutírico (GABA, do inglês *Gamma*-Amino *Butyric Acid*) (Danbolt 2001, Schousboe, Bak et al. 2013), (c) formação e manutenção da BSC e consequentemente da resposta inflamatória uma vez que eles regulam a passagem de células do sistema imune entre a circulação sistêmica e o parênquima do SNC (Abbott, Ronnback et al. 2006), (d) controle da disponibilidade de

substratos energéticos, por estarem em contato direto com os vasos sanguíneos e pelo seu papel no ciclo glutamato-glutamina (McKenna 2007, Stobart and Anderson 2013), (e) defesa contra estresse oxidativo, através da produção do principal antioxidante não enzimático cerebral, a glutationa (GSH) (Dringen 2000), (f) manutenção do pH e homeostase iônica do SNC, evitando a excessiva despolarização neuronal e consequente hiperexcitabilidade (Wang and Bordey 2008). Alguns desses tópicos serão explorados com maior detalhe nas seções seguintes.

Alterações nas funções astrocitárias citadas anteriormente possuem impacto direto em diversas doenças que acometem o SNC, incluindo na doença de Alzheimer (Carter, Herholz et al. 2019), Parkinson (Booth, Hirst et al. 2017), Huntington (Khakh, Beaumont et al. 2017), isquemia (Rossi, Brady et al. 2007), esclerose amiotrófica lateral (Pehar, Harlan et al. 2017) e EAS (Michels, Steckert et al. 2015, Bellaver, Dos Santos et al. 2017). Assim, há um crescente número de estudos propondo modulações da atividade astrocitária para o desenvolvimento de terapias farmacológicas para essas patologias (Gorshkov, Aguisanda et al. 2018).

2.1. Funções astrocitária

2.1.1. Ativação astrocitária

A resposta astrocitária a diferentes tipos de injúrias é um processo comumente denominado reatividade astrocitária. Esse processo é, em geral, transitório e possui como característica hipertrofia e hiperplasia celular, acúmulo de proteínas intermediárias de citoesqueleto, especialmente da proteína glial fibrilar ácida (GFAP, do inglês *glial fibrillary acidic protein*) e liberação de diversas moléculas que impactam de diferentes maneiras todos os tipos celulares no seu microambiente (Kang and Hebert

2011, Sofroniew 2014). A GFAP é uma proteína da classe de filamentos intermediário do tipo III e é a principal proteína que constitui o citoesqueleto de astrócitos, conferindo a essas células a manutenção de sua força mecânica e de suporte estrutural aos neurônios e à BSC (Eng, Ghirnikar et al. 2000, Bramanti, Tomassoni et al. 2010). Adicionalmente à GFAP, os astrócitos também aumentam a expressão de outra importante proteína de citoesqueleto quando se tornam reativos: a vimentina. Nesse contexto, estudos com animais *knockout* para GFAP e vimentina já demonstraram uma diminuição no processo de reatividade e de formação da cicatriz glial (Wilhelmsson, Li et al. 2004, Liu, Li et al. 2014). Apesar da reatividade astrocitária ser considerada um mecanismo de proteção astrocitário evolutivamente conservado, seu papel benéfico ainda é bastante controverso na literatura e parece variar de acordo com o contexto patológico, evidenciando assim a importância de seu estudo específico em diferentes injúrias que acometem o SNC (Pekny, Wilhelmsson et al. 2014).

2.1.2. Modulação do metabolismo energético

O cérebro é um órgão que possui alta demanda energética, chegando a consumir cerca de 25% do total de glicose disponível em todo o corpo. Contudo, esse órgão possui uma baixa reserva de energia, estocada na forma de glicogênio astrocitário. sendo assim, altamente dependente da captação de substratos energéticos da circulação sanguínea (Garcia-Caceres, Quarta et al. 2016). Nesse sentido, os astrócitos são reguladores multifuncionais do acoplamento neurometabólico, desempenhando um importante papel central na regulação do metabolismo energético cerebral. Por ocuparem uma posição privilegiada, com seus pés astrocíticos em contato com cerca de 99% dos capilares sanguíneos cerebrais e também com os neurônios, eles são capazes

de sentir a necessidade energética cerebral e captar substratos da circulação sanguínea fornecendo, com isso, a energia necessária para a manutenção da atividade neuronal (Belanger, Allaman et al. 2011, Stobart and Anderson 2013). A glicose é captada pelos astrócitos através de seus transportadores de glicose específicos, sendo o principal deles o GLUT1. Após ser captada pelos astrócitos, a glicose pode seguir dois destinos: (a) ser estocada na forma de glicogênio para mobilização rápida de glicose (Belanger, Allaman et al. 2011) ou, predominantemente (b) entrar na via glicolítica para liberar intermediários que servirão de substrato energético neuronal ou para serem oxidados no ciclo do ácido cítrico (TCA) para suprir as próprias demandas energéticas (Lovatt, Sonnewald et al. 2007).

2.1.3. Reciclagem de neurotransmissores

Uma das funções astrocitárias melhor caracterizada é a sua participação ativa na refinada regulação dos níveis de glutamato presentes na fenda sináptica. O glutamato é o principal neurotransmissor excitatório do SNC, assim, a adequada captação astrocitária do excesso de glutamato presente na fenda sináptica é de fundamental importância para evitar a chamada excitoxicidade glutamatérgica, que é altamente prejudicial à atividade neuronal. Dessa forma, através dos seus transportadores específicos GLT-1 (transportador de glutamato-1) e GLAST (transportador glutamato-aspartato), os astrócitos são capazes de captar até 90% do glutamato liberado na fenda sináptica (Anderson and Swanson 2000, Nortley and Attwell 2017). Após captado, o glutamato pode ser metabolizado no TCA ou ser reciclado através do ciclo glutamato-glutamina. Esse ciclo é dependente da funcionalidade astrocitária, uma vez que essas células expressam, de maneira exclusiva no SNC, a enzima glutamina sintetase, que vai

converter o glutamato captado à glutamina. Dessa forma, permitindo que a glutamina seja liberada para a fenda sináptica onde pode ser recaptada pelo neurônio pré-sináptico e convertida novamente à glutamato, a fim de manter o pool de glutamato neuronal. Interessantemente, a neurotransmissão glutamatérgica é responsável por 80% da demanda energética cerebral evidenciando um importante link entre metabolismo glutamatérgico e utilização de glicose (Attwell and Laughlin 2001). Nesse sentido, recentemente foi demonstrada a existência de um acoplamento *in vivo* entre captação de glutamato via GLT-1, e metabolismo de glicose cerebral, mediado por astrócitos (Zimmer, Parent et al. 2017).

2.1.4. Resposta inflamatória

Em condições normais, o SNC possui um perfil anti-inflamatório, estando principalmente sob a influência de IL-10 e do fator de crescimento transformante beta (TGF-β, do inglês *transforming growth factor β*), enquanto as citocinas pró-inflamatórias são produzidas apenas em níveis basais, requeridos para o correto funcionamento cerebral (McAfoose, Koerner et al. 2009, Santello, Bezzi et al. 2011, Jensen, Massie et al. 2013). Nesse contexto, os astrócitos atuam controlando a passagem de moléculas, como anticorpos e fatores do sistema complemento, para o SNC. Já no contexto inflamatório, os astrócitos atuam liberando uma gama de citocinas e quimiocinas pró-inflamatórias com o objetivo de atrair células e fatores solúveis sanguíneos para o local da inflamação. Dentre as principais citocinas liberadas pelos astrócitos estão: TNF-α, IL-1β, IL-6 e IL-18 (Jensen, Massie et al. 2013). Após serem secretados pelos astrócitos, esses mediadores estimulam a liberação de enzimas proteolíticas e prostaglandinas, induzindo a produção de espécies reativas de oxigênio e

consequentemente a síntese e liberação de citocinas secundárias que vão recrutar novas células gliais de modo a exacerbar a resposta inflamatória (Cannon 2000).

Essa resposta astrocitária ocorre pois essas células, em cooperação com a microglia, são capazes de reconhecer e responder a diversos patógenos, sejam eles bactérias, fungos ou vírus (Ransohoff and Brown 2012). O reconhecimento desses agentes patológicos é possível devido ao fato de os astrócitos expressarem receptores de reconhecimento padrão específicos, incluindo vários membros da família dos receptores do tipo Toll (TLR) (Hayward and Lee 2014, Kopitar-Jerala 2015). Estudos sugerem uma expressão robusta de TLR3 em astrócitos em condições não patológicas, enquanto que TLR2 e TLR4 têm sua expressão gênica aumentada apenas após as células astrocitárias serem estimuladas por PMAPs (Farina, Aloisi et al. 2007, Gorina, Santalucia et al. 2009, Rossi 2015). Além de os astrócitos serem refinadamente sensíveis a infecções associadas a PMAPs, a presença de citocinas inflamatórias também é capaz de alterar o perfil transcricional astrocitário, fazendo com que essas células adquiram um fenótipo pró-inflamatório e citotóxico.

Tanto a presença de ligandos de TLRs quanto de receptor de TNF ou de IL-1 são capazes de ativar a via de sinalização do fator nuclear kappa B (NFκB, do inglês *nuclear factor kappa B*), que ocorre através da sua translocação do citoplasma para o núcleo. Sabe-se que a sinalização por NFκB é capaz de ativar mais de 500 genes (Chen and Greene 2004, Gupta, Sundaram et al. 2010), sendo uma importante via de sobrevivência celular. Muitos desses genes estão relacionados à atividade cerebral fisiológica, incluindo plasticidade sináptica, aprendizado e memória e proteção contra a excitotoxicidade (Mincheva-Tasheva and Soler 2013). Porém, sua ativação por certas moléculas induz a produção de citocinas e enzimas pró-inflamatórias, como a óxido nítrico sintase induzível (iNOS, do inglês *inducible nitric oxide synthase*), acarretando

na produção aumentada de uma poderosa espécie reativa de nitrogênio, o óxido nítrico (Saha and Pahan 2006).

2.2. Culturas de astrócitos

O cultivo celular primário demonstra-se uma ferramenta bastante útil quando se deseja estudar o papel de um tipo celular individualmente, permitindo assim elucidar suas características e funções específicas. Nesse sentido, a cultura primária de astrócitos vem sendo amplamente utilizada para melhor entendimento do papel dessas células tanto em funções fisiológicas quanto patológicas (Skytt, Madsen et al. 2010, Lange, Bak et al. 2012). Muito do conhecimento sobre a funcionalidade astrocitária é proveniente do estudo utilizando cultura de células de animais neonatos, porém, grande parte das disfunções anteriormente citadas afeta majoritariamente o cérebro maduro. Diferentemente do cérebro em maturação, o tecido adulto apresenta alta interatividade entre as células (especialmente conexões sinápticas), e relações, papéis e funções celulares bem estabelecidas. Assim, células provenientes do tecido maduro tendem a ter um maior grau de diferenciação do que as provenientes do tecido cerebral de neonatos (Souza, Bellaver et al. 2013, Herculano-Houzel 2014, Bellaver, Souza et al. 2016)

Além disso, a utilização do cérebro maduro para a elaboração da cultura astrocitária primária nos permite a realização de diferentes intervenções *in vivo* previamente à obtenção das células para cultivo. Tendo isso em vista, nosso grupo de pesquisa padronizou um protocolo de rotina de cultivo primário de astrócitos provenientes do cérebro de animais maduros que nos permite estudar de maneira mais fidedigna o papel específico dos astrócitos em diferentes patologias que acometem o cérebro adulto ou envelhecido (Bellaver, Souza et al. 2014, Bellaver, Souza et al. 2016,

Souza, Bellaver et al. 2016, Bellaver, Dos Santos et al. 2017, Souza, Bellaver et al. 2017).

OBJETIVOS

Objetivo Geral

Elucidar alterações na funcionalidade dos astrócitos e identificar os eventos sistêmicos responsáveis pela reatividade astrocitária durante a fase aguda de sepse.

Objetivos Específicos

1. Verificar se o perfil sorológico de aminoácidos em modelo experimental de LCP recapitula àquele observado em humanos durante a sepse aguda;
2. Correlacionar o perfil de aminoácidos no soro e no LCR em animais submetidos à LCP;
3. Elucidar a resposta astrocitária hipocampal após episódio de inflamação sistêmica severa e aguda;
4. Investigar diferenças entre análises realizadas no tecido hipocampal total e na cultura celular de astrócitos após indução de LCP *in vivo*;
5. Analisar o transcriptoma de pacientes acometidos por sepse para evidenciar os fatores que possam estar relacionados com a ativação astrocitária observada em modelo experimental;
6. Avaliar o metabolismo energético cerebral após indução de inflamação sistêmica aguda através do modelo experimental de LCP;
7. Avaliar o impacto da comunicação entre PBMCs e astrócitos no metabolismo energético cerebral durante a fase aguda da sepse.

PARTE II

Capítulo 1

Cecal ligation and perforation model recapitulates acute amino acid abnormalities observed in septic patients.

No capítulo 1 apresentamos o artigo a ser submetido ao periódico *Journal of Neurochemistry*

Nesse estudo temos como objetivo investigar a translacionalidade do modelo animal de LCP para o seu uso como ferramenta na busca de biomarcadores para a EAS. De maneira geral, observamos uma alteração no perfil sorológico de aminoácidos em animais submetidos ao modelo de LCP semelhante a que é observada em humanos que desenvolvem EAS. Observamos também em nosso modelo uma correlação entre os níveis sanguíneos e no LCR de aminoácidos de cadeia lateral ramificada (BCAA), aminoácidos aromáticos (AAA), alanina, lisina e ornitina. Finalmente, uma abordagem utilizando uma análise de redes de aminoácidos identificou um fenômeno de hiperassociação entre os aminoácidos analisados, fenômeno evidenciado pela formação de *clusters*.

Cecal ligation and perforation model recapitulates acute amino acid abnormalities observed in septic patients

Bruna Bellaver[1], Fernanda U. Fontella[1], Andréia S. Rocha[1], Douglas T. Leffa[2], Carolina Chatain[1], Pâmela C. Lukazewicz Ferreira[4], Eduarda Ferreira[1], Alessandra V. Amaral[1], Guilherme Schu[1], Débora G. Souza[1], Eduardo R. Zimmer[1,4,5*]

[1]Graduate Program in Biological Sciences: Biochemistry, Universidade Federal do Rio Grande do Sul, Porto Alegre, Brazil;
[2]Graduate Program in Medicine: Medical Sciences, Universidade Federal do Rio Grande do Sul, Porto Alegre, Brazil;
[3]Graduate Program in Biological Sciences: Pharmacology and Therapeutics, Universidade Federal do Rio Grande do Sul, Porto Alegre, Brazil;
[4]Graduate Program in Pharmaceutical Sciences, Universidade Federal do Rio Grande do Sul, Porto Alegre, Brazil
[5]Departament of Pharmacology, Universidade Federal do Rio Grande do Sul, Porto Alegre, Brazil;

***Corresponding author:**
Eduardo R. Zimmer, PhD (E.R. Zimmer)
Department of Pharmacology, Universidade Federal do Rio Grande do Sul (UFRGS)
2500 Ramiro Barcelos St, 90035-003, Porto Alegre, RS, Brazil
Email address: eduardo.zimmer@ufrgs.br
Telephone: +55 51 33085558
Fax: +55 51 33085544
Website: www.zimmer-lab.org

Abstract

Sepsis is a heterogeneous dysfunction presenting high mortality rates associated with the development of sepsis-associated encephalopathy (SAE). Current biomarkers for sepsis diagnosis are not sufficient sensible to be used as SAE predictors. In this sense, animal models have been used in an attempt to elucidate novel biomarkers. Based on that, here we applied a "back-translation" strategy to evaluate whether serum amino acid profile in a rat model of acute cecal ligation and perforation (CLP) recapitulates findings in humans. Additionally, cerebral spinal fluid (CSF) analyzes were performed to investigate a potential correlation with peripheral findings. We observed that sepsis promotes a reduction in serum glutamate levels, along with a decrease in glutamate/glutamine ratio. CLP rats presented increased serum aromatic amino acids (AAA) phenylalanine and tryptophan with no changes in the branched-chain amino acid (BCAA) levels. Impairment in urea cycle-related amino acid ornithine was also observed. In the CSF, a significant decrease in BCAA/AAA ratio was observed. Additionally, significant correlations between serum and CSF levels of phenylalanine and BCAAs were observed. Finally, by network analyses, we identified in the CSF an orchestrated amino acid abnormalities phenomenon in which virtually all amino acids evaluated were associated. Together these findings recapitulate data available from clinical studies regarding amino acid profile in the acute stage of sepsis. In addition, we showed significant correlations between serum and CSF levels of phenylalanine, leucine and valine. Our findings points CLP model as an important tool, with high translational value, for developing innovative therapies to recover amino acids homeostasis during acute sepsis.

Keywords: sepsis; sepsis-associated encephalopathy; biomarkers; cecal ligation and perforation

Introduction

Sepsis is a multifactorial and heterogeneous dysfunction that affects approximately 30 million people globally (1). Mortality rates in sepsis are higher in low-income countries, mainly due to the challenges of early recognition and treatment (2). The development of sepsis-associated encephalopathy (SAE) is a common feature in acute sepsis, increasing its mortality rates and contributing to long-term dysfunction (3-5). In this sense, targeting the recognition of early features in sepsis represents an important strategy to improve the outcome in septic patients.

Currently, multiple biomarkers have been used for diagnosing sepsis. However, none of them are sufficient sensible in the clinical setting to be used as SAE predictors. Thus, the implementation of better biomarkers of SAE is of high interest, as it would improve differential diagnose and early therapeutic intervention (6). In line with this, early amino acid imbalance was observed in serum of patients presenting with SAE (7-9). Based on that, one could argue that amino acid imbalance could be a potential and feasible biomarker to be used in clinics. Indeed, it is possible to speculate that changes in blood levels of amino acid could alter their transport into the central nervous system (CNS). Since, cerebral spinal fluid (CSF) sampling is an invasive technique, a preclinical study investigating relationships between serum and CSF in SAE experimental models is an interesting strategy.

Numerous hypotheses for the pathogenesis of septic encephalopathy have been discussed. However, models recapitulating sepsis in humans are still lacking. One interesting experimental strategy is to find better models that mimic specific phenomena associated with sepsis in humans. Based on that, here we used a "back-translation" strategy to evaluate whether serum amino acid profile in a rat model of acute cecal ligation and perforation (CLP) recapitulates biomarker findings in humans. CSF was

also obtained to evaluate whether serum data is capable of predict CNS amino acid changes. Moreover, metabolic network analyzes was performed to identify amino acid abnormalities patterns during acute sepsis.

Methods

Animals

Male Wistar rats (90 days old) were obtained from the Department of Biochemistry breeding colony (UFRGS, Porto Alegre, Brazil), maintained under controlled environment (12 h light/12 h dark cycle; 22 ± 1 °C; *ad libitum* access to food and water). All animal experiments were performed in accordance with the National Institute of Health (NIH) Guide for the Care and Use of Laboratory Animals and Brazilian Society for Neuroscience and Behavior recommendations for animal care. The experimental protocols were approved by the Federal University of Rio Grande do Sul Animal Care and Use Committee.

Cecal ligation and perforation (CLP) in Wistar rats

For induction of systemic inflammation, rats were subjected to CLP as previously described (10). Rats were anesthetized with a mixture of ketamine and xylazine, given intraperitoneally. Under aseptic conditions, a 3-cm midline laparotomy was performed to allow exposure of the cecum with the adjoining intestine. The cecum was tightly ligated with a 3.0 nylon suture at its base, below the ileocecal valve, maintaining bowel flow continuity, and was perforated once with a 14-gauge needle. The cecum was then gently squeezed to extrude a small amount of fecal material from the perforation site and then returned to the peritoneal cavity; the laparotomy was closed with 4.0 nylon sutures and the animals returned to their cages. Animals were

resuscitated with normal saline (50 ml/kg subcutaneously) immediately and 12 h after CLP. In the sham-operated group, the rats were submitted to all surgical procedures but the cecum was neither ligated nor perforated. Analyses were performed after 24 h of CLP.

High-performance liquid chromatography (HPLC) procedure

High-performance liquid chromatography (HPLC) procedure was performed as previously described (11). The assay was performed with serum or CSF to quantify twelve amino acids [alanine (Ala), aspartate (Asp), tryptophan (Trp), glutamine (Gln), methionine (Met), glutamate (Glu), isoleucine (Ile), leucine (Leu), lysine (Lys), ornitine (Orn), phenylalanine (Phe), tyrosine (Tyr) and valine (Val)]. Briefly, cells were homogenized in 7 % trifluoroacetic acid (TFA) and centrifuged. The supernatant was collected, neutralized with 1.5 M potassium bicarbonate and filtered (0.22 lm pore). Samples were derivatized with o-phthalaldehyde and separation was carried out with a reverse phase column (Supelcosil LC-18, 250 mm 9 4.6 mm, Supelco) in a Shimadzu Class-VP chromatography system. The mobile phase flowed at a rate of 1.4 mL/min and column temperature was 24 C. Buffer composition was A: 0.04 mol/L sodium dihydrogen phosphate monohydrate buffer, pH 5.5, containing 20 % of methanol; B: 0.01 mol/L sodium dihydrogen phosphate monohydrate buffer, pH 5.5, containing 80 % of methanol. The gradient profile was modified according to the content of buffer B in the mobile phase: 0 % at 0.00 min, 100 % at 55 min, 0 % at 55–60.00 min. Absorbance was read at 360 nm and 455 nm, excitation and emission respectively, with a Shimadzu fluorescence detector. For glutamine determination in the CSF, samples were diluted 10x.

Ammonia and urea measurement

Ammonia levels were determined in serum of 24h-post CLP rats using a commercial kit from Randox (catalog number AM1015, Crumlin, UK). The levels of urea were measured using enzymatic kit from Bioclin (catalog number K056, Belo Horizonte, BR) according to manufacturer´s instructions.

Network analyses

Group-based networks of sham and CLP were assembled for both CSF and serum biomarkers as previously described (12). By computing Pearson´s correlation coefficients, networks were constructed based on 50 bootstrap samples. Then, correlation values whose corresponding probability values were not significant ($P \geq 0.05$) were eliminated. In addition, for each bootstrap sample we computed the graph theoretical measures of density and global efficiency.

Statistical Analyses

Data were expressed as median ± quartile. Comparisons between sham and CLP groups were carried out using Student´s t test. P values less than 0.05 were reported as statistically significant. GraphPad Prism 8 was used for statistical analysis.

Results

Serum amino acid profile in CLP rats

Serum glutamate levels were significantly lower in 24h-post CLP rats compared to sham (from mean of 152.25 to 105.98 μmol/L, t_{17}= 3.070, P=0.004, **Fig. 1a**). No changes in glutamine levels were observed (t_{17}=0.6238, P=0.541, **Fig. 1b**), while serum glutamate/glutamine (Glu/Gln) ratio was decreased in CLP rats (19%, t_{17}=2.384,

P=0.029, **Fig. 1c**). Levels of aromatic amino acids (AAA) phenylalanine (from mean of 51.99 to 66.68 µmol/L, t_{17}=2.423, P=0.027, **Fig. 1d**) and tryptophan (from mean of 63.8 to 83.68 µmol/L, t_{17}=5.270, P<0.0001, **Fig. 1e**) were significantly higher in serum during the acute phase of sepsis. No changes in the levels of the branched-chain amino acids (BCAA) leucine (t_{17}=0.051, P=0.96, **Fig. 1f**), isoleucine (t_{17}=0.308, P=0.761, **Fig. 1g**) and valine (t_{17}=0.314, P=0.757, **Fig. 1h**) were noticed. As a result, we observed a significant decrease in BCAA/AAA ratio (30%, t_{16}=2.734, P=0.015, **Fig. 1i**). We also demonstrated a decrease in the levels of a urea cycle intermediate, ornithine (from mean of 34.14 to 22.23 µmol/L, t_{17}=2.389, P=0.029, **Fig. 1j**). Additionally, higher ammonia (31%, t_{10}=2.641, P=0.025, **Fig 1k)** and lower urea (22%, t_{10}=3.631, P=0.005, **Fig 1l)** levels were shown in the CLP model. On the other hand, an increase in aspartate was shown in CLP rats (from mean of 6.98 to 9.71 µmol/L, t_{17}=2.204, P=0.041, **Fig 1m**). Finally, alanine (t_{17}=0.690, P=0.499, **Fig. 1n**), methionine (t_{17}=0.116, P=0.909, **Fig. 1o**) and lysine (t_{17}=1.075, P=0.297, **Fig. 1p**) did not present any alterations in its levels during the acute phase of sepsis in this model.

CSF amino acid profile in CLP rats

An increase in CSF glutamine levels was demonstrated in 24h-post CLP rats (from mean of 492.7 to 572.3 µmol/L, t_{23}=2.346, P=0.01, **Fig. 2a**). CSF glutamate levels did not change (t_{23}=0.990, P=0.3323, **Fig. 2b**), however, we observed a decrease in Glu/Gln ratio in CLP animals (16%, t_{23}=2.1446, P=0.042, **Fig. 2c**). We also demonstrated a significant increase in the levels of AAA tryptophan (from mean of 1.49 to 2.73 µmol/L, t_{23}=2.884, P=0.008, **Fig. 2d**) and phenylalanine (from mean of 4.33 to 5.52 µmol/L, t_{23}=4.122, P=0.0004, **Fig. 2e**) in the CSF of rats submitted to CLP. Regarding to the BCAA, we showed an increase in isoleucine (from mean of 1.91 to

1.67 μmol/L, t_{23}=2.155, P=0.042, **Fig. 2f**), along with no alteration in either leucine (t_{23}=1.434, P=0.165, **Fig. 2g**) or valine (t_{23}=0.927, P=0.364, **Fig. 2h**) levels. A significantly decrease in BCAA/AAA ratio was also observed in the CSF of CLP rats (37%, t_{23}=3.808, P=0.0009, **Fig. 2i**). Among the amino acids with lower levels in CSF during the acute sepsis, we also observed alanine (from mean of 71.97 to 52.82 μmol/L, t_{23}=6.389, P<0.0001, **Fig. 2j**), ornithine (from mean of 2.17 to 1.21 μmol/L, t_{23}=9.872, P<0.0001, **Fig. 2k**), lysine (from mean of 68.46 to 59.25 μmol/L, t_{23}=3.930, P=0.0007, **Fig. 2l**) and the sulfur containing amino acid methionine (from mean of 4.09 to 2.82 μmol/L, t_{23}=3.346, P=0.003, **Fig. 2m**). Finally, CLP did not promote any changes in CSF aspartate levels (t_{23}=0.336, P=0.740, **Fig. 2n**).

Associations between CSF and serum amino acid levels

Correlation analysis between CSF and serum amino acids is depicted in **Table 1**. Cross-correlation matrices evaluating patterns of association among amino acid abnormalities in CSF and serum were depicted in **Fig. 3a-d**. Thresholded binary matrices (P<0.05) were used to identify significant associations (**Fig. 3e-h**). Network representation is showed in **Fig. 3i-l**. Graph measures analyses - indexed by density and global efficiency - were conducted to evaluate differences among amino acids networks. CLP serum network shows increased density (t_{98}=2.255, P=0.0263, **Fig. 3m**) but no changes in global efficiency if compared to sham serum network (t_{98}=1.679, P=0.0963, **Fig. 3n**). CLP CSF network demonstrates increased density (t_{98}= 6.708, P <0.0001, **Fig. 3o**) and global efficiency (t_{98}= 6.155, P<0.0001, **Fig. 3p**).

Discussion

In the present report we demonstrated the amino acid profile in serum and CSF of rats 24h-post CLP induction. We identified a decrease in serum Glu/Gln and BCAA/AAA ratios and an impairment in the urea cycle related markers. We also demonstrated that BCAAs and phenylalanine in serum are strongly correlated with its levels in the CSF. Moreover, the evaluation of CSF from CLP animals evidenced an increase in the neurotransmitter precursors phenylalanine and tryptophan, which might be in part responsible for the damage observed in neural cells during the SAE. Interestingly, amino acids serum abnormalities found here consistently recapitulate findings in human acute sepsis.

It has been previously demonstrated that lower serum glutamate levels and decreased Glu/Gln ratio might be applied as early predictors of mortality in sepsis patients (13). Consistently, we observed a reduction in both parameters in the CLP model. During sepsis, an impairment of the ability to use glucose requires other substrates for energy production. In this sense, Kantrow and colleagues have demonstrated that glutamate is an important energy substrate under this condition (14). It is believed that glutamate is used for *de novo* synthesis of glutamine and alanine (15). In this study, serum levels of glutamine and alanine did not change at the time point evaluated. However, we cannot rule out that the utilization of these amino acids would exceed the endogenous production during the progression of sepsis (16). Alterations in glutamate levels in the CNS are also important in the pathogenesis of SAE, as the development of glutamatergic excitotoxicity is believed to play a role in neuronal damage (17). Interestingly, at 24h-post CLP we did not observe changes in CSF glutamate levels. Thus, it raises the exciting possibility to apply Glu/Gln ratio as an early biomarker of SAE.

AAA serum levels seem to have an important role as predictors, and possibly players, of brain impairment during acute sepsis. On the other hand, the fluctuations in BCAA levels are not a consensus in this pathology (7-9). In this sense, Basler *et al*. suggested a decrease in BCAA/AAA ratio as an early biomarker in SAE patients. Corroborating, a decrease in serum BCAA/AAA ratio 24h-post CLP was showed in our study. AAA are precursors for the synthesis of important neurotransmitters in the CNS. An increased influx of tryptophan into the brain contributes to accelerate the synthesis of serotonin, while phenylalanine is able to promote the synthesis of cerebral catecholamines and false neurotransmitters, contributing to the damage observed during SAE (18). Additionally, AAA and BCAA compete for the same transport system to cross the blood-brain barrier. Accordingly, in our model we observed a prominent decrease in BCAA/AAA ratio in the CSF, mainly driven by an increase in tryptophan and phenylalanine and lower levels of isoleucine. Moreover, we demonstrated a strong correlation between serum and CSF levels of phenylalanine, leucine, isoleucine and valine.

Plasma accumulation of ammonia is an important factor observed in sepsis patients (19). In fact, the development of hyperammonemia seems to be a major issue in the development of SAE. Furthermore, it was demonstrated that higher levels of serum ammonia are correlated with increased mortality in non-survivor sepsis patients with altered sensorium (8). Recently, Numan *et al* has suggested the use of serum ammonia as a novel marker for sepsis (20). In our study, beyond an increase in serum ammonia, we observed a global deficiency in the urea cycle, indexed by a decrease in urea production and ornithine levels. In addition, Keiding *et al*. previously demonstrated that ammonia metabolic flux from blood to CNS results in glutamine synthesis (21). Corroborating, our results from 24h-post CLP rats evidenced a decrease

in ornithine and an increase in glutamine levels in the CSF. Interestingly, the cross-correlation matrices demonstrated increased association between amino acids during sepsis. However, it evidenced glutamine as the single amino acid presenting a hypoassociative profile in the CSF of CLP animals. In this sense, the measurement of urea cycle might be considered for further investigation targeting biomarkers of SAE.

Matrix of correlation coefficient values in serum, identified two clusters in this study. One containing glutamate and leucine as main nodes and the other alanine and methionine. In the CSF, a more organized architectural phenomenon has been identified: a cluster containing 9 amino acids with methionine being the main node. These changes highlight an orchestrated and homogenous phenomenon in CNS but more diluted in serum. Interestingly, methionine was found as the main node in clusters in both serum and CSF. Indeed, it was already demonstrated that methionine metabolites are abnormal in sepsis patients (22) and in animal models (23). This importance of methionine imbalance during acute sepsis is still discussed. While Sprung *et al*. observed that sepsis non-survivors presented higher levels of sulfur-containing amino acids, Su *et al*. correlated higher severity and poor prognosis in septic patients with decreased levels of those amino acids (8, 24). Therefore, further studies are required to understand whether deregulations of methionine metabolism have pathophysiological consequences.

Together, our results demonstrated that CLP animal model recapitulates clinical aspects of amino acids abnormalities during the early stage of SAE. Moreover, we showed associations between peripheral and central amino acids changes. Our finding shed light on the use of CLP model as an important tool, with high translational value, for developing innovative therapies to recover amino acids homeostasis during acute sepsis.

Conflict of interest

The authors declare there are no conflicts of interest.

Funding sources

ERZ receives financial support from CAPES [88881.141186/2017-01], CNPq [460172/2014-0], PRONEX, FAPERGS/CNPq [16/2551-0000475-7], Brazilian National Institute of Science and Technology in Excitotoxicity and Neuroprotection [465671/2014-4],FAPERGS/MS/CNPq/SESRS– PPSUS [30786.434.24734.23112017].

References

C. Fleischmann, A. Scherag, N. K. Adhikari, C. S. Hartog, T. Tsaganos, P. Schlattmann, D. C. Angus and K. Reinhart: Assessment of Global Incidence and Mortality of Hospital-treated Sepsis. Current Estimates and Limitations. *Am J Respir Crit Care Med* 193(3):259-72, 2016.

A. Kwizera, M. Dunser and J. Nakibuuka: National intensive care unit bed capacity and ICU patient characteristics in a low income country. *BMC Res Notes* 5:475, 2012.

T. J. Iwashyna, E. W. Ely, D. M. Smith and K. M. Langa: Long-term cognitive impairment and functional disability among survivors of severe sepsis. *Jama* 304(16):1787-94, 2010.

N. Chaudhry and A. K. Duggal: Sepsis Associated Encephalopathy. *Adv Med* 2014:762320, 2014.

J. C. d'Avila, L. D. Siqueira, A. Mazeraud, E. P. Azevedo, D. Foguel, H. C. Castro-Faria-Neto, T. Sharshar, F. Chretien and F. A. Bozza: Age-related cognitive impairment is associated with long-term neuroinflammation and oxidative stress in a mouse model of episodic systemic inflammation. *J Neuroinflammation* 15(1):28, 2018.

E. P. Rivers, V. Coba and M. Whitmill: Early goal-directed therapy in severe sepsis and septic shock: a contemporary review of the literature. *Curr Opin Anaesthesiol* 21(2):128-40, 2008.

T. Basler, A. Meier-Hellmann, D. Bredle and K. Reinhart: Amino acid imbalance early in septic encephalopathy. *Intensive Care Med* 28(3):293-8, 2002.

C. L. Sprung, F. B. Cerra, H. R. Freund, R. M. Schein, F. N. Konstantinides, E. H. Marcial and M. Pena: Amino acid alterations and encephalopathy in the sepsis syndrome. *Crit Care Med* 19(6):753-7, 1991.

B. A. Mizock, H. C. Sabelli, A. Dubin, J. I. Javaid, A. Poulos and E. C. Rackow: Septic encephalopathy. Evidence for altered phenylalanine metabolism and comparison with hepatic encephalopathy. *Arch Intern Med* 150(2):443-9, 1990.

B. Bellaver, J. P. Dos Santos, D. T. Leffa, L. D. Bobermin, P. H. A. Roppa, I. L. da Silva Torres, C. A. Goncalves, D. O. Souza and A. Quincozes-Santos: Systemic Inflammation as a Driver of Brain Injury: the Astrocyte as an Emerging Player. *Mol Neurobiol*, 2017.

D. G. Souza, B. Bellaver, G. Hansel, B. A. Arus, G. Bellaver, A. Longoni, J. Kolling, A. T. Wyse, D. O. Souza and A. Quincozes-Santos: Characterization of Amino Acid Profile and Enzymatic Activity in Adult Rat Astrocyte Cultures. *Neurochem Res* 41(7):1578-86, 2016.
M. A. Stefani, R. Modkovski, G. Hansel, E. R. Zimmer, A. Kopczynski, A. P. Muller, N. R. Strogulski, M. S. Rodolphi, R. K. Carteri, A. P. Schmidt, J. P. Oses, D. H. Smith and L. V. Portela: Elevated glutamate and lactate predict brain death after severe head trauma. *Ann Clin Transl Neurol* 4(6):392-402, 2017.
M. Poeze, Y. C. Luiking, P. Breedveld, S. Manders and N. E. Deutz: Decreased plasma glutamate in early phases of septic shock with acute liver dysfunction is an independent predictor of survival. *Clin Nutr* 27(4):523-30, 2008.
S. P. Kantrow, D. E. Taylor, M. S. Carraway and C. A. Piantadosi: Oxidative metabolism in rat hepatocytes and mitochondria during sepsis. *Arch Biochem Biophys* 345(2):278-88, 1997.
M. J. Bruins, N. E. Deutz and P. B. Soeters: Aspects of organ protein, amino acid and glucose metabolism in a porcine model of hypermetabolic sepsis. *Clin Sci (Lond)* 104(2):127-41, 2003.
A. M. Karinch, M. Pan, C. M. Lin, R. Strange and W. W. Souba: Glutamine metabolism in sepsis and infection. *J Nutr* 131(9 Suppl):2535S-8S; discussion 2550S-1S, 2001.
M. Michels, A. V. Steckert, J. Quevedo, T. Barichello and F. Dal-Pizzol: Mechanisms of long-term cognitive dysfunction of sepsis: from blood-borne leukocytes to glial cells. *Intensive Care Med Exp* 3(1):30, 2015.
J. D. Fernstrom and M. H. Fernstrom: Tyrosine, phenylalanine, and catecholamine synthesis and function in the brain. *J Nutr* 137(6 Suppl 1):1539S-1547S; discussion 1548S, 2007.
M. C. Machado and F. Pinheiro da Silva: Hyperammonemia due to urea cycle disorders: a potentially fatal condition in the intensive care setting. *J Intensive Care* 2(1):22, 2014.
Y. Numan, Y. Jawaid, H. Hirzallah, D. Kusmic, M. Megri, O. Aqtash and A. Amro: Ammonia vs. Lactic Acid in Predicting Positivity of Microbial Culture in Sepsis: The ALPS Pilot Study. 7(8), 2018.
S. Keiding, M. Sorensen, D. Bender, O. L. Munk, P. Ott and H. Vilstrup: Brain metabolism of 13N-ammonia during acute hepatic encephalopathy in cirrhosis measured by positron emission tomography. *Hepatology* 43(1):42-50, 2006.
O. Wexler, M. S. Gough, M. A. M. Morgan, C. M. Mack, M. J. Apostolakos, K. P. Doolin, R. A. Mooney, E. Arning, T. Bottiglieri and A. P. Pietropaoli: Methionine Metabolites in Patients With Sepsis. *J Intensive Care Med* 33(1):37-47, 2018.
A. Semmler, Y. Smulders, E. Struys, D. Smith, S. Moskau, H. Blom and M. Linnebank: Methionine metabolism in an animal model of sepsis. *Clin Chem Lab Med* 46(10):1398-402, 2008.
L. Su, H. Li, A. Xie, D. Liu, W. Rao, L. Lan, X. Li, F. Li, K. Xiao, H. Wang, P. Yan, X. Li and L. Xie: Dynamic changes in amino acid concentration profiles in patients with sepsis. *PLoS One* 10(4):e0121933, 2015.

Legends

Figure 1. Serum amino acid profile of 24h-post CLP rats. Levels of (a) Glu, (b) Gln, (c) Glu/Gln, (d) Phe, (e) Trp, (f) Leu, (g) Ileu, (h) Val, (i) BCAA/AAA, (j) Orn, (k) Ammonia, (l) Urea, (m) Asp, (n) Ala, (o) Met and (p) Lys were evaluated. *n*=8-11 per group. *P < 0.05, **P < 0.01 and ****P < 0.0001 (t test). Data are presented as median values ± quartiles and individual scatter plots of two independent experimental determinations.

Figure 2. CSF amino acid profile of 24h-post CLP rats. Levels of (a) Gln, (b) Glu, (c) Glu/Gln, (d) Phe, (e) Trp, (f) Ileu, (g) Leu, (h) Val, (i) BCAA/AAA, (j) Ala, (k) Orn, (l) Lys, (m) Met and (n) Asp were evaluated. *n* = 8-11 per group. *P < 0.05, **P < 0.01 and **P < 0.0001 (t test). Data are presented as median values ± quartiles. and individual scatter plots of two independent experimental determinations.

Figure 3. Association between amino acids indexed by cross-correlation analyses. Symmetric matrix of correlation coefficient values between biomarkers in: (a) serum of sham rats, (b) serum of CLP rats, (c) CSF of sham rats and (d) CSF of CLP rats. Binary matrices of (e) serum of sham rats, (f) serum of CLP rats, (g) CSF of sham rats and (h) CSF of CLP rats. Representative networks of (i) serum of sham rats, (j) serum of CLP rats, (k) CSF of sham rats and (l) CSF of CLP rats. (m) Density and (n) average clustering analyses of sham/CLP serum rats network. (o) Density and (p) average clustering analyses of sham/CLP CSF rats network. *n* = 5 per group. *P < 0.05, ****P < 0.0001.

Table 1. Correlation between amino acid levels in serum and CSF. Results with a p-value less than 0.05 were considered as statistically significant.

Amino acid	Pearson´s r	P value
Glu	0.0513	0.8879
Gln	0.1542	0.6705
Phe	0.7118	0.0209*
Trp	0.3585	0.3091
Leu	0.6630	0.0367*
Ileu	0.6154	0.0582
Val	0.6451	0.0440*
Orn	0.4811	0.1592
Asp	-0.1444	0.6906
Ala	0.5197	0.1236
Met	0.3966	0.2564
Lys	0.5880	0.0738

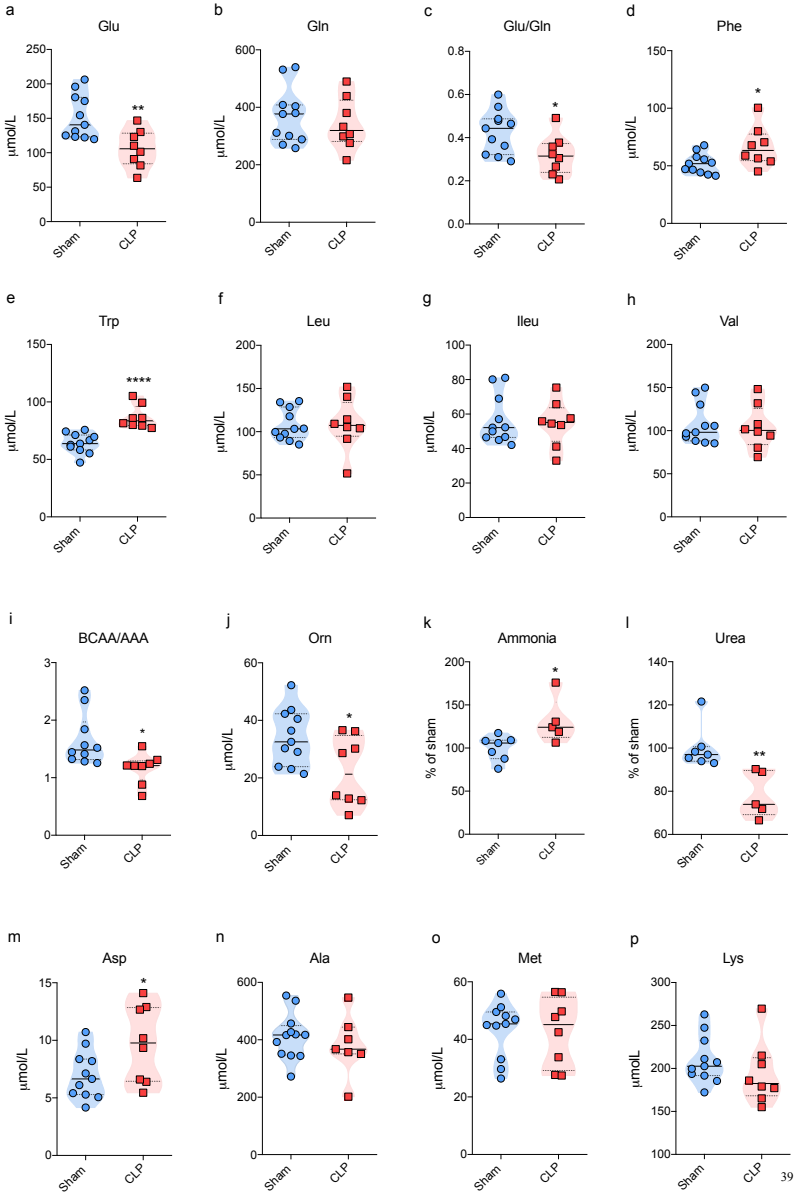
a
Glu
µmol/L
250
200
150
100
50
0
**
Sham
CLP
b
Gln
µmol/L
600
400
200
0
Sham
CLP
c
Glu/Gln
0.8
0.6
0.4
0.2
0.0
*
Sham
CLP
d
Phe
µmol/L
150
100
50
0
*
Sham
CLP
e
Trp
µmol/L
150
100
50
0
****
Sham
CLP
f
Leu
µmol/L
200
150
100
50
0
Sham
CLP
g
Ileu
µmol/L
100
80
60
40
20
0
Sham
CLP
h
Val
µmol/L
200
150
100
50
0
Sham
CLP
i
BCAA/AAA
3
2
1
0
*
Sham
CLP
j
Orn
µmol/L
60
40
20
0
*
Sham
CLP
k
Ammonia
% of sham
200
150
100
50
0
*
Sham
CLP
l
Urea
% of sham
140
120
100
80
60
**
Sham
CLP
m
Asp
µmol/L
15
10
5
0
*
Sham
CLP
n
Ala
µmol/L
600
400
200
0
Sham
CLP
o
Met
µmol/L
60
40
20
Sham
CLP
p
Lys
µmol/L
300
250
200
150
100
Sham
CLP

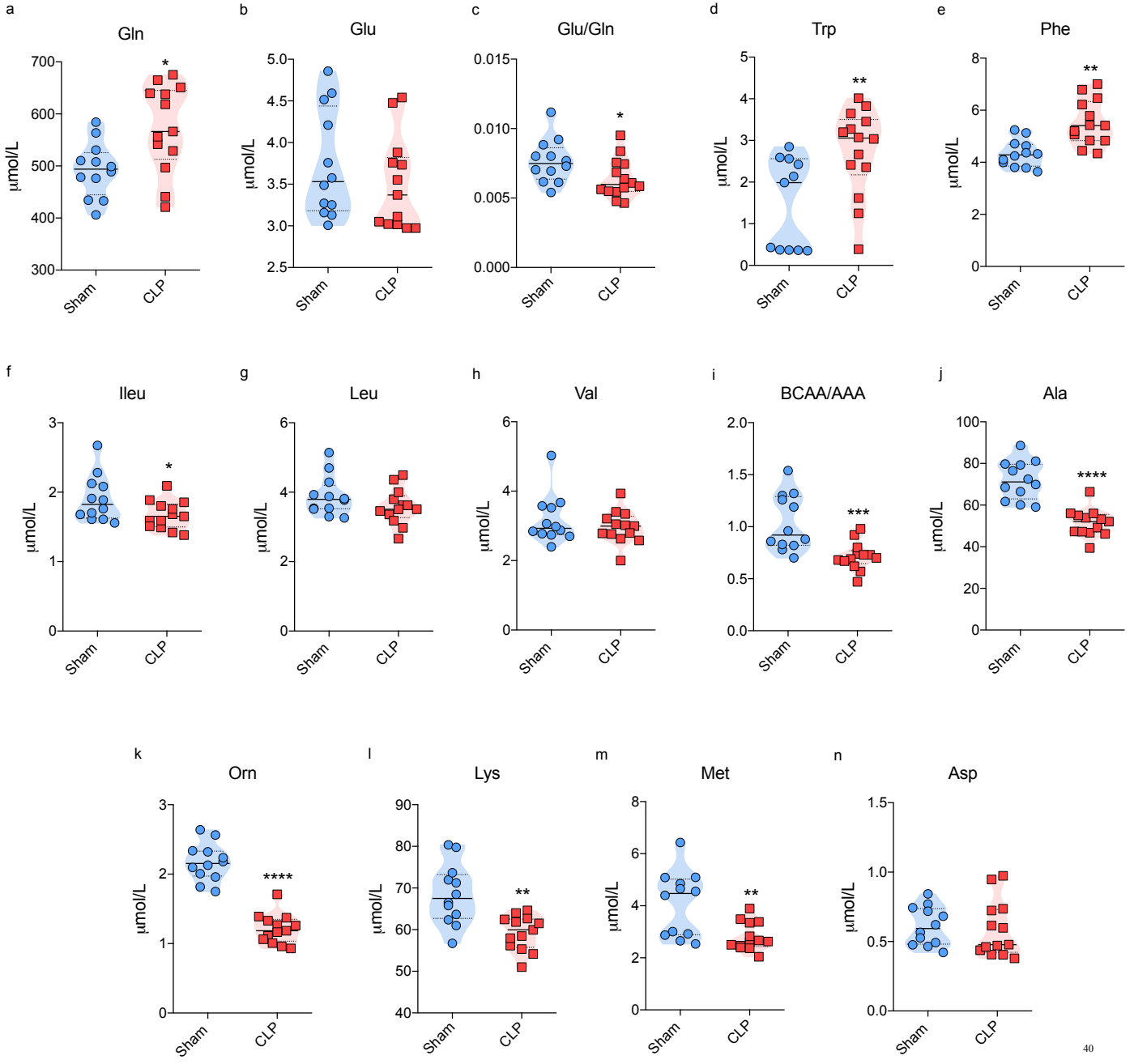
a
Gln
µmol/L
700
600
500
400
300
*
Sham
CLP
b
Glu
µmol/L
5.0
4.5
4.0
3.5
3.0
2.5
Sham
CLP
c
Glu/Gln
0.015
0.010
0.005
0.000
*
Sham
CLP
d
Trp
µmol/L
5
4
3
2
1
0
**
Sham
CLP
e
Phe
µmol/L
8
6
4
2
0
**
Sham
CLP
f
Ileu
µmol/L
3
2
1
0
*
Sham
CLP
g
Leu
µmol/L
6
4
2
0
Sham
CLP
h
Val
µmol/L
6
4
2
0
Sham
CLP
i
BCAA/AAA
2.0
1.5
1.0
0.5
0.0
***
Sham
CLP
j
Ala
µmol/L
100
80
60
40
20
0
****
Sham
CLP
k
Orn
µmol/L
3
2
1
0
****
Sham
CLP
l
Lys
µmol/L
90
80
70
60
50
40
**
Sham
CLP
m
Met
µmol/L
8
6
4
2
0
**
Sham
CLP
n
Asp
µmol/L
1.5
1.0
0.5
0.0
Sham
CLP

Serum

CSF

a)

Sham

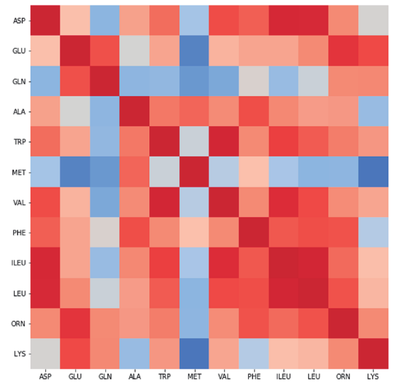

b)

CLP

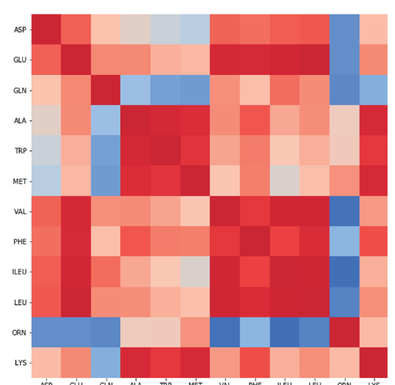

c)

Sham

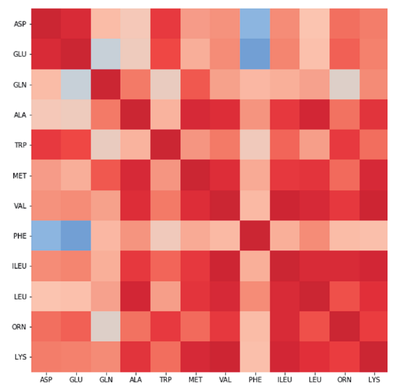

d)

CLP

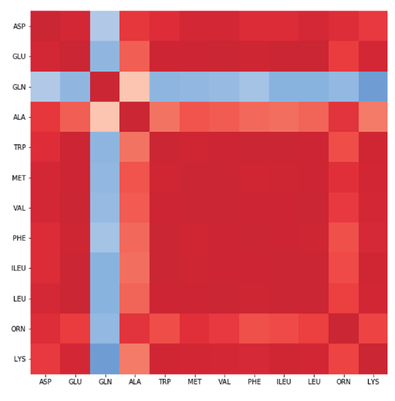

e)

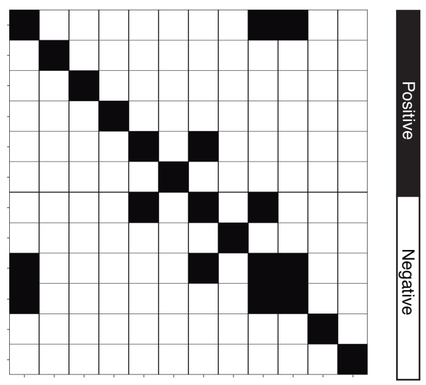

f)

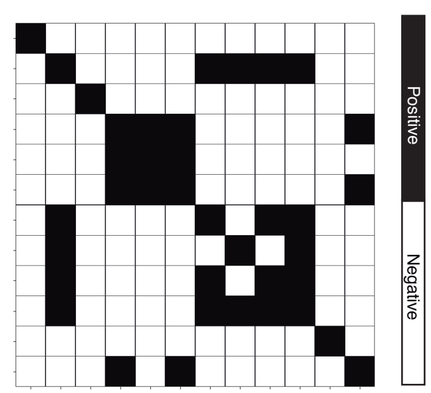

g)

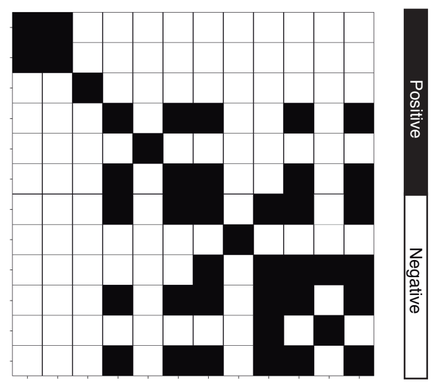

h)

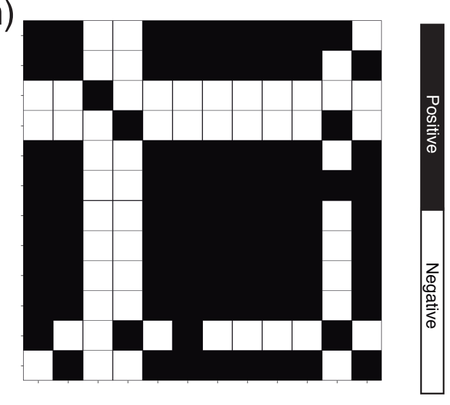

i)

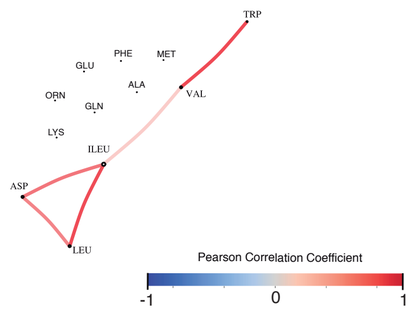

j)

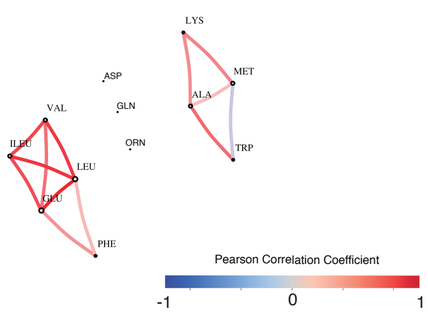

k)

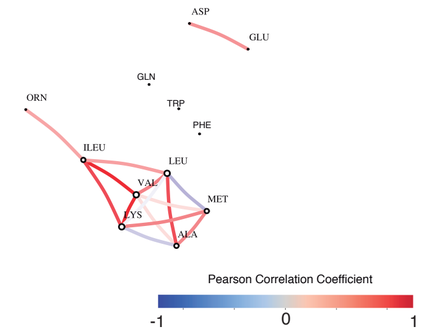

l)

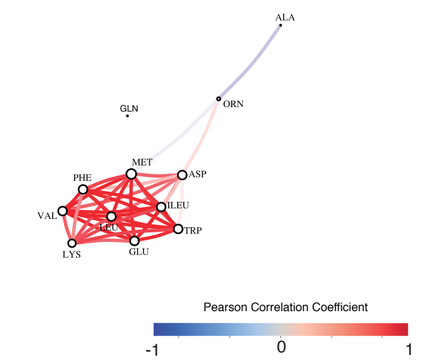

m)

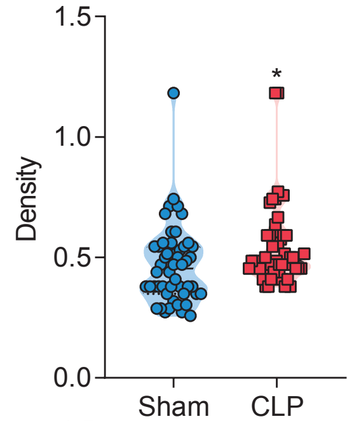

n)

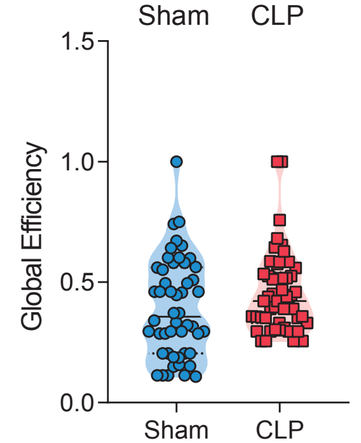

o)

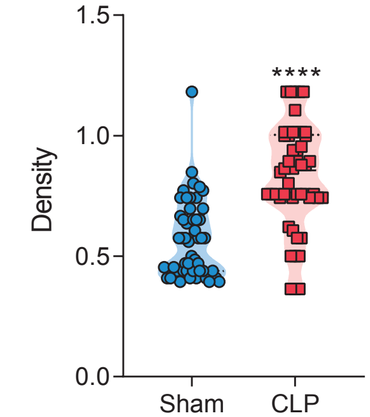

p)

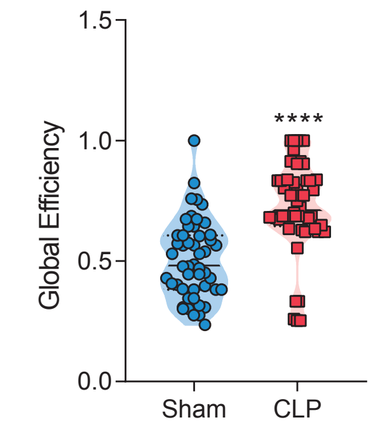

Capítulo 2

Systemic Inflammation as a Driver of Brain Injury: the Astrocyte as an Emerging Player.

No Capítulo 2 apresentamos o artigo publicado no periódico *Molecular Neurobiology*.

No Capítulo anterior demonstramos que o modelo de LCP recapitula anormalidades encontradas em pacientes acometidos por EAS, reiterando a sua utilização como modelo animal para essa patologia. Já neste estudo visamos entender como essas alterações sistêmicas promovidas pelas sepse afetam o SNC, em especial a funcionalidade astrocitária. Além disso, esse Capítulo teve como objetivo elucidar se astrócitos cultivados a partir do cérebro de animais sépticos mantinham o seu fenótipo mesmo após um longo período de cultivo. Com isso, nós observamos que os astrócitos cultivados de animais LCP apresentam um fenótipo pró-inflamatório e que difere, em alguns aspectos, da análise realizada em tecido total.

Systemic inflammation as a driver of brain injury: The astrocyte as an emerging player

Bruna Bellaver[1*], João Paulo dos Santos[1], Douglas Teixeira Leffa[2], Larissa Daniele Bobermin[1], Paola Haack Amaral Roppa[1], Iraci Lucena da Silva Torres[2], Carlos-Alberto Gonçalves[1], Diogo Onofre Souza[1], André Quincozes-Santos[1*]

[1]Departamento de Bioquímica, Programa de Pós-Graduação em Ciências Biológicas: Bioquímica, Instituto de Ciências Básicas da Saúde, Universidade Federal do Rio Grande do Sul, Porto Alegre, RS, Brazil
[2]Programa de Pós-Graduação em Medicina: Ciências Médicas, Faculdade de Medicina, Universidade Federal do Rio Grande do Sul, Porto Alegre, RS, Brazil; Unidade de Experimentação Animal, Hospital de Clínicas de Porto Alegre, Porto Alegre, RS, Brazil.

*Bruna Bellaver, Ph.D. student; *André Quincozes-Santos, Ph.D.
Departamento de Bioquímica
Programa de Pós-Graduação em Ciências Biológicas: Bioquímica
Instituto de Ciências Básicas da Saúde
Universidade Federal do Rio Grande do Sul
Rua Ramiro Barcelos, 2600 – Anexo
Bairro Santa Cecília
90035–003 Porto Alegre, RS, Brazil
Fax: +55 51 3308 5535; Phone: +55 51 3308 5559
Email: brunabellaver90@gmail.com; andrequincozes@ufrgs.br

Abstract

Severe systemic inflammation has strong effects on brain functions, promoting permanent neurocognitive dysfunction and high mortality rates. Additionally, hippocampal damage seems to be directly involved in this process and astrocytes play an important role neuroinflammation and the neuroimmune response. However, the contribution of the astrocytes to the pathology of acute brain dysfunction is not well understood. Recently, our group established a protocol for obtaining astrocyte cultures from mature brain to allow the characterization of these cells and their functions under pathologic conditions. The present study was designed to characterize astrocyte function after acute systemic inflammation induced by cecal ligation and perforation (CLP). Hippocampal astrocyte cultures from CLP animals presented increased levels of tumor necrosis factor-α (TNF-α), interleukin (IL)-1β, IL-6, IL-18 and cyclooxygenase-2 and decreased levels of IL-10. This proinflammatory profile was accompanied by an increase in Toll-like receptor (TLR) 2 mRNA expression levels, and no change in either TLR4 or in vascular endothelial growth factor (VEGF) gene expression. These alterations were associated with increased expressions of p21, nuclear factor kappa B (NFκB) and inducible nitric oxide synthase (iNOS) in astrocytes from CLP animals. The same parameters were also evaluated in whole hippocampal tissue, but differences in this profile were found compared to hippocampal astrocyte cultures from CLP, reflecting an interaction between other central nervous system cell types, which may mask specific astrocytic changes. These results improve our understanding of the mechanisms by which astrocytes react against systemic inflammation, and suggest these cells to be potential targets for therapeutic modulation.

Keywords: astrocytes; systemic inflammation; Toll-like receptors; NFκB.

Introduction

Systemic inflammation, as a result of infection by pathogenic microorganisms or aseptic surgical trauma, can activate the innate immune system, launching a cascade of physiological events and rapidly affecting the central nervous system (CNS) [1,2]. The peripheral immune system has a strong effect on brain functions, as exemplified by the development of sepsis-associated encephalopathy (SAE), a common feature in acute sepsis that increases its morbidity and mortality rate [3]. The increased incidence of sepsis/SAE over the years is thought to be a consequence of advancing age (which accounts for 60 to 85% of all episodes of sepsis), immunosuppression and multidrug-resistant infections [4,5]. The interaction between sepsis and brain homeostasis is an opportunity to elucidate the impact of systemic inflammation on neuroimmune functions.

The pathophysiology of acute brain dysfunction provoked by systemic inflammation remains poorly understood. It has been proposed to be a result of multifactorial events, strongly associated with hippocampal injury, disruption of the blood-brain barrier (BBB), changes in neurotransmitter systems and in redox homeostasis, and increased synthesis and release of proinflammatory mediators, such as tumor necrosis factor alpha (TNF-α) and members of the interleukin (IL) -1 family [6-8]. In addition, Toll-like receptors (TLRs) are closely related to the progression of systemic inflammation, as TLR2 and TLR4 are considered to be the major signal sensors that recognize products implicated in the pathogenesis of polymicrobial sepsis [9].

Astrocytes are important players of neuroinflammation and the neuroimmune response, as these cells express TLRs, which in turn can modulate the activation of nuclear factor kappa B (NFκB). This master regulator of the inflammatory response is able to trigger the release of inflammatory mediators and also promotes the expression of inducible nitric oxide synthase (iNOS) enzyme, increasing nitric oxide (NO) production [10]. Astrocytes also express the cyclin-dependent kinase inhibitor p21, a known cell cycle regulator that emerges as a central regulator of innate and adaptive immunity since it is important for NFκB activation [11,12]. The p21 protein, in turn, appears to participate in the peripheral inflammatory response, but its function in brain cells remains poorly understood [13,14]. Furthermore, astrocytes are suggested to control CNS infiltration, via production of vascular endothelial growth factor (VEGF)

[15] and also regulate the activity of microglia, oligodendrocytes and cells of the adaptive immune system [16].

Although astrocytes actively participate in the inflammatory response, their role in the pathology of acute brain injury has been underexplored. Therefore, characterization of the mechanisms regulating astrocyte activation during this condition identify potential molecular target for therapeutic approaches. To further elucidate changes in astrocyte functionality under different pathologic conditions, our group recently developed a routine protocol for the preparation of astrocyte cultures obtained from mature brain [17-19]. This methodology allows an *in vivo* intervention prior to obtaining the astrocyte primary cultures, representing a more reliable manner for elucidating the specific role of astrocytes in diseases that affect the adult brain.

Considering the detrimental impact of severe systemic inflammation on the CNS, which might lead to SAE, and the pivotal and underexplored functions of astrocytes in the management of associated events, the aim of the present study was to characterize the mechanisms involved in astrocyte cell function after acute systemic inflammation. We hypothesized that inflammatory mediators are over expressed in astrocyte cultures obtained from animals submitted to severe systemic inflammation, and that alterations in molecular expression levels of TLRs, NFκB, iNOS and p21 may be involved in the astrocytic response to acute sepsis.

Material and Methods

Chemicals

DNase was obtained from Sigma-Aldrich (St. Louis, MO, USA). ELISA kits for MCP-1, IL-1β, IL-6, IL-18 and IL-10, TRIzol Reagent, SYBR green PCR master mix, Dulbecco's Modified Eagle's Medium/F12 (DMEM/F12) and other materials for cell cultures were purchased from Gibco/Invitrogen/Thermo (Carlsbad, CA, USA). The ELISA kit for TNF-α was purchased from PeproTech (Rocky Hill, NJ, USA). All other chemicals were purchased from common commercial suppliers.

Animals

Male Wistar rats (90 days old, sham n=16 and CLP n=27) were obtained from our breeding colony (Department of Biochemistry, UFRGS, Porto Alegre, Brazil), and maintained under a controlled environment (12-h light/12-h dark cycle; 22 ± 1 °C; *ad libitum* access to food and water). All animal experiments were performed in accordance with the National Institute of Health (NIH) Guide for the Care and Use of Laboratory Animals and the Brazilian Society for Neuroscience and Behavior´s recommendations for animal care. The experimental protocols were approved by the Federal University of Rio Grande do Sul Animal Care and Use Committee (process number 29180).

Cecal ligation and perforation (CLP) in Wistar rats

For induction of systemic inflammation, male Wistar rats (90-days old) were subjected to CLP as previously described [20]. Rats were anesthetized with a mixture of ketamine and xylazine, given intraperitoneally. Under aseptic conditions, a 3-cm midline laparotomy was performed to allow exposure of the cecum with the adjoining intestine. The cecum was tightly ligated with a 3.0 nylon suture at its base, below the ileocecal valve, maintaining bowel flow continuity, and was perforated once with a 14-gauge needle. The cecum was then gently squeezed to extrude a small amount of fecal material from the perforation site and then returned to the peritoneal cavity; the laparotomy was closed with 4.0 nylon sutures and the animal was returned to its cage. Animals were resuscitated with normal saline (50 ml/kg subcutaneously) immediately and 12 h after CLP. In the sham-operated group, the rats were submitted to all surgical procedures but the cecum was neither ligated nor perforated. The astrocyte primary cultures or the whole hippocampal tissue analyses were performed after 24 h of CLP. Note that 60% of the CLP rats and 100% of the sham rats survived this procedure in our laboratory.

Hippocampal primary astrocyte cultures from sham/CLP Wistar rats

Cerebral hippocampi were aseptically dissected from animals of both groups (sham and CLP) and meninges were removed. The astrocyte cultures were performed as previously described [17]. During the dissection, cerebral tissue was maintained in HBSS (Hank's Balanced Salt Solution) containing 0.05% trypsin and 0.003% DNase

and was kept at 37 ºC for 8 min. The tissue was then mechanically dissociated for 7 min using a Pasteur pipette and centrifuged at 100 g for 5 min. The pellet was resuspended in a solution of HBSS containing only 0.003% DNase and gently mechanically dissociated again for 5 min with a Pasteur pipette and left for decantation for 20 min. The supernatant was collected and centrifuged for 7 min (400 g). The cells from supernatant were resuspended in DMEM/F12 [10% fetal bovine serum (FBS), 15 mM HEPES, 14.3 mM $NaHCO_3$ and 0.04% gentamicin], plated in 6- or 24-well plates pre-coated with poly-L-lysine and cultured at 37 ºC in an incubator with 5% CO_2. The cells were seeded at 3–5x10^5 cells/cm^2. The first medium exchange occurred 24 h after obtaining the culture. During the 1st week, the medium change occurred once every two days and from the 2nd week on, the medium change occurred once every four days. From the 3rd week on, hippocampal astrocytes received the culture medium supplemented with 20% FBS. The cells reached confluence at around the 4th week and were used for experiments. The purity of the primary astrocyte cultures was assessed by immunocytochemistry for glial fibrillary acidic protein (GFAP). OX-42 (CD11b/c) and NeuN were used as microglial and neuronal markers, respectively. Under these conditions, cell cultures were confirmed as more than 98% positive for GFAP, indicating an astrocytic phenotype. Furthermore, approximately 2% of the astrocyte cell cultures stained positive for OX-42.

RNA extraction and quantitative RT-PCR

Total RNA was isolated from whole hippocampal tissue and primary astrocyte cultures using TRIzol Reagent (Invitrogen, Carlsbad, CA). The concentration and purity of the RNA were determined spectrophotometrically at a ratio of 260/280. One μg of total RNA was then reverse transcribed using the Applied Biosystems™ High-Capacity cDNA Reverse Transcription Kit (Applied Biosystems, Foster City, CA) in a 20 μL reaction, according to the manufacturer's instructions. The mRNAs encoding TLR2 and TLR4 were quantified using the TaqMan real-time RT-PCR system using inventory primers and probes purchased from Applied Biosystems (Foster City). mRNA quantification for the genes encoding TNF-α, IL-1β, cyclooxygenase-2 (COX-2), p65 NFκB, iNOS, p21, VEGF and β-actin (Table 1) was performed using pairs and Power SYBR Green PCR Master Mix (Invitrogen). Quantitative RT-PCR was performed in duplicate using the Applied Biosystems 7500 Fast system. No-template and no-reverse

transcriptase controls were included in each assay, and these produced no detectable signals during the 40 cycles of amplification. Target mRNA levels were normalized using β-actin as a housekeeper gene. The results are expressed relative to the levels in astrocyte cultures or whole hippocampus from sham animals using the $2^{-\Delta\Delta Ct}$ method [21].

Inflammatory response measurement

TNF-α levels were measured in extracellular medium (for cell culture analysis) or in hippocampal homogenates (for whole tissue analysis) using a rat TNF-α ELISA kit from PeproTech (catalog number 900-K54). The levels of interleukins were measured using ELISA kits for IL-1β (catalog number ER1L1B), IL-6 (catalog number KRC0062), IL-10 (catalog number ERIL10) and IL-18 (catalog number KRC2341) from ThermoFischer and monocyte chemoattractant protein-1 (MCP-1) levels were determined using an ELISA kit from Invitrogen (catalog number KHC1011). Results are expressed in pg/ml for extracellular medium or pg/mg protein for brain tissue.

Protein assay

Protein content was measured using bicinchoninic acid method with bovine serum albumin as a standard [22].

Statistical analyses

Data are expressed as mean ± standard error of the mean (S.E.M). Comparisons between sham and CLP groups were carried out using Student´s *t* test. All data were normally distributed. *P* values of less than 0.05 were reported as statistically significant. SPSS 19.0 for Windows was used for statistical analysis.

Results

Proinflammatory mediators are increased in astrocyte cultures after severe systemic inflammation

We first analyzed the acute impact of CLP induction on astrocytic expression and the release of major proinflammatory cytokines that trigger the immune response. Fig. 1 shows that severe systemic inflammation promoted an increase in TNF-α and IL-1β mRNA expression levels (80%, P =0.0009, $t_{(10)}$=3.190 and 115%, P =0.012, $t_{(10)}$=3.020, respectively, Fig. 1A,B) and secretion (from 75 to 171 pg/ml, P =0.0006, $t_{(14)}$=4.398 and from 73 to 140 pg/ml, p=0.001, $t_{(14)}$=3.973, respectively, Fig. 1C,D) in astrocyte cultures. In order to better elucidate the inflammatory response, we also evaluated the release of other inflammatory mediators from astrocytes after acute sepsis induction. We observed an augmentation in the secretion of IL-6 (from 51 to 100 pg/ml, P =0.0012, $t_{(14)}$=4.058, Fig. 2A), IL-18 (from 34 to 74 pg/ml, P =0.0002, $t_{(14)}$=5.000, Fig. 2B) and MCP-1 (from 36 to 73 pg/ml, P =0.0005, $t_{(14)}$=4.466, Fig. 2C). We also noticed an increase in the mRNA expression levels of COX-2 (61%, P =0.01, $t_{(10)}$=3.171, Fig. 2D) in astrocyte cultures from CLP animals compared to cultures from the sham group. Additionally, the inflammatory mediators were also assessed in whole hippocampal tissue and showed a similar proinflammatory profile to astrocyte primary cultures from the same groups (Supplementary Fig. 1).

IL-10 levels are altered only in hippocampal astrocyte cultures from CLP animals

Complementing the inflammatory profile analyses, we also determined the production of the major anti-inflammatory cytokine IL-10. We observed decreased levels of IL-10 in hippocampal astrocyte cultures from CLP animals, compared to the sham group (from 24 to 13 pg/ml, P =0.0013, $t_{(14)}$=4.001, Fig. 2E). However, we did not observe this decrease in IL-10 in whole hippocampal tissue (Fig. 2F).

BBB permeability marker expression does not change in astrocyte cultures after CLP

In order to assess the impact of severe systemic inflammation on BBB permeability, we measured VEGF mRNA expression levels. Fig. 3A demonstrates that, compared to the sham group, astrocyte cultures from CLP animals did not present alterations in VEGF expression. In contrast, whole hippocampal tissue samples from CLP animals presented a significant increase in VEGF expression levels (112%, P =0.005, $t_{(10)}$=3.542, Fig. 3B).

Possible role for TLRs in the astrocytic response to severe systemic inflammation

As TLRs seem to be involved in the brain progression of sepsis, we evaluated mRNA expression levels of these receptors. After CLP induction, we observed an increase in TLR2 levels in hippocampal primary astrocytes (65%, P =0.008, $t_{(10)}$=3.296, Fig. 4A), but not in the whole hippocampal tissue homogenate (Fig. 4B). In contrast, TLR4 gene expression demonstrated an opposing pattern; increased TLR4 mRNA expression was observed in the hippocampal tissue (83%, P =0.0019, $t_{(10)}$=4.181, Fig. 4D), but not in hippocampal astrocyte cultures from CLP animals (Fig. 4C).

Astrocytic changes in p21, NFκB and iNOS expression are involved in the progression of inflammation in the brain

Gene expression of p21, a protein that has been increasingly associated with autoimmunity, was evaluated. We observed an augmented p21 mRNA expression in astrocyte cultures after severe systemic inflammation induction (61%, P =0.023, $t_{(10)}$=2.670, Fig. 5A) that was not observed in whole hippocampal tissue analyses (Fig. 5B). As p21 is reported to take part in the activation of the NFκB pathway, we assessed NFκB expression after surgical induction of sepsis; accordingly, NFκB mRNA expression was increased in hippocampal astrocyte cultures (46%, P =0.006, $t_{(10)}$=3.429, Fig. 5C). Finally, we evaluated iNOS expression, as this enzyme activity is modulated by the NFκB transcriptional factor. As expected, we found an increase in the mRNA expression levels of iNOS in primary hippocampal astrocytes from CLP animals (33%, P =0.008, $t_{(10)}$=3.334, Fig. 5D), compared to the sham group. Consistent with this finding, the expression levels of NFκB and iNOS were also increased in the whole hippocampal tissue after severe systemic inflammation (Supplementary Fig. 2).

Discussion

In the present study, we focused on characterizing the impact of an acute severe systemic inflammatory event on astrocytic functions. Astrocytes from CLP animals were found to present increased mRNA expressions and the release of an array of proinflammatory mediators, along with decreased IL-10 levels. Importantly, this

proinflammatory phenotype was not accompanied by an augmentation in astrocytic VEGF expression. Moreover, TLR2 mRNA expression was increased in hippocampal astrocyte cultures, while astrocytic TLR4 expression levels were unchanged after acute systemic inflammation. p21 also participates in the acute astrocytic inflammatory response, and its increased expression after CLP might trigger the translocation of NFκB, consequently promoting iNOS over expression (Fig. 6). The same parameters were also evaluated in whole hippocampal tissue homogenates and, interestingly, some of these proteins presented distinct profiles of expression, when compared to astrocyte cultures from CLP animals, possibly due the interactions of the astrocytes with other CNS cell types, which may in turn mask specific astrocytic changes.

Acute severe systemic inflammation can trigger SAE in up to 70% of cases, often promoting permanent neurocognitive dysfunction and mortality, via process that directly involve hippocampal damage [23,7]. The leading cause of SAE is bacterial infection, triggered by both Gram-positive and Gram-negative bacteria, and the most commonly used experimental model for researching polymicrobial inflammatory pathology is the CLP model [24-26]. Despite increasing knowledge regarding how systemic inflammation affects brain functions, particularly neuron and microglia function, the role of astrocytes in these mechanisms has been largely ignored. In line with this, the use of appropriate models to understand the participation of astrocytes in brain dysfunction has become increasingly important.

Studies using whole brain tissue are the main source of reports regarding the astrocytic molecular changes that occur after systemic inflammation. When comparing gene expression profiles in health and disease, this approach may confuse experimental data for different reasons. Firstly, expression profiles derived from whole tissue mRNA represent the expression of all cells and does not allow the elucidation of a specific cell type that modulates changes in the pathologic condition. Secondly, changes in gene expression that occur in a specific cell type might be imperceptible in the whole tissue mRNA, as a difference may be concealed by a prominent signal from other cell types [27]. Another approach widely used to mimic the impact of Gram-negative inflammation in astrocytes is LPS treatment in primary astrocyte cultures from newborn brain. This model does not accurately reproduce *in vivo* conditions as the inflammatory stimulus directly affects astrocytes instead of the whole body. As such, in order to investigate more reliably the role of astrocytes under physiological and pathological conditions, our group recently established a routine protocol for obtaining astrocyte

cultures from the mature brain of Wistar rats. These primary cultures have been shown to differ from the cultures obtained from neonatal rats in their functional characteristics and molecular expression pattern [17,28,29].

Systemic-derived inflammatory mediators such as TNF-α, interleukins and chemokines are able to drive changes in BBB permeability allowing the influx of inflammatory cells and toxic mediators into the brain, consequently impairing CNS homeostasis and functionality. Accordingly, CLP animals are reported to present a disruption of the BBB, together with an increase in metalloproteinase immunocontent after 24 h of sepsis induction [30,31]. VEGF is considered the major regulator of vascular permeability and reportedly induces leakage of the BBB by decreasing the expression of tight junction claudin-5 [15,32]. We assessed VEGF expression levels in astrocyte cultures from CLP animals and observed no alterations compared to sham animals; however, when we analyzed the whole hippocampal tissue, an increase in VEGF levels was detected. Several cell types can express VEGF, including neurons, astrocytes, microglia and choroid plexus epithelial cells [33,34]. Thus, the high levels of VEGF detected in the hippocampal tissue might reflect an increased expression of this factor in another cell population. Moreover, during the establishment of astrocyte cultures, the cerebral tissue is dissociated and reorganized *in vitro*, interrupting its interaction with pericytes and endothelial cells, which might result in the loss of some of the astrocyte BBB characteristics.

The activation of pattern recognition receptors, such as TLRs, seems to have an important role in the pathogenesis of sepsis. TLR ligands are known stimulators of intracellular signaling pathways that promote enhanced transcription of proinflammatory cytokines [35]. Moreover, TLR2 and TLR4 are the only TLRs known to bind to microbial ligands [36]. However, the role of TLR2 in sepsis is much more indefinite than that of TLR4, as TLR2 appears to have ambivalent roles that seem to vary for different pathogens [37]. Here, we observed an increased expression of TLR2 in astrocyte cultures from CLP animals accompanied by enhanced productions of TNF-α, IL-1β and other proinflammatory mediators, while TLR4 levels remained unchanged. TLR2 classically plays a key role in the pathogenesis of Gram-positive sepsis, although a range of studies has also demonstrated an increase in its expression upon exposure to Gram-negative ligands [38,39]. On the other hand, in the whole tissue analyses, we observed only an augmentation in TLR4 mRNA expression levels. This discrepancy might be explained by the presence of microglia in the whole hippocampal tissue. As

microglial cells are known to respond to TLR ligands faster than astrocytes, producing more proinflammatory cytokines, and may express greater quantities of TLR4 than astrocytes [40,41], it is possible that microglial cell activation may overwhelms the astrocytic response. Furthermore, microglia seem to have a TLR2-independent response to Gram-positive ligands [40], corroborating the unchanged TLR2 levels found in the hippocampal tissue from CLP animals.

Activation of the NFκB signaling pathway by TLR2 and TLR4 ligands in astrocytes contributes to much of the production of proinflammatory cytokines, such as TNF-α and also to the generation of reactive oxygen/nitrogen species (ROS/RNS) [42,43]. Inactive NFκB is located in the cytoplasm, in association with its negative regulator IκB. When agents with the ability to activate NFκB are present, IκB is phosphorylated leading to the release and nuclear translocation of NFκB [44]. Nuclear transcription of NFκB may induce the expression of iNOS, suggesting increased synthesis of NO. In the oxidative environment, NO can react with superoxide anions, to form the powerful oxidant specie, peroxynitrite, which leads to cellular toxicity and neuronal death [45]. Therefore, under physiological conditions, these ROS/RNS are important mediators that provoke or sustain inflammatory processes to protect hosts from harmful stimuli, but when high levels of them are produced, they have cytotoxic effects [46]. Accordingly, we found that astrocyte cultures from CLP animals to present increased mRNA expression levels of NFκB and iNOS. Moreover, an important and differential feature of activated astrocytes is the production of chemokines, including MCP-1 [3]. Previous studies have demonstrated that MCP-1 is a target of NFκB signaling in diverse cell types [47,48]. Consistent with this hypothesis, we demonstrated an increase in NFκB mRNA expression accompanied by high levels of MCP-1 in astrocytes.

Another emerging player in the innate immune system is the p21 protein, whose expression may be stimulated by proinflammatory cytokines [49]. p21 expression is tightly related to cellular senescence and replicative stress might prematurely trigger senescence, compromising the cellular immune response [50]. An immunological role for p21 has been described in macrophages, as $p21^{-/-}$ mice induced to endotoxic shock by LPS demonstrate an increased release of IL-1β and a decreased rate of survival compared to wild type animals [49]. Rackov and colleagues also demonstrated that p21-deficient mice presented decreased LPS tolerance and survival, accompanied by an increase in serum levels of TNF-α and interferon-β [14]. Therefore, p21 seems to have a

role in the brain response to systemic inflammatory events. The p21 immunocontent in the hippocampus from mice induced to chronic intestinal inflammation was increased, together with an augmentation in GFAP and no change in Iba-1 levels, indicating astroglial, but not microglial, activation [51]. Additionally, cultures from newborn p21-deficient mice treated with LPS, presented decreased levels of NFκB compared to cultures from wild type animals [52]. In line with these previous reports, our astrocyte cultures from CLP animals showed an increase in NFκB mRNA and proinflammatory cytokine and chemokine levels, as well as an increase in p21 mRNA expression. Interestingly, analyses of p21 in whole hippocampal tissue homogenates showed no differences between the CLP and sham group.

Taken together, the results presented in this study provide new evidence to suggest the participation of astrocytes in the brain injury derived from acute severe systemic inflammation. The mechanism of astrocyte response involves changes in the expressions of the TLR, p21 and NFκB pathways. Moreover, the differences observed between astrocyte culture and whole hippocampal tissue analyses reinforce the idea that our astrocyte culture model might represent an important new tool for understanding the role of these glial cells under pathological conditions. In summary, this report improves our understanding of the mechanisms by which astrocytes react to systemic inflammation and indicate these cells as a potential target for therapeutic modulation.

Acknowledgements

This work was supported by the Conselho Nacional de Desenvolvimento Científico e Tecnológico (CNPq), Coordenação de Aperfeiçoamento de Pessoal de Nível Superior (CAPES), Fundação de Amparo à Pesquisa do Estado do Rio Grande do Sul (FAPERGS), Federal University of Rio Grande do Sul (UFRGS) and Instituto Nacional de Ciência e Tecnologia para Excitotoxicidade e Neuroproteção (INCTEN/CNPq).

Conflict of interest

The authors declare there are no conflicts of interest.

References

1. Fu HQ, Yang T, Xiao W, Fan L, Wu Y, Terrando N, Wang TL (2014) Prolonged neuroinflammation after lipopolysaccharide exposure in aged rats. PLoS One 9 (8):e106331. doi:10.1371/journal.pone.0106331

2. Terrando N, Monaco C, Ma D, Foxwell BM, Feldmann M, Maze M (2010) Tumor necrosis factor-alpha triggers a cytokine cascade yielding postoperative cognitive decline. Proc Natl Acad Sci U S A 107 (47):20518-20522. doi:10.1073/pnas.1014557107

3. Michels M, Steckert AV, Quevedo J, Barichello T, Dal-Pizzol F (2015) Mechanisms of long-term cognitive dysfunction of sepsis: from blood-borne leukocytes to glial cells. Intensive care medicine experimental 3 (1):30. doi:10.1186/s40635-015-0066-x

4. Esper AM, Martin GS (2009) Extending international sepsis epidemiology: the impact of organ dysfunction. Critical care (London, England) 13 (1):120. doi:10.1186/cc7704

5. Kaukonen KM, Bailey M, Suzuki S, Pilcher D, Bellomo R (2014) Mortality related to severe sepsis and septic shock among critically ill patients in Australia and New Zealand, 2000-2012. Jama 311 (13):1308-1316. doi:10.1001/jama.2014.2637

6. Cotena S, Piazza O (2012) Sepsis-associated encephalopathy. Translational medicine @ UniSa 2:20-27

7. Mazeraud A, Pascal Q, Verdonk F, Heming N, Chretien F, Sharshar T (2016) Neuroanatomy and Physiology of Brain Dysfunction in Sepsis. Clinics in chest medicine 37 (2):333-345. doi:10.1016/j.ccm.2016.01.013

8. Danielski LG, Giustina AD, Badawy M, Barichello T, Quevedo J, Dal-Pizzol F, Petronilho F (2017) Brain Barrier Breakdown as a Cause and Consequence of Neuroinflammation in Sepsis. Mol Neurobiol. doi:10.1007/s12035-016-0356-7

9. Tsujimoto H, Ono S, Efron PA, Scumpia PO, Moldawer LL, Mochizuki H (2008) Role of Toll-like receptors in the development of sepsis. Shock (Augusta, Ga) 29 (3):315-321. doi:10.1097/SHK.0b013e318157ee55

10. Gorina R, Font-Nieves M, Marquez-Kisinousky L, Santalucia T, Planas AM (2011) Astrocyte TLR4 activation induces a proinflammatory environment through the interplay between MyD88-dependent NFkappaB signaling, MAPK, and Jak1/Stat1 pathways. Glia 59 (2):242-255. doi:10.1002/glia.21094

11. Lloberas J, Celada A (2009) p21(waf1/CIP1), a CDK inhibitor and a negative feedback system that controls macrophage activation. European journal of immunology 39 (3):691-694. doi:10.1002/eji.200939262

12. Yang QH, Liu DW, Wang XT, Yang RL, Shi Y, Long Y, Liu HZ, He HW, Zhou X, Tang B (2011) G1 cell cycle arrest signaling in hepatic injury after intraperitoneal sepsis in rats. Inflammation research : official journal of the European Histamine Research Society [et al] 60 (8):783-789. doi:10.1007/s00011-011-0334-5

13. Balomenos D, Martin-Caballero J, Garcia MI, Prieto I, Flores JM, Serrano M, Martinez AC (2000) The cell cycle inhibitor p21 controls T-cell proliferation and sex-linked lupus development. Nat Med 6 (2):171-176. doi:10.1038/72272

14. Rackov G, Hernandez-Jimenez E, Shokri R, Carmona-Rodriguez L, Manes S, Alvarez-Mon M, Lopez-Collazo E, Martinez AC, Balomenos D (2016) p21 mediates macrophage reprogramming through regulation of p50-p50 NF-kappaB and IFN-beta. The Journal of clinical investigation 126 (8):3089-3103. doi:10.1172/jci83404

15. Chapouly C, Tadesse Argaw A, Horng S, Castro K, Zhang J, Asp L, Loo H, Laitman BM, Mariani JN, Straus Farber R, Zaslavsky E, Nudelman G, Raine CS, John GR (2015) Astrocytic TYMP and VEGFA drive blood-brain barrier opening in inflammatory central nervous system lesions. Brain : a journal of neurology 138 (Pt 6):1548-1567. doi:10.1093/brain/awv077

16. Mayo L, Quintana FJ, Weiner HL (2012) The innate immune system in demyelinating disease. Immunological reviews 248 (1):170-187. doi:10.1111/j.1600-065X.2012.01135.x

17. Bellaver B, Souza DG, Souza DO, Quincozes-Santos A (2016) Hippocampal Astrocyte Cultures from Adult and Aged Rats Reproduce Changes in Glial Functionality Observed in the Aging Brain. Mol Neurobiol. doi:10.1007/s12035-016-9880-8

18. Souza DG, Bellaver B, Souza DO, Quincozes-Santos A (2013) Characterization of adult rat astrocyte cutures. PLoS One 8:E60282. doi: 10.1371/journal.pone.0060282

19. Zimmer ER, Parent MJ, Souza DG, Leuzy A, Lecrux C, Kim HI, Gauthier S, Pellerin L, Hamel E (2017) [18F]FDG PET signal is driven by astroglial glutamate transport. Nat Neurosc. doi:10.1038/nn.4492

20. Petronilho F, Perico SR, Vuolo F, Mina F, Constantino L, Comim CM, Quevedo J, Souza DO, Dal-Pizzol F (2012) Protective effects of guanosine against sepsis-induced

damage in rat brain and cognitive impairment. Brain Behav Immun 26 (6):904-910. doi:10.1016/j.bbi.2012.03.007

21. Livak KJ, Schmittgen TD (2001) Analysis of relative gene expression data using real-time quantitative PCR and the 2(-Delta Delta C(T)) Method. Methods (San Diego, Calif) 25 (4):402-408. doi:10.1006/meth.2001.1262

22. Smith PK, Krohn RI, Hermanson GT, Mallia AK, Gartner FH, Provenzano MD, Fujimoto EK, Goeke NM, Olson BJ, Klenk DC (1985) Measurement of protein using bicinchoninic acid. Analytical biochemistry 150 (1):76-85. doi:10.1016/0003-2697(85)90442-7

23. Widmann CN, Heneka MT (2014) Long-term cerebral consequences of sepsis. Lancet Neurol 13 (6):630-636. doi:10.1016/s1474-4422(14)70017-1

24. Dejager L, Pinheiro I, Dejonckheere E, Libert C (2011) Cecal ligation and puncture: the gold standard model for polymicrobial sepsis? Trends in microbiology 19 (4):198-208. doi:10.1016/j.tim.2011.01.001

25. Neves FS, Marques PT, Barros-Aragao F, Nunes JB, Venancio AM, Cozachenco D, Frozza RL, Passos GF, Costa R, de Oliveira J, Engel DF, De Bem AF, Benjamim CF, De Felice FG, Ferreira ST, Clarke JR, Figueiredo CP (2016) Brain-Defective Insulin Signaling Is Associated to Late Cognitive Impairment in Post-Septic Mice. Mol Neurobiol. doi:10.1007/s12035-016-0307-3

26. Comim CM, Freiberger V, Ventura L, Mina F, Ferreira GK, Michels M, Generoso JS, Streck EL, Quevedo J, Barichello T, Dal-Pizzol F (2017) Inhibition of indoleamine 2,3-dioxygenase 1/2 prevented cognitive impairment and energetic metabolism changes in the hippocampus of adult rats subjected to polymicrobial sepsis. J Neuroimmunol 305:167-171. doi:10.1016/j.jneuroim.2017.02.001

27. Srinivasan K, Friedman BA, Larson JL, Lauffer BE, Goldstein LD, Appling LL, Borneo J, Poon C, Ho T, Cai F, Steiner P, van der Brug MP, Modrusan Z, Kaminker JS, Hansen DV (2016) Untangling the brain's neuroinflammatory and neurodegenerative transcriptional responses. Nature communications 7:11295. doi:10.1038/ncomms11295

28. Souza DG, Bellaver B, Bobermin LD, Souza DO, Quincozes-Santos A (2016) Anti-aging effects of guanosine in glial cells. Purinergic Signal. doi:10.1007/s11302-016-9533-4

29. Bellaver B, Souza DG, Souza DO, Quincozes-Santos A (2014) Resveratrol increases antioxidant defenses and deceases proinflammatory cytokines in hippocampal

astocyte cultures from newborn, adult and aged Wistar rats. Toxicology in vitro 28:479-484. doi:10.1016/j.tiv.2014.01.006

30. Dal-Pizzol F, Rojas HA, dos Santos EM, Vuolo F, Constantino L, Feier G, Pasquali M, Comim CM, Petronilho F, Gelain DP, Quevedo J, Moreira JC, Ritter C (2013) Matrix metalloproteinase-2 and metalloproteinase-9 activities are associated with blood-brain barrier dysfunction in an animal model of severe sepsis. Mol Neurobiol 48 (1):62-70. doi:10.1007/s12035-013-8433-7

31. Comim CM, Vilela MC, Constantino LS, Petronilho F, Vuolo F, Lacerda-Queiroz N, Rodrigues DH, da Rocha JL, Teixeira AL, Quevedo J, Dal-Pizzol F (2011) Traffic of leukocytes and cytokine up-regulation in the central nervous system in sepsis. Intensive care medicine 37 (4):711-718. doi:10.1007/s00134-011-2151-2

32. Argaw AT, Asp L, Zhang J, Navrazhina K, Pham T, Mariani JN, Mahase S, Dutta DJ, Seto J, Kramer EG, Ferrara N, Sofroniew MV, John GR (2012) Astrocyte-derived VEGF-A drives blood-brain barrier disruption in CNS inflammatory disease. The Journal of clinical investigation 122 (7):2454-2468. doi:10.1172/jci60842

33. Wang X, Kang K, Wang S, Yao J, Zhang X (2016) Focal cerebral ischemic tolerance and change in blood-brain barrier permeability after repetitive pure oxygen exposure preconditioning in a rodent model. J Neurosurg 125 (4):943-952. doi:10.3171/2015.7.jns142220

34. Ma Y, Zechariah A, Qu Y, Hermann DM (2012) Effects of vascular endothelial growth factor in ischemic stroke. J Neurosci Res 90 (10):1873-1882. doi:10.1002/jnr.23088

35. Hanke ML, Kielian T (2011) Toll-like receptors in health and disease in the brain: mechanisms and therapeutic potential. Clinical science (London, England : 1979) 121 (9):367-387. doi:10.1042/cs20110164

36. Brightbill HD, Modlin RL (2000) Toll-like receptors: molecular mechanisms of the mammalian immune response. Immunology 101 (1):1-10. doi:10.1046/j.1365-2567.2000.00093.x

37. Hanzelmann D, Joo HS, Franz-Wachtel M, Hertlein T, Stevanovic S, Macek B, Wolz C, Gotz F, Otto M, Kretschmer D, Peschel A (2016) Toll-like receptor 2 activation depends on lipopeptide shedding by bacterial surfactants. Nature communications 7:12304. doi:10.1038/ncomms12304

38. Laflamme N, Soucy G, Rivest S (2001) Circulating cell wall components derived from gram-negative, not gram-positive, bacteria cause a profound induction of the gene-

encoding Toll-like receptor 2 in the CNS. J Neurochem 79 (3):648-657. doi:10.1046/j.1471-4159.2001.00603.x

39. Wiersinga WJ, Wieland CW, Dessing MC, Chantratita N, Cheng AC, Limmathurotsakul D, Chierakul W, Leendertse M, Florquin S, de Vos AF, White N, Dondorp AM, Day NP, Peacock SJ, van der Poll T (2007) Toll-like receptor 2 impairs host defense in gram-negative sepsis caused by Burkholderia pseudomallei (Melioidosis). PLoS medicine 4 (7):e248. doi:10.1371/journal.pmed.0040248

40. Kielian T (2006) Toll-like receptors in central nervous system glial inflammation and homeostasis. J Neurosci Res 83 (5):711-730. doi:10.1002/jnr.20767

41. Carpentier PA, Begolka WS, Olson JK, Elhofy A, Karpus WJ, Miller SD (2005) Differential activation of astrocytes by innate and adaptive immune stimuli. Glia 49 (3):360-374. doi:10.1002/glia.20117

42. Troutman TD, Bazan JF, Pasare C (2012) Toll-like receptors, signaling adapters and regulation of the pro-inflammatory response by PI3K. Cell cycle (Georgetown, Tex) 11 (19):3559-3567. doi:10.4161/cc.21572

43. Marinelli C, Di Liddo R, Facci L, Bertalot T, Conconi MT, Zusso M, Skaper SD, Giusti P (2015) Ligand engagement of Toll-like receptors regulates their expression in cortical microglia and astrocytes. Journal of neuroinflammation 12:244. doi:10.1186/s12974-015-0458-6

44. Wakabayashi N, Slocum SL, Skoko JJ, Shin S, Kensler TW (2010) When NRF2 Talks, Who's Listening? Antioxid Redox Signal. doi:10.1089/ars.2010.3216

45. Brown GC, Neher JJ (2010) Inflammatory neurodegeneration and mechanisms of microglial killing of neurons. Mol Neurobiol 41 (2-3):242-247. doi:10.1007/s12035-010-8105-9

46. Aruoma OI, Grootveld M, Bahorun T (2006) Free radicals in biology and medicine: from inflammation to biotechnology. BioFactors (Oxford, England) 27 (1-4):1-3. doi:10.1002/biof.5520270101

47. Ueda A, Okuda K, Ohno S, Shirai A, Igarashi T, Matsunaga K, Fukushima J, Kawamoto S, Ishigatsubo Y, Okubo T (1994) NF-kappa B and Sp1 regulate transcription of the human monocyte chemoattractant protein-1 gene. J Immunol 153 (5):2052-2063

48. Dranse HJ, Muruganandan S, Fawcett JP, Sinal CJ (2016) Adipocyte-secreted chemerin is processed to a variety of isoforms and influences MMP3 and chemokine

secretion through an NFkB-dependent mechanism. Molecular and cellular endocrinology 436:114-129. doi:10.1016/j.mce.2016.07.017

49. Scatizzi JC, Mavers M, Hutcheson J, Young B, Shi B, Pope RM, Ruderman EM, Samways DS, Corbett JA, Egan TM, Perlman H (2009) The CDK domain of p21 is a suppressor of IL-1beta-mediated inflammation in activated macrophages. European journal of immunology 39 (3):820-825. doi:10.1002/eji.200838683

50. Montes M, Lund AH (2016) Emerging roles of lncRNAs in senescence. The FEBS journal 283 (13):2414-2426. doi:10.1111/febs.13679

51. Zonis S, Pechnick RN, Ljubimov VA, Mahgerefteh M, Wawrowsky K, Michelsen KS, Chesnokova V (2015) Chronic intestinal inflammation alters hippocampal neurogenesis. Journal of neuroinflammation 12:65. doi:10.1186/s12974-015-0281-0

52. Tusell JM, Saura J, Serratosa J (2005) Absence of the cell cycle inhibitor p21Cip1 reduces LPS-induced NO release and activation of the transcription factor NF-kappaB in mixed glial cultures. Glia 49 (1):52-58. doi:10.1002/glia.20095

Figure legends

Fig. 1. Hippocampal astrocyte cultures from CLP animals presented changes in (A) TNF-α and (B) IL-1β mRNA expression levels and in (C) TNF-α and (D) IL-1β release. Data represent the means + S.E.M. of groups (n= 6-8). **P* <0.05, ***P* <0.01 and ****P* <0.001 (*t* test), compared to the sham group.

Fig. 2. Astrocytes showed a proinflammatory profile after acute systemic inflammation. The levels of (A) IL-6, (B) IL-18, (C) MCP-1 and (E,F) IL-10 and (D) COX-2 mRNA expression were measured. Data represent the means + S.E.M. of groups (n= 6-8). **P* <0.05, ***P* <0.01 and ****P* <0.001 (*t* test), compared to the sham group.

Fig. 3. The mRNA expression levels of a BBB permeability marker in hippocampus and astrocyte cultures after CLP. VEGF mRNA expression levels were measured in (A) hippocampal astrocyte cultures and (B) hippocampus. Data represent the means + S.E.M. of groups (n= 6). ***P* <0.01 (*t* test), compared to the sham group.

Fig. 4. Changes in the expression levels of TLRs were observed in hippocampal astrocyte cultures and hippocampal tissue from CLP. TLR2 mRNA expression in (A) astrocyte cultures and (B) hippocampus and TLR4 mRNA expression in (C) astrocyte cultures and (D) hippocampus. Data represent the means + S.E.M. of groups (n= 6). ***P* <0.01 (*t* test), compared to the sham group.

Fig. 5. p21, NFκB and iNOS expression levels were altered in hippocampal astrocyte cultures from CLP animals. mRNA expression levels of p21 were measured in (A) astrocyte cultures and (B) hippocampus. (C) NFκB and (D) iNOS mRNA expression levels were measured in astrocyte cultures. Data represent the means + S.E.M. of groups (n= 6). **P* <0.05 and ***P* <0.01 (*t* test), compared to the sham group.

Fig. 6. Schematic illustration of the impact of severe systemic inflammation on hippocampal astrocyte cultures. Systemic mediators released by CLP animals induced an increase in TLR2 and no changes in TLR4 mRNA expression levels. CLP also promoted an augmentation in astrocytic p21 levels accompanied by increased NFκB expression. NFκB induced the expression of proinflammatory target genes, such as

iNOS, TNF-α, IL-1β, IL-6, IL-18 and COX-2 and inhibited the release of IL-10. Green cells represent astrocytes; yellow cells represent neurons; blue cells represent microglia and purple oligodendrocytes.

Supplementary Fig. 1. Inflammatory profile in the whole hippocampus. (A) TNF-α, (B) IL-1β and (G) COX-2 mRNA expression levels. (C) TNF-α, (D) IL-1β, (E) IL-6, (F) IL-18 and MCP-1 levels. Data represent the means + S.E.M. of groups (n= 6-8). *P <0.05, **P <0.01 and ***P <0.001 (t test), compared to the sham group.

Supplementary Fig. 2. CLP promoted increases in mRNA expression levels of (A) NFκB and (B) iNOS in hippocampal tissue. Data represent the means + S.E.M. of groups (n= 6). **P <0.01 (t test), compared to the sham group.

Table 1. Oligonucleotide Primers or Assay number for Real-Time RT-PCR

mRNA target	Sense/anti-sense or Assay number
TNF-α	5′- GCGACGTGGAACTGGCAGAAG-3′
	5′-GGTACAACCCATCGGCTGGCA-3′
IL-1β	5′-TGTTTCCATCCTGGAAGGTC-3′
	5′-TCACAGCAGCACATCAACAA-3′
COX-2	5′-GATTGACAGCCCACCAACTT-3′
	5′-CGGGATGAACTCTCTCCTCA-3′
VEGF	5′-TAACGATGAAGCCCTGGAGTG-3′
	5′-AGGTTTGATCCGCATGATCTG-3′
p21	5′-GAGGCCTCTTCCCCATCTTCT-3′
	5′-AATTAAGACACACTGAATGAAGGCTAAG-3′
p65 NFκB	5′-CCTAGCTTTCTCTGAACTGCAAA-3′
	5′-GGGTCAGAGGCCAATAGAGA-3′
iNOS	5′-GGCAGCCTGTGAGACCTTTG-3′
	5′-GAAGCGTTTCGGGATCTGAA-3′
β-actin	5′-CAACGAGCGGTTCCGAT-3′
	5′- GCCACAGGATTCCATACCCA-3′
TLR4	*Rn00569848_m1*
TLR2	Rn02133647_s1

Figure 1

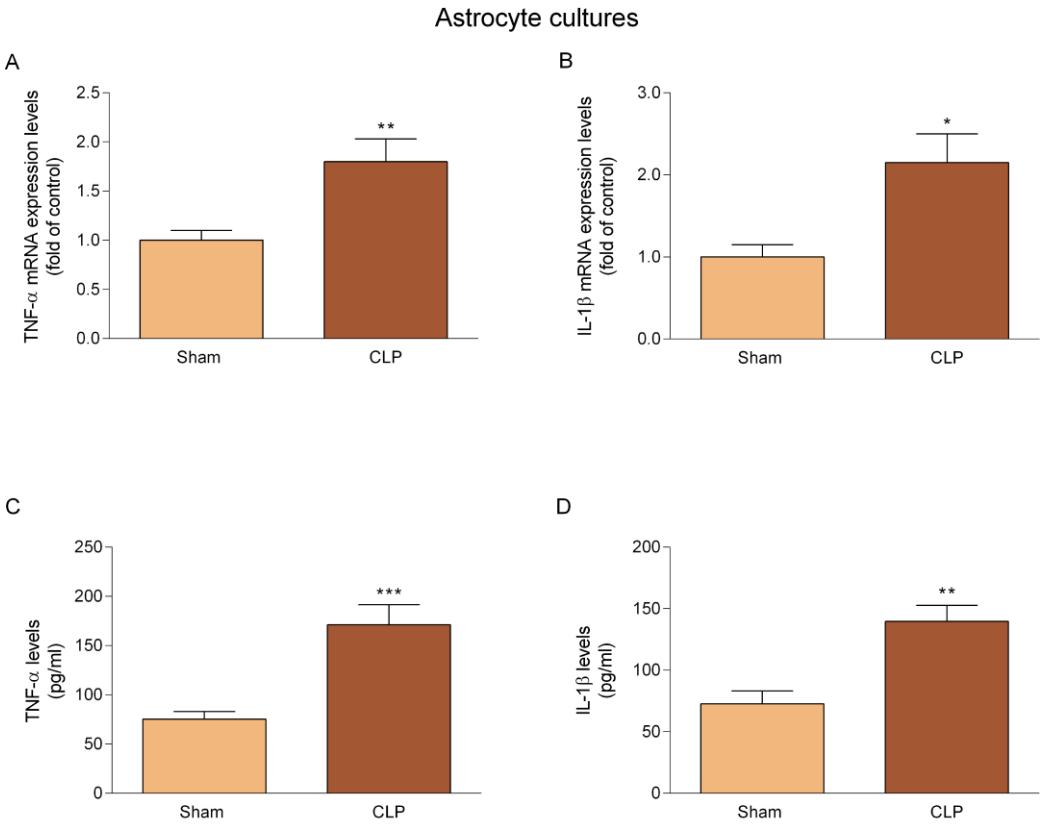
Astrocyte cultures
A
TNF-α mRNA expression levels (fold of control)
2.5
2.0
1.5
1.0
0.5
0.0
**
Sham
CLP
B
IL-1β mRNA expression levels (fold of control)
3.0
2.0
1.0
0.0
*
Sham
CLP
C
TNF-α levels (pg/ml)
250
200
150
100
50
0
***
Sham
CLP
D
IL-1β levels (pg/ml)
200
150
100
50
0
**
Sham
CLP

Figure 2

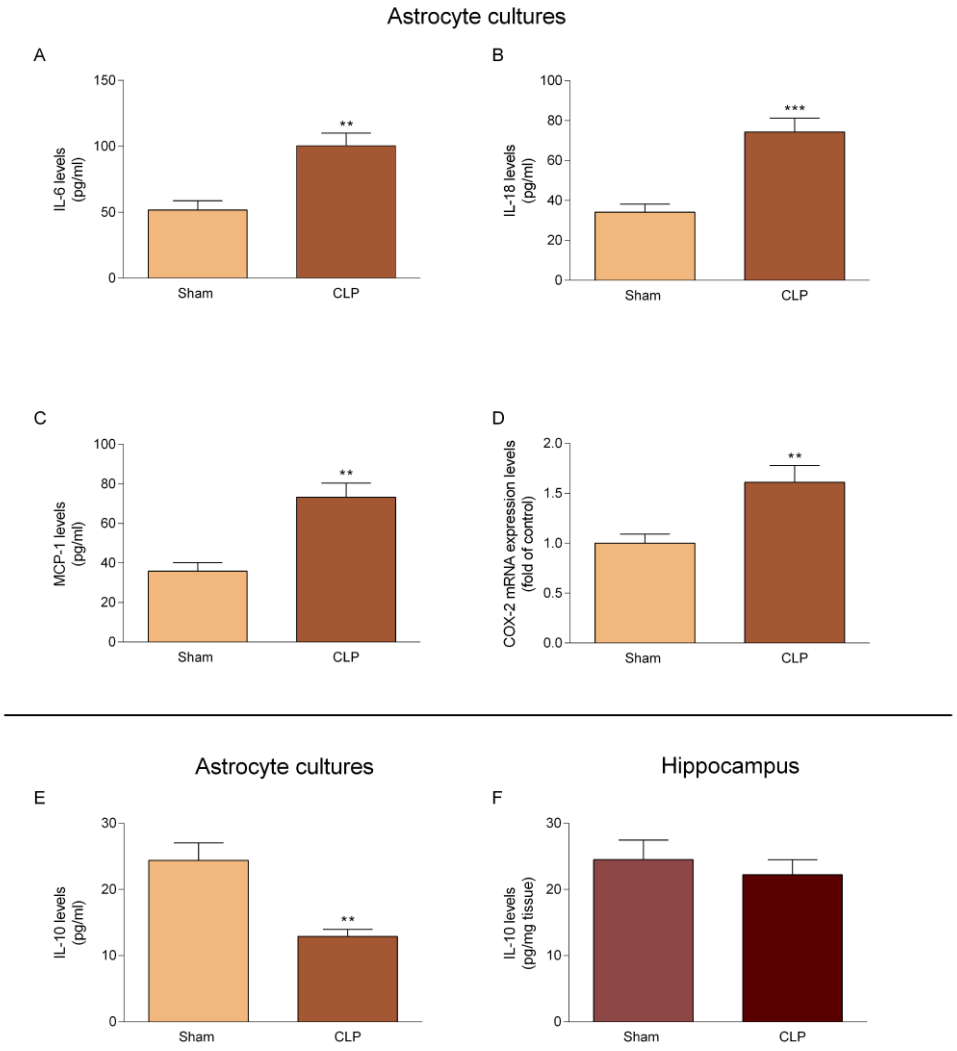
Astrocyte cultures
A
IL-6 levels (pg/ml)
150
100
50
0
**
Sham
CLP
B
IL-18 levels (pg/ml)
100
80
60
40
20
0
***
Sham
CLP
C
MCP-1 levels (pg/ml)
100
80
60
40
20
0
**
Sham
CLP
D
COX-2 mRNA expression levels (fold of control)
2.0
1.5
1.0
0.5
0.0
**
Sham
CLP
Astrocyte cultures
E
IL-10 levels (pg/ml)
30
20
10
0
**
Sham
CLP
Hippocampus
F
IL-10 levels (pg/mg tissue)
30
20
10
0
Sham
CLP

Figure 3

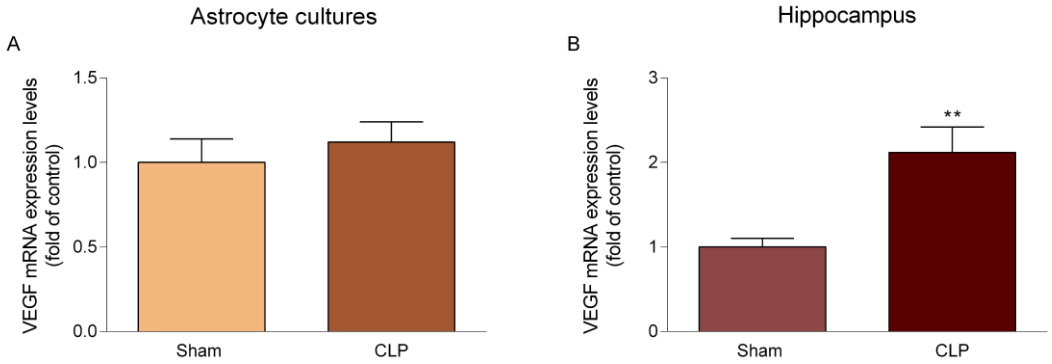
Astrocyte cultures
A
VEGF mRNA expression levels (fold of control)
1.5
1.0
0.5
0.0
Sham
CLP
Hippocampus
B
VEGF mRNA expression levels (fold of control)
3
2
1
0
**
Sham
CLP

Figure 4

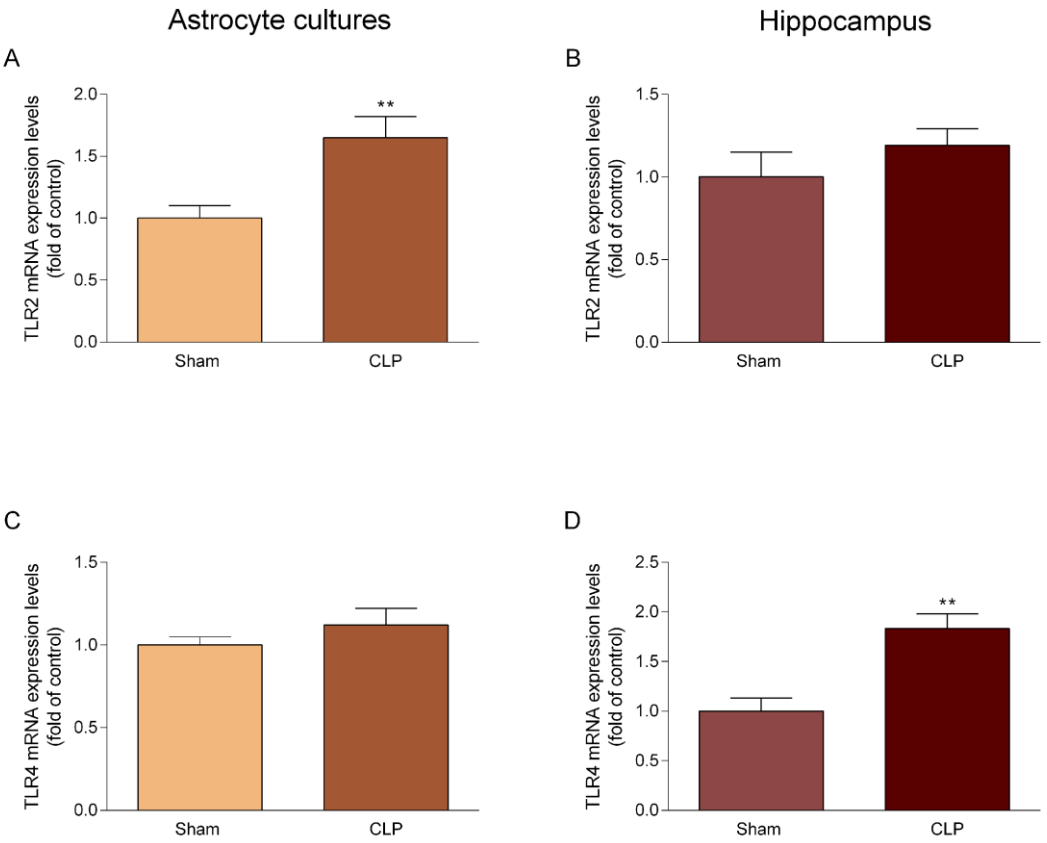
Astrocyte cultures
Hippocampus
A
B
C
D
TLR2 mRNA expression levels (fold of control)
TLR4 mRNA expression levels (fold of control)
Sham
CLP
**

Figure 5

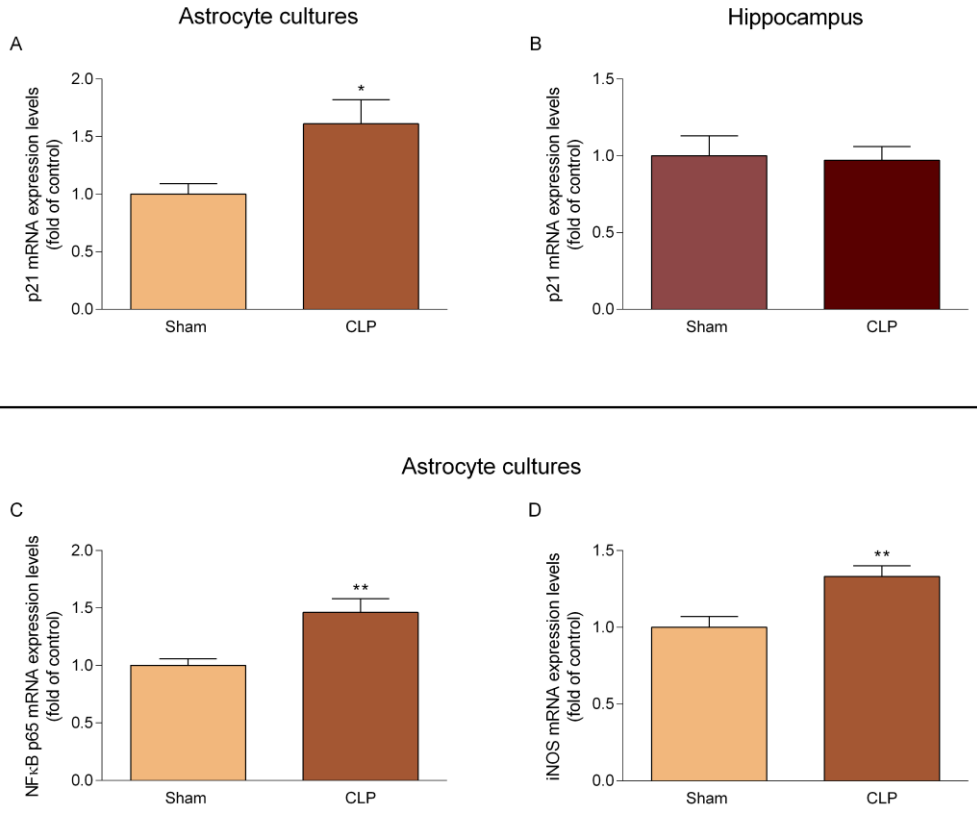
Astrocyte cultures
A
p21 mRNA expression levels (fold of control)
2.0
1.5
1.0
0.5
0.0
*
Sham
CLP
Hippocampus
B
p21 mRNA expression levels (fold of control)
1.5
1.0
0.5
0.0
Sham
CLP
Astrocyte cultures
C
NFκB p65 mRNA expression levels (fold of control)
2.0
1.5
1.0
0.5
0.0
**
Sham
CLP
D
iNOS mRNA expression levels (fold of control)
1.5
1.0
0.5
0.0
**
Sham
CLP

Figure 6

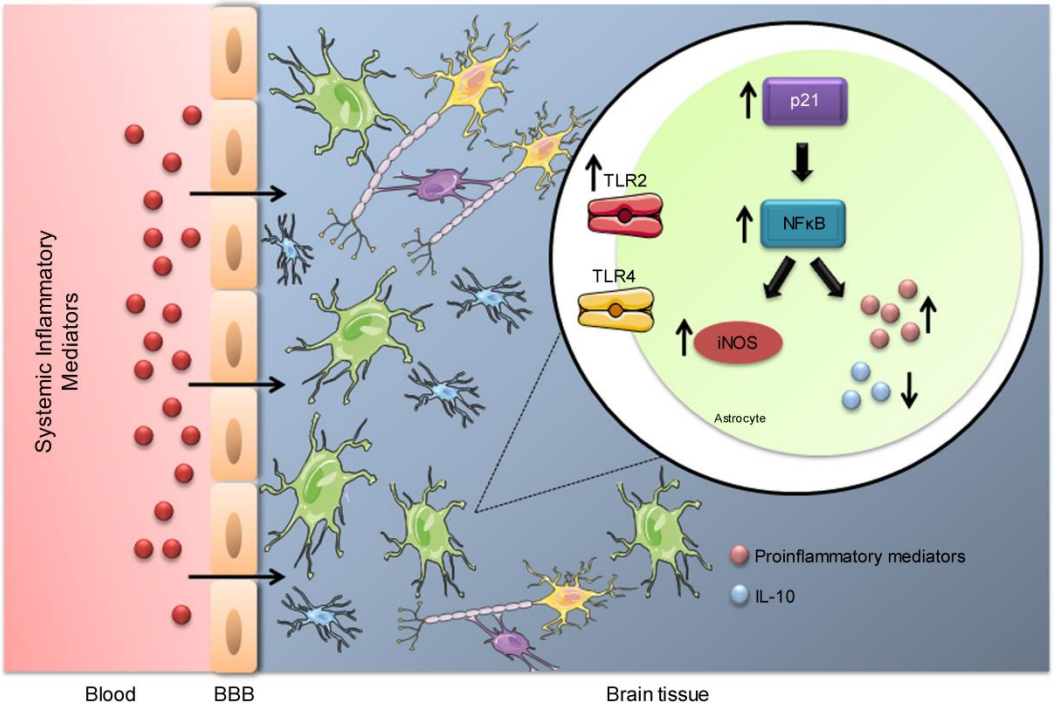
Systemic Inflammatory Mediators
p21
TLR2
NFκB
TLR4
iNOS
Astrocyte
Proinflammatory mediators
IL-10
Blood
BBB
Brain tissue

Supplementary Figure 1

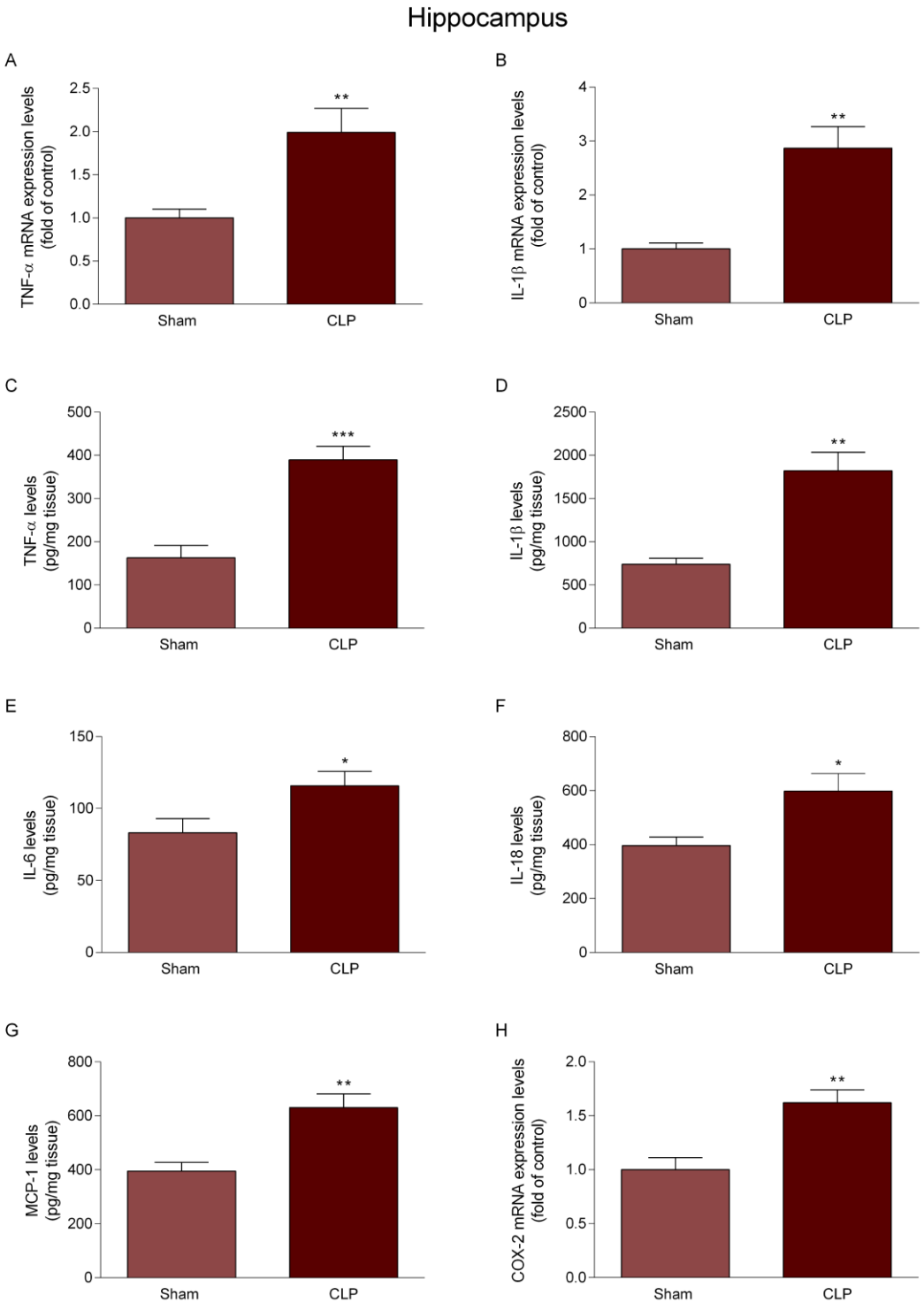

Supplementary Figure 2

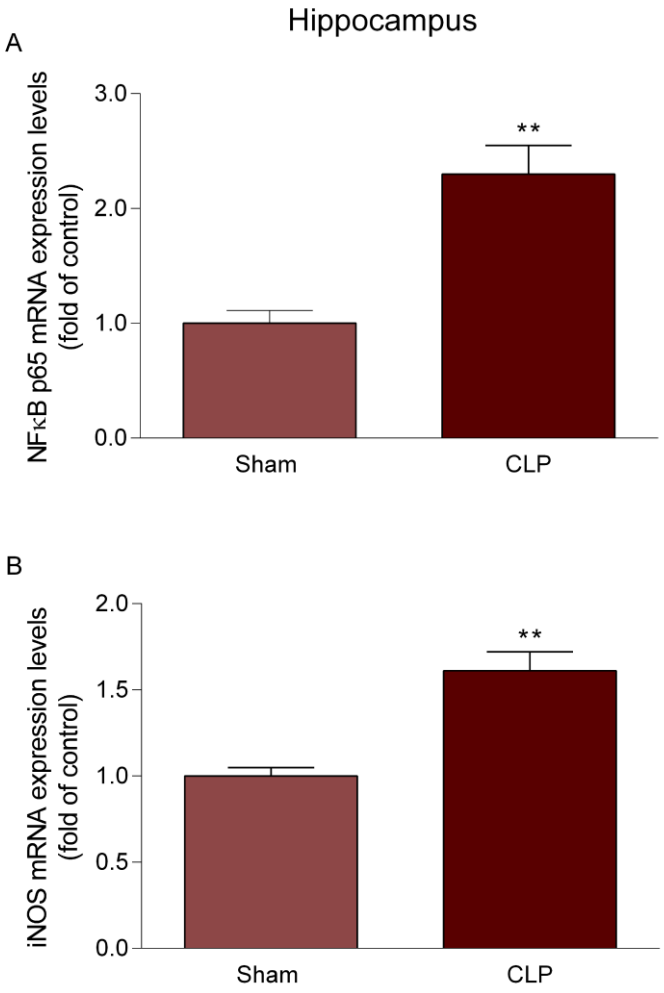

Capítulo 3

Activated peripheral blood mononuclear cell mediators trigger astrocyte reactivity.

No Capítulo 3 apresentamos o artigo aceito para publicação no periódico *Brain, Behavior and Immunity*.

No Capítulo anterior demonstramos a resposta astrocitária durante a fase aguda da sepse. Neste Capítulo temos como objetivos entender os mecanismos pelos quais essa inflamação sistêmica severa impacta tão fortemente a habilidade dos astrócitos manterem a homeostasia celular. Assim, realizamos uma análise de transcriptoma de pacientes acometidos por sepse, com o intuito de entender quais as funções mais fortemente acometidas nesse processo. Posteriormente, avaliamos se as PBMCs seriam capazes de promover essas alterações em astrócitos. Desse modo, observados que as vias envolvidas no metabolismo energético são as predominantemente afetadas durante a sepse em humanos. Corroborando, a indução de LCP em modelo animal promoveu um hipometabolismo cerebral de glicose, que é acompanhado de uma diminuição na captação de glutamato astrocitária. Astrócitos expostos a fatores liberados pelas PBMCs reproduziram a diminuição da captação de glicose e glutamato observadas *in vivo*.

Activated peripheral blood mononuclear cell mediators trigger astrocyte reactivity

Bruna Bellaver[1], Andréia S. da Rocha[1], Débora G. Souza[1], Douglas T. Leffa[2], Marco Antônio De Bastiani[1], Guilherme Schu[1], Pâmela C. Lukasewicz Ferreira[3], Gianina T. Venturin[4], Samuel Greggio[4], Camila T. Ribeiro[1], Jaderson C. da Costa[4], José Cláudio Fonseca Moreira[1,5], Daniel P. Gelain[1,5], Iraci Lucena da S. Torres[2,6,8], Fábio Klamt[1,7], Eduardo R. Zimmer[1,4,6,8*]

[1]Graduate Program in Biological Sciences: Biochemistry, Universidade Federal do Rio Grande do Sul, Porto Alegre, Brazil;

[2] Graduate Program in Medicine: Medical Sciences, Universidade Federal do Rio Grande do Sul, Porto Alegre, Brazil;

[3] Graduate Program in Pharmaceutical Science, Universidade Federal do Rio Grande do Sul, Porto Alegre, Brazil;

[4] Preclinical Imaging Center, Brain Institute (BraIns) of Rio Grande do Sul, Porto Alegre, Brazil;

[5] Department of Biochemistry, Universidade Federal do Rio Grande do Sul, Porto Alegre, Brazil;

[6] Graduate Program in Biological Sciences: Pharmacology and Therapeutics, Universidade Federal do Rio Grande do Sul, Porto Alegre, Brazil;

[7] Laboratory of Cellular Biochemistry, Instituto de Ciências Básicas da Saúde, Universidade Federal do Rio Grande do Sul, Porto Alegre, Brazil;

[8]Departament of Pharmacology, Universidade Federal do Rio Grande do Sul, Porto Alegre, Brazil

***Corresponding author:**

Eduardo R. Zimmer, PhD (E.R. Zimmer)

Department of Pharmacology, Universidade Federal do Rio Grande do Sul (UFRGS)

2500 Ramiro Barcelos street, 90035-003, Porto Alegre, RS, Brazil

Email address: eduardo.zimmer@ufrgs.br

Telephone: +55 51 33085558

Fax: +55 51 33085544

Website: www.zimmer-lab.org

Abstract

Sepsis is characterized by a severe and disseminated inflammation. In the central nervous system, sepsis promotes synaptic dysfunction and permanent cognitive impairment. Besides sepsis-induced neuronal dysfunction, glial cell response has been gaining considerable attention with microglial activation as a key player. By contrast, astrocytes' role during acute sepsis is still underexplored. Astrocytes are specialized immunocompetent cells involved in brain surveillance. In this context, the potential communication between the peripheral immune system and astrocytes during acute sepsis still remains unclear. We hypothesized that peripheral blood mononuclear cell (PBMC) mediators are able to affect the brain during an episode of acute sepsis. With this in mind, we first performed a data-driven transcriptome analysis of blood from septic patients to identify common features among independent clinical studies. Our findings evidenced pronounced impairment in energy-related signaling pathways in the blood of septic patients. Since astrocytes are key for brain energy homeostasis, we decided to investigate the communication between PBMC mediators and astrocytes in a rat model of acute sepsis, induced by cecal ligation and perforation (CLP). In the CLP animals, we identified widespread *in vivo* brain glucose hypometabolism. *Ex vivo* analyses demonstrated astrocyte reactivity along with reduced glutamate uptake capacity during sepsis. Also, by exposing cultured astrocytes to mediators released by PBMCs from CLP animals, we

reproduced the energetic failure observed *in vivo*. Finally, by pharmacologically inhibiting phosphoinositide 3-kinase (PI3K), a central metabolic pathway downregulated in the blood of septic patients and reduced in the CLP rat brain, we mimicked the PBMC mediators effect on glutamate uptake but not on glucose metabolism. These results suggest that PBMC mediators are capable of directly mediating astrocyte reactivity and contribute to the brain energetic failure observed in acute sepsis. Moreover, the evidence of PI3K participation in this process indicates a potential target for therapeutic modulation.

Keywords: astrocyte; glucose; glutamate; energy metabolism; PBMC; sepsis.

1. Introduction

Sepsis is characterized by a severe and disseminated systemic inflammation as a result of a microorganism invasion in the bloodstream. In this inflammatory scenario, the activation of the peripheral immune system also affects brain function. Reports have demonstrated that sepsis impairs the brain even earlier than other organs, which increases morbidity and mortality rates in this condition (Michels et al., 2015; Young, 2010; Ziaja, 2013). Moreover, long-term brain dysfunction is commonly observed in sepsis-survivors (Iwashyna et al., 2010). However, key systemic features triggering brain impairment during acute sepsis are still elusive. In this context, it has been suggested that glial cells have a significant role in mediating the crosstalk between systemic immune signals and the central nervous system (CNS) (Bellaver et al., 2017; Michels et al., 2015; Richards et al., 2015).

In the acute phase of sepsis, inflammation is coordinated by the innate immune system. In this scenario, the activation of peripheral blood mononuclear cells (PBMCs), is thought to play an important role in orchestrating this immune response as PBMCs actively change their transcriptomic and secretory profile (Godini and Fallahi, 2018; Ransohoff et al., 2015; Tang et al., 2009), being able to release mediators to the affected sites, which include the brain (Ransohoff et al., 2015). Additionally, an elevated rate of PBMC infiltration into the CNS under inflammatory conditions was previously demonstrated (Kyrkanides et al., 2008). Based on this, it is very likely that infiltrated PBMCs, or their mediators, are capable of activating brain immune cells, such as microglia and astrocytes. In this way, recent evidence suggests a potential microglial-independent direct activation of astrocytes by PBMCs (Horng et al., 2017; Richards et al., 2015). When activated, astrocytes overexpress the astrocytic glial fibrillary acidic protein (GFAP) and undergo morphological changes, becoming reactive (Sofroniew, 2009).

Astrocytes are important regulators of brain homeostasis. They directly modulate glutamatergic neurotransmission by taking up glutamate from the synaptic cleft trough highly efficient glutamate transporters (Souza et al., 2019). Astroglial glutamate transport is suggested as a main signaling trigger for glucose uptake in astrocytes (Pellerin and Magistretti, 2012). In fact, glutamate transport activation via glutamate transporter-1 (GLT-1) increases glucose metabolism *in vivo* as indexed by [^{18}F]fluorodeoxyglucose ([^{18}F]FDG) positron emission micro-tomography (microPET) (Zimmer et al., 2017). Therefore, it suggests that [^{18}F]FDG signal also reflects astrocyte metabolism, reinforcing a central participation of these glial cells in brain energy metabolism (Nortley and Attwell, 2017; Zimmer et al., 2017).

Based on this, this study is intended to evaluate the crosstalk between peripheral mediators and astrocytes during the acute phase of sepsis. We hypothesized that peripheral immune signals sent by PBMCs are capable of triggering astrocyte reactivity and, consequently, impacting brain energetic metabolism.

2. Material and Methods

2.1. Microarray data acquisition, differential gene expression (DEG) and enrichment analysis

Human blood expression datasets from 250 healthy subjects and 277 sepsis patients were obtained from the Gene Expression Omnibus repository (GEO) (http://www.ncbi.nlm.nih.gov/geo/). **Table 1** summarizes the data from the 10 selected GEO datasets used in this study. All transcriptomic analyses were implemented in an R statistical environment. Differential expression analysis was computed for each dataset independently, using the LIMMA package (Ritchie et al., 2015), and considering FDR-adjusted p-value < 0.05 as DEG criteria. Only genes significantly expressed in more than 7 datasets were included in further analyses. Hierarchical clustering of DEGs median logFC was constructed using Euclidean distance and Ward´s hierarchical agglomerative clustering criterion (Murtagh and Legendre, 2014). Finally, functional enrichment analyses of gene ontology (GO) biological processes and KEGG pathways were computed using the cluster Profiler and GOplot packages (Yu et al., 2012).

2.2. Chemicals

DNase and LY 294002 were obtained from Sigma-Aldrich (St. Louis, MO, USA). TRIzol Reagent, Dulbecco's modified Eagle's medium/F12 (DMEM/F12), and other

materials for cell culture were purchased from Gibco/Invitrogen/Thermo (Carlsbad, CA, USA). Polyclonal anti-GFAP was purchased from Dako (Carpinteria, CA, USA). Monoclonal β-actin and 4,6-diamino-2-phenylindole (DAPI) were purchased from Millipore (Billerica, MA, USA). Alexa Fluor® 488 (Amax = 493; Emax = 519) conjugated AffiniPure antibodies were purchase from Jackson ImmunoResearch (West Grove, PA, USA). L-[^{3}H]-glutamate, 2-Deoxy-D-[1,2-^{3}H]glucose ([^{3}H]2DG), nitrocellulose membrane and ECL kit were from Amersham. All other chemicals were purchased from common commercial suppliers.

2.3. Animals

Adult male Wistar rats (90 days old) were divided into two groups: sham (n = 13; bodyweight = 375 ± 36 g) and CLP (n = 14; bodyweight = 390 ± 34 g). Newborn rats (1-2 days old) were used for experimental primary astrocyte cultures (n = 40). All animals were obtained from our breeding colony (Department of Biochemistry, UFRGS, Porto Alegre, Brazil), maintained in a controlled environment (12 h light/12 h dark cycle; 22 ± 1 °C; ad libitum access to food and water). All animal experiments were performed in accordance with the National Institute of Health (NIH) Guide for the Care and Use of Laboratory Animals and the Brazilian Society for Neuroscience and Behavior recommendations for animal care. The experimental protocols were approved by the Federal University of Rio Grande do Sul Animal Care and Use Committee.

2.4. Cecal ligation and perforation (CLP) in Wistar rats

For induction of systemic inflammation, male Wistar rats were subjected to CLP as previously described (Petronilho et al., 2012). Rats were anesthetized with a mixture of ketamine and xylazine, given intraperitoneally. A 3 cm midline laparotomy was

performed to allow exposure of the cecum with the adjoining intestine. The cecum was tightly ligated with a 3.0 nylon suture at its base, below the ileocecal valve, maintaining bowel flow continuity, and was perforated once with a 14-gauge needle. The cecum was then gently squeezed to extrude a small amount of fecal material from the perforation site and then returned to the peritoneal cavity. The laparotomy was closed with 4.0 nylon sutures and the rats were returned to their cages. Animals were resuscitated with normal saline (50 ml/kg subcutaneously) immediately and 12 h after CLP. In the sham-operated group, rats were submitted to all surgical procedures but the cecum was neither ligated nor perforated. In absence of antibiotic therapy, the mortality rate in this model was 100% after 72 h. All *in vivo* and *in vitro* analyses were performed after 24 h. of CLP when there was no mortality but the animals were lethargic, presenting piloerection, diarrhea, huddling along with an increase in BBB permeability (**Supplementary Figure 1**). After surgery, no differences in food intake between groups were identified.

2.5. Micro-PET Brain Scan

Twenty-four hours after surgical induction of sepsis, the animals from each group (sham n = 13 and CLP n = 14) were individually anesthetized using a mixture of isoflurane and medical oxygen (3–4% induction dose), and injected with 0.4 mL [^{18}F]FDG (sham = 38.05 ± 1.06 MBq and CLP = 37.56 ± 1.08 MBq) in the tail vein, after overnight fasting. Then, each rat was returned to its home cage for a 40 min period of conscious (awake) *in vivo* metabolism of [^{18}F]FDG. After the uptake period, each rat was placed in a head-first prone position and scanned with the Triumph™ micro-PET [LabPET-4, TriFoil Imaging, Northridge, CA, USA, (for LabPET-4 technical information see Bergeron et al., 2014)] under inhalational anesthesia (2–3% maintenance dose). Throughout these procedures, the animals were kept on a pad heated at 37 °C. For

radiotracer readings, 10 min list mode static acquisitions were acquired with the field of view (FOV; 3.75 cm) centered on each rat's head (Zanirati et al., 2018). All data were reconstructed using the maximum likelihood estimation method (MLEM-3D) algorithm with 20 iterations. Each micro-PET image was reconstructed with a voxel size of 0.2 x 0.2 x 0.2 mm and spatially normalized into an [^{18}F]FDG template using brain normalization in PMOD v3.8 and the Fuse It Tool (PFUSEIT) (PMOD Technologies, Zurich, Switzerland). An MRI rat brain volume of interest (VOI) template was used to overlay the normalized images previously coregistered to the micro-PET image database. Activity values were normalized for the injected dose and the animal bodyweight, and were therefore expressed in standard uptake values (SUVs). Mean SUVs of 14 brain regions were extracted using a predefined VOI template. For analysis at the voxel level, MINC tools (www.bic.mni.mcgill.ca/ServicesSoftware) were used for image processing and analysis.

2.6. Metabolic networks

Metabolic brain networks of groups were constructed by computing Pearson correlation coefficients based on 10,000 bootstrap samples. Graph theoretical measures such as density, global efficiency, small-world, assortativity coefficient, average degree and average clustering coefficient were calculated for each of the bootstrap samples. Networks were corrected for multiple comparisons using false discovery rate $P < 0.005$ (Rubinov and Sporns, 2010).

2.7. Hippocampal primary astrocyte cultures and maintenance

Twenty-four hours after CLP induction, animals from both groups had their cerebral hippocampi aseptically dissected and their meninges removed. The astrocyte

cultures were performed as previously described (Bellaver et al., 2017; Bellaver et al., 2016b). During the dissection, cerebral tissue was kept in HBSS (Hank's Balanced Salt Solution) containing 0.05% trypsin and 0.003% DNase at 37 ºC for 8 min. The tissue was then mechanically dissociated for 7 min using a Pasteur pipette and centrifuged at 100 xg for 5 min. The pellet was resuspended in a solution of HBSS containing only 0.003% DNase and again gently mechanically dissociated for 5 min with a Pasteur pipette and left for decantation for 20 min. The supernatant was collected and centrifuged for 7 min. (100 xg). The cells from the supernatant were resuspended in DMEM/F12 [10% fetal bovine serum (FBS), 15 mM HEPES, 14.3 mM $NaHCO_3$, 0.04% gentamicin and 1% Fungizone®], plated in 6- or 24-well plates pre-coated with poly-L-lysine and cultured at 37 ºC in an incubator with 5% CO_2. The cells were seeded at 3–5x10^5 cells/cm^2. The same protocol was applied to cultivate astrocytes from newborn (naive) animals. The first medium exchange occurred 24 h. after obtaining cultures. During the 1st week, the change occurred once every two days and from the 2nd week on, the change occurred once every four days. From the 3rd week on, hippocampal astrocytes received the culture medium supplemented with 20% FBS. Around the 4th week, the cells reached confluence, and biochemical and molecular analyses were performed by researchers blinded for group allocation.

2.8. 2-Deoxy-D-[1,2-^{3}H] glucose ([^{3}H]2DG) uptake

After cells reached confluence, glucose was assessed as previously described (Souza et al., 2013). Briefly, cells were rinsed once with HBSS and incubated with DMEM/F12 containing only 1 mCi/ml [^{3}H]2DG (basal) or 1 mCi/ml [^{3}H]2DG + 100 μM glutamate (stimulated) for 20 min at 37 ºC. After incubation, astrocytes were rinsed with HBSS and lysed overnight with NaOH 0.3 M. Incorporated radioactivity was measured

in a scintillation counter. Cytochalasin B (10 mM) was used as a specific glucose transporter inhibitor. Glucose uptake was determined by subtracting uptake with cytochalasin B from total uptake.

2.9. Glutamate uptake

After the cells reached confluence, glutamate uptake was determined as previously described (Bellaver et al., 2016a). Briefly, astrocyte cultures were incubated at 37 °C in HBSS containing the following components (in mM): 137 NaCl, 5.36 KCl, 1.26 $CaCl_2$, 0.41 $MgSO_4$, 0.49 $MgCl_2$, 0.63 Na_2HPO_4, 0.44 KH_2PO_4, 4.17 $NaHCO_3$, and 5.6 glucose, adjusted to pH 7.4. The assay was started by the addition of 100 μM L-glutamate and 0.33 μCi/ml L-[2,3-^{3}H] glutamate. The incubation was stopped after 7 min by removing the medium and rinsing the wells twice with ice-cold HBSS. The cells were then lysed in a solution containing 0.5 M NaOH. Incorporated radioactivity was measured in a scintillation counter. Sodium-independent uptake was determined using methyl-D-glucamine instead of sodium chloride. Sodium-dependent glutamate uptake was obtained by subtracting the sodium-independent uptake from the total uptake.

2.10. High-performance liquid chromatography (HPLC) procedure

The assay was performed to measure glutamate levels in the cerebrospinal fluid (CSF) of animals 24 h. after CLP or sham surgery. Briefly, the CSF was filtered (0.22 μm pore), samples were derivatized with o-phthalaldehyde and separation was carried out with a reverse phase column (Supelcosil LC-18, 250 mm 9 4.6 mm, Supelco) in a Shimadzu Class-VP chromatography system. The mobile phase flowed at a rate of 1.4 mL/min. and column temperature was 24 °C. Buffer composition was A: 0.04 mol/L sodium dihydrogen phosphate monohydrate buffer, pH 5.5, containing 20% of methanol;

B: 0.01 mol/L sodium dihydrogen phosphate monohydrate buffer, pH 5.5, containing 80% of methanol. The gradient profile was modified according to the content of buffer B in the mobile phase: 0% for 0.00 min, 100% for 55 min, 0% for 55–60.00 min. Absorbance was read at 360 nm and 455 nm, excitation and emission respectively, with a Shimadzu fluorescence detector.

2.11. RNA extraction and quantitative RT-PCR

Total RNA was isolated from primary astrocyte cultures obtained from sham/CLP animals using TRIzol Reagent (Invitrogen, Carlsbad, CA). The concentration and purity of the RNA were determined spectrophotometrically at a ratio of 260/280. Then, 1 μg of total RNA was reverse transcribed using Applied Biosystems™ High-Capacity cDNA Reverse Transcription Kit (Applied Biosystems, Foster City, CA) in a 20 μL reaction, according to manufacturer's instructions. The mRNAs of GLT-1 and glutamate-aspartate transporter (GLAST) were quantified using a TaqMan real-time RT-PCR system with inventory primers and probes purchased from Applied Biosystems (Foster City, CA). Quantitative RT-PCR was performed in duplicate using the Applied Biosystems 7500 Fast system. No-template and no-reverse transcriptase controls were included in each assay, and these produced no detectable signal during the 40 cycles of amplification. Target mRNA levels were normalized using β-actin as a housekeeper gene. The results were expressed as fold of change of sham group using the $2^{-\Delta\Delta Ct}$ method (Livak and Schmittgen, 2001).

2.12. Western blot analysis

Hippocampal astrocytes from sham/CLP animals or PBMC CM treated animals were solubilized in lysis solution containing 4% SDS, 2-mM EDTA and 50-mM Tris-

HCl (pH 6.8). Samples were separated by SDS/PAGE (15 mg protein per sample), and transferred to nitrocellulose membranes, which were then incubated overnight (4 °C) with one of the following antibodies: anti-GFAP (1:1000), anti-GLT-1 (1:1000), anti phospho-phosphoinositide 3-kinase (PI3K) p85 (Tyr458)/p55 (Tyr199) (1:1000) or anti-β-actin (1:5000). β-actin was used as a loading control. Then, the membranes were incubated with a peroxidase-conjugated anti-rabbit or anti-mouse immunoglobulin (IgG) (1:7000) for 1 h. Chemiluminescence signals were detected in an Image Quant LAS4010 system (GE Healthcare) using an ECL kit (Souza et al., 2016b).

2.13. Immunofluorescence analysis

Immunofluorescence was performed as described previously by our group (Souza et al., 2016a). Cell cultures were fixed with 4% paraformaldehyde for 20 min and permeabilized with 0.1% Triton X-100 in PBS for 5 min at room temperature. After blocking overnight with 4% albumin, the cells were incubated overnight with anti-GFAP (1:400) at 4 ºC. Then, an incubation with a secondary antibody conjugated with Alexa Fluor® 488 for 1 h at room temperature was performed. For all the immunostaining-negative control reactions, the primary antibody was omitted. No reactivity was observed when the primary antibody was excluded. For actin-labeling analyses, the cells were incubated with 10 mg/ml rhodamine-labeled phalloidin in PBS for 45 min. Cell nuclei were stained with 0.2 mg/ml of 4',6'-diamino-2-phenylindole (DAPI) for 10 min. Astrocyte immunofluorescence was analyzed and photographed with a Nikon microscope and a TE-FM Epi-Fluorescence accessory.

2.14. Multiplex assays

Cell-free supernatants of cultivated PBMCs and serum of sham and CLP rats were assayed for the presence of the following inflammatory mediators: interleukin (IL)-1α, IL-1β, granulocyte-macrophage colony-stimulating factor (GM-CSF), granulocyte colony-stimulating factor (G-CSF), interferon gamma (INF-ɣ), IL-2, IL-4, IL-5, IL-6, IL-10, IL-12p70, IL-13, IL17A and tumor necrosis factor alpha (TNF-α). Data were collected using the ProcartaPlex Rat Th Complete Panel 14plexdetection kit (catalog number EPX140-30120-901) following the manufacturer´s instructions.

2.15. Newborn astrocyte treatments

After cells reached the confluence, 0.25 mM dibutyryl-cAMP was added for 3 days to induce GLT-1 expression. Then, astrocytes were treated with serum from CLP/sham rats (10% v/v), PBMC CM from CLP/sham rats (10% v/v) and/or 10 μM LY294002 (a PI3K inhibitor) for different periods (6 h, 24 h and 72 h).

2.16. Peripheral blood mononuclear cells isolation and culture

Fresh heparinized blood from CLP and sham animals was collected 24 h after surgery. Then, blood was gently added over an equal volume of Ficoll-Histopaque. Tubes were centrifuged for 30 min. at 400 xg at room temperature. Next, the opaque interface containing mononuclear cells was transferred into a conical centrifuge tube. PBMCs were washed (centrifuged at 100 xg for 10 min.) twice with sterile HBSS. PBMCs were plated at a density of $1x10^6$ cells/mL in a 24-well plate using RPMI-1640 medium supplemented with 10% FBS and kept for 24 h at 37 ºC in an incubator with 5% CO_2 (Shalova et al., 2015). After incubation, the supernatant was collected to perform astrocyte treatments and multiplex analyses.

2.17. Protein determination

Protein content was measured using bicinchoninic acid method with bovine serum albumin as a standard (Smith et al., 1985).

2.18. Statistical analyses

Data were expressed as mean ± standard deviation (s.d). Normality was evaluated using histograms and quantile plot. All data were normally distributed and comparisons between sham and CLP groups were carried out using Student´s t test. P-values less than 0.05 were reported as statistically significant. Networks were corrected for multiple comparisons using false discovery rate (FDR) $P < 0.005$. GraphPad Prism 6 was used for statistical analysis.

3. Results

3.1. Transcriptome analysis in blood of acute sepsis patients

Transcriptome analysis of peripheral blood cells from 250 healthy subjects and 277 sepsis patients identified a total of 746 differentially expressed genes (DEGs) between groups. Among them, 295 were upregulated and 451 downregulated (**Fig. 1a**; **Supplementary Table 1;** for log Fold change and p-values of each independent dataset, see **Supplementary Table 2** and **3**, respectively). Additionally, to verify the biological processes associated with these DEGs we performed an enrichment analysis of gene ontology (GO) biological processes (**Supplementary Table 4**). **Fig. 1b** revealed enrichment of DEGs in GO terms related to inflammatory response, energy metabolism, immune cell differentiation and RNA regulation. Top 10 enriched biological processes during sepsis are depicted in **Fig. 1c**. GO terms associated with immune response are predominant among the upregulated genes, while genes related to RNA processing are

dominant in the downregulated DEGs. Finally, to recognize the most affected pathways related to changes in transcriptome profile, we also performed an enrichment analysis using canonical pathways described in the KEGG pathway database. This revealed a significant enrichment of DEGs in four pathways in septic patients compared to healthy subjects: measles, carbon metabolism, glycolysis/gluconeogenesis and tricarboxylic acid (TCA) cycle (**Fig. 1d-h**) (for a complete list of up- and downregulated genes in each process, see **Supplementary Figure 2**). Interestingly, carbon metabolism, glycolysis/gluconeogenesis and TCA cycle are pathways associated with energy metabolism.

3.2. Acute severe systemic inflammation promotes a shift in astrocyte-mediated cerebral metabolism

Representative micro-PET studies using [^{18}F]FDG images showed widespread global [^{18}F]FDG hypometabolism in the CLP group (sham standardized uptake value (SUV) = 2.57 ± 0.38; CLP SUV = 2.07 ± 0.35; **Fig. 2a,b**). Acute sepsis induced ~20% hippocampal [^{18}F]FDG hypometabolism (**Fig. 2c**). **Fig. 2d** depicts hippocampal t-statistical map with peak effect in the posterior area (peak t_{25} = 4.53; P = 0.0007). Whole brain and hippocampal metabolism were chosen as volume of interest (VOIs, **Fig. 2e,f**). In this way, we identified whole brain (t_{25} = 3.562, P = 0.0015; **Fig. 2g**) and hippocampal [^{18}F]FDG hypometabolism (t_{25} = 3.636, P = 0.0013; **Fig. 2h**) in animals submitted to CLP. VOIs from all other analyzed brain areas are available in **Supplementary Figure 3**. Metabolic networks analyses across previously delineated VOIs were performed to identify brain reorganization patterns during acute sepsis. Sepsis changed multiple

connections within the metabolic network, promoting a metabolic hyposynchronicity, especially in hippocampal and cortical areas ($P < 0.005$, FDR corrected, **Fig. 2i-l**). Graph measures demonstrated a consistent reorganization in the brain metabolic network indexed by lower density ($P < 0.0001$, **Fig. 2m**), reduced global efficiency ($P = 0.00011$, **Fig. 2n**), assortativity ($P < 0.0001$, **Fig. 2o**), small-world ($P < 0.0001$, **Fig. 2p**), degree ($P < 0.0001$, **Fig. 2q**) and clustering coefficient ($P < 0.0001$, **Fig. 2r**) in CLP rats. Aiming to verify a potential coupling between astrocyte glucose and glutamate metabolism during sepsis, astrocyte cultures from CLP and sham rats were performed. Under basal condition, we did not observe any differences in glucose uptake in *ex vivo* astrocytes cultivated from septic rats ($t_8 = 1.148$, $P = 0.284$; **Fig. 2s**). However, when CLP astrocytes were stimulated with glutamate, we observed a tendency to decrease glucose uptake levels compared to the control ($t_8 = 1.947$, $P = 0.087$; **Fig. 2s**). Hippocampal astrocytes cultivated from CLP rats presented a significant decrease in glutamate uptake (from 1.22 to 0.78 $nmol^3$[H]/mg prot/min, $t_{20} = 3.715$, $P = 0.0014$; **Fig. 2t**). A similar decrease in glutamate uptake was observed in the hippocampal brain slices from rats submitted to surgical sepsis (**Supplementary Fig. 4**). Complementarily, no changes in glutamate levels in the CSF were verified between groups (**Fig. 2u**). Astrocytes from CLP animals presented a substantial increase in the mRNA expression levels of GLT-1 (3.4-fold; $t_6 = 4.359$, $P = 0.005$; **Fig. 2v**). On the other hand, a 2.5-fold decrease in the expression of GLAST was observed in CLP astrocytes when compared to the control group ($t_7 = 2.40$, $P = 0.047$; **Fig. 2v**). However, no changes in protein levels of GLT-1 were found ($t_6 = 0.801$, $P = 0.454$; **Fig. 2w**).

3.3. PBMC-released mediators trigger astrocyte reactivity

First, we investigated how the induction of severe systemic inflammation affect astrocytic phenotype in cultivated astrocytes at 24 h post-CLP. We did not observe any major changes in the morphology of astrocytes cultivated from CLP, compared to sham animals (**Fig. 3a,b**), but CLP astrocytes showed an intense immunostaining for GFAP (**Fig. 3c,d**). Additionally, astrocytes cultivated from septic rats presented a pronounced diffuse organization of stress fibers, when compared to the parallel and well-organized actin filaments observed in sham astrocytes (**Fig. 3e,f**). An increase in GFAP protein content was confirmed by western blotting analysis (47%; $P = 0.027$; $t_4 = 3.408$; **Fig. 3g**). Subsequently, astrocytes cultivated from healthy animals were exposed to the serum collected from CLP animals (serum pro-inflammatory cytokine activation panel is depicted in **Fig. 3h**; see the absolute values for cytokines in **Supplementary Table 5**). Interestingly, we observed a dual phase change in astrocytic glutamate uptake after CLP serum exposure. As observed in **Fig. 3i**, 6 h of septic serum treatment promoted a prominent increase in glutamate uptake (25%, $t_4 = 4.666$, $P = 0.0096$). At the 24 h time-point no changes between astrocytes treated with septic or sham serum were verified ($t_4 = 0.2972$, $P = 0.781$), while a significant decrease in glutamate uptake levels was observed after 72 h of exposure to serum from septic animals compared to sham (31%, $t_4 = 3.080$, $P = 0.036$). Consistently, glucose uptake decreased in astrocytes exposed to 72 h of serum from septic animals (18%, $t_5 = 2.926$, $P = 0.032$; **Fig. 3j**), mimicking our *in vivo* data. We further analyzed the involvement of PBMC mediators in the activation and shift of astrocyte functions. Conditioned medium collected from PBMCs (PBMC CM), previously isolated from septic or sham animals, was used to treat astrocytes. Cytokine analysis of PBMC CM pool from septic rats revealed an increase in TNF-α (42%) and IL-10 (15%) and a decrease in G-CSF levels (from 10.02 pg/μl to undetectable) compared

to sham (**Fig. 3k**). In this way, 72 h of sepsis-activated PBMC CM exposure induced astrocyte reactivity, evidenced by a 2.3-fold increase in the GFAP protein levels (**Fig. 3l**). Also, a significant decrease in glutamate uptake levels was observed in astrocytes treated with PBMC CM from septic animals ($t_7 = 4.178$, $P = 0.0041$; **Fig. 3m**), despite no changes in GLT-1 protein expression ($t_6 = 0.827$, $P = 0.004$; **Fig. 3n**). Additionally, astrocytes exposed to sepsis PBMC CM also showed a prominent decrease in glucose uptake ($t_6 = 4.540$, $P = 0.0039$; **Fig. 3o**). Corroborating the observations after serum exposure, 24 h of sepsis PBMC CM treatment did not significantly change either glutamate or glucose uptake levels compared to the control conditions (**Supplementary Figure 5**). Of note, no significant changes were verified in cell viability after serum or PBMC CM treatments at the time point evaluated in this study (**Supplementary Figure 6**). In an attempt to understand the mechanism involved in the astrocytic energetic failure promoted by PBMC mediators, we looked for a potential target among the DEGs found in our transcriptomic analysis. In this sense, we observed a downregulation in two PI3K subunit genes (PIK3C2B and PIK3CD; **Supplementary Table 1**) along with an upregulation of PTEN (**Supplementary Table 1**), an important PI3K negative regulator, in septic patients. Based on the evident impairment in the PI3K pathway observed in our transcriptomic analysis and the putative role that this route plays in the management of energetic metabolism, including in glycolysis/gluconeogenesis, we decided to investigate this pathway in our animal model. In this regard, we verified a significant decrease in PI3K phosphorylation in astrocyte cultures exposed to PBMC CM from CLP animals (46%, $t_8 = 4.216$, $P = 0.003$; **Fig. 3p**). The specific inhibition of PI3K pathway by LY294002 (10 μM) presented a detrimental effect in astrocytes treated with PBMC CM from sham animals, while it exacerbated the decrease observed in glutamate uptake

in astrocytes treated with CLP PBMC CM (about 30%, **Fig. 3q**). Interestingly, LY294002 treatment did not significantly affect glucose uptake levels (**Fig. 3r**).

4. Discussion

In the present report we described a potential link between peripheral factors and central metabolic failure during the acute phase of a systemic and severe inflammatory episode. We first showed, through a data-driven gene transcription analysis, that pathways related to energy metabolism are the main altered features in the blood of patients during the acute phase of sepsis. Then, in a rat model of sepsis we observed widespread brain energetic abnormalities, including glucose hypometabolism, lower glutamate uptake and astrocyte reactivity. Also, we provided, to the best of our knowledge, the first evidence of mediators released by PBMCs directly promoting astrocyte reactivity during sepsis, in a microglia-independent manner. Finally, by inhibiting PI3K signaling we exacerbated astrocyte dysfunctional glutamate uptake in both sham and CLP groups.

Data-driven transcriptome analysis of blood cells indicated multiple changes in energy metabolism pathways as main features among septic patients. More specifically, we found DEGs overrepresented in carbon metabolism, glycolysis/gluconeogeonesis and TCA pathways, indicating a clear impairment in glucose metabolism-related genes. Interestingly, GO terms associated with inflammatory processes were enriched in septic patients but this was not observed in inflammatory KEGG pathways. Our findings associating sepsis-activated PBMCs with peripheral energy metabolism dysfunction

motivated us to investigate brain energetics. Since astrocytes are the main glucose handlers in the brain, we decided to assess their functionality during acute sepsis.

Interestingly, we found that the energetic crisis observed in the blood of septic patients was also present in the brains of our CLP rat model. More specifically, we identified widespread brain glucose hypometabolism, as indexed by [^{18}F]FDG PET, in CLP rats. In clinical settings, [^{18}F]FDG PET is considered a biomarker of synaptic dysfunction and its values are associated with cognitive impairment (Gardener et al., 2016; Pagani et al., 2015; Weise et al., 2018). Not surprisingly, sepsis has been associated with increased risk for developing dementia (Chou et al., 2017; Cunningham and Hennessy, 2015). Our [^{18}F]FDG PET regional analysis demonstrated hypometabolism in several brain regions, including the hippocampus. Semmler et al. previously demonstrated [^{18}F]FDG hypometabolism in a lipopolysaccharide (LPS) model of acute sepsis. However, no changes in hippocampal [^{18}F]FDG PET metabolism were observed in their study (Semmler et al., 2008). Human hippocampi are extremely vulnerable to sepsis, as indexed by hippocampal atrophy in sepsis patients (Semmler et al., 2013). Based on this, one could argue that the CLP model resembles human sepsis with more accuracy than the LPS injection model (Lee and Huttemann, 2014). In addition, by using refined network analysis, we demonstrated that region-to-region communication in the CLP rat model is largely disrupted. Metabolic network is hyposynchronic in the CLP group and graph measures revealed that brain regions, including the hippocampus, are exchanging information less efficiently.

A recent report demonstrated that glutamate and glucose uptake by astrocytes are coupled, as indexed by [^{18}F]FDG signal, which suggests that the [^{18}F]FDG signal also reflects astrocyte metabolism (Zimmer et al., 2017). However, cellular interpretation of

[^{18}F]FDG is still under discussion and we cannot exclude neuronal participation in [^{18}F]FDG hypometabolism induced by sepsis. For testing this hypothesis, we then evaluated glucose and glutamate uptake *ex vivo* in astrocytes obtained from CLP rats. Interestingly, we did not observe changes in basal glucose uptake between groups. In fact, it seems that the long incubation period required for cultivating mature astrocytes (3-4 weeks) allows them to adapt to environmental conditions, such as high availability of glucose and other nutrients present in the medium. However, we noticed a tendency of lower glucose uptake in CLP astrocytes stimulated with glutamate, which suggests that these cells still preserved a septic phenotype. Next, we identified that astrocyte glutamate uptake is reduced during acute sepsis but no changes in GLT-1 density, the main glutamate astrocyte transporter (Anderson and Swanson, 2000), were observed. Interestingly, we found increased GLT-1 mRNA expression in CLP astrocytes. Here, we hypothesize that GLT-1 could be either internalized or have its activity reduced, which could explain the lack of changes in transporter density despite reduced glutamate uptake. Also, the 3-fold increase in GLT-1 mRNA suggests that CLP astrocytes are unsuccessfully attempting to replace defective transporters, likely due to the decreased ribosomal protein translation, a process already related to the detrimental effects of sepsis (Hato et al., 2019).

It has been well established that astrocytes are activated during inflammation. Reactive astrocytes overexpress GFAP and release a range of inflammatory cytokines and chemokines (Brahmachari et al., 2006; Gorina et al., 2009). Here we demonstrated PBMC-released factors driving astrocyte reactivity. Serum from CLP animals presented increased levels of pro-inflammatory cytokines, as IL-1β, IL-12p70, IFN-ɣ and TNF-α, compared to sham rats. Interestingly, PBMC CM activation was much more subtle

(increased TNF-α and IL-10 and decreased G-CSF levels). Indeed, it has been previously demonstrated that even a slight increase in brain TNF-α levels is able to promote a decrease in glutamate transporter activity (Clark and Vissel, 2016), corroborating the deficient glutamate transport observed in our model. In addition, mice lacking TNF-α type 1 receptors had memory preservation after CLP induction (Calsavara et al., 2015). From that, one could argue that astrocyte energy crisis during sepsis seems to be independent of other canonical inflammatory mediators, such as IL-1β and IFN-ɣ. However, more studies are required to determine if IL-10 and G-CSF actively play a role in astrocyte activation during sepsis. Of note, we measured only a limited variety of cytokines/chemokines present in the PBMC CM. It is possible that factors not evaluated here are also important for promoting astrocyte reactivity.

The mechanisms involved in the regulation of cerebral energy metabolism during sepsis are poorly understood. The downregulation of PI3K identified in our transcriptome analysis was also observed in astrocytes treated with PBMC CM from CLP rats. Trying to mimic sepsis-induced abnormalities in glutamate and glucose metabolism we conducted a pharmacological inhibition of PI3K in cultured astrocytes. The pharmacological inhibition of PI3K reduced astrocytic glutamate uptake in PBMC CM treated sham and CLP astrocytes. In fact, Zhang et al., also observed that the activation of PI3K signaling increases glutamate uptake by upregulating GLT-1 (Zhang et al., 2013). Additionally, it has been demonstrated that the inhibition of PI3K signaling decreases survival between animals submitted to CLP as well as promotes an early and more severe onset of sepsis (Wrann et al., 2007). The inhibition of PI3K pathway has also been shown to enhance LPS-induced inflammation in different cell types (Guha and Mackman, 2002). Controversially, the inhibition of PI3K did not affect glucose uptake in sham or CLP rats

treated with PBMC CM. Based on that, one could argue that PI3K is involved in sepsis-induced glutamate abnormalities but not in mediating glucose hypometabolism, thus inhibiting the signaling at the level of PI3K uncoupled glutamate and glucose metabolism in astrocytes. In this sense, other molecular energy sensors, such as the AMP-activated protein kinase (AMPK), might be acting in parallel with PI3K signaling to regulate glucose uptake (Domise and Vingtdeux, 2016). However, further investigations are needed to completely decode this complex regulation.

Taken together, our results pointed to PBMCs as important triggers of astrocyte reactivity, metabolic and energetic dysfunction during the early stage of sepsis. In addition, we demonstrated that impaired PI3K signaling drives glutamate abnormalities but not glucose hypometabolism during acute sepsis. In summary, this report improves the understanding of the mechanisms by which systemic inflammation impacts brain functionality, indicating potential targets for therapeutic modulation.

5. Data Availability

Datasets used in this study can be accessed via NCBI GEO portal (https://www.ncbi.nlm.nih.gov/geo/). Further intermediate data and codes generated to implement the MRCMap adaptation are available from the corresponding author upon request.

6. Conflict of interest

The authors declare there are no conflicts of interest.

7. Funding sources

ERZ receives financial support from CAPES [88881.141186/2017-01], CNPq [460172/2014-0], PRONEX, FAPERGS/CNPq [16/2551-0000475-7], Brazilian National Institute of Science and Technology in Excitotoxicity and Neuroprotection [465671/2014-4],FAPERGS/MS/CNPq/SESRS– PPSUS [30786.434.24734.23112017].

8. References

Anderson, C.M., Swanson, R.A., 2000. Astrocyte glutamate transport: review of properties, regulation, and physiological functions. Glia 32, 1-14.
Bellaver, B., Bobermin, L.D., Souza, D.G., Rodrigues, M.D., de Assis, A.M., Wajner, M., Goncalves, C.A., Souza, D.O., Quincozes-Santos, A., 2016a. Signaling mechanisms underlying the glioprotective effects of resveratrol against mitochondrial dysfunction. Biochim Biophys Acta 1862, 1827-1838.
Bellaver, B., Dos Santos, J.P., Leffa, D.T., Bobermin, L.D., Roppa, P.H.A., da Silva Torres, I.L., Goncalves, C.A., Souza, D.O., Quincozes-Santos, A., 2017. Systemic Inflammation as a Driver of Brain Injury: the Astrocyte as an Emerging Player. Mol Neurobiol.
Bellaver, B., Souza, D.G., Souza, D.O., Quincozes-Santos, A., 2016b. Hippocampal Astrocyte Cultures from Adult and Aged Rats Reproduce Changes in Glial Functionality Observed in the Aging Brain. Mol Neurobiol.
Bergeron, M., Cadorette, J., Tetrault, M.A., Beaudoin, J.F., Leroux, J.D., Fontaine, R., Lecomte, R., 2014. Imaging performance of LabPET APD-based digital PET scanners for pre-clinical research. Physics in medicine and biology 59, 661-678.
Brahmachari, S., Fung, Y.K., Pahan, K., 2006. Induction of glial fibrillary acidic protein expression in astrocytes by nitric oxide. J Neurosci 26, 4930-4939.
Calsavara, A.C., Soriani, F.M., Vieira, L.Q., Costa, P.A., Rachid, M.A., Teixeira, A.L., 2015. TNFR1 absence protects against memory deficit induced by sepsis possibly through over-expression of hippocampal BDNF. Metabolic brain disease 30, 669-678.
Chou, C.H., Lee, J.T., Lin, C.C., Sung, Y.F., Lin, C.C., Muo, C.H., Yang, F.C., Wen, C.P., Wang, I.K., Kao, C.H., Hsu, C.Y., Tseng, C.H., 2017. Septicemia is associated with increased risk for dementia: a population-based longitudinal study. Oncotarget 8, 84300-84308.
Clark, I.A., Vissel, B., 2016. Excess cerebral TNF causing glutamate excitotoxicity rationalizes treatment of neurodegenerative diseases and neurogenic pain by anti-TNF agents. Journal of neuroinflammation 13, 236.
Cunningham, C., Hennessy, E., 2015. Co-morbidity and systemic inflammation as drivers of cognitive decline: new experimental models adopting a broader paradigm in dementia research. Alzheimer's research & therapy 7, 33.
Domise, M., Vingtdeux, V., 2016. AMPK in Neurodegenerative Diseases. Experientia supplementum (2012) 107, 153-177.

Gardener, S.L., Sohrabi, H.R., Shen, K.K., Rainey-Smith, S.R., Weinborn, M., Bates, K.A., Shah, T., Foster, J.K., Lenzo, N., Salvado, O., Laske, C., Laws, S.M., Taddei, K., Verdile, G., Martins, R.N., 2016. Cerebral Glucose Metabolism is Associated with Verbal but not Visual Memory Performance in Community-Dwelling Older Adults. J Alzheimers Dis 52, 661-672.
Godini, R., Fallahi, H., 2018. Network analysis of inflammatory responses to sepsis by neutrophils and peripheral blood mononuclear cells 13, e0201674.
Gorina, R., Santalucia, T., Petegnief, V., Ejarque-Ortiz, A., Saura, J., Planas, A.M., 2009. Astrocytes are very sensitive to develop innate immune responses to lipid-carried short interfering RNA. Glia 57, 93-107.
Guha, M., Mackman, N., 2002. The phosphatidylinositol 3-kinase-Akt pathway limits lipopolysaccharide activation of signaling pathways and expression of inflammatory mediators in human monocytic cells. The Journal of biological chemistry 277, 32124-32132.
Hato, T., Maier, B., Syed, F., Myslinski, J., Zollman, A., Plotkin, Z., Eadon, M.T., Dagher, P.C., 2019. Bacterial sepsis triggers an antiviral response that causes translation shutdown. The Journal of clinical investigation 129, 296-309.
Horng, S., Therattil, A., Moyon, S., Gordon, A., Kim, K., Argaw, A.T., Hara, Y., Mariani, J.N., Sawai, S., Flodby, P., Crandall, E.D., Borok, Z., Sofroniew, M.V., Chapouly, C., John, G.R., 2017. Astrocytic tight junctions control inflammatory CNS lesion pathogenesis. J Clin Invest 127, 3136-3151.
Iwashyna, T.J., Ely, E.W., Smith, D.M., Langa, K.M., 2010. Long-term cognitive impairment and functional disability among survivors of severe sepsis. Jama 304, 1787-1794.
Kyrkanides, S., Miller, A.W., Miller, J.N., Tallents, R.H., Brouxhon, S.M., Olschowka, M.E., O'Banion, M.K., Olschowka, J.A., 2008. Peripheral blood mononuclear cell infiltration and neuroinflammation in the HexB-/- mouse model of neurodegeneration. J Neuroimmunol 203, 50-57.
Lee, I., Huttemann, M., 2014. Energy crisis: the role of oxidative phosphorylation in acute inflammation and sepsis. Biochim Biophys Acta 1842, 1579-1586.
Livak, K.J., Schmittgen, T.D., 2001. Analysis of relative gene expression data using real-time quantitative PCR and the 2(-Delta Delta C(T)) Method. Methods (San Diego, Calif.) 25, 402-408.
Michels, M., Steckert, A.V., Quevedo, J., Barichello, T., Dal-Pizzol, F., 2015. Mechanisms of long-term cognitive dysfunction of sepsis: from blood-borne leukocytes to glial cells. Intensive care medicine experimental 3, 30.
Murtagh, F., Legendre, P., 2014. Ward's Hierarchical Agglomerative Clustering Method: Which Algorithms Implement Ward's Criterion? Journal of Classification 31, 274-295.
Nortley, R., Attwell, D., 2017. Control of brain energy supply by astrocytes. Curr Opin Neurobiol 47, 80-85.
Pagani, M., De Carli, F., Morbelli, S., Oberg, J., Chincarini, A., Frisoni, G.B., Galluzzi, S., Perneczky, R., Drzezga, A., van Berckel, B.N., Ossenkoppele, R., Didic, M., Guedj, E., Brugnolo, A., Picco, A., Arnaldi, D., Ferrara, M., Buschiazzo, A., Sambuceti, G., Nobili, F., 2015. Volume of interest-based [18F]fluorodeoxyglucose PET discriminates MCI converting to Alzheimer's disease from healthy controls. A European Alzheimer's Disease Consortium (EADC) study. NeuroImage. Clinical 7, 34-42.

Pellerin, L., Magistretti, P.J., 2012. Sweet sixteen for ANLS. J Cereb Blood Flow Metab 32, 1152-1166.
Petronilho, F., Perico, S.R., Vuolo, F., Mina, F., Constantino, L., Comim, C.M., Quevedo, J., Souza, D.O., Dal-Pizzol, F., 2012. Protective effects of guanosine against sepsis-induced damage in rat brain and cognitive impairment. Brain Behav Immun 26, 904-910.
Ransohoff, R.M., Schafer, D., Vincent, A., Blachere, N.E., Bar-Or, A., 2015. Neuroinflammation: Ways in Which the Immune System Affects the Brain. Neurotherapeutics : the journal of the American Society for Experimental NeuroTherapeutics 12, 896-909.
Richards, M.H., Narasipura, S.D., Kim, S., Seaton, M.S., Lutgen, V., Al-Harthi, L., 2015. Dynamic interaction between astrocytes and infiltrating PBMCs in context of neuroAIDS. Glia 63, 441-451.
Ritchie, M.E., Phipson, B., Wu, D., Hu, Y., Law, C.W., Shi, W., Smyth, G.K., 2015. limma powers differential expression analyses for RNA-sequencing and microarray studies. Nucleic acids research 43, e47.
Rubinov, M., Sporns, O., 2010. Complex network measures of brain connectivity: uses and interpretations. NeuroImage 52, 1059-1069.
Semmler, A., Hermann, S., Mormann, F., Weberpals, M., Paxian, S.A., Okulla, T., Schafers, M., Kummer, M.P., Klockgether, T., Heneka, M.T., 2008. Sepsis causes neuroinflammation and concomitant decrease of cerebral metabolism. Journal of neuroinflammation 5, 38.
Semmler, A., Widmann, C.N., Okulla, T., Urbach, H., Kaiser, M., Widman, G., Mormann, F., Weide, J., Fliessbach, K., Hoeft, A., Jessen, F., Putensen, C., Heneka, M.T., 2013. Persistent cognitive impairment, hippocampal atrophy and EEG changes in sepsis survivors. Journal of neurology, neurosurgery, and psychiatry 84, 62-69.
Shalova, I.N., Lim, J.Y., Chittezhath, M., Zinkernagel, A.S., Beasley, F., Hernandez-Jimenez, E., Toledano, V., Cubillos-Zapata, C., Rapisarda, A., Chen, J., Duan, K., Yang, H., Poidinger, M., Melillo, G., Nizet, V., Arnalich, F., Lopez-Collazo, E., Biswas, S.K., 2015. Human monocytes undergo functional re-programming during sepsis mediated by hypoxia-inducible factor-1alpha. Immunity 42, 484-498.
Smith, P.K., Krohn, R.I., Hermanson, G.T., Mallia, A.K., Gartner, F.H., Provenzano, M.D., Fujimoto, E.K., Goeke, N.M., Olson, B.J., Klenk, D.C., 1985. Measurement of protein using bicinchoninic acid. Analytical biochemistry 150, 76-85.
Sofroniew, M.V., 2009. Molecular dissection of reactive astrogliosis and glial scar formation. Trends Neurosci 32, 638-647.
Souza, D.G., Almeida, R.F., Souza, D.O., Zimmer, E.R., 2019. The astrocyte biochemistry. Seminars in cell & developmental biology.
Souza, D.G., Bellaver, B., Bobermin, L.D., Souza, D.O., Quincozes-Santos, A., 2016a. Anti-aging effects of guanosine in glial cells. Purinergic Signal.
Souza, D.G., Bellaver, B., Hansel, G., Arus, B.A., Bellaver, G., Longoni, A., Kolling, J., Wyse, A.T., Souza, D.O., Quincozes-Santos, A., 2016b. Characterization of Amino Acid Profile and Enzymatic Activity in Adult Rat Astrocyte Cultures. Neurochem Res 41, 1578-1586.
Souza, D.G., Bellaver, B., Souza, D.O., Quincozes-Santos, A., 2013. Characterization of adult rat astrocyte cutures. PLoS One 8, E60282.

Tang, B.M., McLean, A.S., Dawes, I.W., Huang, S.J., Lin, R.C., 2009. Gene-expression profiling of peripheral blood mononuclear cells in sepsis. Critical care medicine 37, 882-888.
Weise, C.M., Chen, K., Chen, Y., Kuang, X., Savage, C.R., Reiman, E.M., 2018. Left lateralized cerebral glucose metabolism declines in amyloid-beta positive persons with mild cognitive impairment. NeuroImage. Clinical 20, 286-296.
Wrann, C.D., Tabriz, N.A., Barkhausen, T., Klos, A., van Griensven, M., Pape, H.C., Kendoff, D.O., Guo, R., Ward, P.A., Krettek, C., Riedemann, N.C., 2007. The phosphatidylinositol 3-kinase signaling pathway exerts protective effects during sepsis by controlling C5a-mediated activation of innate immune functions. J Immunol 178, 5940-5948.
Young, G.B., 2010. Sparing brain damage in severe sepsis: a beginning. Critical care (London, England) 14, 159.
Yu, G., Wang, L.G., Han, Y., He, Q.Y., 2012. clusterProfiler: an R package for comparing biological themes among gene clusters. Omics : a journal of integrative biology 16, 284-287.
Zanirati, G., Azevedo, P.N., Venturin, G.T., Greggio, S., Alcara, A.M., Zimmer, E.R., Feltes, P.K., DaCosta, J.C., 2018. Depression comorbidity in epileptic rats is related to brain glucose hypometabolism and hypersynchronicity in the metabolic network architecture. Epilepsia 59, 923-934.
Zhang, X., Shi, M., Bjoras, M., Wang, W., Zhang, G., Han, J., Liu, Z., Zhang, Y., Wang, B., Chen, J., Zhu, Y., Xiong, L., Zhao, G., 2013. Ginsenoside Rd promotes glutamate clearance by up-regulating glial glutamate transporter GLT-1 via PI3K/AKT and ERK1/2 pathways. Frontiers in pharmacology 4, 152.
Ziaja, M., 2013. Septic encephalopathy. Current neurology and neuroscience reports 13, 383.
Zimmer, E.R., Parent, M.J., Souza, D.G., Leuzy, A., Lecrux, C., Kim, H.I., Gauthier, S., Pellerin, L., Hamel, E., 2017. [18F]FDG PET signal is driven by astroglial glutamate transport.

Figure legends

Figure 1. Transcriptome analyses of blood cells from sepsis patients. The analysis of 10 datasets available on online repositories show differentially expressed genes (DEGs) (a), gene ontology (GO) network (b), the top 10 GO terms up- and downregulated (c) and the enriched KEGG pathways (d-g) and their respective p-value and q-value (h). Only DEGs found in more than 7 datasets were included. In the network, node colors represent the summarized up/downregulation state of the term, while edge widths represent the number of common genes between two terms, summarized in the Jaccard coefficient.

Figure 2. Astrocytic glucose and glutamate metabolism. Whole-brain [^{18}F]FDG uptake of sham (a) and CLP (b) animals. Percentage of change between sham and CLP (c). T-statistical map overlaid on histological template (d). Brain mask showing VOIs overlaid on histological template (e,f). Whole brain (g) and hippocampal (h) [^{18}F]FDG uptake. Cross-correlation matrices: intersubject cross-correlation maps displaying region-to-region associations in sham (i) and CLP (j) rats. Metabolic networks: 3D brain surfaces displaying large-scale metabolic cross-correlation maps in sham (k) and in CLP (l) animals. Metabolic network graph measures of global efficiency (m), assortativity (n), average degree (o), average clustering (p), density (q) and small world (r). Glucose uptake in astrocytes cultivated from sham and CLP rats (s) Glutamate uptake in astrocytes cultivated from sham and CLP rats (t). Glutamate levels in the CSF (u). GLT-1 and GLAST mRNA levels (v) and immunocontent in astrocytes cultivated from sham and CLP rats (w). Cumulative frequencies are depicted in the upper left of graph measures (m-r). n = 5-14 rats per group. *P < 0.05, **P < 0.01, ***P < 0.001 (t test). Data are

presented as mean values ± s.d. and individual scatter plots or as correlation values with FDR-corrected ($P < 0.005$) thresholds for brain networks.

Figure 3. PBMC released mediators trigger astrocyte activation. Phase contrast (a,b), GFAP immunostaining (c,d) and actin cytoskeleton (e,f) and western blotting for GFAP (g) of astrocytes cultivated from sham and CLP rats. Cytokine profile of serum from sham/CLP rats (h). Glutamate uptake of astrocytes treated with 10% serum from sham/CLP animals for 6 h, 24 h and 72 h (i). Glucose uptake of astrocytes treated with 10% serum from sham/CLP animals for 72 h (j). Cytokine profile of PBMC CM from sham/CLP rats (k). Western blotting for GFAP (l), glutamate (m) and glucose uptake (n) of astrocytes treated with 10% PBMC CM from sham/CLP animals for 72 h Western blotting for p-PI3K of astrocytes treated with 10% PBMC CM from sham/CLP animals for 72 h (o). Glutamate (q) and glucose uptake (r) by astrocytes pre-treated with 10% PBMC CM from sham/CLP rats and/or 10 μM LY 294002. n = 4-6 per group. *$P < 0.05$, **$P < 0.01$ (t test). Data are presented as mean values ± s.d. and individual scatter plots.

Table 1

GEO ID	Description	Sample (n)	Reference
GSE95233	Gene expression data of whole blood collected from patients at day 1 of sepsis and from healthy subjects	Whole blood from septic patients (n=51) Whole blood from healthy subjects (n=22)	(Venet et al., 2017)
GSE49757	Gene expression data of polymorphonuclear neutrophils collected from septic patients in the first admission at hospital and from healthy subjects	Polymorphonuclear neutrophils from septic patients (n=35) Polymorphonuclear neutrophils from healthy subjects (n=19)	Not published
GSE67652	Gene expression data of polymorphonuclear neutrophils collected from septic patients and from healthy subjects with paired age	Polymorphonuclear neutrophils from septic patients (n=6) Polymorphonuclear neutrophils from healthy subjects (n=6)	(Vieira da Silva Pellegrina et al., 2015)
GSE57065	Gene expression data of whole blood collected from patients 24 h after septic shock and from healthy subjects	Whole blood from septic patients (n=28) Whole blood from healthy subjects (n=25)	(Cazalis et al., 2014)
GSE54514	Gene expression data of whole blood collected from patients at day 1 of sepsis and from healthy subjects	Whole blood from septic patients (n=26) Whole blood from healthy subjects (n=18)	(Parnell et al., 2013)

GSE32707	Gene expression data of whole blood collected from septic patients in the first admission at hospital and from healthy subjects	Whole blood from septic patients (n=34) Whole blood from healthy subjects (n=38)	(Dolinay et al., 2012)
GSE28750	Gene expression data of polymorphonuclear neutrophils collected from septic patients in the first admission at hospital and from healthy subjects	Polymorphonuclear neutrophils from septic patients (n=27) Polymorphonuclear neutrophils from healthy subjects (n=20)	(Sutherland et al., 2011)
GSE13015	Gene expression data of whole blood collected from septic patients and healthy subjects	Whole blood from septic patients (n=31) Whole blood from healthy subjects (n=29)	(Pankla et al., 2009)
GSE69063	Gene expression data of whole blood collected from septic patients and healthy subjects	Whole blood from septic patients (n=33) Whole blood from healthy subjects (n=57)	Not published
GSE46955	Gene expression data of monocytes collected from septic patients in the first admission at hospital and from healthy subjects	Monocytes from septic patients (n=6) Monocytes from healthy subjects (n=16)	(Shalova et al., 2015)

a)

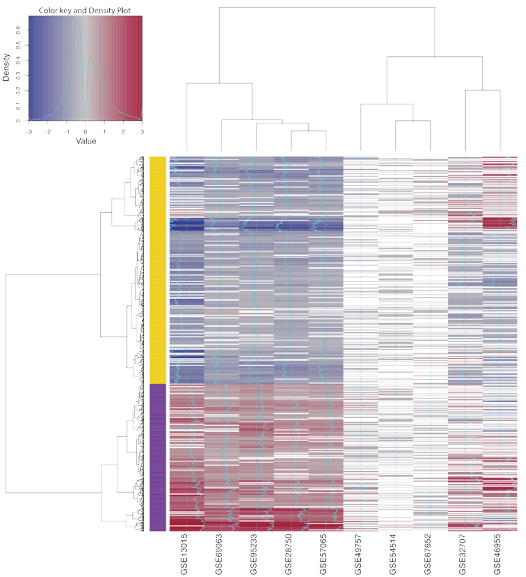

b)

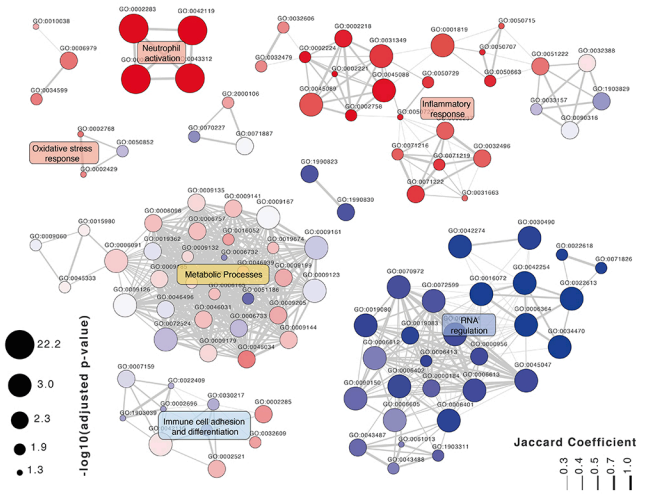

c)

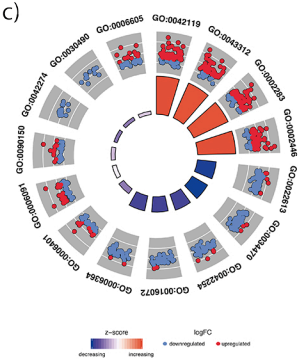

ID	Description
GO:0042119	neutrophil activation
GO:0043312	neutrophil degranulation
GO:0002283	neutrophil activation involved in immune response
GO:0002446	neutrophil mediated immunity
GO:0022613	ribonucleoprotein complex biogenesis
GO:0034470	ncRNA processing
GO:0042254	ribosome biogenesis
GO:0016072	rRNA metabolic process
GO:0006364	rRNA processing
GO:0006401	RNA catabolic process
GO:0006091	generation of precursor metabolites and energy
GO:0090150	establishment of protein localization to membrane
GO:0042274	ribosomal small subunit biogenesis
GO:0030490	maturation of SSU-rRNA
GO:0006605	protein targeting

d)

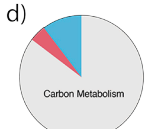

e)

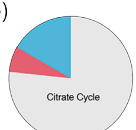

f)

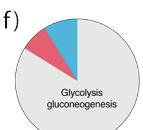

g)

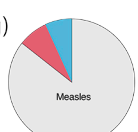

h)

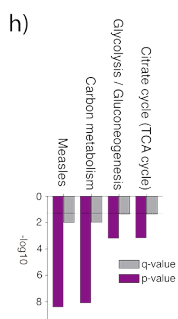

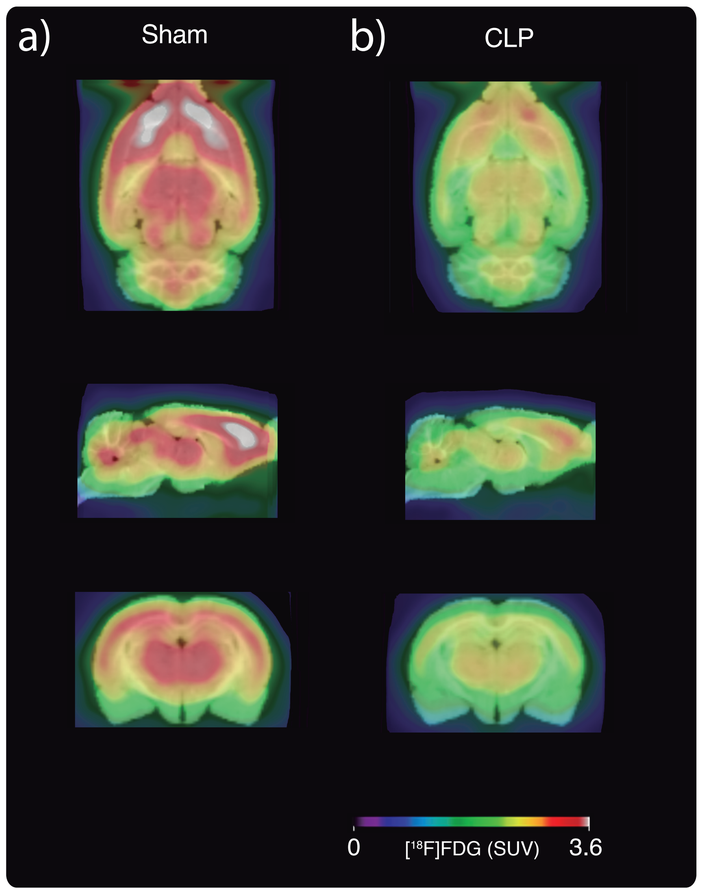
a)
Sham
b)
CLP
0
[18F]FDG (SUV)
3.6

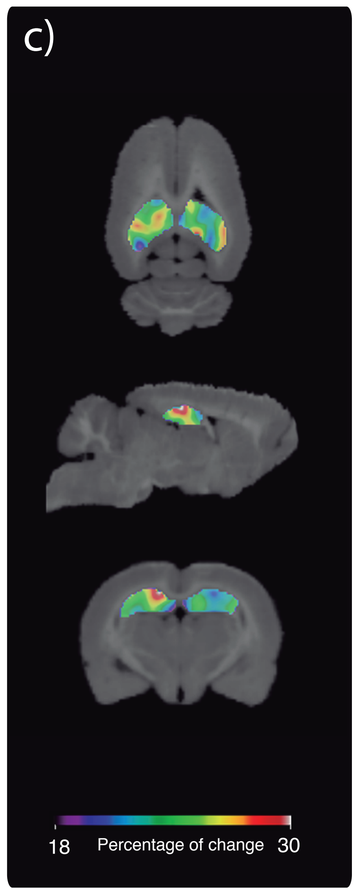
c)
18
Percentage of change
30

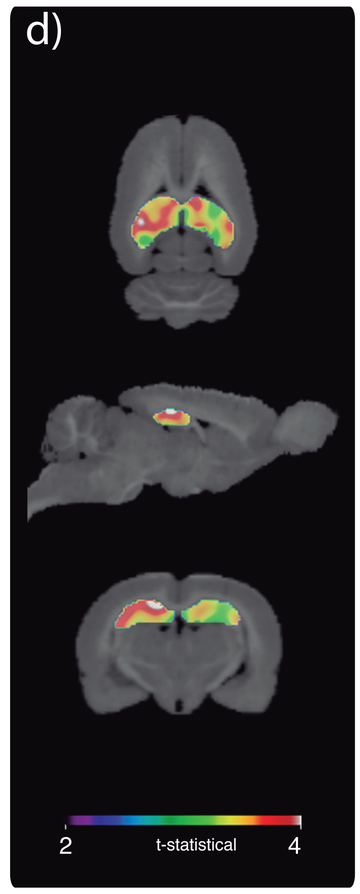
d)
2
t-statistical
4

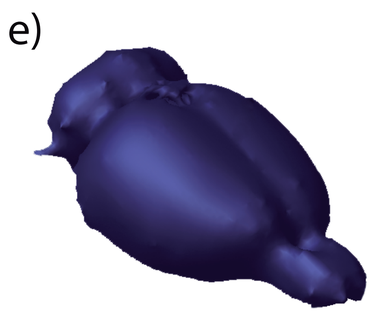
e)

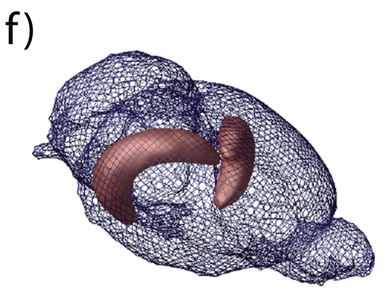
f)

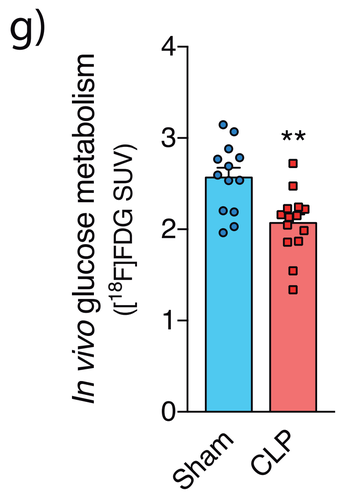
g)
In vivo glucose metabolism
([18F]FDG SUV)
Sham
CLP
**

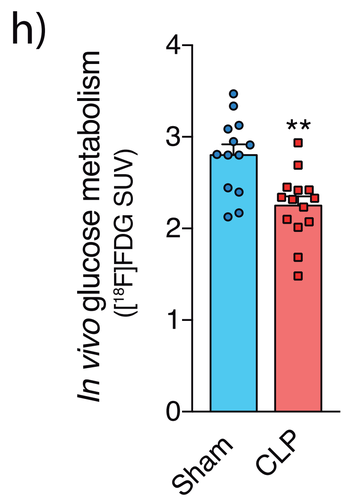
h)
In vivo glucose metabolism
([18F]FDG SUV)
Sham
CLP
**

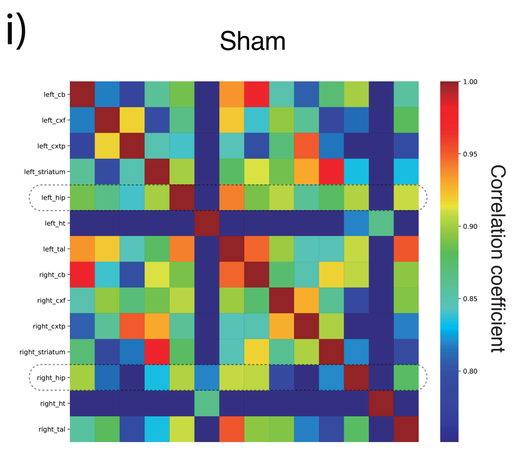
i)
Sham
Correlation coefficient

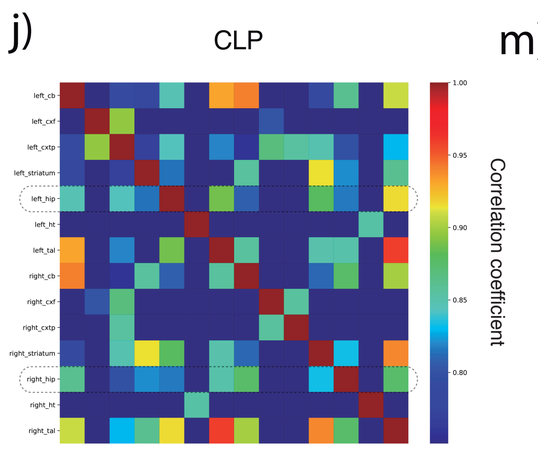
j)
CLP
Correlation coefficient

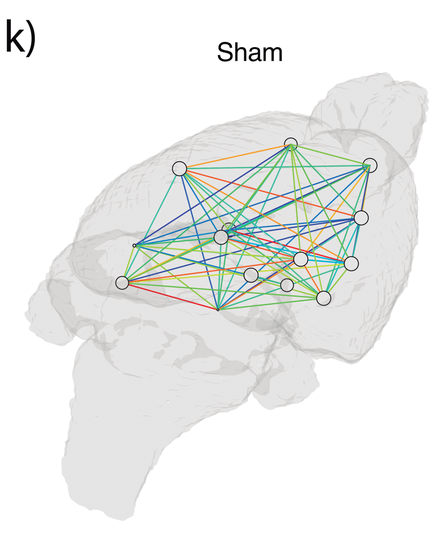
k)
Sham

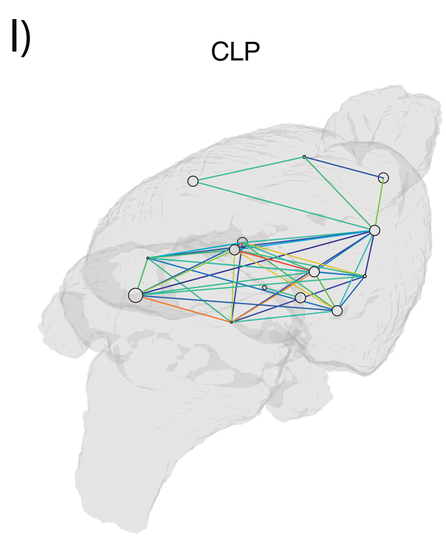
l)
CLP

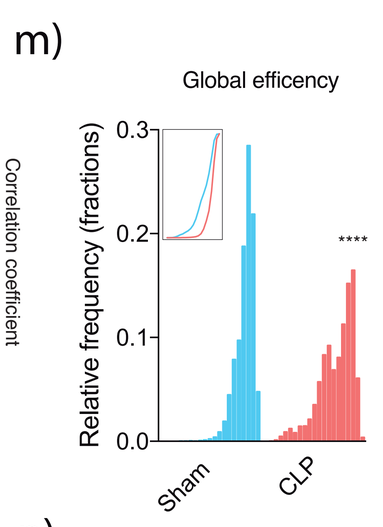
m)
Global efficency
Relative frequency (fractions)
Sham
CLP
****

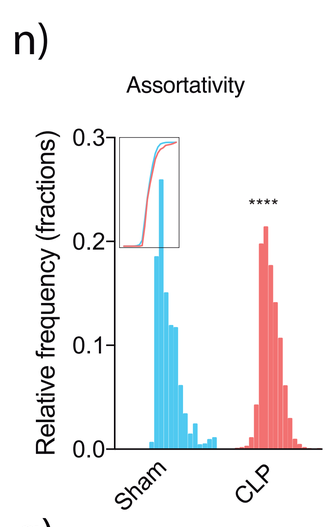
n)
Assortativity
Relative frequency (fractions)
Sham
CLP
****

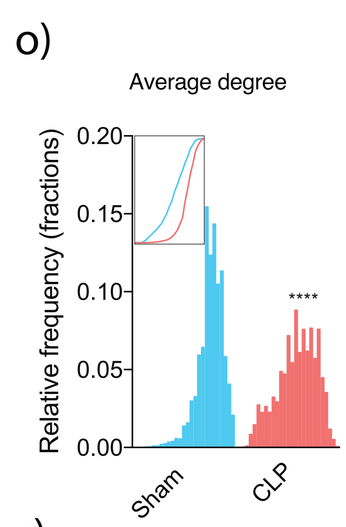
o)
Average degree
Relative frequency (fractions)
Sham
CLP
****

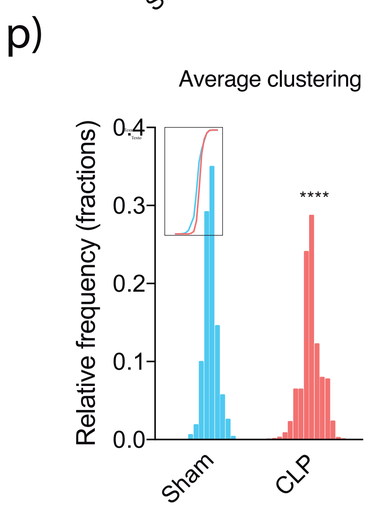
p)
Average clustering
Relative frequency (fractions)
Sham
CLP
****

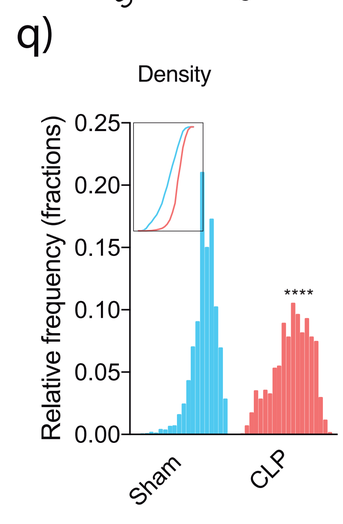
q)
Density
Relative frequency (fractions)
Sham
CLP
****

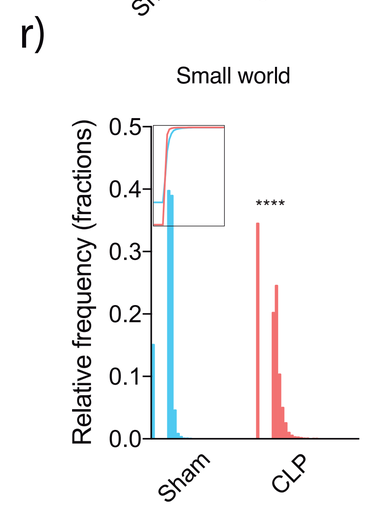
r)
Small world
Relative frequency (fractions)
Sham
CLP
****

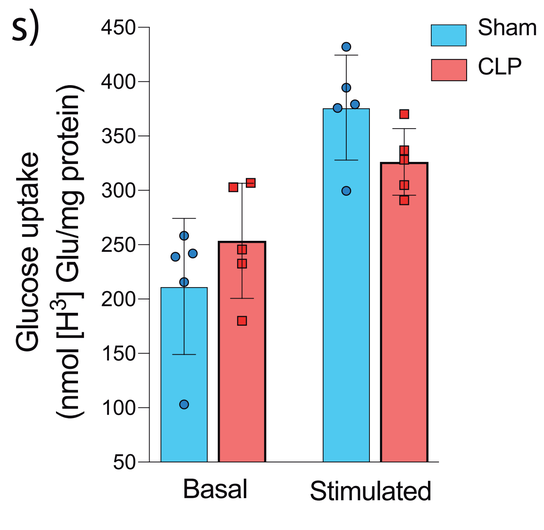
s)
Glucose uptake
(nmol [H3] Glu/mg protein)
Sham
CLP
Basal
Stimulated

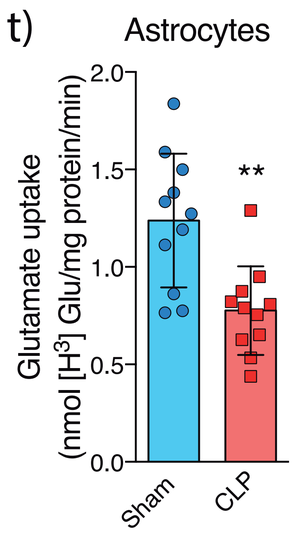
t)
Astrocytes
Glutamate uptake
(nmol [H3] Glu/mg protein/min)
Sham
CLP
**

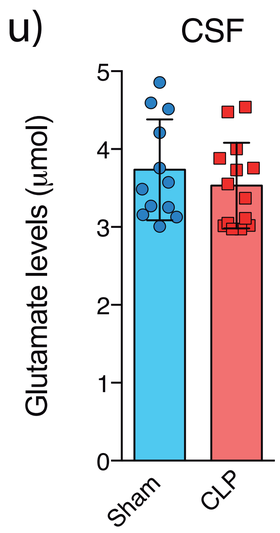
u)
CSF
Glutamate levels (µmol)
Sham
CLP

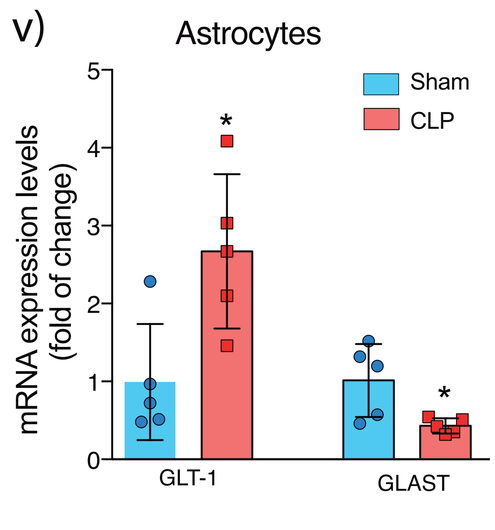
v)
Astrocytes
mRNA expression levels
(fold of change)
Sham
CLP
GLT-1
GLAST
*
*

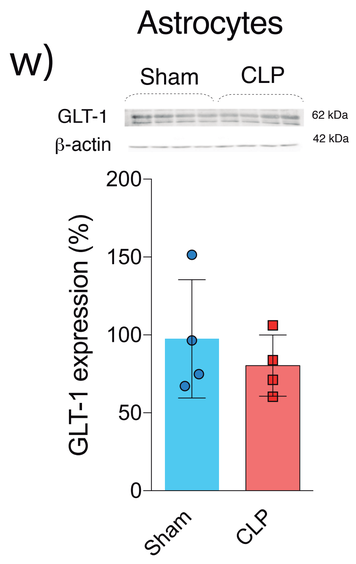
w)
Astrocytes
Sham
CLP
GLT-1
62 kDa
β-actin
42 kDa
GLT-1 expression (%)

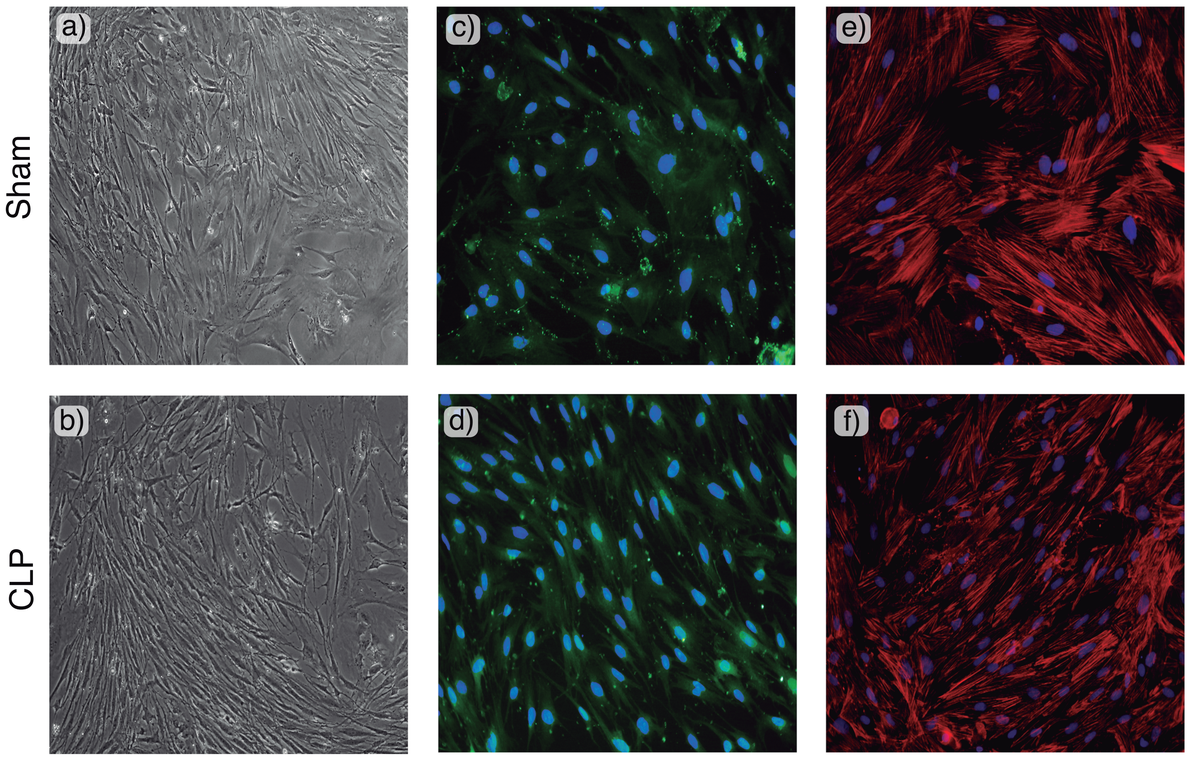
Sham
CLP
a)
b)
c)
d)
e)
f)

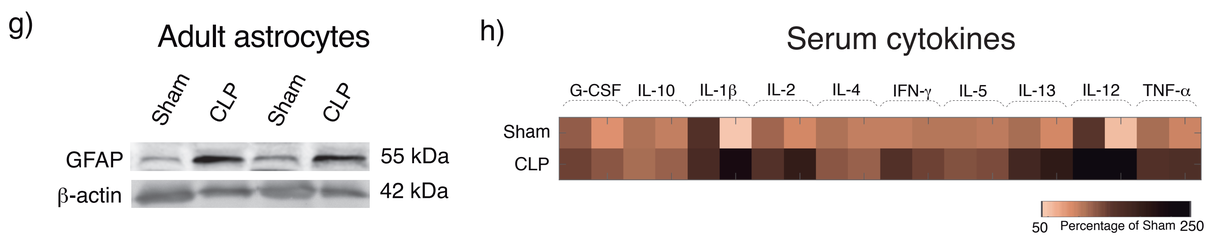
g)
Adult astrocytes
Sham
CLP
Sham
CLP
GFAP
55 kDa
β-actin
42 kDa
h)
Serum cytokines
G-CSF
IL-10
IL-1β
IL-2
IL-4
IFN-γ
IL-5
IL-13
IL-12
TNF-α
Sham
CLP
50
Percentage of Sham
250

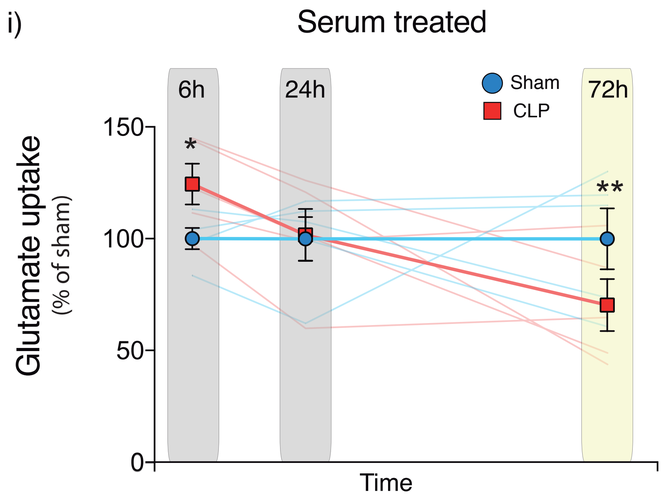
i)
Serum treated
6h
24h
72h
Sham
CLP
Glutamate uptake
(% of sham)
150
100
50
0
*
**
Time

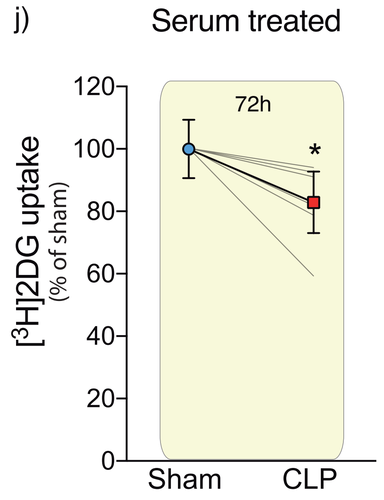
j)
Serum treated
72h
[3H]2DG uptake
(% of sham)
120
100
80
60
40
20
0
*
Sham
CLP

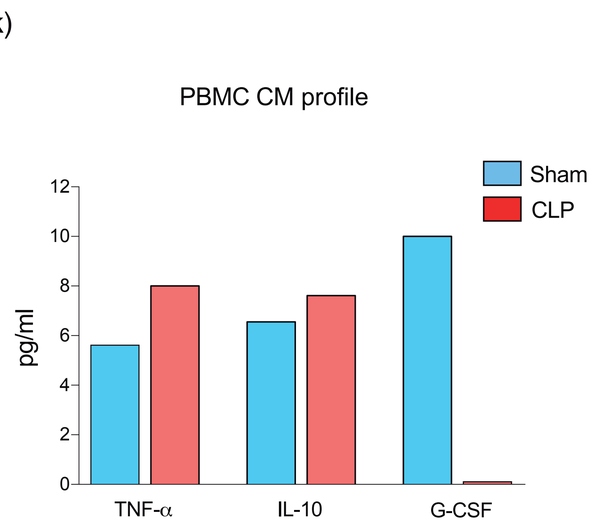
k)
PBMC CM profile
Sham
CLP
pg/ml
12
10
8
6
4
2
0
TNF-α
IL-10
G-CSF

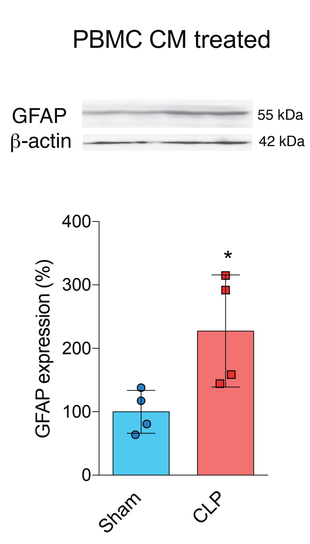
l)
PBMC CM treated
GFAP
55 kDa
β-actin
42 kDa
GFAP expression (%)
400
300
200
100
0
*
Sham
CLP

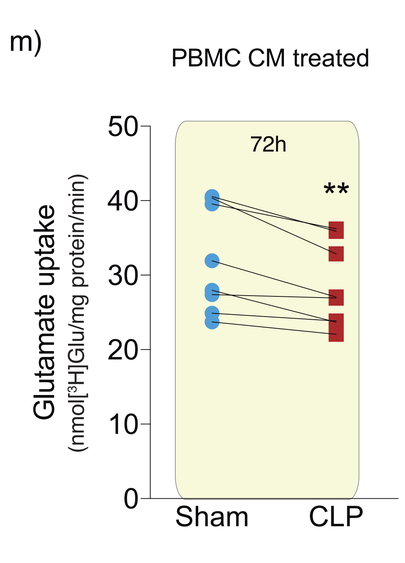
m)
PBMC CM treated
72h
Glutamate uptake
(nmol[3H]Glu/mg protein/min)
50
40
30
20
10
0
**
Sham
CLP

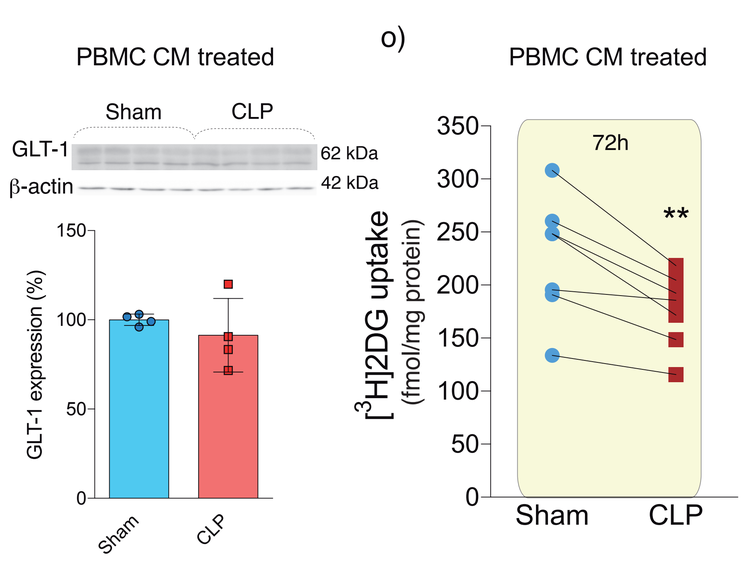
n)
PBMC CM treated
Sham
CLP
GLT-1
62 kDa
β-actin
42 kDa
GLT-1 expression (%)
150
100
50
0
Sham
CLP
o)
PBMC CM treated
72h
[3H]2DG uptake
(fmol/mg protein)
350
300
250
200
150
100
50
0
**
Sham
CLP

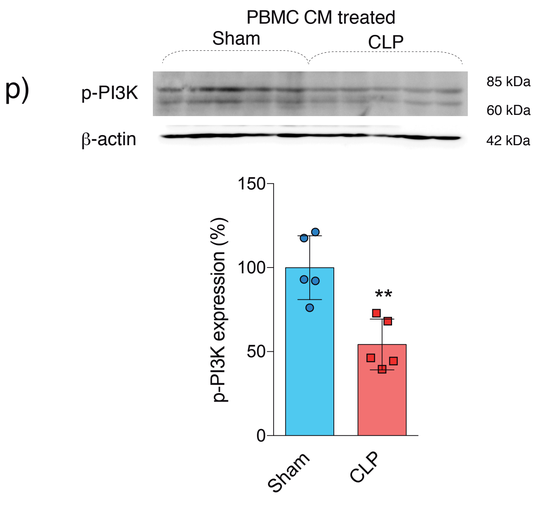
PBMC CM treated
Sham
CLP
p)
p-PI3K
85 kDa
60 kDa
β-actin
42 kDa
p-PI3K expression (%)
150
100
50
0
**
Sham
CLP

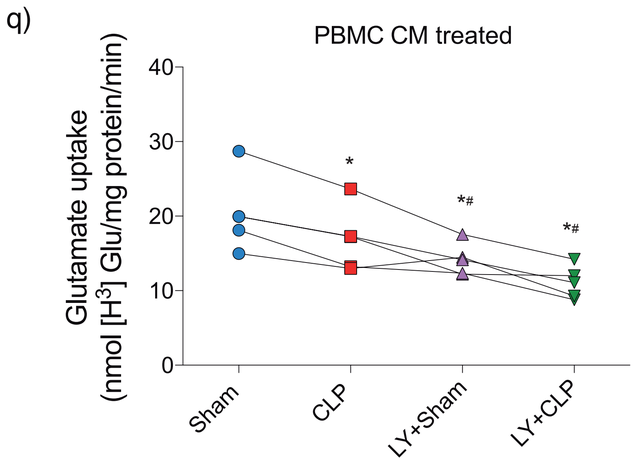
q)
PBMC CM treated
Glutamate uptake
(nmol [H3] Glu/mg protein/min)
40
30
20
10
0
*
*#
*#
Sham
CLP
LY+Sham
LY+CLP

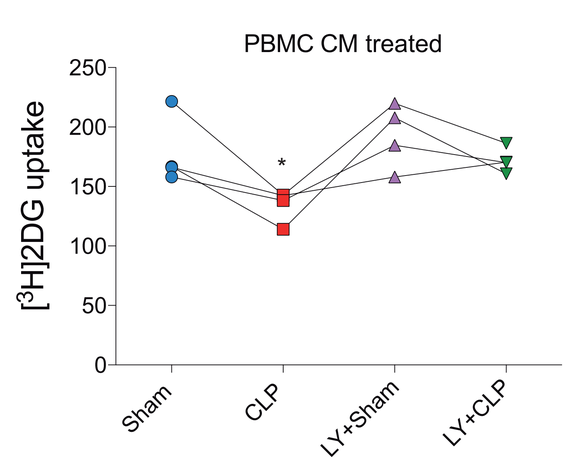
r)
PBMC CM treated
[3H]2DG uptake
250
200
150
100
50
0
*
Sham
CLP
LY+Sham
LY+CLP

Supplemental information

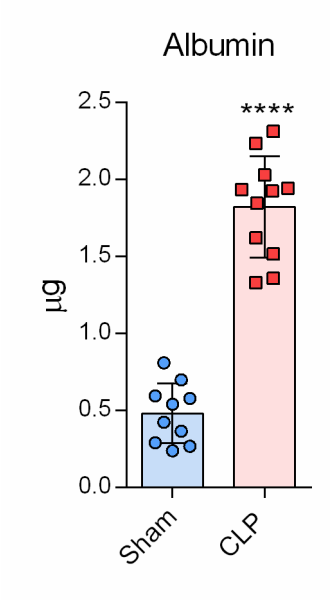

Supplementary Figure 1: 24h-CLP promoted a decrease in albumin levels in cerebrospinal fluid. Data are represented as mean values ± s.d. and individual scatter plots. ****P<0.0001. (t test), compared to the sham group.

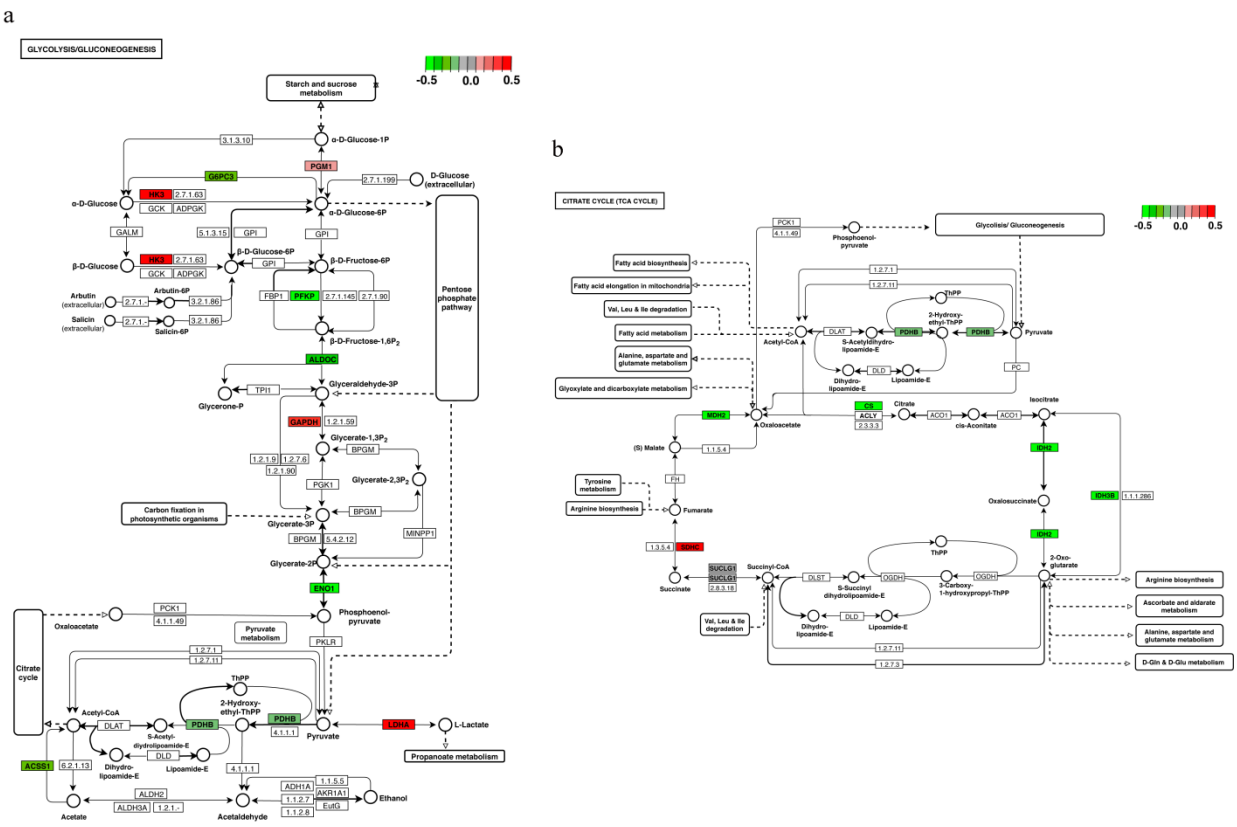

Supplementary Figure 2. Transcriptome analysis revealed enrichment of differentially expressed genes in energy-related KEGG pathways. Representation of upregulated and downregulated genes in **(a)** glycolysis/gluconeogenesis and **(b)** citrate cycle (TCA cycle). Color code refers to median logFC expression direction over all sepsis *versus* controls datasets utilized.

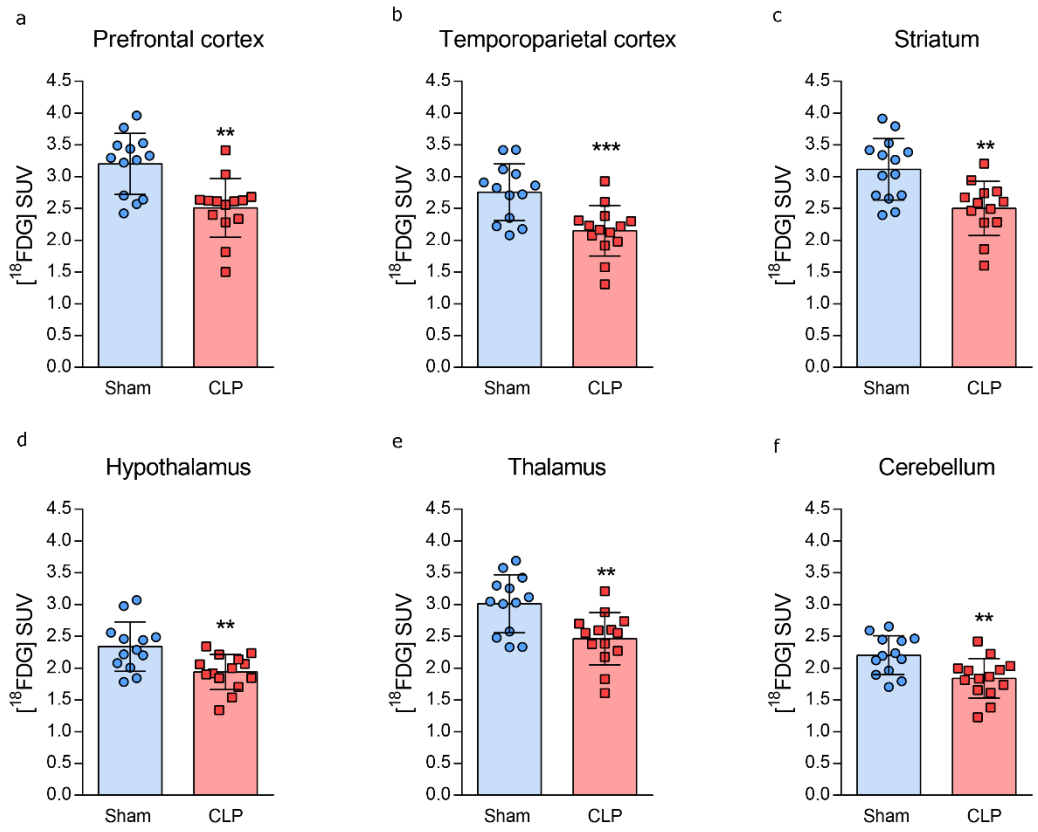

Supplementary Figure 3. Sepsis promoted a global decrease in standard uptake values (SUVs). SUV for **(a)** prefrontal cortex, **(b)** temporoparietal cortex, **(c)** striatum, **(d)** hypothalamus, **(e)** thalamus and **(f)** cerebellum are represented as mean values ± s.d. and individual scatter plots. **P<0.01 and ***P<0.001. (t test), compared to the sham group.

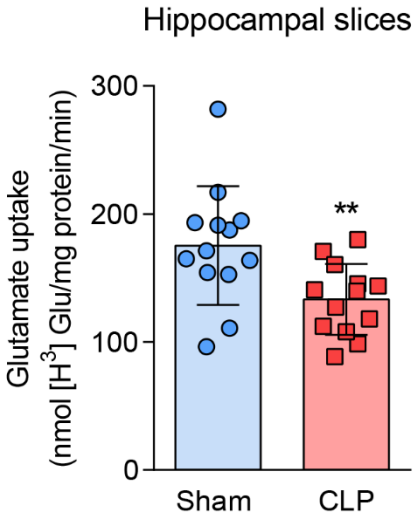

Supplementary Figure 4.CLP induction promoted a decrease in glutamate uptake in hippocampal slices. Data are represented as mean values ± s.d. and individual scatter plots. **P<0.01. (t test), compared to the sham group.

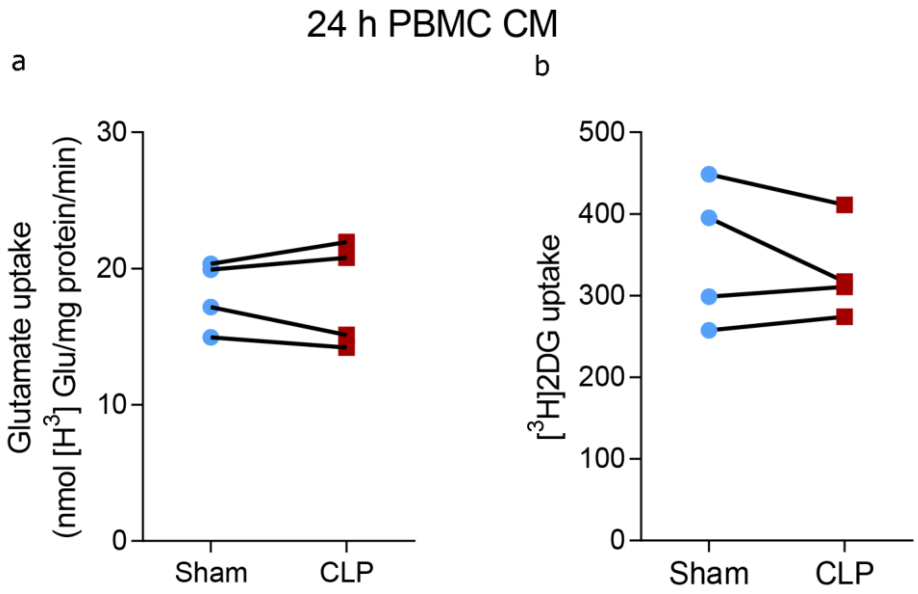

Supplementary Figure 5. 24 h of treatment with peripheral blood mononuclear cells conditioned medium (PBMC CM) from sham/CLP animals does not affects **(a)** glutamate and **(b)** glucose uptake in astrocytes. (t test), compared to the sham group.

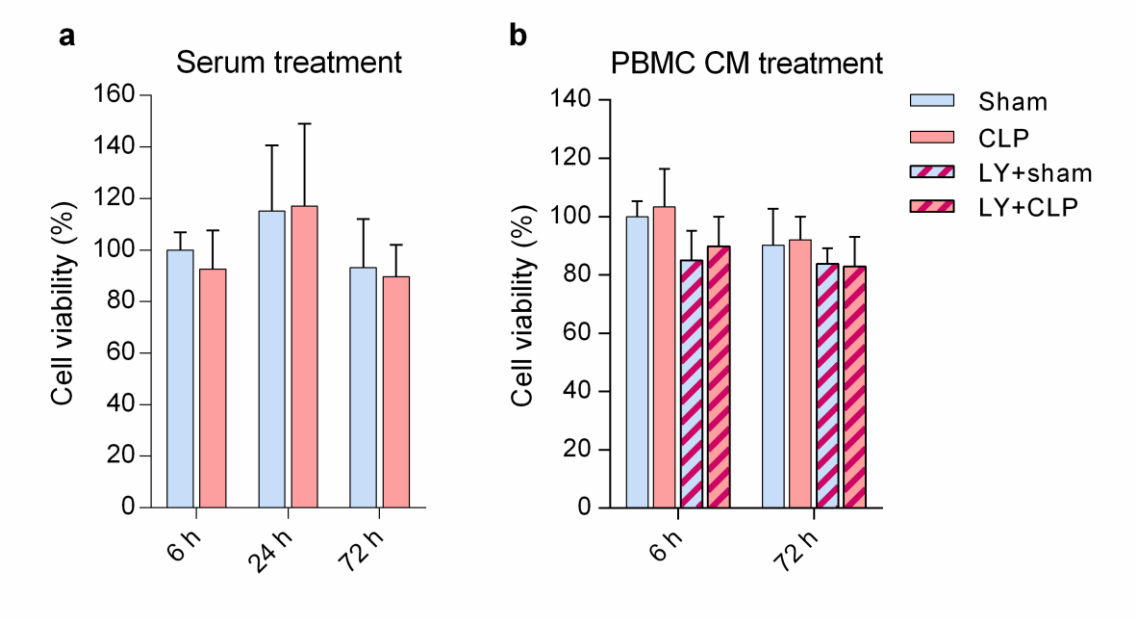

Supplementary Figure 6. Cell viability in astrocytes treated with **(a)** serum and **(b)** peripheral blood mononuclear cells conditioned medium (PBMC CM) from sham and CLP animals. Values are represented as percentage of 6 h sham. $n = 4$.

Supplementary table 1: differentially expressed genes in blood of sepsis and control subjects

Downregulated genes	Upregulated genes
AARSD1	ABCC2
ABCB7	ABHD5
ABHD12	ACAA1
ACD	ACSL1
ACSS1	ADAM17
ACTR1B	ADORA2A
ACTR5	AIM2
ADCK1	ALOX5AP
ADK	ANXA3
AFG3L2	AP3S1
AKNA	APH1B
AKR1B1	AQP9
AKR7A2	ARF5
ALDH16A1	ARL6IP5
ALDOC	ARPC1B
ALG1	ARPC3
ALKBH2	ARPC5
ANGEL2	B3GNT8
ANKRD54	BASP1
APEH	BATF
APEX1	BCORL1
ARHGEF18	BLOC1S1
ARHGEF3	BRI3
ARL2BP	BUD31
ASB13	C16orf72
ASF1B	C1orf162
ATIC	C3AR1
B3GALT6	CARD6
BBS2	CARS2
BBX	CASP5
BCAT2	CCDC17
BCS1L	CCND3
BIN1	CCNDBP1
BMP6	CD300LF
BZW2	CD44
C1orf174	CD55
C7orf26	CD63

CAD	CD82
CAMK1	CDA
CARD11	CDC20
CBY1	CDCA5
CCDC107	CEACAM3
CCDC115	CEBPA
CCDC6	CEBPD
CCR7	CHIC2
CCT4	CKAP2L
CCT8	CKAP4
CD160	CLEC4E
CD19	CLIC1
CD2	CLTC
CD27	CMTM6
CD300LB	CNIH4
CD3E	COX8A
CD3G	CST7
CD52	CSTA
CD6	CTSA
CD7	CTSD
CDC42SE2	CXCL16
CDK4	CYB5R4
CFDP1	CYBB
CHD4	DCTN6
CHD9	DCUN1D3
CHST11	DDAH2
CIRBP	DENND3
CLC	DIRC2
CNNM3	DNASE1L1
CNOT10	DNTTIP1
COPS6	DOK3
COPS7B	DRAM1
COPZ1	DUSP3
COQ10A	DYNLT1
COX10	DYSF
COX4I1	EDEM2
CREB1	EMILIN2
CS	ENO1
CSE1L	ENTPD1
CTCF	ERLIN1

CTDSPL2	EVI2A
CWF19L2	FAM49B
CYB5D1	FAM53C
DDX1	FAM89A
DDX17	FAM96A
DDX18	FBXO34
DDX21	FBXO6
DDX27	FBXW2
DDX46	FCER1G
DDX55	FEM1C
DDX56	FERMT3
DEXI	FES
DGCR8	FGFR1OP2
DHPS	FGR
DIABLO	FLOT1
DISP1	FLOT2
DKC1	FOXN2
DNAJA3	FPR1
DNMT1	FURIN
DOCK8	GADD45B
DOLK	GADD45G
DPEP2	GAPDH
DRG1	GBGT1
DUS1L	GCA
DUSP2	GLA
E2F5	GLT1D1
E4F1	GMFG
EARS2	GNA15
ECHS1	GNG5
EDF1	GNS
EEF2K	GOLGA1
EEF2K	GOLPH3
EIF2B1	GPR160
EIF3A	GPR84
EIF5B	GRAMD1A
ELP4	GSR
ENDOG	HBD
ENO2	HCK
ENOPH1	HEBP2
EOMES	HIF1A

EP400	HIST1H2AC
EPHX2	HIST1H2BE
EPRS	HIST1H3D
ERCC1	HIST2H2BE
EXOSC5	HK3
EXOSC7	HP
EXOSC8	HSPA1B
FARS2	IER3
FARSA	IFITM1
FASN	IFITM2
FBL	IFNAR1
FBXO21	IFNGR1
FGD3	IFNGR2
FGFBP2	IGSF6
FMNL1	IL10RB
FUNDC1	IL17RA
FXYD5	IL18R1
G6PC3	IL18RAP
GALNT11	IMPA1
GGA2	INSIG2
GIMAP1	ITGAM
GIMAP7	JUNB
GLOD4	KCNJ2
GOLGA3	KIF20A
GORASP2	KLHL2
GOT2	LDHA
GPD1L	LEPROT
GRWD1	LGALS1
GSS	LHFPL2
GSTP1	LILRB2
GTF2H4	LILRB3
GTF3C1	LILRB3
GZMA	LILRB3
GZMH	LILRB3
GZMK	LMNB1
GZMM	LMO2
HACL1	LRP10
HADH	LRPAP1
HCP5	LTB4R
HDDC3	LY96

HNRNPA0	MAN2A2
HSH2D	MAP3K5
HSPA8	MFN2
HSPA9	MICAL1
ICAM2	MMP9
ICOS	MOSPD2
ID3	MSRA
IDH2	MTF1
IDH3B	MXD1
IDS	MYD88
IKBKE	MYL6
IKZF1	NARF
IL10RA	NCF4
IL2RB	NDUFAF1
IL7R	NDUFS5
IMP3	NFE2
IMP4	NFIL3
IMPDH2	NFKB1
INPP5D	NFKBIA
INPP5E	NLK
INTS9	NMI
IRF9	NPTN
ISOC1	NTSR1
ITGAL	ORM1
ITGB7	OSBPL9
ITK	OSM
ITPR1	PAG1
IVD	PFKFB3
JARID2	PGLYRP1
KDELR1	PGM1
KIF3B	PGS1
KLHL22	PHF21A
KLRB1	PHKA2
LAGE3	PIK3AP1
LANCL2	PLEKHO2
LARP1	POR
LARS	PPM1M
LAS1L	PPP2R5A
LBH	PQLC1
LCP2	PRDX5

LEO1	PRDX6
LEPROTL1	PRKAR2A
LFNG	PROK2
LIG1	PRTN3
LIPA	PSMC6
LONP1	PSTPIP2
LRMP	PTEN
LSM4	PTGES
LTB	PTPN12
LYSMD2	PYGL
MAN2B1	QPCT
MAP4K1	RAB10
MARCKSL1	RAB11A
MAZ	RAB24
MBP	RAB27A
MCM3	RAB32
MCM5	RAB33B
MDH2	RAB8B
METAP1	RABAC1
MFNG	RANBP9
MGMT	RETN
MORC2	RGL4
MPHOSPH10	RGS18
MRPL4	RGS19
MRPL54	RHBDF2
MRPS17	RNASE2
MRPS23	RNF175
MRPS27	RPL26L1
MRPS9	S100A12
MYBBP1A	S100A6
MYCBP2	S100A8
MYO1F	S100A9
MYO1G	SAP30L
NADK	SDCBP
NAP1L1	SDF2
NAT10	SDHC
NAT9	SELL
NCAPD3	SEMA4A
NCL	SEPHS2
NCOA5	SERPINB1

NCOR2	SFXN5
NDE1	SH2B2
NELL2	SH3GLB1
NIP7	SIL1
NOL11	SIPA1
NOL8	SKAP2
NOSIP	SLA
NOV	SLC11A1
NPM3	SLC12A9
NSUN2	SLC22A4
NSUN4	SLC35A5
NUBP1	SNRPG
NUDC	SNX10
NUDCD3	SORT1
NUP107	SPATA5L1
NUP210	SPPL2A
NUP85	SRGN
NUP93	ST3GAL2
ODF2	STAM2
OGFOD1	STOM
P2RY8	SUCLG1
PAAF1	SUMF1
PAK1	TBC1D14
PALB2	TK1
PAQR8	TLR2
PARP1	TLR5
PAXIP1	TMBIM4
PBXIP1	TMEM120A
PCSK7	TMEM165
PDHB	TNFAIP3
PEX11B	TNNI2
PFAS	TOLLIP
PFKP	TOR1AIP1
PHB	TPD52L2
PHF1	TPM3
PI4KAP2	TPST2
PIH1D1	TRIM25
PIK3C2B	TRIP6
PIK3CD	TROAP
PIK3IP1	TRPM2

PILRA	TSPAN14
PIP5K1C	TYROBP
PLCB2	UBA3
PLEKHG4	UBAP1
PLEKHO1	UBE2A
PNPO	UBE2C
POGK	UBE2W
POLE3	UBTD1
POLR1C	UGCG
POLR2I	UQCRQ
POLR3A	USP3
POP7	VAMP7
PPAN	VNN2
PPHLN1	XPO6
PPM1G	ZC3H12A
PPP1R13B	ZDHHC12
PPP1R2	ZDHHC3
PPP2R1A	ZNF281
PPRC1	
PRKD2	
PRKRA	
PRMT7	
PRPF19	
PRPF31	
PRPF4	
PRPS1	
PRPSAP2	
PRR7	
PTBP1	
PTDSS1	
PTMA	
PTPRCAP	
PUS7	
PWP1	
RASGRP1	
RAVER1	
RBBP7	
RBM14	
RBM15B	
RBM28	

RBM4B	
RBMX	
RCC2	
RCSD1	
RDH11	
REV1	
RFTN1	
RFX5	
RHOF	
RHOT2	
RING1	
RNASE6	
RNASEH1	
RNF4	
RNH1	
RNMT	
RPA1	
RPL18	
RPL29	
RPL32	
RPL36	
RPL36A	
RPL37A	
RPL4	
RPS13	
RPS15	
RPS16	
RPS19	
RPS9	
RPUSD4	
RRN3	
RRS1	
RSAD1	
RUSC1	
SCRN1	
SDHAF1	
SENP5	
SET	
SF3A3	
SH2D1A	

SIN3B	
SKAP1	
SLC25A5	
SLC35B2	
SLC39A10	
SLC41A1	
SLC5A6	
SLC9A3R1	
SMAD4	
SMAD7	
SMARCC1	
SMCHD1	
SMYD3	
SND1	
SNRPA	
SPNS3	
SPOCK2	
SRFBP1	
SRM	
SRP68	
SRP72	
SRPRB	
SRRM1	
SSRP1	
ST3GAL1	
ST6GAL1	
ST6GALNAC6	
STARD7	
STAT4	
STK10	
STK40	
SUPT16H	
SUPV3L1	
SURF6	
TAF15	
TAF4	
TARBP2	
TATDN2	
TBC1D10A	
TBC1D10C	

TBC1D9	
TBCD	
TBL3	
TGIF2	
THOC1	
TIGD2	
TIMM44	
TIMM9	
TMC8	
TMCC1	
TMEM106B	
TMEM109	
TMEM14A	
TMEM50B	
TNFAIP2	
TNFRSF1B	
TNFRSF25	
TRAF3IP3	
TRAM2	
TRAP1	
TRIM28	
TRIT1	
TSFM	
TSPYL1	
TXNIP	
UBA52	
UBE2E2	
UBE2Q2	
UFSP2	
UPF1	
UPRT	
UROS	
UTP14A	
UTP6	
UXT	
VAMP2	
VDAC1	
VIPR1	
WBP11	
WDR46	

WDR54	
WDR74	
WDR77	
WDR82	
XPO5	
XRCC6	
YWHAQ	
YY1	
ZBTB2	
ZBTB4	
ZBTB9	
ZMYND19	
ZNF329	
ZNF559	

Supplementary table 2: log fold change for differentially expressed genes in each GSE

Gene	nsigstudies	GSE13015	GSE28750	GSE32707	GSE46955	GSE49757	GSE54514	GSE57065	GSE67652	GSE69063	GSE95233
AARSD1	7	-1227	-0.2017	-0.5956	-1146	NA	0.0851	-0.2540	0.1027	NA	-0.3638
ABCB7	8	-0.7543	-0.4645	-0.6068	0.1681	-0.3589	0.0870	-0.3728	0.1117	-0.3868	-0.2898
ABCC2	7	1141	0.4231	-0.5809	0.0123	NA	0.0386	0.7193	-0.4519	0.3881	0.5325
ABHD12	7	-1029	-0.4026	-0.2674	-1264	NA	-0.0120	-0.2194	NA	-0.2815	-0.2746
ABHD5	7	0.8143	0.5065	0.2341	0.5099	0.6905	-0.1333	NA	0.1283	0.3324	0.7139
ACAA1	7	0.9421	0.3725	0.8797	-0.2274	0.0102	0.2353	0.4364	-0.0700	0.5701	0.7801
ACD	7	-1311	-0.9342	-0.4427	0.1693	-0.1101	0.0631	-0.5259	0.1332	-0.4946	-0.6278
ACN9	7	0.8251	1425	NA	-0.7590	0.7576	-0.1104	1508	-0.3835	NA	2201
ACSL1	9	2260	1492	1041	1364	0.7062	-0.4547	1422	0.0817	1198	1260
ACSS1	7	-0.8334	-0.5520	0.5229	-0.4259	-0.1748	0.1902	-0.8814	0.2782	-0.7719	-0.0558
ACTR1B	8	-1316	-0.4920	-0.3211	-0.6072	-0.5491	0.1095	-0.4800	0.1434	-0.8610	-0.6146
ACTR5	7	-1218	-0.7304	-0.3014	-0.4938	NA	0.0532	-0.6511	NA	-0.7067	-0.5901
ADAM17	7	0.8727	0.4595	0.0567	0.0186	0.2496	-0.0201	0.7539	-0.2640	0.3872	0.3453
ADCK1	7	-1297	-0.3616	-0.2212	-0.4672	NA	0.1504	-0.4907	NA	-0.6916	-0.3971
ADK	7	-1634	-0.8404	-0.1638	-0.6418	-0.1726	-0.0043	NA	0.4700	-0.7212	-0.4755
ADORA2A	7	0.8466	0.2427	1110	3451	-0.5623	0.4303	0.6492	NA	0.2093	1083
AFG3L2	7	-1251	-0.4005	-0.8075	-0.8424	-0.1575	0.0665	-0.3794	NA	-0.7695	-0.5871
AIM2	7	2452	1926	0.0513	2137	-0.1059	-0.0856	1708	NA	1914	1990
AKNA	7	-0.2966	-0.8789	1218	0.2218	-0.2806	0.3432	-0.8738	NA	-0.2687	-0.9722
AKR1B1	8	-1713	-1564	-0.4796	2490	0.1962	0.0527	-0.9084	0.0147	-0.5788	-1180
AKR7A2	8	-0.8125	-0.8162	-0.4350	-0.6383	-0.3441	-0.0689	-0.4078	0.0955	-0.6460	-0.5221
ALDH16A	7	-1001	-0.5389	-0.0938	-0.6696	-0.1482	0.0843	-0.5317	0.1056	-0.3767	-0.2555
ALDOC	8	-0.7667	-0.5925	-0.6299	0.9952	-0.6957	-0.0131	-0.4834	-0.0235	-0.3671	-0.3806
ALG1	7	-1461	-0.2862	-0.3014	-0.2819	NA	0.0583	-0.2663	-0.1077	-0.5052	-0.1970
ALKBH2	8	-1921	-0.4378	-0.4444	-0.7521	NA	0.0682	-0.3438	-0.2602	-0.4342	-0.3247
ALOX5AP	7	1453	1100	2441	1667	-0.0034	-0.0155	1149	0.2333	0.6095	1233
ANGEL2	7	-0.5764	0.1974	-0.2536	0.4114	-0.2549	-0.0017	-0.4967	0.1108	-0.2409	-0.6084
ANKRD54	7	-0.8191	-0.2126	-0.2937	-0.0879	-0.3106	0.0232	-0.2840	NA	-0.2216	-0.4810
ANXA3	9	4321	4007	0.8394	0.5569	1005	-0.2083	4170	NA	2778	4134

AP3S1	7	0.5301	0.6829	0.1188	-1070	-0.0292	-0.1722	0.5481	NA	1015	1174
APEH	7	-0.3079	-0.6071	-0.4051	-0.7908	-0.1039	0.1876	-0.3673	-0.0551	-0.3026	-0.3374
APEX1	7	-1654	-1382	NA	-0.8379	-0.2384	0.1153	-0.8495	0.0798	-0.9030	-0.8605
APH1B	8	1286	0.6329	0.8359	0.5586	0.4120	0.0660	0.5410	-0.0167	0.6255	0.6327
AQP9	8	1658	0.8116	2141	2170	0.0965	-0.0385	0.6109	0.3600	0.4450	0.9920
ARF5	7	0.4384	-0.0407	0.4820	-0.0934	-0.1373	0.1775	-0.0136	0.3039	0.3225	0.4459
ARHGEF1	7	-0.7572	-1257	0.3322	0.0930	-0.2712	0.0899	-1091	0.1555	-1140	-1139
ARHGEF3	8	-0.7088	-0.7250	0.3457	1812	-0.2945	-0.2522	-1038	0.1530	-0.4002	-0.7825
ARL2BP	7	-0.9495	-0.4677	-0.2630	-0.0556	-0.1019	-0.2210	-0.4355	0.2127	-0.2177	-0.3282
ARL6IP5	7	0.5287	0.3978	0.5369	0.9530	-0.4486	-0.4761	0.4353	0.0017	0.1513	0.3280
ARPC1B	7	0.8422	0.4870	1316	NA	-0.1493	-0.1573	0.3852	0.0752	0.4499	0.6148
ARPC3	7	0.2707	0.6993	0.6512	-0.9036	-0.0609	-0.0728	0.9435	0.2610	0.6632	0.7549
ARPC5	7	0.9078	0.4832	0.5828	0.1282	-0.0829	-0.6519	0.3108	NA	0.4591	0.6870
ASB13	7	-1316	-0.5785	-0.3937	-0.6646	NA	0.1013	-0.0990	0.0133	-0.3910	-0.4280
ASF1B	7	-0.8559	-0.4880	-0.7913	0.6606	-0.4630	-0.1022	-0.2572	0.2048	-0.7054	-0.0131
ATIC	7	-1715	-1538	-0.5278	-0.7957	-0.0477	0.1613	-1161	0.0317	-0.9557	-1427
B3GALT6	7	-1659	-0.7541	-0.2370	-0.4911	-0.1579	0.1718	NA	-0.0980	-0.2489	-0.7281
B3GNT8	7	1496	0.6059	0.6223	-0.2730	-0.0603	0.2151	0.6770	0.1365	0.9194	0.7573
BASP1	7	1487	0.8802	0.1907	1799	0.1709	0.2880	0.6212	0.0118	0.9735	0.6022
BATF	8	1468	0.7454	0.8934	0.4085	0.9903	0.0741	0.7009	-0.4062	1103	1454
BBS2	7	-1312	-0.8345	-0.2828	0.8493	NA	-0.0333	-0.9764	0.0964	-0.8829	-0.8092
BBX	7	-0.0039	-0.7819	0.4009	0.6360	-0.2806	0.2191	-0.5676	NA	-0.2509	-0.4620
BCAT2	7	-1745	-0.5767	-0.7678	-1256	NA	0.0403	-0.4154	-0.0078	-0.2885	-0.4181
BCORL1	7	0.7437	0.2757	0.1688	0.1127	-0.3684	0.1307	0.0103	-0.1925	0.2434	0.3554
BCS1L	7	-1563	-0.4491	-0.5758	-0.6593	NA	0.0721	-0.1254	-0.0125	-0.4010	-0.2342
BIN1	7	-2172	-0.7464	NA	0.4923	0.2428	NA	-1227	0.1034	-0.9347	-0.9145
BLOC1S1	7	0.9031	1360	0.6192	0.2942	0.1420	0.3696	1253	-0.0962	1013	1839
BMP6	7	0.0431	0.1559	-0.9397	-1047	0.5845	-0.1387	0.1893	-0.0487	-0.4506	0.0596
BRI3	8	1331	0.4226	0.8789	-0.6677	0.0920	0.3073	0.8267	NA	1019	0.8587
BUD31	7	0.0640	0.0634	-0.0469	-0.4790	-0.1615	0.1679	0.4951	0.1168	0.2633	0.9605
BZW2	8	-1429	-0.9276	-1229	-1141	-0.2611	0.0342	-0.5302	0.0400	-0.5424	-0.7402

C14orf169	7	-1487	-0.5785	-0.5034	-0.5570	0.2742	-0.0490	-0.6579	0.1602	NA	-0.9060
C16orf72	7	0.9497	1093	0.6937	-0.0142	0.3620	-0.1205	0.7558	-0.0943	0.8342	0.7721
C16orf80	7	-1062	-1102	-0.3053	-0.1401	-0.4468	-0.0637	-0.9022	0.2225	NA	-0.5767
C17orf62	7	1212	0.5186	1156	0.5848	0.2927	0.4915	0.5185	-0.0607	NA	0.8590
C1orf162	7	1308	0.9217	2012	-0.2000	0.3886	-0.1227	0.8759	NA	0.6588	0.9303
C1orf174	7	NA	-0.6435	-0.3023	-0.3388	-0.2026	NA	NA	0.2063	-0.3195	-0.3756
C21orf33	7	-1021	-0.7707	-0.2341	-0.8282	0.2833	0.0527	-0.5620	-0.0958	NA	-0.8879
C3AR1	9	21949	1743	0.6757	1911	0.4191	0.3485	1882	-0.1250	1774	2017
C7orf26	8	-0.3952	-0.4196	0.2976	0.1647	-0.3398	0.2301	-0.3090	0.0328	-0.3206	-0.1710
C9orf91	8	-1268	-0.9198	-0.2944	0.2987	-1191	0.0954	-1205	0.4797	NA	-1278
CAD	7	-1262	-0.4787	-0.7088	-0.7464	NA	0.0354	-0.5198	-0.0555	-0.6747	-0.3715
CAMK1	7	-3088	-0.7247	0.3407	-1395	-0.2969	0.1328	-0.6080	NA	-0.3630	-0.6311
CARD11	7	-1762	-0.6550	0.3296	1586	-0.0222	-0.1638	-0.8005	NA	-1304	-0.7984
CARD6	7	1373	1708	0.1661	0.6815	NA	-0.0807	1639	-0.2102	1543	1674
CARS2	8	0.9963	0.5595	0.1170	-0.5822	-0.2987	-0.1572	0.2637	0.2362	0.4420	0.6034
CASP5	7	2378	0.4584	0.5005	0.7661	0.7358	0.1362	1085348	0.1300	2412	1262
CBY1	7	-1246	-0.2871	-0.1472	-0.3883	NA	0.0237	-0.5234	NA	-0.4677	-0.4149
CCDC107	7	-1408	-0.4775	0.0068	-0.6194	NA	0.0149	-0.4464	0.2739	-0.3440	-0.6900
CCDC115	8	-1001	-0.8624	0.3170	0.7787	-0.1694	-0.0726	-0.8880	0.2622	-0.5262	-0.4377
CCDC17	7	1030	0.4144	0.0349	-0.1852	0.3474	0.1007	0.6393	NA	0.4510	0.9135
CCDC6	7	-1020	-0.5627	-0.5679	-0.5478	0.2617	0.0841	NA	-0.3113	-0.6559	-0.8449
CCND3	7	0.7817	-0.0127	0.9737	0.7635	1578	-0.0889	0.3096	-0.0185	0.6093	0.5561
CCNDBP1	7	0.6370	0.5949	-0.0154	0.8028	0.0313	0.0296	0.5930	0.1792	0.7726	0.7552
CCR7	7	-2083	-2525	0.8355	4811	-0.0462	0.1972	-2099	0.4635	-1431	-1855
CCT4	7	-0.9577	-0.9453	-0.4647	-0.4236	NA	-0.0046	0.1684	0.0400	-0.4964	-0.3369
CCT8	7	-0.6786	-0.6009	-0.6446	-0.4614	-0.0566	0.1384	-0.3972	-0.0002	-0.3791	-0.2228
CD160	7	-3145	-1812	0.1553	0.2660	0.0444	-0.1633	-1736	NA	-1259	-1362
CD19	7	-1610	-0.8503	-0.1510	2779	-0.1697	0.2526	-0.6137	NA	-0.5579	-0.5288
CD2	7	-2844	-2490	1069	2561	-0.1428	-0.1269	-1918	NA	-1576	-1976
CD27	7	-2552	-1898	0.9597	0.7852	NA	0.0170	-1544	NA	-1611	-1507
CD300LB	7	-2558	-0.6093	0.4202	-1123	-0.5144	0.0865	-0.7564	NA	-1059	NA

CD300LF	8	0.8609	0.4855	0.8842	0.7576	-0.3963	-0.2905	0.2408	NA	0.3801	0.8725
CD3E	8	-2664	-2620	0.8924	0.8114	NA	0.3602	-1901	NA	-1918	-2007
CD3G	8	-2732	-2276	0.4648	1121	NA	-0.2443	-1560	0.4284	-1885	-2513
CD44	7	0.9157	0.7270	0.3255	0.8735	0.2809	0.0083	0.3754	-0.3729	0.6660	0.1726
CD52	7	-2768	-0.9011	1763	-0.9633	-0.1267	0.1933	NA	0.7870	-0.5815	-0.4986
CD55	8	1853	1772	-0.4158	2729	0.6485	-0.3524	1572	-0.1595	0.4799	1182
CD6	7	-2998	-1689	0.9430	2187	0.1424	-0.0162	-1435	0.2988	-2007	-0.9223
CD63	7	1515	1506	0.5229	-0.8215	0.1744	0.1240	1468	-0.0194	0.8165	0.8987
CD7	7	-2009	NA	0.8804	1640	0.7445	-0.0868	-1589	-0.0571	-0.7967	-0.3565
CD82	7	1874	0.5982	NA	2469	-0.2730	0.0288	0.8286	0.0103	0.6326	0.7944
CDA	8	1430	0.6984	0.6038	0.7125	-0.3716	0.1783	0.8384	0.1442	0.7555	0.9011
CDC20	8	1543	0.8706	-1147	-0.4074	NA	0.2198	1012	-0.1065	0.5887	0.7206
CDC42SE2	8	-0.0913	-0.6847	-0.0180	1182	-0.3167	-0.1567	-0.8753	0.3425	-0.3792	-0.6239
CDCA5	8	1569	0.4605	-0.8200	0.6349	NA	0.2085	0.5842	-0.1400	0.2354	1046
CDK4	7	-1744	-1140	-0.7658	-0.8838	-0.1377	0.0302	-0.6482	-0.0650	-0.6911	-0.8039
CEACAM3	7	1364	0.3325	1162	1098	-0.4033	0.1165	0.3879	NA	0.3045	NA
CEBPA	8	0.8209	0.6482	0.9219	-2728	0.1604	0.2354	0.4132	-0.3520	0.4809	1137
CEBPD	7	1262	0.8402	1000	-0.2224	1098	0.0198	0.9863	0.0075	1594	1244
CECR5	7	-1041	-0.7714	-0.3162	-1330	-0.4677	0.0306	-0.3229	-0.0800	NA	-0.3193
CFDP1	7	-0.1924	0.1472	-0.6512	-0.9145	-0.3328	-0.0836	0.1934	0.0400	-0.4053	0.6930
CHD4	8	-0.4497	-0.4368	0.0830	-0.3921	-0.2100	0.4245	-0.4806	-0.0228	-0.5202	-0.1648
CHD9	8	-0.7778	0.2756	0.7182	-0.0585	-0.3639	0.3301	-0.2485	0.0550	-0.6070	-0.2851
CHIC2	7	0.7227	0.3919	0.8179	0.7789	0.1522	-0.0063	0.5303	0.0852	0.8217	0.6746
CHST11	7	2016	-1074	0.0305	-0.0705	-0.4638	NA	-0.8356	0.2033	-0.5244	-0.8752
CIRBP	7	-1097	-0.7364	-0.1420	-0.2335	0.2035	0.0410	-0.6861	0.4080	-0.7091	-0.9076
CKAP2L	7	1560	0.1215	-0.4282	0.1202	-0.4090	0.0565	0.2730	NA	0.7789	0.4315
CKAP4	7	2586	2085	1229	0.0120	-0.2240	0.3646	NA	-0.3986	2016	1966
CLC	7	-2223	-0.6598	1295	1708	-0.4015	0.2814	-0.7978	1131	-0.6826	-0.4892
CLEC4E	7	2056	1416	0.4001	2313	1065	-0.1326	NA	NA	0.8898	2127
CLIC1	8	0.7888	0.7625	0.6474	-0.6520	-0.0239	0.1791	0.8599	0.1272	0.8744	1172
CLTC	7	0.6329	0.7681	-0.3615	0.0566	0.1189	-0.1516	0.3652	NA	0.1531	0.6858

CMTM6	7	0.9023	0.5037	0.9990	0.2366	-0.1032	-0.2363	0.3307	0.2457	0.8313	0.5048
CNIH4	7	1639	2266	-0.1536	0.9555	0.4707	-0.2123	0.8362	-0.3073	1807	2535
CNNM3	7	-1156	-1355	-0.2186	0.4482	-0.1077	-0.0972	-1051	0.1364	-0.8491	-0.9826
CNOT10	7	-0.5972	-0.5546	-0.2604	0.1518	-0.3561	0.1002	-0.2964	0.0849	-0.4207	-0.1208
COPS6	7	-1198	-0.4672	-0.6251	-0.3865	-0.3520	0.0621	-0.2058	0.1327	-0.2670	-0.1500
COPS7B	8	-0.8834	-0.4699	-0.3110	-0.5024	-0.1955	0.1042	-0.4753	NA	-0.5923	-0.8135
COPZ1	7	-1136	-0.6803	-0.3787	-0.6977	-0.0055	0.1086	-0.5062	0.0820	0.2375	0.5803
COQ10A	7	-1973	-0.8062	0.6820	0.7169	-0.1459	0.0256	-0.7894	0.2152	-0.6431	-1068
COX10	7	-1313	-0.2915	-0.5667	-0.6559	NA	0.0490	-0.4493	NA	-0.4957	-0.6345
COX4I1	7	-0.5033	-0.3904	-0.1342	-0.4378	-0.2218	-0.0384	-0.0980	0.2545	0.2736	0.3918
COX8A	7	0.1320	0.2832	-0.1298	-0.8684	-0.0347	0.3328	0.3267	0.1142	0.4523	0.5529
CREB1	7	0.3028	-0.3074	0.4507	0.4440	0.0241	-0.1074	-0.6226	0.2443	-0.4560	-0.5201
CS	7	-0.5652	-0.6517	-0.0294	-0.3597	-0.2480	0.0227	-0.6723	-0.0472	-0.5540	-0.5838
CSE1L	8	-1176	-0.6019	-0.5318	0.0164	-0.5472	0.0192	-0.4170	0.1605	-0.3693	-0.3827
CST7	9	1758	2234	2344	1494	0.6191	0.0441	1999	-0.7422	1245	1781
CSTA	7	0.5738	1154	0.5156	0.8646	-0.4204	-0.0550	1334	NA	1091	2516
CTCF	7	-0.5472	-0.5708	-0.0329	0.2995	-0.2991	0.0399	-0.5727	0.0958	-1000	-0.6530
CTDSPL2	7	-0.9955	-0.2259	-0.0502	0.1679	-0.3607	-0.0486	NA	0.4163	-0.5675	-0.6879
CTSA	9	1209	0.8550	0.6298	-0.7518	0.5800	0.3654	0.7598	NA	0.1718	0.6398
CTSD	8	1719	1073	1043	-0.4667	-0.1917	0.4224	0.9609	-0.2796	0.2310	1013
CWF19L2	7	-0.8486	-0.0857	-0.2976	0.6066	-0.3563	-0.0192	NA	0.4608	-0.6505	-0.4450
CXCL16	7	1512	0.4407	-0.0139	1373	0.3646	-0.0261	0.4247	NA	1199	0.5178
CYB5D1	7	0.009	-0.1735	-0.8159	-0.3707	-0.4567	0.1101	-0.0933	-0.3871	0.4535	-0.1256
CYB5R4	8	1226	NA	0.6932	0.4245	0.0467	-0.3864	0.6502	0.2000	0.7594	1014
CYBB	7	1332	0.0642	1248	0.8082	-1016	0.3231	NA	0.3175	0.1796	0.6430
DCTN6	8	-0.0264	0.4749	-0.1940	-0.0467	0.4266	-0.0748	0.5308	0.1237	0.8023	1253
DCUN1D3	7	1697	0.2941	0.1990	1008	0.2563	-0.0402	0.2697	-0.0778	1788	0.5886
DDAH2	8	2695	1735	0.7923	-0.8178	0.2990	0.0317	1626	-0.4513	1596	1868
DDX1	8	-0.6467	-0.4868	-0.6747	-0.5323	-0.0258	0.1838	-0.2385	0.0692	-0.3825	-0.2298
DDX17	7	1207	-0.4199	NA	0.3562	-0.1932	0.0546	-0.3455	0.1807	-0.2975	-0.3094
DDX18	8	-1466	-0.7542	-0.2668	-0.4081	-0.2189	0.1018	-0.7750	0.2418	-0.7282	-0.8378

DDX21	7	-0.8345	-0.6009	-0.6095	-0.8250	0.0083	0.0668	NA	0.2388	-0.4836	-0.5987
DDX27	7	-0.1807	-0.3474	-0.1700	-0.0987	0.4632	-0.1576	-0.5712	0.1495	-0.6463	-0.3120
DDX46	7	-0.7259	-0.1139	-0.4983	-0.4248	-0.3328	-0.0676	-0.2650	0.1362	-0.6047	-0.1117
DDX55	7	-1225	-0.3953	-0.3319	-0.6011	-0.0767	0.0246	-0.3746	0.0628	-0.7804	-0.3419
DDX56	8	-1044	-0.6977	-0.4645	-0.4593	-0.1868	0.1500	-0.7120	0.0057	-0.4734	-0.5881
DENND3	7	1108	0.2711	0.6619	1087	-0.1775	0.2743	0.3673	NA	0.4371	0.5436
DEXI	7	-1214	-0.6227	-0.3662	-0.3930	-0.0880	-0.0742	-0.4870	0.0562	-0.4356	-0.8193
DGCR8	7	-1143	-0.6119	0.0044	-0.8784	0.1152	0.1074	-0.2787	-0.0812	-0.6140	-0.6352
DHPS	7	-0.7015	-0.4737	NA	-0.4572	-0.0137	0.1946	-0.2894	0.1378	0.0795	-0.4004
DIABLO	7	-0.3721	-0.4046	-0.0670	-0.4258	-0.1330	0.0021	-0.1594	0.1310	0.2173	0.0641
DIRC2	7	1387	0.9809	-0.2019	1521	0.3792	-0.1178	1083	-0.2317	0.6756	NA
DISP1	7	-2432	-0.3761	-0.2425	-0.4389	NA	0.0194	-0.3370	-0.0985	-0.4349	-0.5900
DKC1	7	-1040	-0.9440	-1093	-0.8446	0.1539	0.1203	-0.8287	0.0012	-0.7272	-0.6753
DNAJA3	7	-1401	-0.6556	-0.9377	-0.7645	-0.1036	0.0694	-0.6406	0.0562	-0.5460	-0.7768
DNASE1L1	7	1112	0.7086	0.0169	-0.0754	0.4585	0.0166	0.8297	-0.1698	0.5600	0.9672
DNMT1	7	-1422	-1478	-0.8330	-0.5980	-0.0561	-0.0385	-1273	0.2188	-1110	-1148
DNTTIP1	7	0.5674	0.3540	0.0934	0.5547	-0.1684	-0.0734	0.4534	0.1185	0.4940	0.8208
DOCK8	7	0.1530	0.4737	0.9559	0.9673	-0.2367	0.0015	-0.4067	0.1817	-0.3894	-0.8977
DOK3	8	2104	0.7579	0.5895	0.6077	0.2590	0.0478	0.5755	0.1333	0.7979	0.6043
DOLK	7	-1564	-0.2865	-0.5556	-0.4222	NA	0.0678	-0.4467	0.0047	-0.3374	-0.2632
DPEP2	7	-1259	-1588	1371	-1337	0.0465	0.0555	-1116	0.1900	-1145	-1175
DRAM1	7	NA	1519	0.3231	NA	-0.3253	NA	1392	-0.2677	1915	1989
DRG1	7	-0.5142	-0.0489	-0.3567	-0.3237	-0.2444	0.1577	0.0966	0.1372	-0.1838	0.2829
DUS1L	7	-1567	-0.6014	-0.4330	-0.7461	NA	0.0385	-0.4552	0.0342	-0.3647	-0.3626
DUSP2	8	-2078	-0.7534	0.3034	-0.2215	-0.7628	-0.0464	-1014	0.1663	-0.4464	-0.4647
DUSP3	8	1511	0.4894	0.6919	-0.5978	0.0532	0.4148	0.3677	-0.4272	1231	0.3912
DYNLT1	7	1149	0.8642	0.6627	0.4494	0.3064	0.1778	0.7791	0.1052	1112	1853
DYSF	8	2613	1436	1612	0.3116	0.5836	0.4325	1304	0.1533	1299	1327
E2F5	7	-1685	-0.7586	-0.2969	0.6978	0.0980	0.0580	-0.6709	NA	-0.7300	-0.4540
E4F1	8	-0.5639	-0.2110	-0.4115	-0.0369	-0.3161	-0.2798	-0.2253	0.1232	-0.2714	-0.1835
EARS2	7	-0.9943	-0.3043	-0.3420	-1197	NA	0.0215	-0.3362	NA	-0.3249	-0.5580

ECHS1	7	-0.9488	-0.8315	-1056	-1245	-0.3414	0.0545	-0.5527	0.0472	-0.4410	-0.8301
EDEM2	7	0.8957	0.4805	0.4386	0.2967	-0.1466	0.0514	0.4918	-0.1610	0.8173	0.6721
EDF1	7	-0.7132	-0.6251	NA	-0.1362	-0.2203	0.3442	-0.2087	0.1650	-0.2951	-0.4966
EEF2K	7	-2022	-0.7485	-0.5297	-0.8056	-0.0142	0.0579	NA	0.3993	-1290	-1330
EIF2B1	7	-1056	-0.4301	-0.3003	-0.6334	-0.3458	0.0281	-0.4586	0.1038	-0.4687	-0.3240
EIF3A	7	-0.7389	-0.5627	-0.7386	NA	0.1072	-0.3003	-0.6094	-0.0637	-0.8739	-1077
EIF5B	7	-0.6183	-0.7405	-0.5318	-0.6973	-0.1466	0.1085	-0.9364	0.2028	-1024	-0.9124
ELP4	7	-0.9624	-0.3868	-0.4016	-0.4817	NA	0.0304	-0.2033	0.0835	-0.3497	-0.4907
EMILIN2	7	1768	1652	1078	-0.3716	0.5008	0.1954	NA	-0.5707	1066	1010
ENDOG	7	-1844	-0.7832	-0.6722	-0.4888	NA	0.0799	-0.3472	-0.0422	-0.1226	-0.5237
ENO1	8	0.1250	0.4470	-0.6531	-1011	-0.2896	0.1813	0.4729	-0.3642	0.2770	0.6159
ENO2	7	-1062	-0.7236	-0.4329	-0.0868	-0.7171	0.0838	-0.8350	-0.0913	-1007	-1172
ENOPH1	7	-1558	-0.5994	-0.5600	-0.6070	0.1764	-0.1050	-0.4925	0.1267	-0.5504	-0.4640
ENTPD1	8	1309	0.9817	0.7814	1887	0.4936	0.1462	0.9115	-0.1807	0.5328	1000
EOMES	7	-3107	-2002	0.8953	1997	-0.0434	-0.2186	-1949	NA	-1180	-2007
EP400	8	-1473	-0.3474	-0.3850	-0.4363	-0.4963	0.0735	-0.4955	-0.0410	-1165	-0.8294
EPHX2	8	-1095	-1052	-0.2293	0.3516	NA	-0.1232	-1065	0.2812	-1215	-1377
EPRS	8	-0.9206	-0.8136	-0.5185	-0.8458	-0.2540	0.0723	-0.4312	0.0283	-0.6995	-0.7173
ERCC1	8	-1327	-0.5279	-0.2053	-0.2033	0.2868	0.0446	-0.1932	0.1717	-0.3511	-1253
ERLIN1	7	2245	1425	-0.1389	-0.4588	1084	0.0407	1391	-0.3585	1969	1332
EVI2A	7	0.1043	0.9671	0.0296	0.6018	0.1540	-0.0247	0.4866	0.2667	0.7111	1134
EXOSC5	8	-2026	-0.5476	-0.6187	-1400	NA	0.1051	-0.2824	-0.1010	-0.8394	-0.1956
EXOSC7	7	-1488	-0.5152	-0.7133	-0.8268	NA	0.0526	-0.1848	0.0080	-0.8216	-0.4909
EXOSC8	7	-1380	-0.6750	-0.3371	0.1280	-0.1231	-0.1098	-0.3442	0.2215	-0.5677	-0.4925
FAIM3	7	-2802	-2592	0.7896	1464	0.3793	0.0493	-2369	NA	NA	-2539
FAM49B	7	NA	0.6611	NA	0.8529	-0.0905	-0.6081	0.4973	0.2993	0.7352	0.9441
FAM53C	7	1072	0.4962	0.5658	0.2902	0.2359	-0.2924	0.4727	0.0540	0.3998	0.6793
FAM89A	8	2530	1735	0.1389	-0.8230	0.3995	-0.0037	1456	-0.6192	1251	2190
FAM96A	7	-0.3374	0.5555	NA	-0.6467	-0.1557	-0.1706	0.4074	0.1818	0.6283	0.8796
FARS2	7	-1637	-0.3036	-0.4326	-0.1635	NA	0.0965	-0.2941	NA	-0.6270	-0.1183
FARSA	8	-1104	-0.4063	-0.6369	-0.9553	NA	0.1333	-0.2446	0.0378	-0.3161	-0.4774

FASN	7	-1312	-0.3731	-1522	-1179	NA	0.0549	-0.2623	-0.1657	-0.1888	0.0252
FBL	7	-1925	-1573	-0.9512	-0.9980	-0.1364	-0.0267	-1084	0.1723	-0.4825	-1208
FBXO21	7	-1360	0.0495	-0.3099	0.4393	0.0170	-0.0102	-1521	0.1927	-0.9128	-0.9091
FBXO34	7	0.9311	0.4302	-0.2525	0.3525	0.0403	-0.2171	0.1369	-0.1517	0.5360	0.4381
FBXO6	7	2024	0.8312	0.6784	1252	-0.0251	0.0340	0.7924	NA	1717	1349
FBXW2	7	1067	0.8389	-0.0251	-0.1747	-0.1647	0.0686	0.7888	-0.2656	0.4631	1062
FCER1G	8	2115	1466	2612	1333	0.2935	0.3825	1829	-0.0247	1023	1344
FEM1C	8	0.9336	1467	0.3753	-0.1828	-0.2168	-0.0581	1014	-0.1487	1232	1119
FERMT3	7	0.8737	0.6712	NA	NA	-0.2232	0.3062	0.4896	-0.0467	0.3756	0.6842
FES	8	1503	0.8157	1464	-0.8867	0.6648	0.0290	0.7374	0.0300	0.9936	1237
FGD3	7	0.5335	-0.5844	1401	0.9794	0.0740	-0.0483	-0.1872	0.1967	-0.2310	-0.1791
FGFBP2	7	-4076	-2241	0.8845	1498	-0.1244	-0.2304	-2105	NA	-1100	-2705
FGFR1OP2	7	1134	0.8588	0.1792	0.3409	-0.1291	-0.3615	0.2890	NA	0.6012	0.9724
FGR	7	1382	0.9128	-0.0352	-1985	-0.0317	-0.0029	0.6671	0.3033	0.7064	0.7626
FLOT1	8	1878	0.3615	0.5754	0.9840	-0.0042	0.1552	1160	-0.2012	1422	1362
FLOT2	7	1453	0.7236	0.7198	1683	0.2902	0.0791	0.8034	-0.0317	0.9331	1075
FMNL1	7	0.6641	-0.2560	0.3311	0.2018	0.0510	0.2364	-0.4492	0.1633	-0.1730	-0.3816
FOXN2	8	0.8034	NA	0.4794	1085	0.1890	-0.4400	0.8257	NA	0.6780	1042
FPR1	9	1509	0.6366	2097	1913	0.3555	0.0869	0.5799	0.3917	0.6391	0.5527
FUNDC1	8	-1531	-1293	-0.2707	0.4158	-0.3689	-0.0667	-0.4352	0.3802	-0.2593	-0.0301
FURIN	7	1011	0.6111	0.4242	0.0709	0.4546	0.3073	0.3199	NA	0.5595	0.5803
FXYD5	7	-0.5931	-1065	0.0379	-0.7581	0.1488	0.0503	-0.8272	-0.0662	-0.4398	-0.8388
G6PC3	7	-0.7663	-0.3692	-0.6925	-0.6570	NA	0.1226	-0.0685	-0.1703	-0.5517	-0.1982
GADD45B	7	1748	0.4138	0.5458	-0.1503	0.3804	0.0400	0.3777	-0.0807	1334	1193
GADD45G	7	1416	0.2977	0.2081	0.0084	-0.5530	0.0637	0.5777	-0.2027	0.5281	0.8584
GALNT11	7	-0.6286	-0.4181	-0.0693	-0.6936	0.1132	0.1123	-0.3642	0.0116	-0.3261	-0.2550
GAPDH	7	0.9961	0.8692	0.0842	-0.0426	-0.1481	0.2834	0.7683	-0.2605	0.3280	0.8380
GBGT1	9	1007	0.3561	0.5537	0.6034	0.4175	-0.0858	0.3412	-0.1367	0.7692	0.7579
GCA	9	1201	1530	1826	0.7223	0.2908	-0.4411	1184	0.3617	1003	0.7558
GGA2	7	-1661	-0.4904	-0.2938	-1026	-0.3159	0.1324	-0.4831	0.3915	-0.8668	-1271
GIMAP1	7	-0.9637	-1241	0.3842	1538	NA	-0.2507	-1232	NA	-0.9413	-0.9141

GIMAP7	7	-2101	-1250	NA	2574	-0.0647	-0.2172	-0.7845	NA	-1178	-0.6580
GLA	7	0.8173	0.6004	-0.1170	0.1678	0.4073	0.2159	0.6648	-0.1101	0.8714	0.9182
GLOD4	7	-1838	-1122	-0.5915	NA	-0.0064	-0.0615	-0.9016	0.4085	-0.9883	-0.6926
GLT1D1	7	1531	0.6545	0.6312	-0.2452	-0.0009	-0.0511	0.8105	0.2867	0.5003	0.9629
GMFG	8	0.7792	1042	1905	-0.1428	0.2561	0.0030	1211	0.3483	0.6193	1153
GNA15	8	1182	0.7776	0.7396	1304	-0.3791	0.1468	0.7706	NA	0.8817	0.9390
GNG5	7	1086	0.6589	0.2763	-1180	0.1873	0.1548	0.7995	-0.1617	1175	1158
GNS	7	1313	0.9823	0.3238	0.3718	0.3168	0.1634	0.7235	-0.2474	0.6176	0.9365
GOLGA1	8	0.8233	0.7435	-0.1498	-0.3175	-0.3686	0.1052	0.5789	-0.2423	0.2851	0.6241
GOLGA3	7	-0.6451	-0.0789	-0.0733	-1101	-0.2359	0.2706	-0.1267	-0.0983	-0.5375	-0.9762
GOLPH3	7	0.5881	0.5883	-0.3784	0.3948	-0.1821	-0.2686	0.0743	-0.0678	0.2892	0.2832
GORASP2	7	-0.8436	-0.5872	-0.4229	-0.4562	-0.2071	0.0165	-0.5977	-0.0183	-0.5222	-0.6954
GOT2	8	-1290	-0.9568	-0.9819	-0.5818	0.1273	0.2029	-0.7670	0.0218	-0.5202	-0.9683
GPD1L	7	-1210	-0.3927	-0.4063	-1070	0.1799	-0.0742	-0.7410	0.0878	-0.6081	-0.6556
GPR160	7	1788	1988	0.0459	0.4234	-0.0990	-0.3567	1870	0.0047	1676	2551
GPR84	7	6290	3981	0.9222	2545	-0.3706	0.1786	3888	NA	4011	4430
GRAMD1A	7	1950	0.7910	0.5653	3474	0.0599	-0.0063	0.8583	NA	1468	0.9287
GRWD1	7	-0.8153	-0.3888	-0.7829	-0.8297	NA	0.0573	-0.4739	0.0147	-0.5413	-0.1828
GSR	7	1070	1272	NA	-0.9531	0.4353	-0.0166	0.9206	NA	0.5079	0.9907
GSS	8	-1016	-0.4254	-0.5160	-0.4551	NA	0.1013	-0.4227	-0.0420	-0.4649	-0.4573
GSTP1	7	-1344	-0.7432	1060	-0.3427	-0.0151	0.0304	-0.5552	0.2133	-0.5021	-1167
GTF2H4	7	-1400	-0.4581	-0.4027	-0.8189	-0.0916	0.1020	-0.5835	-0.0077	-0.1334	-0.0680
GTF3C1	8	-0.8040	-0.6425	-0.2678	0.1177	-0.3861	0.1067	-0.4964	NA	-0.4051	-0.1987
GZMA	7	-2770	-1811	1341	2149	-0.0200	-0.2472	-1469	NA	-0.8026	-1524289
GZMH	8	-2971	-1799	1275	1838	-0.0003	-0.2543	-1207	0.7585	-0.6293	-2303
GZMK	7	-3524	-2006	1169	2211	-0.0978	-0.3601	-1851	NA	-1406	-2039
GZMM	7	-3727	-1382	0.5302	0.8176	-0.0738	0.0362	-0.8379	0.1037	-1047	-0.8507
HACL1	7	-0.9152	-0.7507	-0.4840	0.1212	-0.0436	-0.0271	-0.4417	0.1483	-0.5314	-0.2914
HADH	8	-1167	-0.2756	-0.9439	-0.9216	NA	-0.1381	-0.1705	-0.0448	-0.7739	-0.4304
HBD	7	1678	1461	2056	0.0376	NA	-0.1789	0.9898	0.6622	1270	0.6149
HCK	9	1338	0.5489	1718	1954	-0.3544	0.1636	0.5951	0.2333	0.5447	0.5945

HCP5	7	0.2238	-0.8921	0.9211	1951	-0.1882	-0.2694	-0.7225	NA	-0.3145	-0.8383
HDDC3	7	-0.5474	-0.2475	-0.4500	-0.9715	0.7688	0.1336	0.0315	-0.1625	0.1401	0.4148
HEBP2	7	0.6283	0.8541	0.4462	0.1908	0.2317	-0.3932	1051	-0.0210	1066	1421
HIF1A	7	1367	0.9131	-0.0892	2921	-0.1513	-0.1424	0.3639	NA	0.4892	1213
HIST1H2A	7	1180	0.5536	0.7384	1497	0.0409	-0.2739	0.3882	NA	0.1169	1035
HIST1H2B	7	0.9415	0.8863	0.1625	0.7321	0.1183	-0.1613	1036	NA	0.9467	0.7317
HIST1H3D	7	1623	1189	0.2464	0.5420	-0.0471	-0.0532	1618	0.1318	1135	1752
HIST2H2B	7	2057	1415	0.6802	1400	0.2935	0.0751	0.8425	NA	1042	1720
HK3	8	2700	2439	1856	-1023	0.3686	0.5737	2226	NA	1799	2351
HNRNPA0	7	-1181	NA	-0.6142	NA	0.0020	-0.2092	-0.9998	0.3148	-0.2468	-0.9150
HP	7	5742	4664	1652	0.0275	0.3797	0.1940	4239	-0.6962	4662	3999
HSH2D	7	-1060	-1394	0.9007	1811	-0.3811	0.0422	-1249	NA	-0.9662	-1121
HSPA1B	8	1694	0.8684	-0.3209	-1157	0.8131	0.0714	0.4525	-0.3240	1352	0.3523
HSPA8	7	-1141	-0.9427	NA	-0.9680	0.0611	NA	-0.9097	0.2217	-0.4717	-0.7348
HSPA9	7	-0.9366	-0.6825	-0.9292	-0.7911	-0.0513	0.0915	-0.7195	-0.0117	-1032	-0.7653
ICAM2	8	-1204	-1406	1217	1058	-0.4354	0.2206	NA	0.3698	-0.8542	-1273
ICOS	7	-2290	-0.9021	0.3398	1369	NA	-0.0352	-0.7261	NA	-1275	-1257
ID3	8	-2913	-1539	-1330	1874	-0.5094	-0.0297	-1287	0.0487	-0.9354	-0.3062
IDH2	7	-1004	-0.6146	0.1479	-0.5237	-0.5671	0.2953	-0.2473	0.2078	-0.4336	-0.4018
IDH3B	8	-0.5779	-0.4813	0.0825	-0.5440	-0.1268	0.1650	-0.4828	0.1282	-0.3319	-0.5496
IDS	7	-0.1613	-0.6728	NA	0.7351	-0.1236	-0.3800	-0.6059	0.3163	-0.4087	-0.5716
IER3	7	2310	1079	-0.1973	2735	-0.1614	0.0771	0.9458	NA	1124	1313
IFITM1	8	1377	0.4106	1146	3543	0.6454	0.0673	0.5770	NA	0.6910	1104
IFITM2	7	0.7760	0.2414	0.3486	1424	0.1331	0.0662	0.3402	0.2450	0.1748	0.2468
IFNAR1	7	1403	0.8435	0.8083	0.4342	0.0885	0.0446	0.4928	-0.0127	0.7815	0.6744
IFNGR1	7	1202	1251	1150	0.5798	0.2237	-0.2071	1152	0.1233	1071	1541
IFNGR2	8	1244	0.5246	0.8478	0.6635	-0.3148	-0.0308	0.3924	-0.0217	0.6004	0.7535
IGSF6	7	1388	0.5072	1366	-0.7574	-0.1634	-0.0370	0.9916	NA	0.4575	0.5262
IKBKE	7	-0.3591	-0.0981	0.3372	0.6177	-0.7126	0.1711	-0.2165	NA	-0.4760	-0.2490
IKZF1	7	0.0309	-0.3767	0.6599	0.8317	-0.1715	-0.4081	-0.5732	0.0327	-0.4030	-0.9573
IL10RA	7	-0.9992	-1206	1128	1527	0.0527	-0.0042	-1308	0.1367	-0.5577	-1224

IL10RB	7	1166	0.7335	NA	0.7263	-0.0822	-0.3039	0.9379	0.0850	0.8961	1260
IL17RA	10	1496	1124	1309	-0.7187	0.4076	0.3779	0.7957	0.1150	0.3398	0.4722
IL18R1	7	3871	29358	0.6808	0.9182	2480	-0.0804	2896	NA	2975	3565
IL18RAP	8	2668	1988	1660	1464	1694	0.0221	2101	0.0700	1998	2719
IL2RB	8	-2936	-2386	0.5420	2793	-0.3841	-0.3704	-2412	NA	-1472	-2352
IL7R	7	-2248	-2293	NA	2661	0.4387	NA	-1890	NA	-1925	-2031
IMP3	8	-1483	-1198	-0.6958	0.1110	-0.3901	0.0074	-1174	0.1958	-0.5297	-1030
IMP4	7	-1001	-0.8497	-0.6007	-1047	-0.0575	0.1431	-0.4019	0.0690	-0.8289	-0.5593
IMPA1	7	0.1243	0.5968	-0.0029	1225	-0.2719	-0.2537	0.4074	0.2298	0.5374	1074
IMPDH2	7	-1399	-1453	-1061	-0.5545	-0.1747	0.1382	-0.9748	-0.0488	-1117	-0.7681
INPP5D	7	0.2424	-0.4615	0.9992	0.1977	-0.1656	0.2857	-0.4846	0.1383	-0.6166	-0.5063
INPP5E	7	-2648	-0.6245	-0.2842	-0.5225	-0.0906	0.0515	-0.8051	-0.0138	-0.3606	-0.6854
INSIG2	7	0.7939	1137	-0.0049	1312	-0.2819	-0.1283	0.5025	-0.0671	0.4447	1012
INTS9	7	-0.7452	-0.8028	-0.2475	NA	-0.7136	-0.1432	-1003	0.1384	-0.7091	-0.4155
IRF9	8	0.5914	-0.5328	1072	NA	-0.0068	0.2889	-0.4887	0.1883	0.2643	-0.2698
ISOC1	8	-1092	-0.9956	-0.7727	-0.3010	-0.1502	-0.2092	-0.9077	0.0586	-0.5305	-0.2651
ITGAL	8	-0.4623	-0.4631	1068	0.5442	-0.5336	0.2797	-0.6393	NA	-0.5360	-0.9401
ITGAM	8	2030	1672	1243	-1388	0.3576	0.2720	1326	NA	0.8285	0.8632
ITGB7	7	-1994	-0.7631	1126	-0.6613	-0.0034	0.3150	-1081	0.2945	-1425	-1911
ITK	8	-2121	-2415	0.6933	2981	0.3366	-0.1010	-2249	NA	-1746	-2021
ITPR1	7	-0.4690	-0.1928	-0.3738	-0.7872	0.5283	0.0877	-0.5047	0.0769	-1031	-0.7568
IVD	7	-1023	-0.5258	-0.1571	-0.5650	NA	0.0561	-0.6112	0.0397	-0.5206	-0.3643
JARID2	7	-0.6844	-0.7608	0.1471	-1601	0.1407	-0.0885	-1036	0.1978	-1184	-0.8126
JUNB	7	1841	0.5270	0.4962	-0.0597	-0.1572	0.1353	0.6421	0.1678	0.9672	0.6292
KCNJ2	9	1770	0.7155	1052	1482	0.2039	-0.0152	0.6368	0.2533	1190	0.6725
KDELR1	7	-0.0455	-0.2771	-0.6201	-0.2947	0.0480	0.1745	-0.2261	-0.1232	0.1562	-0.2067
KIAA0141	7	-0.7321	-0.4037	0.0183	-0.2614	-0.0557	0.1173	-0.4008	0.1151	NA	-0.3210
KIF20A	7	2347	0.7195	-0.7582	0.1449	NA	0.0729	0.7842	-0.1562	0.3944	0.7081
KIF3B	7	-0.2425	-0.2661	-0.3288	0.3252	-0.5383	0.0135	-0.5181	0.1543	-0.1903	-0.1639
KLHL2	8	2184	2262	0.1977	0.7395	0.5295	-0.4912	1825	NA	1696	2344
KLHL22	8	-1614	-0.8925	0.4035	-0.3696	-0.2306	-0.1030	-0.7297	0.2796	-0.7708	-1045

KLRB1	7	-3253	-2034	0.9176	0.8613	0.0812	-0.5073	-1902	NA	-0.8555	-1473
LAGE3	7	-1185	-0.8758	-0.6752	-1243	-0.1537	0.2003	-0.4461	-0.0078	0.2001	-0.2547
LANCL2	7	-1299	-0.3467	-0.1837	-0.2083	NA	-0.0250	-0.1378	NA	-0.2561	-0.3125
LARP1	7	0.6592	0.0284	0.0159	-0.4410	-0.1655	0.1396	-0.2574	-0.2780	-0.4186	-0.8317
LARS	7	-1359	-0.6006	-0.5860	-0.8732	-0.1397	0.0545	-0.8347	0.0310	-1031	-0.7936
LAS1L	7	-2092	-0.6372	-1004	-0.5259	NA	-0.0162	-0.5913	0.0395	-1032	-0.8531
LBH	7	-2249	-2113	-0.0455	0.4676	-0.1445	-0.0575	-2090	NA	-1105	-2119
LCP2	7	0.7878	-0.3450	0.5218	0.9417	0.1663	-0.0864	-0.4898	0.1218	-0.1791	-0.3534
LDHA	7	1504	1779	-0.0991	0.7495	-0.1806	0.3752	1462	-0.2825	1441	1972
LEO1	8	-1258	-0.4807	-0.2364	-0.4773	-0.5659	0.0292	-0.3156	0.0250	-0.8176	-0.4493
LEPROT	8	0.6196	0.7142	1180	0.5180	0.2410	0.0584	0.7818	-0.0253	0.1770	0.3930
LEPROTL1	8	-0.7679	-0.8667	-0.0179	0.4267	0.0121	-0.4890	-1219	0.2593	-0.5412	-0.4612
LFNG	7	-1753	-1124	0.1294	-0.5138	-0.7681	-0.0209	-1224	NA	-0.7330	-0.9350
LGALS1	7	-0.0185	1345	0.5063	-0.8281	-0.4692	0.3609	1148	-0.1005	0.7139	0.9337
LHFPL2	7	1651	0.7539	0.2326	-0.3288	0.4572	0.2452	0.6430	-0.0997	1176	0.7295
LIG1	7	-1182	-0.4977	-0.2661	-0.3138	0.0374	0.1025	-0.5382	0.1235	-0.4518	-0.6131
LILRB2	8	1006	0.5643	0.1608	0.0498	-0.1761	-0.0646	0.4832	0.2517	0.1919	0.2921
LILRB3	7	0.5188	0.8429	0.4942	0.1126	0.0034	-0.0651	0.6894	0.2017	1012	0.7026
LIPA	7	-0.9745	-0.4922	-0.1680	-2984	-0.1192	0.0542	-0.5001	0.3193	-0.4664	-0.6314
LMNB1	7	2388	1324	0.2985	0.7016	0.9949	-0.1092	0.3965	-0.4825	1409	12066
LMO2	7	0.8053	0.2099	1044	0.7596	0.3317	-0.2347	0.2712	NA	0.4896	0.2956
LONP1	9	-1384	-0.7614	-0.6931	-0.8559	-0.6165	0.1395	-0.4680	-0.0205	-0.4035	-0.3788
LRMP	7	-0.6089	-0.5222	0.9627	1112	-0.2484	-0.1222	-0.3465	0.3100	-0.6962	-0.0498
LRP10	7	1073	0.2372	0.7730	1413	0.2181	-0.0699	0.3136	0.0913	0.6598	0.2801
LRPAP1	8	1058	0.7567	-0.0129	-0.5569	0.3122	0.2016	0.8082	-0.0782	0.5853	0.8938
LSM4	9	-1290	-0.7437	-0.7177	-0.7240	-0.4304	0.0287	-0.3793	0.1487	-0.2250	-0.7515
LTB	8	-0.9482	-1506	NA	1739	-0.6492	NA	0.3548	0.2783	-0.8841	-0.7173
LTB4R	7	2093	0.9529	0.6197	0.1248	0.3211	0.3245	1302	-0.0085	0.9525	0.4480
LY96	7	1188	2327	1467	0.2644	0.3044	-0.1739	1451	0.0850	2148	2489
LYSMD2	7	-0.2650	-1454	0.2739	1734	-0.7336	-0.3593	-1120	0.3720	0.1277	-0.5904
MAN2A2	7	0.7392	0.4553	0.2730	-0.5577	0.3491	0.1301	0.4545	-0.0910	0.3547	0.5068

MAN2B1	7	0.0216	-0.4626	0.5508	-0.3906	-0.4596	0.2594	-0.3988	0.0172	-0.4245	-0.3893
MAP3K5	7	1076	0.5295	0.9624	0.9691	0.0748	0.1125	0.2809	0.1217	0.2130	0.3799
MAP4K1	7	-2200	-1278	NA	1268	0.0378	0.0805	-1136	NA	-1362	-1867
MARCKSL	7	-1891	-1901	-0.0347	1543	-0.9304	-0.0059	-1750	0.1076	-0.6014	-1371
MAZ	7	NA	-0.4818	0.0104	-0.2288	0.4111	-0.0661	-0.5125	-0.1242	-0.3184	-0.5477
MBP	7	-0.1099	-0.5044	NA	-1461	0.2563	-0.2460	-0.6136	NA	-0.3128	-0.7714
MCM3	7	-1169	-0.7134	NA	-0.0698	-0.3210	0.0840	-0.9010	0.0900	-1052	-0.9917
MCM5	7	-1193	-0.5679	-0.3398	0.4907	0.0763	0.1948	-0.2497	0.2712	-0.9369	NA
MDH2	7	-0.3834	-0.6634	-0.5983	-0.7214	-0.0535	0.1912	-0.3530	-0.0070	-0.3069	-0.4401
METAP1	7	-1391	-0.8110	-0.3437	-0.5981	0.0271	-0.0269	-0.6728	0.0485	-0.8047	-0.5637
MFN2	7	1089	0.4409	0.0565	-0.8895	0.0386	0.3776	NA	-0.3051	0.2507	0.2237
MFNG	7	-1297	-1169	0.9442	-0.7613	-0.1094	-0.2248	-0.8807	NA	-0.8000	-1014
MGMT	7	-1683	-0.7527	-0.7593	-0.5382	NA	-0.0905	-0.4452	0.2132	-0.6853	-0.5851
MICAL1	8	0.8672	0.7716	1047	-0.9895	0.1033	0.2386	0.5307	-0.0735	0.5455	0.6857
MMP9	9	4031	2717	2071	0.5903	-1652	0.6575	2900	0.1550	2036	3228
MORC2	7	-1947	-1265	-0.3137	-0.6212	NA	0.0793	-1140	-0.1126	-0.9120	-0.5261
MOSPD2	7	1037	0.6396	NA	-0.5128	0.0665	0.2181	0.2909	NA	0.6950	0.8274
MPHOSPH	7	-1570	-0.7954	0.0681	-0.7766	-0.1563	-0.0479	-0.4954	0.0635	-0.7079	-0.4324
MRPL4	7	NA	-0.5793	-0.0919	-0.5340	NA	0.0622	-0.1941	0.0013	-0.3113	-0.2374
MRPL54	7	-1034	-0.4767	-0.1562	-0.4645	-0.3970	0.2780	0.1193	0.2678	0.1040	0.2237
MRPS17	8	-1418	-0.5075	-0.9318	-0.7927	-0.3882	-0.0036	0.3170	-0.0200	-0.3979	0.6008
MRPS23	8	-0.6526	-0.2268	-0.5257	-0.5247	NA	-0.0137	-0.1865	0.2278	-0.3263	0.4437
MRPS27	7	-1410	-1165	-0.6354	-0.6591	NA	0.0692	-0.8804	0.0012	-0.8533	-0.9287
MRPS9	7	-1597	-0.9692	-0.5987	-0.9367	NA	0.1021	-0.4877	0.1078	-0.8827	-0.4240
MSRA	7	1290	1066	0.3962	-0.7520	0.1675	-0.1079	0.8216	-0.0107	0.7274	0.5014
MTF1	9	2469	0.8297	1076	1195	-0.0196	0.5316	0.9711	-0.4257	0.7312	0.9368
MXD1	7	0.9792	0.5036	1467	1528	-0.0471	0.0299	0.3433	0.1850	0.2119	0.0437
MYBBP1A	8	-1533	-0.2946	-0.3273	-0.4819	NA	NA	-0.3069	-0.1598	-0.8541	-0.3715
MYCBP2	7	-0.6415	-0.9804	0.0017	0.4416	-0.3137	0.2629	-1013	NA	-0.8354	-0.8472
MYD88	8	1271	0.3004	1246	-0.2281	0.2751	0.2167	0.3926	-0.0383	0.4597	0.6071
MYL6	7	0.6216	0.3039	0.4082	-0.4824	0.0297	0.0914	1207	0.3495	1058	1043

MYO1F	7	0.7330	-0.2467	1440	0.1714	-0.2046	0.3847	-0.0740	0.3110	-0.2559	-0.1692
MYO1G	8	-0.4832	-0.5298	0.5838	2235	0.0589	0.2983	-0.2951	0.2162	-0.4380	-0.2728
NADK	7	0.7233	-0.4137	0.7689	0.6161	-0.3800	0.3485	-0.1546	0.1533	0.0092	0.1441
NAP1L1	9	-0.8495	-1123	-0.1612	-0.4202	-0.1832	-0.0581	-0.9944	0.2193	-0.5188	-0.6539
NARF	7	0.7325	0.6684	0.4831	0.6369	-0.1036	0.1808	1007	-0.0055	0.7105	0.8361
NAT10	8	-1696	-0.7884	-0.9075	-0.8072	-0.1778	0.0325	-0.9088	-0.1358	-1133	-1524
NAT9	7	-0.9780	-0.2608	-0.1633	-0.5600	-0.5772	0.0506	-0.3631	-0.0837	-0.4705	-0.1726
NCAPD3	7	-1149	-0.4767	-0.4465	-0.3533	NA	0.0327	-0.4787	-0.0502	-1040	-0.4032
NCF4	8	1233	0.7536	NA	0.5342	-0.1182	0.3279	0.6579	0.2467	0.7343	0.7794
NCL	9	-1264	-1298	-0.3326	-0.6701	-0.2978	0.0116	-0.9755	0.1585	-1483	-1272
NCOA5	7	-0.9507	-0.6868	-0.2911	-0.0356	-0.0836	0.1525	-0.9447	NA	-0.4716	-1007
NCOR2	7	-1138	-0.0562	-0.0308	-0.9904	-0.4711	0.2078	-0.8695	0.0882	-0.6575	-0.2129
NDE1	7	-0.3869	-0.9412	0.8972	0.6907	-0.2122	-0.0528	-0.5346	0.2377	-0.9096	-0.8008
NDUFAF1	7	1019	0.9750	0.0340	-0.2427	-0.2860	0.0576	1200	-0.1729	0.6515	1715
NDUFS5	7	-0.2159	0.3485	-0.7339	-0.9385	-0.2120	0.2020	0.9120	0.1483	0.2548	1812
NELL2	7	-4061	-2507	0.3089	1584	-0.4929	-0.0368	-2597	NA	-2631	-2236
NFE2	7	1209	0.8378	1434	0.8144	0.2549	0.0580	0.7498	0.0817	1066	0.8863
NFIL3	8	1730	0.8275	0.3099	1894	0.4714	-0.4561	1024	0.0627	1613	1213
NFKB1	7	0.8027	-0.0391	0.5190	1171	-0.5710	0.2409	-0.0628	-0.1902	0.2300	0.0997
NFKBIA	7	2012	0.1954	0.9931	1201	0.2303	0.0524	0.8602	NA	1043	0.9497
NIP7	7	-1084	NA	-0.6127	-0.6351	-0.3365	-0.0723	NA	-0.1448	-0.1489	-0.2257
NLK	7	0.8119	0.7927	-0.2073	0.2551	NA	-0.1328	0.9380	-0.0703	0.4638	0.4222
NMI	7	0.6220	0.6691	0.2006	0.8180	-0.0581	-0.2193	0.6326	0.1800	0.6910	1063
NOL11	7	-1501	-0.9070	-0.6988	-0.1915	-0.1002	-0.0894	-0.7513	0.1553	-0.8509	-0.3145
NOL8	8	-0.8709	-0.6456	-0.4704	-0.5615	0.2089	0.0299	-0.5665	-0.0058	-0.2848	-0.3184
NOSIP	8	-0.7370	-1202	0.2499	0.5391	-0.0834	0.2998	-0.7392	0.1363	-0.2098	-0.4763
NOV	8	-3255	-0.3866	0.0134	-0.8229	-0.2535	-0.1830	-0.9823	1047	-1863	-0.5535
NPM3	7	-1071	-0.3090	-0.9737	-0.0431	0.1491	0.1159	-0.2939	-0.2305	0.1463	0.1773
NPTN	7	0.8534	0.8018	0.0328	-0.0742	-0.1678	-0.3420	0.4023	NA	0.4209	0.4746
NSUN2	7	-0.5875	-0.4703	-1041	-0.2569	-0.1321	-0.0577	-0.7129	-0.0018	-0.6936	-0.4848
NSUN4	7	-1275	-0.0452	-0.2947	-0.3193	0.4618	0.0145	NA	-0.1432	-0.5128	-0.1821

NTSR1	7	3680	0.4507	0.2563	0.1359	0.6195	0.0420	0.4467	NA	0.8972	0.6894
NUBP1	8	-1705	-0.5919	-0.3636	-0.4313	NA	0.0952	-0.2611	0.2461	-0.3194	-0.3491
NUDC	7	-0.7190	-0.5658	-0.8025	-0.5559	-0.2081	-0.1229	-0.3485	0.0062	0.0220	-0.5335
NUDCD3	8	-0.9414	-0.5521	-0.2861	-0.2946	-0.2866	0.1615	-0.4018	0.0670	-0.8652	-0.8337
NUP107	7	-0.7402	-0.4751	-0.6435	-0.0484	-0.1524	-0.0351	-0.3757	0.1697	-0.6135	-0.3674
NUP210	7	-1445	-1080	-0.3453	0.0808	NA	0.1302	-1163	0.0717	-1107	-0.5042
NUP85	8	-0.9610	-0.6917	-0.4800	-0.4247	-0.3736	0.1141	-0.4759	0.0472	-0.3010	-0.2957
NUP93	7	-1338	-0.8085	-0.8066	-0.3947	-0.2873	0.1020	-1044	0.3957	-0.7913	-1404
ODF2	7	-0.7541	-0.3834	-0.1649	-0.1759	-0.2504	0.1421	NA	0.2333	-0.5945	-0.8258
OGFOD1	7	-1236	-0.8167	-0.0969	0.1979	NA	0.0976	-0.7963	-0.0037	-0.6422	-0.1458
ORM1	7	2951	1689	1402	0.5756	-0.7296	0.2921	2108	-0.2456	1462	2116
OSBPL9	8	0.5174	0.5217	0.0508	0.4851	0.5777	0.0157	0.6549	-0.1394	0.3674	0.8168
OSM	8	2478	0.3512	0.4658	3093	-0.6845	-0.1168	NA	0.2967	2510	0.1720
P2RY8	7	-1595	-1411	1081	1534	0.2359	0.1398	-1309	0.0117	-1072	-1472
PAAF1	7	-1524	-0.7075	-0.5866	NA	NA	0.0658	-0.1584	0.1865	-0.5207	-0.7173
PAG1	8	1587	0.9974	NA	14113	0.6128	0.0662	0.7158	-0.3583	0.8300	1124
PAK1	8	0.0826	-0.3119	0.7526	-0.7264	-0.5921	0.1985	-0.5043	0.2370	-0.3909	-0.5135
PALB2	7	-1444	-0.5400	-0.3006	-0.4103	NA	-0.0186	-0.7117	NA	-0.3901	-0.2441
PAQR8	7	-1767	-0.7370	0.4811	-0.6513	NA	0.0420	-0.8745	NA	-1272	-1007
PARP1	7	-1161	-0.9945	-0.9456	0.4680	0.1067	0.1480	-1059	0.0320	-0.9847	-0.7038
PAXIP1	7	-0.6159	-0.6169	-0.4017	-0.3059	-0.0269	0.0204	-0.6425	0.0773	-0.4141	-0.3724
PBXIP1	7	-1327	-1340	0.0362	0.4102	-0.1517	0.1068	-1203	0.2838	-1142	-1891
PCNX	8	1580	0.5765	0.7610	1837	0.4217	0.1481	0.6578	-0.1268	NA	0.5686
PCSK7	7	-0.9050	-0.8500	0.4143	-0.3303	-0.0504	0.1222	-0.7038	NA	-0.9890	-1733
PDHB	7	-0.8863	-0.4557	-0.5233	-0.2731	-0.1002	-0.1079	-0.1810	0.1227	-0.4634	0.0803
PEX11B	7	-0.4984	-0.3823	0.0786	-0.1662	0.2002	0.1191	-0.3742	0.1573	0.2260	-0.0999
PFAS	7	-1221	-0.9643	-1301	-1077	NA	0.0705	-1029	-0.0031	-0.7877	-1184
PFKFB3	7	3244	3098	NA	2169	0.1578	NA	2301	-0.3428	1996	1900
PFKP	7	-0.9140	-0.5487	-0.7133	-1450	-0.3695	0.1286	-0.5317	-0.0755	-0.0421	-1109
PGLYRP1	8	2857	2021	2418	0.2971	-0.1818	0.6585	2351	0.2550	1904	1990
PGM1	7	0.4804	0.4430	-0.1964	0.0721	-0.4368	0.1478	0.6687	-0.1365	0.6120	0.7023

PGS1	7	2692	1879	0.9733	NA	0.3488	0.1492	1699	0.0235	1065	1828
PHB	7	-1492	-0.4595	-0.7619	-1344	-0.0148	-0.0079	-0.4502	0.0657	-0.3070	-0.6408
PHF1	8	-0.5209	-0.9343	0.2182	0.4010	-0.2733	0.0263	-0.8160	0.1827	-0.1582	-0.6010
PHF21A	7	1434	0.2392	0.4214	1478	-0.1193	0.0351	0.8341	-0.2067	0.5919	0.4238
PHKA2	8	1122	0.3473	0.6080	-0.4306	-0.2093	0.2277	0.4202	-0.2262	0.4987	0.7903
PI4KAP2	7	-0.9652	-1091	0.3258	NA	-0.1037	0.1373	-0.5925	0.1557	NA	-0.5845
PIH1D1	7	-0.9806	-0.3925	-0.0931	-0.2997	0.0033	0.1232	-0.2816	0.0662	-0.3515	-0.2433
PIK3AP1	7	1947	1408835063	0.7425	2220	-0.2907	-0.3173	0.9006	NA	0.8721	NA
PIK3C2B	7	-1856	-1061	-0.3779	-0.0611	0.6303	0.0305	-1108	0.0765	-1317	-1487
PIK3CD	9	0.7855	-0.3745	0.9875	0.6832	0.2653	0.2345	-0.3814	0.1833	-0.0933	-0.4331
PIK3IP1	7	-1700	-0.8120	0.6150	NA	0.4800	-0.0036	-13164	NA	-1136	-0.3953
PILRA	7	0.7311	-1031	NA	1860	-0.1447	0.1740	-0.4862	0.2252	-0.4352	-0.7547
PIP5K1C	7	-0.7147	-0.3472	-0.1266	-0.6051	-0.1301	0.2011	-0.4330	-0.0265	-0.5414	-0.2649
PLCB2	7	-0.3126	0.1347	0.9938	-1033	-0.6640	0.2890	-0.2117	0.2367	-0.7982	0.1086
PLEKHG4	7	-1411	-0.6620	-0.3207	-0.4068	NA	0.0200	-0.4561	-0.1688	-0.1121	-0.4480
PLEKHO1	7	-0.9442	-1126	0.3178	1019	-0.6584	-0.0700	-1170	NA	-0.8281	-1026
PLEKHO2	8	1095	0.2248	1033	NA	-0.2376	0.2639	0.2830	0.1350	0.5171	0.3670
PNPO	8	-1049	-0.5961	-0.7988	-0.9322	-0.1389	-0.1341	-0.6062	-0.1235	-0.3190	-0.9400
POGK	7	-0.7379	-0.7087	-0.3446	-0.4678	-0.0147	-0.0201	-0.7508	0.0238	-0.2844	-0.6250
POLE3	7	-0.9271	-0.7587	-0.6797	-0.3855	-0.0850	-0.0612	-0.4352	0.0935	-0.2288	-0.2813
POLR1C	7	-1822	-0.7390	NA	-0.6688	-0.1002	0.0859	-0.5866	-0.0593	-0.7445	-0.5778
POLR2I	7	-1046	-0.4053	-0.5478	-0.4435	-0.3577	0.2501	-0.0804	0.1193	-0.1584	0.1027
POLR3A	7	-0.5978	-0.4070	-0.0500	-0.2510	-0.1703	0.1073	-0.2671	-0.0800	-0.3554	-0.1435
POP7	7	-0.6228	-0.0173	-0.3280	-0.5935	NA	0.0151	0.2325	0.1245	0.1999	0.2076
POR	7	1667	1075	0.2932	-0.6620	0.5424	0.1490	1102	-0.0057	1479	0.8437
PPAN	7	-2112	-0.4115	-0.5055	-0.7759	NA	0.0565	-0.4161	-0.0676	NA	-0.2413
PPHLN1	8	-0.5298	-0.2073	-0.1281	0.1123	-0.1999	-0.0631	-0.4193	0.2012	-0.3043	-0.4131
PPM1G	7	-0.5869	-0.5247	-0.0238	-0.4509	-0.0975	0.1960	-0.4231	0.0542	-0.3659	-0.4756
PPM1M	7	1261	0.8731	1092	-0.4991	0.0708	-0.0276	0.6748	NA	0.6650	1172
PPP1R13B	7	-2677	-0.5528	-0.2721	0.5860	NA	-0.0180	-0.5407	-0.0175	-0.6486	-1067
PPP1R2	8	-0.7342	-1056	-0.3760	0.5510	-0.1061	-0.3036	-0.7337	NA	0.4006	-0.5853

PPP2R1A	8	-0.4270	-0.5231	-0.2957	-0.6300	-0.2913	0.2001	-0.5258	-0.1251	-0.3468	-0.1189
PPP2R5A	7	0.6064	0.5094	0.6731	-0.9720	0.0462	-0.0257	0.2399	-0.0007	0.5327	0.2613
PPRC1	7	-1689	-0.6804	-0.8518	-0.6244	-0.2177	0.0452	-0.7886	-0.0868	-0.6939	-0.9635
PQLC1	8	0.7059	0.6167	0.7788	-0.4513	0.2903	-0.0206	0.8092	NA	0.5289	0.7390
PRDX5	7	0.5499	0.4420	NA	0.0841	-0.5171	0.2128	0.6487	0.0887	0.5461	0.6045
PRDX6	7	0.5849	0.4193	-0.5429	0.1566	0.1758	-0.3923	0.4018	-0.2735	0.0304	0.4497
PRKAR2A	7	1578	0.4885	0.2221	-0.6769	0.0930	0.0376	0.3787	NA	0.5753	-0.2691
PRKD2	7	NA	-0.9958	0.3128	1573	-0.0133	0.1327	-0.6288	0.1342	-0.2805	-0.7482
PRKRA	7	-1228	NA	-0.3380	-0.2652	-0.2597	-0.1465	-0.8325	0.0983	-0.6819	-0.4123
PRMT7	7	-0.9456	-0.7277	-0.3993	-0.6511	NA	0.0321	-0.4434	0.0360	-1096	-0.4420
PROK2	8	1189	1316	1733	1932	1138	-0.3545	0.8743	NA	1301	0.7231
PRPF19	7	-1730	-0.5869	-0.9871	-0.8878	NA	0.0968	-0.6212	0.0693	-0.7745	-0.8846
PRPF31	8	-0.9074	-0.8900	-0.3498	-0.3210	-0.2855	0.2503	-0.5452	0.0797	-0.4190	-0.2869
PRPF4	7	-0.5692	-0.5569	-0.7260	-0.3194	-0.1130	0.0667	-0.5537	0.0157	-0.4130	-0.3163
PRPS1	8	-1518	-1181	-0.7217	0.2731	0.4682	0.0244	-0.8434	0.1343	-0.5123	-0.6570
PRPSAP2	7	-0.7025	-0.5615	NA	0.0092	-0.3921	-0.0475	-0.3612	0.1813	-0.2206	-0.2099
PRR7	7	-0.9023	-0.2687	-0.1529	-0.0491	-0.5974	0.0859	-0.1227	-0.0438	0.2489	0.3244
PRTN3	7	1986	1667	0.9343	-0.0750	NA	0.6682	1945	NA	1039	0.6678
PSMC6	7	0.1209	1082	NA	-0.4944	-0.2633	-0.1062	0.9679	0.0693	0.7144	1683
PSTPIP2	7	2298	1935	0.9461	2707	-0.1619	0.0105	1862	NA	2016	2125
PTBP1	8	-0.6650	-0.5412	-0.5835	-0.5023	-0.0460	0.3431	-0.6207	0.0175	-0.7433	-0.7977
PTDSS1	7	-0.7317	-0.5829	-0.0737	-0.8973	0.1007	0.2120	-0.6889	0.0773	-0.4821	-0.4029
PTEN	7	0.9732	0.7244	-0.1364	0.1853	0.3621	-0.2644	0.6842	0.2043	1005	0.6759
PTGES	7	2631	0.3327	-0.9870	4897	-1477	0.0538	NA	NA	1091	0.3396
PTMA	7	-1032	-0.8895	-0.9052	0.6013	-0.2854	-0.5838	-0.7487	0.2867	NA	-0.6819
PTPN12	7	0.8512	0.1338	NA	0.9347	-0.0308	-0.4275	0.4291	0.1967	0.6083	0.6291
PTPRCAP	7	-2387	-1540	1162	2524	-0.0437	0.1803	-1025	0.3542	-0.9934	-1452
PUS7	7	-1881	-0.4530	-0.7281	-1181	-0.4247	0.0307	-0.9162	0.0867	-0.3316	-0.7181
PWP1	7	-1265	-0.9129	-0.4777	-0.5311	0.0016	0.0892	-0.5970	0.1582	-0.6546	-0.2524
PYGL	8	2020	1470	0.6570	-0.8065	0.3523	-0.1486	1401	-0.1980	0.7832	1248
QPCT	7	1173	0.9110	0.1164	2238	-0.3976	0.0297	1327	NA	0.9783	0.9485

RAB10	7	0.6368	1228	-0.0583	-0.3952	-0.1596	-0.2700	1037	-0.1282	0.4884	0.9415
RAB11A	7	0.7049	0.4015	-0.0829	-0.0615	-0.0682	-0.4830	0.4371	0.1813	0.4415	0.7587
RAB24	7	1414	0.6998	NA	0.3417	-0.2439	0.0161	0.6551	0.1040	1357	1239
RAB27A	8	1200	1172	0.0935	0.3077	0.5159	0.0082	0.7280	-0.1988	0.9739	1201
RAB32	7	1567	1305	0.5431	-0.0547	-0.1154	0.1793	1448	-0.1802	1290	1991
RAB33B	7	1056	1286	0.0272	0.7302	0.2703	-0.4242	0.4488	NA	1284	1237
RAB8B	7	0.7715	1381	0.7827	-0.2436	-0.1534	-0.1861	0.4556	0.1278	0.3773	0.9487
RABAC1	8	0.4577	0.4156	0.8586	0.2870	0.1750	0.4309	0.6587	-0.0462	0.6850	0.6996
RANBP9	7	1787	NA	-0.1450	0.1657	0.0218	-0.0875	0.4769	-0.3132	0.4235	0.7112
RASGRP1	8	-2084	-2096	0.2404	2066	-0.3786	-0.2744	-1972	NA	-1617	-1872
RAVER1	7	-0.6196	-0.4835	-0.3363	0.3409	-0.1965	0.1630	-0.3664	-0.0935	-0.0611	-0.1696
RBBP7	7	-1270	-1009	-0.9658	0.3625	-0.0283	-0.1703	-0.6637	0.1253	-0.8448	-0.6835
RBM14	7	-0.8289	-0.4562	-0.5996	-0.6809	-0.0600	0.0113	-0.6110	-0.0300	-0.6660	-0.6534
RBM15B	7	-1534	-0.2739	-0.2107	-0.4556	NA	0.0113	-0.6321	NA	-0.2527	-0.3949
RBM28	7	-0.8892	-0.3552	-0.1791	-0.5198	0.2007	0.0530	-0.1883	-0.0047	-0.8773	-0.2889
RBM4B	8	-1102	-0.8196	-0.2980	0.1410	-0.6026	0.0628	-0.7872	0.1463	-0.5348	-1219
RBMX	7	-0.5735	-0.6226	-0.4271	0.6569	0.0281	-0.0033	-0.5775	-0.0893	-0.5439	-0.5867
RCC2	7	-1111	-0.7161	-0.7577	-0.7591	-0.2356	-0.0014	-0.7157	0.0685	-0.6308	-1230
RCSD1	9	-0.1417	-0.5015	0.6854	1393	-0.6471	0.1004	-0.9063	0.2707	-0.3683	-0.3681
RDH11	7	-0.2497	-0.1523	-0.4686	1110	-0.0922	-0.2241	-0.5364	0.1980	-0.4452	-0.2161
RETN	7	4390	4846	1623	1364	0.1961	0.4411	3900	-0.3797	2095	2687
REV1	8	-1009	-0.2655	-0.2966	0.1089	-0.2323	-0.1120	-0.3496	0.0097	-0.6235	-0.4706
RFTN1	7	-1790	-1647	0.4357	2243	0.1668	-0.1230	-1513	0.4888	-1198	-1773
RFWD2	7	0.7551	0.4881	0.0942	-0.0220	-0.2039	-0.2420	0.2086	0.1945	NA	0.2961
RFX5	7	-0.8003	-0.6267	NA	1235	-0.7030	0.0708	-0.6901	0.1012	-0.6479	-1184
RGL4	8	3145	2577	1664	NA	-0.3039	-0.0296	2758	0.2567	1289	3255
RGS18	9	0.1224	1022	1059	1182	0.5466	-0.7070	0.6180	0.3633	0.7234	1563
RGS19	7	0.8798	0.3960	1010	0.0900	-0.2155	0.1693	0.2631	0.0987	0.9272	0.8332
RHBDF2	7	1615	0.4290	0.0439	0.6625	-0.1252	0.1116	0.4592	-0.2148	0.9333	0.9104
RHOF	7	-1417	-1243	-0.3620	0.1571	-0.7976	0.0239	-0.9819	NA	-0.9361	-1163
RHOT2	8	-0.5611	-0.2210	0.0511	-0.5425	-0.2048	0.1489	-0.1803	0.1233	-0.3127	-0.3616

RING1	7	-0.7586	-0.5995	-0.3978	-0.0910	-0.1952	0.1780	-0.4381	-0.0167	-0.2734	-0.7535
RNASE2	7	-0.1051	2817	2234	1306	-0.0208	0.8438	3135	NA	1615	2732
RNASE6	7	-1851	-0.8361	0.9937	-0.1426	0.5708	-0.0207	-0.5289	NA	-0.6699	-0.5276
RNASEH1	7	-1274	-0.2651	0.1380	-0.9747	-0.2077	0.0464	-0.2212	0.0887	-0.6000	-0.7185
RNF175	7	-0.3696	0.3297	-0.0422	0.2540	0.3410	-0.1014	0.3587	NA	0.5690	1555
RNF4	8	-0.5816	-0.7819	0.2413	-0.0953	-0.1991	-0.1083	-0.6267	0.1298	-0.1837	-0.5669
RNH1	7	-0.8132	-0.4199	0.0337	-1389	NA	0.1455	-0.3514	0.0195	-0.2261	-0.5405
RNMT	7	-1395	-0.7831	-0.2229	-0.5843	-0.3785	0.1017	-0.8137	0.0563	-0.6368	-1092
RPA1	7	-1265	-1136	-0.2458	-0.3057	-0.1748	-0.0930	-1073	0.3303	-0.8802	-0.9048
RPL18	7	-1294	-1427	-0.3118	NA	-0.1141	0.0153	-0.9036	0.3453	-0.5948	-1257
RPL26L1	7	-0.5574	0.6661	-0.3915	-0.6615	0.2521	0.0329	0.8520	-0.0603	-0.1833	1202
RPL29	8	NA	-0.9939	-1031	-0.9164	NA	0.0780	-0.5351	0.2507	-0.3801	-0.7447
RPL32	7	-0.9101	-0.8451	-0.0010	-0.1887	-0.1247	-0.0030	-0.4625	0.3633	-0.7267	-0.2864
RPL36	7	-1495	-1163	-0.2340	0.0911	-0.0015	0.0119	-0.6999	0.2655	-0.3571	-0.5322
RPL36A	7	NA	0.3180	-1081	-0.1358	NA	-0.0563	0.4049	0.3680	-0.4168	0.6362
RPL37A	7	-0.8739	-0.6155	-0.1404	-0.5702	-0.0741	-0.0128	-0.6025	0.3430	NA	-0.4223
RPL4	7	-1468	-1070	-0.5771	-0.7385	0.0160	-0.0138	-0.5424	0.2918	-0.7910	-0.6174
RPS13	7	-0.9926	-0.6324	-0.5417	-0.6154	-0.0823	-0.0616	-0.4082	0.2370	-0.0024	-0.1990
RPS15	9	-1166	-0.8418	-0.4925	-0.8488	0.0338	0.0922	-0.6080	0.3007	-0.5968	-0.6624
RPS16	7	-0.8017	-0.6789	-0.0643	-0.2239	0.1677	-0.1742	-0.4744	0.3388	-0.8580	-0.6479
RPS19	7	-0.6976	-0.8979	-0.1873	-0.0388	-0.1196	-0.0234	-0.5021	0.3020	-0.6981	-0.7129
RPS9	7	-0.4845	-0.3524	-0.0443	-0.2244	0.2107	0.2326	-0.0249	0.2947	0.3030	0.2208
RPUSD4	7	-1277	-0.8092	-0.5028	-0.4674	-0.1095	0.0244	-0.6266	-0.0393	-0.3140	-0.9402
RRN3	7	-1488	-0.6501	-0.5717	-0.3272	-0.1902	-0.0778	-0.7839	0.3442	-0.7449	-0.8487
RRS1	7	-1713	-0.9144	-0.6941	-1262	NA	0.0639	-1143	0.0738	-0.3055	-0.9235
RSAD1	7	-1621	-1152	-0.2604	-0.5725	NA	0.0106	-1086	0.1505	-0.7041	-0.9363
RUSC1	7	-0.9274	-0.4549	-0.8769	-0.4730	0.0301	0.1451	-0.5401	-0.0971	0.1787	-0.3184
S100A12	8	3179	3376	2459	2496	-0.0276	0.4381	3234	0.1883	1965	3506
S100A6	7	0.9528	0.8264	0.4043	-0.8508	-0.1367	-0.3078	0.8422	0.0818	0.5639	1060
S100A8	8	0.9531	1298	2591	2672	0.0249	0.1596	1128	0.3317	1548	2422
S100A9	8	0.8986	1362	2238	3318	-0.0541	0.0801	1505	0.3567	1157	2223

SAP30L	7	1181	0.3112	-0.1292	0.6875	-0.0425	-0.3152	0.4211	NA	0.4234	1063
SCRN1	7	-1543	-1302	-0.0392	-0.6325	NA	0.1065	-1280	0.4153	-0.5716	-0.9078
SDCBP	7	1533	0.4198	NA	-0.1350	0.0568	-0.3893	0.3529	0.1747	0.4741	0.4593
SDF2	7	0.6842	0.6202	0.2716	0.3602	-0.2284	0.0103	0.7250	0.1073	0.6031	1223
SDHAF1	7	NA	-0.5086	-0.1627	NA	-0.4149	NA	-0.2685	0.1053	-0.2194	-0.2042
SDHC	7	0.6576	0.4637	NA	-0.9551	-0.0089	-0.0425	0.3488	-0.2051	0.8487	0.5069
SELL	8	1519	0.2594	2199	2331	0.1351	0.2592	0.3431	0.3027	0.2188	0.4853
SEMA4A	8	1603	0.5967	1022	2100	-0.2761	0.3953	0.7471	NA	0.7320	NA
SENP5	7	0.8974	-0.1726	-0.0794	0.3287	-0.1890	-0.0545	-0.3448	-0.0263	-0.2127	-0.1761
SEPHS2	7	1296	0.5262	0.2670	-0.1837	0.0891	-0.2413	0.7033	-0.2232	1096	1195
SERPINB1	8	1993	2293	0.7577	0.9335	0.0027	0.2177	1827	-0.1703	1412	1464
SET	7	-1018	-0.8132	-0.7531	-0.4266	-0.3611	0.0584	-0.4764	0.3077	-0.1576	-0.5795
SF3A3	7	-1648	-1030	-0.3909	-0.5770	-0.4115	-0.0376	-0.7957	-0.0390	-0.6253	-0.9132
SFXN5	7	0.7346	0.3944	0.2461	-0.4978	NA	0.1768	0.3495	NA	0.6126	0.9542
SH2B2	7	1042	-0.3004	0.6076	0.0982	-0.1755	0.1509	0.4685	-0.0043	0.5987	0.2462
SH2D1A	9	-2500	-0.2216	0.5304	0.9929	0.0551	-0.2342	-0.4833	0.5462	-0.9048	-0.6259
SH3GLB1	7	1883	0.7652	0.8302	0.2292	0.4258	-0.0207	1365	NA	1298	1577
SIL1	7	1346	0.3996	-0.0290	-0.7526	0.2331	0.0479	0.4803	-0.2526	0.5414	0.6244
SIN3B	7	-0.6470	-0.5930	0.0234	-0.3616	-0.3990	0.1198	-0.5753	0.1514	-0.5225	-0.2942
SIPA1	7	0.5197	-0.2904	0.7749	0.8450	-0.3038	-0.2671	-0.1452	0.0617	0.1592	0.2431
SKAP1	7	-3022	-1549	NA	1575	NA	-0.0487	-1362	0.6445	-1519	-1697
SKAP2	7	1212	1150	NA	-0.1672	0.3116	-0.0263	0.4105	0.2502	0.7940	0.9117
SLA	8	1515	0.8058	NA	2520	0.5645	-0.0945	0.8261	0.1800	0.7315	0.9017
SLC11A1	7	NA	0.8181	NA	1280	0.3555	0.1017	0.9404	0.1533	0.5415	0.4250
SLC12A9	7	1007	0.3694	0.8990	-0.1769	0.4317	0.1370	0.5635	0.0697	0.9073	0.7099
SLC22A4	7	NA	1471	NA	0.8514	0.2262	NA	1690	-0.2568	1514	1739
SLC25A5	7	-0.7192	-0.7125	-0.5987	-0.5593	-0.0675	-0.0128	-0.3988	0.0905	-0.3293	-0.3824
SLC35A5	8	0.7116	0.8087	0.4888	0.5800	-0.1802	-0.1943	0.5193	-0.0152	0.6476	0.7976
SLC35B2	9	-0.9764	-0.6854	-0.4117	0.4798	-0.6840	0.1766	-0.3965	-0.1180	-0.4178	-0.4616
SLC39A10	7	-1551	-1122	-0.5281	-0.5062	NA	-0.0015	-1088	NA	-0.8353	-0.6516
SLC41A1	7	-2534	-1017	-0.3790	0.4113	NA	0.0296	-0.7718	NA	-0.7146	-1045

SLC5A6	8	-1124	-0.3240	-0.5830	-1129	0.0420	0.1518	-0.2732	-0.0725	-0.3140	-0.6741
SLC9A3R1	9	-0.8568	-0.7930	0.4707	0.7416	-0.3524	-0.0841	-0.5423	0.1933	-0.6200	-0.9987
SMAD4	7	-0.1147	-0.5725	-0.2591	0.5421	-0.0645	-0.3361	-0.4416	-0.3269	-0.2719	-0.7329
SMAD7	7	NA	-0.7782	-0.0580	0.9663	-0.6749	-0.0503	-0.9340	0.1421	-0.3266	-0.6682
SMARCC1	7	-0.6121	-0.5971	-0.7491	-0.7273	0.0758	0.0404	-0.7523	-0.0622	-0.4942	-0.3844
SMCHD1	7	-0.0041	-0.5942	0.4260	NA	0.3132	-0.0136	-0.7067	0.2937	-0.4549	-0.6948
SMYD3	7	-1896	-0.5122	-0.3682	0.1237	NA	-0.0430	-0.4424	0.2420	-0.8623	-0.3851
SND1	7	-0.4295	-0.5722	-0.4964	-1086	0.0655	0.2284	-0.4892	0.0012	-0.5410	-0.6488
SNRPA	8	-0.7231	-0.8618	-0.5869	-0.5656	NA	0.1763	-0.4836	0.0045	-0.2495	-0.3713
SNRPG	7	-0.4717	0.8246	-0.6732	-0.5127	-0.1976	0.1627	0.9959	0.1617	NA	1560
SNX10	8	1440	0.9225	0.2582	1558	-0.0681	-0.7789	0.4141	0.1328	0.9261	1001
SORT1	7	2709	1624	0.3069	-2067	1131	0.4064	1283	-0.2750	1623	NA
SPATA5L1	7	0.0861	0.2643	-0.4580	-0.2753	-0.2172	0.0223	0.2632	-0.0447	0.3153	0.2601
SPNS3	8	-3069	-0.5394	0.3029	NA	-0.2130	0.0934	-0.2150	0.4308	-0.6860	-0.4691
SPOCK2	7	-2750	-0.7197	0.7699	2908	-0.1517	-0.0798	-1036	NA	-1562	-1387
SPPL2A	8	1590	1358	0.4457	0.8606	-0.3926	0.0908	1095	-0.0585	0.7220	1272
SRFBP1	7	-1339	-0.236	-0.1686	-0.5557	NA	-0.0447	-0.2459	-0.1550	-0.3528	-0.3013
SRGN	8	0.7517	0.424	NA	0.6052	-0.0304	-0.2876	0.8230	0.3483	0.3421	0.6888
SRM	7	-1332	-0.962	-0.8002	-1303	-0.0089	0.1898	-0.3862	-0.0678	-0.4970	-0.4403
SRP68	9	-0.8930	-0.622	-0.3637	0	-0.2897	0.2001	-0.5911	0.1137	-0.4721	-0.4023
SRP72	7	-0.9245	-0.555	-0.3050	-0.5069	-0.1304	0.0570	-0.4980	-0.0098	-0.5226	-0.2429
SRPRB	7	-1560	-1268	-0.6285	-1768	NA	0.1123	-0.6123	0.2365	-0.4285	-1042
SRRM1	7	-0.4958	-0.6979	-0.4521	-0.0265	-0.1053	-0.0692	-1174	0.1459	-0.6669	-0.9162
SSRP1	7	-1057	-0.9197	-0.4751	-0.5796	0.0050	-0.0076	-0.9151	0.0505	-1005	-1144
ST3GAL1	7	-0.0365	-0.4319	0.1614	1998	0.4593	0.0014	-0.7450	-0.0415	-0.2951	-0.6841
ST3GAL2	8	1090	0.2232	0.2671	0.6454	-0.2933	0.0145	0.4270	-0.1080	0.6535	0.2117
ST6GAL1	7	NA	-1321	-0.0011	0.2425	-0.3073	0.0162	-1512	0.2763	-1093	-1710
ST6GALN	7	-1572	-0.2776	0.3097	-0.2111	0.3432	0.0275	-1	0.2095	-0.6989	-0.4765
STAM2	7	1014	0.3988	0.1519	0.7679	-0.0997	-0.0802	0.2237	NA	0.4957	0.4836
STARD7	7	-0.7261	-0.3611	0.1429	-0.7831	-0.2288	0.1736	-0.5655	0.0860	-0.5221	-0.6118
STAT4	7	-1591	-1644	0.6156	3171	-0.1177	0.0015	-1498	NA	-1022	-1629

STK10	7	0.2687	-0.4570	0.6961	-0.0394	-0.1906	0.1807	-0.3528	0.1283	-0.5385	-0.4843
STK40	7	0.3309	-0.4980	0.2104	-0.3196	-0.1659	-0.0242	-0.4447	0.1582	-0.0554	-0.2532
STOM	7	2206	2672	NA	1751	NA	-0.1268	2054	-0.7320	1606	1921
SUCLG1	7	0.2048	0.3333	-0.1853	-0.6166	-0.3525	-0.1666	0.4267	-0.0896	0.5429	0.8965
SUMF1	8	0.7006	0.7057	-0.1327	-0.6872	0.5163	-0.1920	0.3743	-0.1374	0.0485	0.8099
SUPT16H	9	-0.9037	-0.5900	-0.6110	-0.6549	-0.2258	0.1989	-0.6706	-0.1046	-0.8505	-0.4302
SUPV3L1	7	-1253	-0.5066	-0.4505	-0.0957	NA	0.0649	-0.4488	-0.0008	-0.6506	-0.7491
SURF6	7	-0.8368	-0.4505	-0.7297	-0.2108	-0.4692	0.1074	-0.3465	0.1204	-0.5427	-0.0163
TAF15	7	-0.6782	-0.9450	NA	-0.3290	-0.2524	0.0353	-0.4338	-0.2523	-0.8938	-1536
TAF4	7	-1338	0.0911	-0.4594	-0.2185	-0.2885	-0.1585	-1158	0.2276	-0.8033	-0.4505
TARBP2	8	-1340	-0.3484	-0.5166	-0.8385	0.1399	0.0495	-0.1633	-0.0045	0.1456	-0.3294
TATDN2	7	-0.7039	-0.3856	0.2747	-0.1281	-0.1820	0.1459	-0.4138	-0.0242	-0.8325	-0.6771
TBC1D10A	8	-0.9096	-0.7332	0.1553	0.5781	-0.5082	0.0169	-0.6564	0.1720	-0.2557	-0.1666
TBC1D10C	8	-0.6220	-0.7808	1608	0.9601	-0.3686	0.1763	-0.4266	0.2650	-0.1324	-0.3468
TBC1D14	8	1030	0.4231	0.5795	-0.4870	1309	0.2741	0.2110	-0.0893	0.4382	0.7059
TBC1D9	7	-2065	-0.2849	-0.1887	2415	NA	-0.0684	-0.3458	-0.1871	-1047	-0.1980
TBCD	7	-1011	-0.2882	-0.1245	-0.0359	0.0190	0.1509	-0.4769	0.1062	-0.4965	-0.5375
TBL3	8	-1180	-0.5016	-0.2550	-0.5121	NA	0.0562	-0.3296	0.0977	-0.2818	-0.3187
TGIF2	7	-0.7214	-0.7403	-0.2946	0.3160	-0.7186	-0.0301	-0.7755	NA	-0.6188	-0.6150
THOC1	7	-1705	-0.5725	-0.5265	-0.2673	-0.7235	-0.0257	-0.6638	NA	-0.9605	-0.7919
TIGD2	7	-1121	-0.5322	-0.1505	-0.2664	NA	0.0516	-0.3989	NA	-0.0490	-0.3356
TIMM44	7	-2119	-0.3988	-0.4826	-0.8441	NA	0.0639	-0.1547	-0.0055	-0.5016	-0.0371
TIMM9	7	-1731	-0.8405	-0.6592	-0.5759	0.1582	0.0526	-0.4709	0.0483	-0.3171	-0.4971
TK1	8	1399	0.5577	-0.8414	0.6576	NA	0.2216	0.7321	-0.1367	0.5353	0.5910
TLR2	7	2623	0.5921	0.1784	1665	2346	-0.0116	0.8493	NA	0.9794	0.8085
TLR5	8	2893	2407	1553	-0.7302	0.9072	0.3242	2232	-0.2747	2244	2198
TMBIM4	7	0.4384	0.3155	0.5150	0.2343	-0.1347	-0.2313	0.5992	NA	0.4368	0.7631
TMC8	7	-1058	-1231	0.2929	0.1418	-0.3539	-0.0070	-1319	0.1475	-1155	-1237
TMCC1	7	NA	-0.8907	0.0167	-0.4680	-0.3842	-0.0777	0.0196	0.4577	-0.5610	0.1338
TMEM106	7	-1178	-0.8566	-0.0840	0.0271	0.4313	-0.2223	-0.3917	-0.0212	-0.3167	-0.6565
TMEM109	9	-1529	-0.9417	-0.4742	0.0564	-0.3192	0.1608	-1103	0.3405	-0.8052	-0.8988

TMEM120	7	1225	0.7815	0.6567	NA	0.2171	0.0926	0.9782	0.1207	1292	1272
TMEM14A	7	-2858	-0.7370	-0.7082	0.5065	NA	0.0167	-0.6888	0.0995	-0.5128	-0.8180
TMEM165	7	2388	0.3037	-0.0118	0.9180	0.0530	-0.1097	1072	-0.3131	1203	0.5090
TMEM50B	8	-1050	-0.5495	0.1129	0.1914	-0.2756	0.0678	-0.4452	0.2177	-0.4565	-0.8954
TMEM55A	7	0.7303	0.9715	0.3678	0.0268	-0.3011	-0.2813	0.7226	0.1963	NA	1344
TNFAIP2	8	0.4110	-1356	0.4590	-0.6880	-0.7578	0.2274	-1077	0.5083	-0.5594	NA
TNFAIP3	7	1665	0.2286	0.5070	1573	0.4120	-0.0337	0.2375	-0.2832	0.8173	0.6126
TNFRSF1B	8	0.7116	-0.3942	1735	0.9467	-0.1915	-0.1531	-0.3138	0.0583	-0.3408	-0.4768
TNFRSF25	7	-2918	-0.9263	0.0826	2190	-0.3170	0.0021	-0.1416	0.4133	-1035	-0.4051
TNNI2	7	1112	0.3062	0.1468	-1727	-0.4388	-0.0037	0.4726	0.0593	0.3584	0.7626
TOLLIP	7	0.9153	0.4728	0.3831	-0.7089	-0.0709	0.0981	0.2641	-0.0188	0.4376	0.5506
TOR1AIP1	7	0.4440	1022	0.4885	0.7698	-0.1907	-0.2891	0.0906	NA	0.3383	0.7735
TPD52L2	8	0.8269	0.3755	NA	-0.8495	0.2524	-0.2301	0.4410	-0.0108	0.4932	0.6106
TPM3	7	1115	0.3058	0.1324	-0.4474	0.1568	-0.0122	0.1618	0.1062	0.1623	0.1422
TPST2	7	1350	1032	NA	-0.1441	0.5977	-0.0979	1317	-0.2593	0.6508	1289
TRAF3IP3	8	-1084	-0.9901	0.9521	0.8512	0.1095	0.2047	-0.5727	NA	-0.3459	-0.5340
TRAM2	7	-0.7622	-0.3934	-0.3214	-0.7241	NA	0.1334	-0.3614	0.0265	-0.4435	-0.4097
TRAP1	8	-1940	-0.5924	-0.8546	-1016	NA	0.0974	-0.4730	-0.0590	-0.9420	-0.8005
TRIM25	8	1547	0.6809	0.9085	-0.4310	1425	0.2985	0.8264	-0.1132	0.8813	0.7786
TRIM28	7	-1206	-1328	-0.2460	-0.0900	-0.2797	0.2018	-1003	-0.0203	-0.6696	-0.5282
TRIP6	7	0.3448	-0.0389	-0.7522	-0.8011	0.0936	0.1163	0.3555	-0.3588	0.7784	0.3416
TRIT1	7	-1941	-0.7887	-0.6594	-0.0685	-0.1756	-0.1123	-0.8171	-0.0070	-0.9609	-1105
TROAP	7	1595	0.3320	-0.6112	0.2352	NA	0.0723	NA	-0.1193	0.3327	0.5519
TRPM2	7	NA	0.5240	0.0390	0.1285	0.9064	0.0597	0.5573	-0.6504	1458	0.7464
TSFM	7	-0.9422	-0.2548	-0.3358	0.7339	NA	0.0196	-0.3751	0.0733	-0.4964	-0.2870
TSPAN14	7	1098	0.4127	0.5230	0.9741	0.4927	0.0823	0.1559	NA	0.3751	0.4346
TSPYL1	8	-0.5023	-0.6697	0.1388	0.6793	-0.1194	-0.2039	-0.7037	0.2586	-0.1147	-0.8409
TXNIP	8	0.1222	-0.8072	0.9431	-0.6712	0.3129	-0.2881	-0.6557	0.3275	-0.4435	-0.7045
TYROBP	7	0.5326	0.3346	2571	0.0256	-0.0866	0.1622	0.4284	0.4187	0.1112	0.2627
UBA3	7	0.7493	0.7061	0.2130	NA	-0.2303	-0.0795	0.6410	0.1232	0.3377	0.9694
UBA52	8	-0.4664	-0.2449	-0.3657	-0.4967	-0.0237	-0.1202	-0.3370	0.3025	-0.1509	-0.2123

UBAP1	7	0.9814	0.6758	0.5291	0.6209	0.1402	-0.0938	0.6790	-0.1020	0.6093	0.6185
UBE2A	7	0.4985	0.3416	NA	0.3703	0.1306	-0.0822	0.4846	-0.0693	1049	0.6618
UBE2C	7	NA	0.6204	-0.3474	0.4449	NA	-0.0171	1049	-0.3005	0.6394	0.9338
UBE2E2	7	-1618	-0.6297	-0.4702	-0.5517	0.0510	-0.0606	-0.7653	NA	-0.3112	-0.7176
UBE2Q2	7	-1386	-1166	-0.1727	-0.0190	0.1096	-0.2569	-10896518	0.3948	-0.5669	-0.6049
UBE2W	7	0.9172	0.9399	-0.0032	0.1399	0.1633	-0.0812	0.7693	0.1480	1098	NA
UBTD1	7	0.9526	0.4504	0.8371	-0.7243	0.0908	0.2184	0.4151	0.0092	0.6928	0.5079
UFSP2	7	-1389	-0.8665	-0.3098	NA	-0.3860	0.0264	-0.4623	0.0070	-0.7821	-0.3298
UGCG	8	3108	2292	0.7518	1391	0.5244	0.2591	NA	-0.4981	2417	2377
UPF1	7	0.0062	-0.4455	0.1741	-0.4774	0.2156	0.1559	-0.4188	0.0313	-0.2166	-0.2089
UPRT	7	-1079	-0.6725	-0.3976	-0.1847	-0.1049	-0.0350	-0.8049	0.2247	-0.4206	-0.4002
UQCRQ	7	-0.4393	0.6027	-0.6053	-0.6862	-0.0893	0.4978	0.9973	0.2737	0.2446	1787
UROS	7	-1184	-0.5155	-0.4780	-1011	0.0603	0.0235	-0.3507	0.3027	-0.1900	-0.1870
USP3	9	0.8324	0.3466	0.4607	0.4092	0.2349	0.1950	0.3761	NA	0.2261	0.3918
UTP14A	7	-1028	-0.6598	-0.2759	-0.4375	NA	0.0801	-0.1317	-0.0293	-0.5293	-0.2210
UTP6	7	-0.4606	-0.6130	-0.3854	-0.2190	-0.3775	-0.1464	-0.1910	0.3194	-0.6423	-0.2927
UXT	7	-0.6771	-0.5537	-0.2192	0.2534	-0.1677	0.1760	-0.2396	0.1187	0.1981	0.1318
VAMP2	7	-0.7742	-0.7679	0.6534	0.1458	-0.0074	0.1912	-1005	NA	-0.1915	-0.6144
VAMP7	7	0.5348	0.8423	0.0202	NA	-0.1808	-0.0976	0.6063	0.1249	0.9273	1282
VDAC1	8	-0.6655	0.1759	-0.6400	-0.8456	-0.3012	0.3027	-0.3558	-0.1158	0.2484	-0.5865
VIPR1	7	-1135	-0.7691	0.3867	0.3517	0.0125	0.0855	-0.6402	NA	-0.8810	-0.9299
VNN2	7	1287	1197	-0.0060	0.4449	0.1930	0.0349	1275	0.3683	0.3423	0.8356
WBP11	8	-0.9854	-1138	-0.1068	-0.1123	-0.3870	-0.0215	-1071	0.2458	-0.7676	-0.5449
WDR46	8	-1298	-0.2804	-0.5209	-0.8083	-0.2043	0.2169	-0.4168	0.0035	-0.4646	-0.4055
WDR54	7	-2212	-1365	-0.9207	0.9382	-0.2383	-0.0178	-0.8828	0.0143	-0.5914	-1356
WDR74	7	-2395	-0.8731	NA	-0.1708	0.3006	-0.0059	-0.3071	0.0095	-0.5264	-0.4698
WDR77	8	-1391	-0.3531	-0.4701	-0.3472	-0.0118	0.0949	-0.2687	-0.0008	-0.6952	-1191
WDR82	7	-0.6459	-0.8255	0.6965	NA	-0.1470	0.2130	-0.8770	NA	-0.5535	-0.8664
XPO5	7	-1533	-0.3921	-0.6189	-0.5137	NA	0.0182	-0.4918	0.0715	-0.7472	-0.5007
XPO6	7	1101	0.1135	0.7783	-0.2591	0.9796	0.2671	0.3172	0.0800	0.1704	0.2527
XRCC6	7	-1	-0.9041	NA	-0.1350	-0.0987	0.2342	-0.5597	0.2948	-0.2730	-0.7702

YWHAQ	8	-0.6238	-0.4144	-0.6234	-0.4648	-0.0012	-0.3958	-0.5066	0.0198	-0.3001	-0.2767
YY1	7	-0.0819	-0.5354	NA	0.2860	-0.2330	-0.4709	-0.3018	0.1756	-0.1418	-0.3430
ZBTB2	7	-0.9999	-0.5737	-0.1414	0.4974	-0.2204	-0.0989	-0.7992	-0.0490	-0.2781	-0.3738
ZBTB4	7	-1499	-0.7238	NA	0.2050	-0.2207	-0.1087	-0.6413	0.3188	-0.7208	-1533
ZBTB9	7	-2073	-0.6368	-0.4368	-0.6536	NA	0.0626	-0.5928	NA	-0.2987	-0.5524
ZC3H12A	9	1978	0.3764	0.5785	1456	-0.2232	0.1805	0.4818	-0.2188	0.6718	0.7471
ZDHHC12	7	1023	0.3633	0.2811	0.0996	-0.1959	0.2239	0.3467	NA	0.8635	0.8167
ZDHHC3	7	1389	1180	0.2169	-0.2116	0.1381	0.1696	0.5437	NA	0.9065	1445
ZMYND19	7	-1922	-0.3181	-0.7605	-0.5745	NA	0.0429	-0.2665	NA	-0.3709	-0.2576
ZNF281	7	1104	0.9704	0.7133	0.9846	1003	0.1590	0.7569	-0.0930	0.8877	NA
ZNF329	8	-2348	-1189	-0.1799	-0.1207	-0.2407	-0.0017	-0.9658	0.3292	-0.3012	-0.7565
ZNF559	8	-1516	-1138	-0.2231	0.1710	-0.3451	-0.1039	-1018	NA	-0.4366	-0.9328

Supplementary table 3: p-values for differentially expressed genes in each GSE

Gene	nsigstudies	GSE13015	GSE28750	GSE32707	GSE46955	GSE49757	GSE54514	GSE57065	GSE67652	GSE69063	GSE95233
FCER1G	8	3.14E+03	8.03E+06	1.27E+09	2.07E+09	0.0084618	0.1055214	1.11E-10	0.8065696	2.77E-10	1.11E-15
GPR84	7	5.70E+03	1.13E+03	3.41E-04	7.06E+09	0.1328291	0.5590299	3.95E-03	NA	6.21E-08	2.21E-16
DYSF	8	7.87E+03	8.76E+06	6.51E-04	0.7592669	0.0107861	0.027234	1.26E-06	0.1452541	1.15E-05	1.44E-02
TLR5	8	1.67E+04	1.13E+03	1.56E+09	0.3654939	0.0278729	0.1558305	8.39E-14	0.0037686	5.42E-11	3.38E-09
MMP9	9	3.09E+04	2.53E+06	3.42E-04	3.12E-01	8.47E+08	0.0393654	2.74E-06	0.0326073	1.20E-03	3.72E-06
HP	7	3.67E+04	1.75E+03	7.32E+09	9.14E-01	0.1119298	0.6193582	8.09E-07	0.0024331	2.07E-13	5.51E-20
RAB32	7	1.55E+05	7.26E+05	0.0382286	0.8893501	0.4971537	0.2258945	3.15E-08	0.0272385	2.09E-03	1.86E-13
S100A12	8	3.65E+05	4.04E+01	3.12E+09	0.0001841	0.8818664	0.1182596	1.11E-14	0.0411347	4.20E-18	8.29E-21
PFKFB3	7	4.31E+04	5.43E+04	NA	0.000321	0.4605598	NA	8.28E-03	0.004812	5.01E-10	3.39E-08
DDAH2	8	4.31E+04	2.26E+07	9.05E+09	0.0169819	0.0584674	0.8170874	1.34E-03	0.0040862	7.25E-05	1.63E-09
SH3GLB1	7	4.31E+04	0.00025989	0.0033377	0.3419421	0.0011166	9.34E-01	1.70E-03	NA	3.97E-06	5.42E-07
PGLYRP1	8	6.54E+05	1.33E+07	8.11E+07	0.479304	1.88E-01	0.0080864	1.08E-05	0.0036683	3.51E-05	1.04E-04
IFNGR2	8	8.11E+05	0.00987831	0.0013776	0.012446	0.0008162	0.8168352	1.19E+09	0.7432529	6.05E-04	7.28E+02
FPR1	9	9.10E+05	4.19E-04	7.15E+09	0.0400248	2.02E-04	6.31E-01	1.41E+03	0.0021367	2.86E+06	7.29E+04
PGS1	7	1.09E+06	1.85E+07	0.0029496	NA	0.032722	0.6039737	9.90E-08	0.7556796	1.33E-06	1.26E-10
HK3	8	1.11E+06	2.21E+04	1.22E+09	7.83E-02	0.0037616	0.0261197	7.90E-08	NA	3.84E-07	3.10E-15
AQP9	8	1.16E+06	6.35E+09	0.0003152	1.99E+09	0.1903581	0.8468034	1.78E+06	0.0057495	2.81E+03	2.12E+04
RGL4	8	1.27E+06	3.88E+06	2.19E+09	NA	0.0179863	0.9453887	1.98E-02	0.0058659	1.56E-03	1.13E-19
GADD45B	7	1.59E+06	1.00E-03	0.0032458	7.87E-01	0.014045	0.7280176	1.19E-03	0.3289707	1.39E-09	2.76E-04
ID3	8	1.96E+06	1.72E+04	1.56E+08	0.0001641	0.0026489	0.7015292	2.45E-05	0.3741736	2.33E+03	1.94E-04
TRIM25	8	1.99E+06	3.25E-03	0.0007804	0.0756835	0.0003681	0.043671	1.37E+03	0.1616623	1.90E-03	5.11E+04
CNIH4	7	2.70E+06	4.48E+04	6.29E-01	0.0107821	0.0777265	0.3018905	1.23E+01	0.006246	5.89E-14	1.80E-17
ANXA3	9	3.66E+06	7.83E+03	1.20E-02	0.003152	4.73E-02	0.3678683	3.14E-14	NA	1.09E-18	2.14E-17
ACSL1	9	4.14E+06	1.03E+08	0.0397904	3.69E-02	0.0052866	0.00539	1.97E-01	0.1813689	1.31E-15	1.61E-02
FLOT1	8	4.19E+06	2.73E-04	3.38E-02	0.0005288	0.9715024	0.365475	8.52E-03	0.0053993	8.97E-13	6.48E-11
LMNB1	7	4.69E+06	4.93E+08	1.17E-01	0.0992537	0.0047543	0.4327227	2.31E-02	0.0021367	4.36E-04	1.64E+01
SORT1	7	5.49E+06	3.92E+06	0.2845243	0.0002008	0.0037413	0.0316943	9.34E+02	0.0505777	1.58E-03	NA
IL18R1	7	5.49E+06	9.41E+08	0.1493638	0.0002623	3.76E+07	0.8587684	5.09E-03	NA	2.56E-16	2.26E-14
IL18RAP	8	7.50E+06	1.65E+07	0.0006953	0.0128446	0.0002046	0.9579791	1.14E-06	0.1970552	1.10E-07	5.66E-15

CKAP4	7	8.27E+06	2.30E+06	9.39E+09	0.9856811	0.0441474	0.0996788	NA	0.0021367	2.24E-10	4.76E-18
MYD88	8	8.73E+04	1.83E-02	6.37E+09	0.3027634	0.0001185	0.0281235	8.28E+07	0.5919174	6.46E+02	5.15E+04
ITGAM	8	9.30E+06	3.86E+06	1.76E-03	4.04E-02	0.0298729	0.1228347	5.47E-05	NA	9.81E+02	1.04E-01
BRI3	8	1.00E+07	0.00193317	0.0032696	0.0043267	0.5017974	0.0055582	9.52E+03	NA	5.17E-06	3.01E-04
TPST2	7	1.24E+07	1.12E+08	NA	0.1329261	0.0115231	0.4411075	2.56E-08	0.0090378	4.65E+05	6.30E-09
SELL	8	1.27E+07	0.12106582	8.38E+09	0.0008679	0.2658512	0.0395039	8.94E+08	0.0027604	1.87E+06	1.60E+07
PSTPIP2	7	1.48E+07	3.02E+07	0.0022508	3.72E+09	0.7007554	0.9671686	3.15E-01	NA	1.12E-07	6.73E-09
CST7	9	1.48E+07	4.13E+04	5.09E+08	0.0014852	0.0365756	0.8827977	8.62E-08	0.0005796	1.26E-07	1.02E-04
PHF21A	7	1.49E+07	2.27E-02	1.99E-01	7.90E+09	0.3750616	0.7995419	1.10E+05	0.0298743	1.16E+02	5.60E+06
STOM	7	1.52E+07	1.06E+04	NA	5.97E+08	NA	2.50E-01	2.41E-02	0.0006499	1.22E-11	1.59E-18
CTSD	8	2.02E+07	1.17E+07	9.75E+09	0.1866086	0.5129912	0.0011773	3.10E+03	0.0147398	1.19E-02	1.45E+04
S100A9	8	2.34E+07	1.75E+03	2.19E+09	2.47E+09	0.5392234	0.1068696	3.52E-16	0.0036954	1.09E-12	2.18E-22
JUNB	7	2.60E+06	2.16E-02	0.0388258	0.4802375	0.2274305	0.2747504	7.01E+05	0.0347967	1.41E-08	5.28E+04
FAIM3	7	2.71E+07	9.45E+04	0.0338452	0.0059397	0.0044705	0.8695988	2.70E-10	NA	NA	8.59E-09
SDCBP	7	3.42E+07	2.57E-02	NA	7.34E-01	0.4331405	0.013572	9.51E+08	0.0165344	8.35E+01	1.62E+06
CDA	8	3.49E+07	6.52E-03	7.17E-03	0.0712957	0.0375483	0.233197	9.70E+06	0.032871	2.94E-02	1.81E+06
FGFBP2	7	3.55E+07	1.45E-04	0.0085225	0.0069535	0.2061774	0.2397635	3.91E+05	NA	4.11E+06	1.22E-01
BASP1	7	3.78E+07	8.80E+09	4.04E-01	5.90E+08	0.0178906	0.0594805	4.22E+05	0.9035138	4.06E-02	3.08E+05
MTF1	9	3.88E+07	8.36E+05	0.0001056	0.0014495	0.9139693	9.24E+09	1.01E-04	0.026054	7.71E+04	7.00E-05
OSM	8	4.03E+07	3.40E-03	1.20E-02	8.43E+09	5.22E+08	0.3563131	NA	0.0026794	3.86E-11	6.25E-03
FLOT2	7	4.03E+07	8.08E-04	3.26E-02	5.60E+08	0.1645145	0.6657358	7.43E+02	0.6153604	6.56E-02	1.28E+00
CXCL16	7	4.95E+07	1.04E-02	0.9219969	0.0002443	6.01E+06	0.509069	1.51E-02	NA	8.27E-06	8.89E-04
IL10RB	7	5.46E+07	0.00016355	NA	0.0066881	0.1602656	0.0180194	1.53E-02	0.1414105	3.16E-08	8.35E-10
KLHL2	8	6.47E+07	7.09E+08	5.79E-01	0.032605	0.0088187	0.0115639	6.71E-01	NA	2.70E-12	2.13E-06
TMEM165	7	7.40E+07	0.0009856	9.63E-01	0.0026934	0.8540853	0.266118	3.68E+01	0.0097564	1.30E-11	4.09E+07
GRAMD1A	7	7.40E+07	1.31E-04	4.19E-02	1.25E+08	0.7421849	9.74E-01	1.53E+05	NA	2.13E-07	5.52E-02
AIM2	7	7.40E+07	1.86E+09	0.4017583	0.0079405	7.51E-01	0.0270692	1.27E+02	NA	5.52E-06	1.08E-02
ENTPD1	8	8.81E+07	1.63E+09	2.24E-03	9.03E+09	0.0006698	7.36E-02	5.20E+00	0.0561154	1.51E+07	8.26E-01
PIK3AP1	7	8.88E+07	5.12E+07	2.03E-02	0.0004626	0.0123143	0.0539378	4.67E+06	NA	6.62E+00	NA
GNS	7	9.62E+07	4.25E+08	0.3704314	0.0896493	0.0013806	0.3438336	2.26E+07	0.0036174	4.41E+05	8.90E+03
CD160	7	9.92E+07	1.72E+07	0.4130903	0.0361713	1	0.0014802	2.72E+03	NA	4.50E+02	3.31E-06

NCF4	8	1.08E+08	1.35E-04	NA	0.0323963	0.3493764	1.48E+08	2.90E+03	0.0054482	3.77E-06	1.65E-02
VNN2	7	1.10E+08	1.19E+09	0.9321742	0.0001425	0.1100305	0.8827977	2.53E+01	0.0024331	9.14E+07	8.16E+05
KLRB1	7	1.10E+08	3.84E+08	0.0016436	1.17E-01	0.2013392	7.24E-03	6.44E+01	NA	4.44E+08	7.01E+01
FGR	7	1.21E+08	4.72E+09	0.6497458	1.39E+09	0.722467	0.9189468	1.38E+05	0.0039255	1.46E-02	3.92E+01
SEMA4A	8	1.28E+08	1.08E-02	0.0024224	5.49E+08	0.0211453	0.0059192	1.82E+05	NA	4.49E+04	NA
IER3	7	1.29E+08	6.16E+09	0.5926209	0.0012794	0.0486614	0.6756075	4.12E+04	NA	3.24E+02	3.30E-06
EOMES	7	1.29E+08	1.43E+08	0.0005499	0.017297	0.7724763	0.1989757	2.53E+01	NA	1.59E+04	1.98E-07
CD6	7	1.33E+08	2.79E+06	0.0038913	3.82E-03	0.1058934	0.9557351	3.47E-06	0.2062753	1.70E-06	8.73E-04
CD2	7	1.33E+08	6.05E+06	0.0010428	0.0009539	0.1132488	0.6279737	4.24E-01	NA	4.47E-02	9.73E-07
NFKBIA	7	1.35E+08	0.07815391	0.0019248	0.0012442	0.0091363	0.8324099	1.23E+04	NA	5.95E+03	1.12E+00
UGCG	8	1.65E+08	2.10E+07	0.0036747	0.0068927	0.0308621	0.2611001	NA	0.0028531	5.13E-10	1.20E-14
PCNX	8	1.72E+08	0.00030551	0.0022651	3.48E+09	0.0009874	0.2111311	6.65E+05	0.0313208	NA	1.13E+06
RHBDF2	7	1.75E+08	0.02610173	0.3571162	0.0190349	0.3964457	0.0656179	3.55E-04	0.0449196	8.30E+02	3.93E+02
ALOX5AP	7	1.80E+08	6.68E+08	5.28E+09	0.1036802	9.47E-01	0.9455392	1.53E-02	0.0086692	3.22E+01	1.05E-09
NTSR1	7	1.85E+08	5.49E-04	0.0092221	4.79E-01	0.0408149	0.7916274	1.27E+09	NA	2.96E-04	2.04E+08
SLA	8	1.85E+08	1.95E-03	NA	7.13E+09	0.0181356	0.2371982	4.81E+04	0.0202086	5.03E-07	1.44E+01
PTPRCAP	7	2.06E+08	1.01E+06	2.84E-04	0.0006307	0.6758535	0.3860607	1.19E+06	0.0890838	3.72E+05	8.79E+00
TLR2	7	2.13E+08	1.79E-02	0.4840663	8.18E+08	8.55E+08	0.9381336	1.27E+07	NA	2.11E-01	4.52E+07
IFNAR1	7	2.50E+07	1.19E-04	0.0003716	0.0377185	0.5216913	0.7654936	2.16E-04	0.8873546	9.40E+01	2.11E+03
CTSA	9	2.56E+08	0.00019761	0.0068628	0.0106861	0.0283727	0.0077579	7.77E+06	NA	4.86E-02	2.95E+09
SPOCK2	7	2.59E+08	7.39E+08	4.73E-02	0.0006992	0.1763956	0.811919	5.89E-09	NA	5.59E-03	1.32E-07
S100A8	8	2.70E+08	3.35E+05	1.62E+09	0.0003432	0.8760581	0.065566	3.15E-08	0.0449196	6.66E-15	2.56E-20
GPR160	7	3.05E+08	3.28E+07	0.8650717	0.0102629	0.1651905	0.0063445	1.70E-01	0.9640948	3.15E-16	6.70E-10
SH2D1A	9	3.09E+08	0.04940154	0.001543	0.0208596	0.5008826	2.64E-04	1.36E+07	0.0317486	8.50E+03	6.85E+01
SPPL2A	8	3.09E+08	1.09E+07	0.0494031	5.30E+08	3.12E+06	0.6284021	7.20E+01	0.4117019	7.73E+00	1.65E-02
LY96	7	3.12E+08	2.91E+07	8.52E+09	0.5430897	0.0255825	0.5525968	1.27E+05	0.1826623	2.37E-12	3.71E-08
CD82	7	3.27E+08	0.00640921	NA	3.28E-04	0.0004102	0.8127916	2.56E+03	0.897688	8.14E+08	3.41E+00
IFNGR1	7	3.38E+08	2.57E+08	0.003128	7.98E-02	0.0058681	0.2786359	1.62E-01	0.1141394	1.69E-07	1.45E-06
GNA15	8	3.40E+08	1.97E+07	0.0007777	1.49E-04	0.0037927	0.1666456	2.02E+05	NA	8.45E+05	2.29E+03
BIN1	7	3.50E+08	1.06E+08	NA	0.0497765	0.0494819	NA	2.07E-06	0.5263574	4.84E-02	1.54E+00
PYGL	8	3.57E+08	1.76E+07	0.0639424	3.99E-02	0.0213803	0.4442449	5.58E-06	0.0093815	5.25E+05	1.03E-02

DDX18	8	3.65E+07	2.34E+09	0.2638456	0.0039094	2.28E-02	0.2452073	7.64E+00	0.0058659	8.99E-01	1.62E-01
C17orf62	7	3.86E+08	1.63E-03	9.80E+09	0.0077916	0.0647775	6.46E+07	4.15E+07	0.3560475	NA	6.61E-03
RASGRP1	8	3.91E+08	6.71E+08	0.2457724	0.0006269	0.0039047	0.0012379	2.06E+00	NA	4.93E-06	7.30E-07
EP400	8	3.94E+07	1.80E-03	0.0044668	0.0013568	0.0001251	0.2776441	1.74E+04	0.6054053	1.86E-11	2.47E-07
GAPDH	7	4.06E+08	6.09E+05	0.805639	0.9305574	0.0452481	0.0610678	3.90E-02	0.0063148	5.62E-04	4.41E-05
HCK	9	4.11E+08	1.32E-02	4.12E+09	3.08E+07	1.11E-02	0.2770428	2.26E+07	0.0187224	1.45E+01	2.09E+06
LBH	7	4.21E+08	1.04E+06	5.64E-01	0.0016149	0.0835593	0.0189468	9.88E-07	NA	2.12E+04	1.65E-07
CD55	8	4.35E+08	1.52E+06	0.0811636	3.59E+08	0.0005996	0.1357499	1.77E-04	0.0250045	3.79E-01	1.44E-03
IFITM1	8	4.48E+07	0.00639724	0.0004175	0.0058647	3.78E-04	0.7636443	2.43E+07	NA	8.12E-02	3.48E-02
DOK3	8	4.58E+08	2.18E-04	0.0011072	1.06E-02	0.230584	0.6966368	1.32E+06	0.0492792	2.83E+03	1.25E+07
ACAA1	7	5.06E+08	0.00041561	7.63E+09	0.5034814	0.9437272	1.58E-02	1.36E+07	0.2782577	1.06E+04	1.81E-04
GZMH	8	5.11E+08	4.76E-03	0.0012139	0.0149466	0.9988811	0.3833839	4.65E-04	0.0121954	8.59E+09	5.67E+02
CEBPD	7	5.17E+08	0.0001002	0.0029082	0.5569872	5.67E+07	0.9364082	1.10E+00	0.9086592	3.32E-06	1.59E-06
LTB4R	7	5.51E+08	6.66E+08	0.0006043	0.6638795	0.1472392	0.0318463	6.55E-01	0.9035138	4.66E-04	1.15E+08
CD3G	8	5.54E+07	5.39E+07	0.0118089	0.0048022	NA	0.0006953	5.58E+03	0.099017	4.76E-07	2.52E-09
NFE2	7	6.14E+08	5.18E+08	1.38E-03	0.0206731	0.4717044	0.713058	1.92E+03	0.2500556	6.83E-04	2.75E-01
HIST2H2B	7	6.54E+08	5.21E+09	5.25E-03	1.87E+09	0.0515659	0.7041515	1.15E+08	NA	1.14E-08	1.52E-06
RAB24	7	6.57E+08	2.43E-04	NA	0.0484717	0.0229452	0.7267084	2.17E+07	0.1833323	2.95E-07	5.83E-05
ICOS	7	6.70E+08	5.91E+08	0.045098	1.11E-02	NA	0.4597591	4.48E+03	NA	4.43E+02	2.02E+01
HNRNPA0	7	7.64E+08	NA	6.13E+08	NA	0.9865416	0.0150837	4.15E+00	0.040819	6.98E-03	1.73E-04
PRPS1	8	7.86E+07	1.70E+07	0.0003065	0.3739585	0.0056561	0.6938285	1.30E-02	0.0453489	2.33E+08	3.44E+03
C1orf162	7	8.09E+07	2.24E+08	2.92E+09	0.8222679	0.0295526	0.5989937	1.47E+05	NA	2.40E+07	2.93E-02
SRGN	8	8.24E+08	8.64E-04	NA	0.0019358	0.395456	0.0456611	2.05E-06	0.0033186	2.20E+00	3.86E-03
SERPINB1	8	8.42E+08	1.56E+06	0.0116193	0.0025316	0.9933919	0.4323425	6.67E-04	0.0259919	7.73E-09	3.54E-10
NFIL3	8	8.85E+08	0.00282836	0.3688418	2.72E+05	8.03E+09	8.33E+09	2.31E+03	0.5099232	2.64E-11	1.12E+01
KLHL22	8	9.19E+08	4.94E+07	0.0031769	0.0360066	0.1495491	0.2718276	1.43E-03	0.0151133	1.34E-02	1.90E-05
MAP4K1	7	9.23E+08	1.73E+07	NA	0.013336	0.8098299	3.18E-02	6.29E-04	NA	3.07E-03	7.91E-11
WDR74	7	9.28E+08	3.89E+06	NA	0.0344474	0.0196545	0.8689793	1.61E-04	0.846917	3.12E+08	4.36E+07
ZC3H12A	9	9.49E+08	2.05E-02	5.57E+09	0.0012115	0.1055488	0.0288647	8.70E+08	0.0139723	5.71E+09	1.61E+02
CD52	7	1.00E+09	0.01467488	0.0002113	8.73E+09	0.1997789	0.4333836	NA	0.009247	3.01E+09	4.20E-03
CLIC1	8	1.02E+09	9.36E+05	0.0047271	2.09E-02	0.7856149	0.1672896	1.67E+00	0.0472646	3.07E-11	1.37E-16

SNX10	8	1.03E+09	1.61E-02	4.24E-01	0.0035655	0.5219259	8.80E+05	9.11E-03	0.0397716	8.45E-02	3.12E+06
GNG5	7	1.08E+07	1.48E+09	2.48E-01	5.14E+09	6.68E-02	1.68E-01	9.63E+00	0.0178077	4.01E+01	7.61E-11
DYNLT1	7	1.08E+07	3.58E+08	7.64E-04	0.2010583	0.011867	0.2079517	1.10E+04	0.3471391	3.68E-04	1.20E-14
ZNF329	8	1.12E+09	8.12E+07	0.0114848	0.5558849	0.0100212	0.9782301	3.26E+00	0.0095448	2.13E+09	1.17E+05
IFITM2	7	1.16E+09	0.0689834	1.38E-02	0.2315708	0.0121617	0.4603625	2.45E+08	0.0200553	2.06E-03	1.65E-04
DIRC2	7	1.16E+09	5.38E+07	4.62E-01	0.0017845	0.0006408	0.4311347	6.09E-01	0.0028435	6.59E+06	NA
IMP3	8	1.17E+09	1.72E+07	1.35E-02	0.7149962	0.0006368	0.9718371	2.61E-05	0.0211151	3.80E+04	2.26E-06
GIMAP7	7	1.18E+09	6.07E+09	NA	0.0015484	0.5466657	1.95E+09	2.23E-04	NA	7.56E+03	2.43E+09
FES	8	1.21E+09	1.33E+09	1.11E+09	0.0400276	6.26E-03	0.898772	3.03E+05	0.6413626	1.88E-02	9.63E-04
RNMT	7	1.30E+09	6.85E+07	0.1526179	4.38E+09	0.0129554	0.0679405	4.55E+00	0.677844	6.26E+02	1.54E-09
FBL	7	1.50E+09	6.11E+06	1.62E-03	0.0265059	1.05E-01	0.8814821	8.56E+03	0.2667132	1.69E-04	2.66E-02
GZMA	7	1.57E+09	0.00146607	0.0009017	0.0009229	8.89E-01	0.2343003	1.34E+07	NA	3.94E+09	4.18E+06
APEX1	7	1.66E+09	2.89E+06	NA	3.07E-02	0.0295458	0.2001125	9.28E+05	0.2476189	1.90E+02	2.43E+01
RETN	7	1.68E+09	8.33E+00	2.69E+09	0.0582124	0.4523545	0.2647522	2.44E-02	0.0308956	1.37E+02	7.87E-02
IL2RB	8	1.78E+09	3.62E+05	0.067609	1.51E-04	0.0044277	0.0302279	1.93E-09	NA	2.44E+03	6.73E-14
SKAP1	7	1.81E+07	8.48E+05	NA	0.0038524	NA	0.4989646	5.93E-01	0.0421408	6.00E-03	2.91E-08
RPL36	7	1.88E+09	2.87E+08	0.0099596	0.8449033	0.9855273	0.6806007	3.32E+09	0.0143613	7.01E-03	1.44E+09
FERMT3	7	1.95E+09	2.27E-04	NA	NA	0.0435985	0.0038817	7.20E+08	0.4022814	2.19E-04	5.77E-01
GZMK	7	2.03E+09	0.00011399	2.03E-04	0.0032032	0.602173	0.0544084	4.20E+01	NA	2.20E+04	9.49E-02
ZBTB4	7	2.04E+08	1.18E+08	NA	0.4715825	0.0167498	0.1129455	9.62E+01	0.0106393	8.99E+05	3.49E-12
RPL18	7	2.05E+09	6.81E+05	0.1460317	NA	0.0121617	0.9510087	1.27E+05	0.0114218	2.15E+05	1.10E+01
UBAP1	7	2.05E+09	6.11E+08	4.58E-02	0.0024552	0.218887	0.4391242	3.96E+01	0.0705055	3.59E+00	7.42E+00
APH1B	8	2.06E+09	2.93E+09	0.0014737	1.33E-02	0.000545	0.5957998	6.22E+08	0.8362993	6.25E+05	2.75E+08
STAT4	7	2.08E+09	1.09E+07	0.0050128	8.67E+05	0.408341	0.9926893	5.52E-04	NA	2.41E+05	4.36E-01
TMEM109	9	2.11E+09	2.41E+08	0.0136757	0.8457429	0.0489165	0.0384393	2.27E-06	0.0104476	1.95E+03	4.60E-08
FBXO6	7	2.17E+09	9.98E-03	0.0010803	0.0286435	0.9645726	0.8647693	9.10E-04	NA	6.01E+01	3.78E+03
CASP5	7	2.23E+09	0.13404416	0.0397904	2.88E-03	0.0863194	0.4220029	3.55E+08	0.0413181	4.58E-04	3.29E+07
COQ10A	7	2.29E+08	1.32E+07	4.75E-03	3.28E-04	0.1431762	0.5169853	4.24E+00	0.0850097	1.69E+08	3.12E-04
WDR54	7	2.40E+09	3.43E+04	6.56E-04	0.0006285	0.0769698	0.9095375	8.15E-02	0.7990997	1.10E+00	2.15E-06
CD7	7	2.52E+09	NA	0.0010964	2.30E-03	1.77E+08	0.7313119	3.64E-07	0.6818203	1.57E+08	3.62E+08
PAG1	8	2.53E+08	3.82E+09	NA	0.0009685	0.0023975	0.4048996	6.50E+06	0.0320425	1.19E+04	2.68E-01

ZDHHC3	7	2.65E+09	1.89E+07	0.0456881	0.5243102	0.2595438	0.0348483	1.23E+04	NA	1.19E-08	1.66E-13
POR	7	2.80E+09	8.21E+08	2.16E-01	0.0420693	0.0385821	0.2798827	4.06E+02	0.9247385	8.36E-05	1.05E+02
MXD1	7	2.80E+09	0.0189841	1.24E-03	0.0083231	0.4526296	0.8633579	3.21E-04	0.0063614	3.74E+08	5.41E-01
CD3E	8	2.81E+09	5.19E+05	7.13E-04	0.0192568	NA	0.0395945	4.96E-05	NA	3.09E-05	4.54E-07
CYB5R4	8	2.96E+09	NA	0.0031059	0.0402602	0.6255381	0.0026745	1.79E+06	0.0047711	1.95E+00	5.64E+02
FAM89A	8	3.13E+09	4.56E+07	0.0344734	0.0002719	0.1042628	0.9278054	1.04E+04	0.0028909	1.01E+08	1.96E-01
GLOD4	7	3.18E+09	4.39E+09	0.001665	NA	0.9816821	0.276408	6.70E+04	0.0278904	5.04E-06	3.38E+05
ORM1	7	3.19E+09	3.96E+09	3.12E-04	0.1221315	0.0001392	0.3189191	3.71E+04	0.3954678	7.80E+08	1.84E+02
XRCC6	7	3.45E+09	1.78E+08	NA	0.6516215	0.2690863	0.0039734	1.60E+07	0.0028909	1.58E+09	5.94E-04
PCSK7	7	3.60E+08	3.39E+07	1.89E-02	0.02519	0.689652	0.0908969	1.10E-04	NA	5.35E-07	1.22E-17
NAT10	8	3.61E+09	3.99E+08	3.11E+09	0.0057253	0.2924575	0.6908434	1.82E-05	0.0380333	3.68E-10	3.85E-12
PPP1R13B	7	3.73E+08	6.71E+08	0.0004245	0.0046524	NA	0.7180988	4.08E+05	0.7817715	1.11E+00	5.88E-09
PPM1M	7	3.81E+09	1.02E+08	0.0006614	3.12E-02	0.5248702	0.9031289	8.47E+06	NA	1.03E+06	1.97E-01
LDHA	7	3.83E+09	5.33E+06	1.75E-01	1.59E-03	0.070984	0.1074304	2.34E+00	0.0028531	1.30E-02	1.47E-12
SLC9A3R1	9	4.02E+09	1.74E+08	0.0324921	0.0010347	0.0158634	0.5121724	1.23E+07	0.0097239	2.67E+04	1.33E-08
MFNG	7	4.11E+09	1.36E+06	0.0023131	0.0069508	0.4532831	0.1209211	7.79E+02	NA	1.08E+02	7.75E-05
TBCD	7	4.46E+09	8.48E-03	0.0198486	0.8630072	0.9105828	0.0032476	1.29E+05	0.1001406	2.07E+03	6.66E+00
CAMK1	7	4.47E+09	0.00096044	0.0799082	0.0029296	0.1582038	0.0393092	2.95E+09	NA	2.96E-03	8.83E+05
EIF2B1	7	4.49E+09	5.61E-03	0.0679605	0.0005894	0.0279722	0.703005	1.02E+06	0.1940629	1.18E+04	1.15E+09
NUP93	7	4.49E+09	1.94E+08	2.68E+09	0.0625124	0.1669326	0.1101269	8.82E-07	0.0021953	7.57E-03	8.65E-15
XPO6	7	4.64E+09	6.27E-01	1.02E-02	0.34902	1.83E+08	0.0230318	7.98E-04	0.1361614	2.34E-02	2.35E-02
HIST1H3D	7	4.74E+09	5.92E-04	0.068547	0.0012086	0.796819	0.6022628	1.64E+02	0.039386	3.74E-02	8.97E-06
CARD11	7	4.82E+09	2.67E+08	1.51E-02	3.50E-03	0.9104234	0.0953955	2.34E-05	NA	8.03E-05	2.66E-02
GPD1L	7	4.95E+09	2.20E-02	0.0197158	0.000228	0.2149301	0.1997837	4.65E+02	0.3554171	1.63E+02	2.39E+07
MARCKSL	7	5.08E+09	1.13E+07	0.9093305	0.0027221	0.0004177	0.9756361	4.29E-04	0.2291697	4.83E+08	3.97E-02
GCA	9	5.26E+09	1.61E+08	0.0011166	1.67E-02	0.2480172	0.0167564	2.60E+02	0.0096656	5.97E-08	2.81E+00
SF3A3	7	5.30E+09	5.46E+08	0.103243	0.0088493	0.0047454	0.7895508	6.44E+05	0.5793783	8.14E+03	3.62E+00
UFSP2	7	5.43E+09	3.21E+08	0.0255288	NA	0.0176532	0.4753538	1.14E-04	0.9631257	5.40E-03	2.82E-04
KCNJ2	9	5.43E+09	2.97E-03	0.0026646	8.71E-04	0.6710429	0.9419686	0.0002614	0.0230792	4.47E-01	1.51E-04
BATF	8	5.44E+09	2.23E+07	1.36E+09	2.70E-01	0.0413383	0.630327	1.57E+05	0.0027853	1.70E+02	6.02E-07
NELL2	7	5.44E+09	1.07E+05	1.03E-01	0.0012776	0.0003077	0.8124171	1.01E-08	NA	1.02E-07	1.45E-06

CD63	7	5.48E+08	2.32E+06	3.58E-02	6.02E+09	0.3076869	0.4645261	5.89E-09	0.8326212	7.33E+04	1.59E-08
SAP30L	7	5.50E+09	2.00E-03	0.4199421	5.14E-03	0.6713549	4.07E+09	5.85E+09	NA	1.34E+07	1.38E-04
UBE2Q2	7	5.50E+09	0.00132525	0.4264012	0.942689	0.1763956	0.001399	1.09E+05	0.0095892	3.46E+09	9.67E+07
NPTN	7	5.56E+09	3.66E-02	0.4451582	0.2945012	0.0286129	0.0135366	4.17E-03	NA	4.89E+07	8.96E+09
IL7R	7	5.61E+09	1.84E+07	NA	1.56E-03	0.0001468	NA	2.21E+00	NA	1.97E-02	1.69E-03
C3AR1	9	5.64E+08	5.62E+06	0.0022508	0.0021409	0.016951	0.0393287	2.56E+01	0.6235126	3.11E-03	3.85E-05
ITK	8	5.71E+09	1.62E+07	0.013549	0.0004626	0.0048085	0.6188752	1.30E-03	NA	2.61E+00	3.42E-04
DCUN1D3	7	5.81E+09	0.00552661	0.0124837	0.0116791	0.1030135	0.6072299	9.14E+09	0.1627041	3.73E-01	6.68E+07
USP3	9	6.06E+09	0.02408319	3.80E-03	0.0322919	0.0257556	0.0192175	6.06E+09	NA	6.45E+05	3.84E+09
FBXO21	7	6.16E+09	7.19E-01	0.0001685	0.0040434	0.9265011	0.7488447	1.04E-06	0.0440936	4.73E-03	2.03E-05
RPS15	9	6.27E+09	1.19E+07	0.0024629	0.0049993	0.6562848	0.0016663	1.78E+06	0.0073807	2.52E+04	9.91E+05
RPL4	7	6.44E+09	3.29E+08	0.0240337	0.0547192	0.8418272	0.9548815	8.33E+09	0.0137765	3.31E+01	1.06E+05
UPRT	7	6.48E+09	0.01238934	1.62E+09	0.1032294	0.550398	0.424633	1.17E+05	0.0184558	2.82E+08	3.00E-04
PI4KAP2	7	7.18E+08	4.23E+08	2.87E-02	NA	0.4168119	0.0152814	4.75E+03	0.0484848	NA	4.74E+02
ACD	7	7.20E+09	4.47E+07	6.62E-04	4.70E-01	0.5043245	0.1657122	3.29E+08	0.0179108	6.73E+03	1.15E+02
ENOPH1	7	7.53E+09	2.80E-02	0.0003487	0.0022754	0.3039984	0.0542856	1.16E-03	0.4257854	1.82E+04	1.41E-03
IL10RA	7	7.60E+09	7.75E+07	0.0001434	4.87E+09	0.7614561	0.9765628	1.06E-02	0.3492778	7.11E+05	7.53E-12
SIL1	7	7.71E+09	1.64E-04	6.26E-01	0.0096075	0.0686971	0.6406854	2.66E+06	0.0060829	2.29E+06	9.75E+03
LEO1	8	7.71E+09	5.86E-03	0.0002651	0.0358535	0.0003681	4.22E-01	9.38E-04	0.757327	2.81E+01	2.83E+09
LILRB2	8	7.84E+09	0.0006712	0.005519	0.4975696	0.0471208	0.2180977	3.27E+08	0.004817	4.37E-02	2.87E-03
EEF2K	7	8.19E+09	1.70E+08	0.0013347	0.0013762	0.9505854	2.03E-01	NA	0.0276044	1.13E-08	1.85E-06
FARS2	7	8.26E+09	9.35E-03	0.0034081	4.83E-01	NA	0.046121	1.14E+08	NA	1.98E+03	4.75E-02
UXT	7	8.26E+08	5.44E+09	0.0348734	0.3819614	0.0058657	0.0539375	2.77E-02	0.0479563	1.92E-02	1.19E-01
CMTM6	7	8.27E+09	0.00085245	0.0012488	8.36E-02	0.069524	0.1545876	5.48E+07	0.0352969	2.90E-06	6.56E+05
RFTN1	7	8.28E+09	4.98E+06	0.1943768	1.39E+09	0.0059118	4.10E-01	1.21E-04	0.0594536	3.87E-01	5.47E-10
LFNG	7	8.46E+09	1.79E+09	0.0432476	0.0827259	0.0001089	0.1919518	1.31E+04	NA	1.91E+04	2.34E-01
SUPV3L1	7	8.50E+09	0.01105686	5.90E-03	0.6466111	NA	0.0299692	4.14E+08	0.9893771	3.31E+05	6.82E+02
CEACAM3	7	8.56E+09	5.82E-03	4.28E+08	0.0009707	0.0058657	0.4535039	0.0011902	NA	0.0147084	NA
NUP210	7	8.59E+09	1.07E+07	0.0258721	0.7704812	NA	0.0154034	4.30E-06	0.4880974	1.01E-01	3.27E+02
IGSF6	7	8.59E+09	1.19E-02	3.01E+09	0.0088374	0.2903136	0.8374634	3.46E+03	NA	3.42E+06	1.05E+07
COPS6	7	8.93E+09	0.00056256	0.0014014	0.0234952	0.1250011	0.1989157	0.0225402	0.0301818	2.54E+09	1.10E-01

ST6GALN	7	8.95E+09	2.93E-02	0.0345222	0.5359101	0.0344227	0.8474414	1.65E+03	0.0947661	4.20E+08	4.08E+09
SPNS3	8	9.05E+09	0.00183191	0.0005665	NA	0.1899702	0.0342345	3.35E-02	0.0206837	4.58E+02	3.63E+07
MPHOSPH	7	9.05E+09	1.68E+09	0.8075941	0.0105833	0.3022816	0.0164102	5.16E+07	0.1652121	6.66E+04	1.43E+07
GZMM	7	9.10E+09	4.53E+08	0.0033448	0.0047291	0.6964219	0.7889797	4.90E+05	0.3741583	4.63E-01	3.40E-02
DKC1	7	9.23E+09	7.74E+06	2.52E+09	0.0001109	0.091472	0.1069317	1.79E-01	0.9853273	5.92E-06	4.32E+00
NIP7	7	9.62E+09	NA	0.0008835	0.0319166	0.0013229	0.0999934	NA	0.0148808	1.54E-02	4.24E-03
ITGB7	7	9.79E+09	2.52E+09	6.31E+09	0.1245701	0.9861732	0.1105285	8.35E-02	0.0113794	3.20E-06	4.78E-11
RGS19	7	1.02E-04	9.35E-03	2.40E+09	0.7656126	0.003194	3.12E-01	0.0064895	0.1225018	6.87E-03	7.59E-07
GLA	7	0.000103	7.24E+07	0.6954591	0.3496839	0.0327286	0.012468	6.57E+03	0.1738454	9.96E-07	4.37E-01
NOV	8	1.08E-04	1.15E-04	0.9606309	0.0018852	0.3498167	0.0364168	1.20E-07	0.0036925	9.63E-03	3.35E-01
COPZ1	7	0.0001086	1.81E+09	0.0280585	0.0283489	0.9739635	0.1642911	2.43E+04	0.0865587	4.32E-03	2.75E+05
MOSPD2	7	0.0001091	1.07E-04	NA	0.001259	0.2869922	0.0139294	3.97E-03	NA	1.20E+04	5.41E+02
CLEC4E	7	1.09E-04	1.31E-04	0.0344263	5.01E+08	2.78E+09	0.1243257	NA	NA	8.07E+02	2.18E-11
DUSP3	8	1.10E-04	1.47E-03	0.0040725	1.32E-01	0.785936	0.0001313	3.22E-03	0.0079119	1.03E-05	8.83E-04
C21orf33	7	1.11E-04	9.58E+06	0.0161026	0.0065792	0.0098053	0.0978243	4.18E+02	0.3150315	NA	2.90E-06
EXOSC7	7	0.0001123	5.32E+08	0.0007957	1.43E+09	NA	0.4345454	5.49E-03	0.9045188	2.24E-01	4.54E+07
PTEN	7	0.0001159	0.00031644	5.99E-01	0.1770487	0.0151239	0.0627488	7.35E+04	0.0045165	3.52E-01	1.67E+04
VIPR1	7	0.0001173	9.81E+05	0.0088798	0.004127	0.9552428	2.86E-01	7.61E+00	NA	1.93E-02	2.06E+01
B3GNT8	7	0.000119	0.00234539	0.0002836	0.229202	0.7934164	0.1215581	8.04E+03	0.0283469	1.18E-02	8.22E+02
RPS16	7	0.0001209	1.79E+08	8.72E-01	0.1141624	0.0140022	0.2312665	2.39E+07	0.0190336	3.06E+00	2.89E+03
ARPC5	7	1.21E-04	1.73E-02	0.0433911	0.7642502	0.1017602	5.86E+06	3.80E+09	NA	2.17E+04	2.19E+03
S100A6	7	1.21E-04	7.04E+07	0.1645778	0.0105522	0.2915592	0.028901	1.82E+02	0.2682257	5.86E+08	4.99E-12
ATIC	7	1.23E-04	2.72E+06	0.0142606	3.17E-02	0.7235795	0.1469072	8.04E-01	0.5431481	1.51E-03	8.37E-06
IL17RA	10	1.24E-04	2.09E+07	6.50E+09	1.88E-02	0.0103201	0.0008744	3.74E+00	0.033698	5.41E+06	9.05E+07
PAQR8	7	0.0001262	1.68E+08	2.38E-02	0.0028198	NA	0.6676587	2.93E-04	NA	9.50E-06	3.94E-09
GMFG	8	0.000127	8.09E+09	2.06E+09	0.6728912	0.0014326	0.9895042	4.96E+00	0.0086692	1.43E+03	4.93E-09
WBP11	8	0.0001284	6.46E+05	0.0319525	0.3952726	7.84E+09	0.2554447	2.04E-08	0.0149933	1.06E+03	1.90E-01
MORC2	7	0.0001328	4.58E+06	0.0029012	0.0017705	NA	0.0526347	6.19E-04	0.1627952	4.62E-05	5.60E+04
OGFOD1	7	0.000135	5.29E+07	0.0014405	0.1970981	NA	0.0286797	4.78E-06	0.9597726	1.14E+03	3.92E-03
SLC12A9	7	0.0001355	7.60E-03	0.0043329	0.6592064	0.0488567	0.3947835	1.26E+04	0.4412141	1.29E+04	4.03E+03
CIRBP	7	1.37E-04	2.23E+07	0.5046274	0.5326829	0.047979	0.7702712	7.46E+06	0.0103003	1.46E+00	9.57E+04

DNASE1L	7	1.38E-04	6.83E+08	0.7374698	0.3939301	0.0045074	0.7447463	1.37E+02	0.0259125	1.19E+08	9.60E+00
WDR46	8	1.46E-04	4.61E-02	0.0003449	2.46E-03	0.1856709	0.0003418	3.92E+06	0.9538456	1.26E+05	2.45E+06
RFWD2	7	1.49E-04	1.16E-02	0.6188499	0.9241531	0.0125957	1.61E-02	1.87E-02	0.0067058	NA	8.16E-04
TRAF3IP3	8	0.0001545	1.80E+07	0.0002534	0.0101812	0.4017311	0.012468	1.57E+06	NA	1.95E+06	2.46E+06
RPA1	7	0.0001546	5.55E+07	3.04E-02	0.1147275	0.0994791	0.2600216	1.88E-02	0.0019786	2.41E-06	6.93E+03
NCOA5	7	0.0001565	3.34E-04	0.0024419	8.63E-01	0.4539326	0.0006192	1.39E-01	NA	2.15E+01	6.76E-06
RAB27A	8	1.58E-04	1.18E+09	1.25E-02	1.93E-02	0.0059936	0.7944027	4.51E+03	0.1166617	3.99E-05	4.23E-08
NUDCD3	8	0.0001585	4.83E+07	0.0030271	0.0800231	0.0471208	0.0001262	1.88E+05	0.1632161	7.26E-04	2.28E-06
IMPDH2	7	0.0001643	2.70E+06	0.0018268	2.82E-01	0.0196142	0.1627841	5.81E+03	0.3204749	9.16E-04	2.90E+04
SKAP2	7	0.0001651	1.12E+08	NA	6.49E-01	5.25E+09	0.898772	2.33E+09	0.0255256	5.27E+02	3.47E+01
LONP1	9	0.0001778	1.42E+09	0.0005065	0.0032559	0.0011385	3.25E-03	1.30E+08	0.683709	4.44E+04	2.64E-03
MRPS9	7	1.80E-04	4.13E+07	0.001921	0.0001284	NA	0.0509774	7.32E+09	0.1466105	6.18E-02	2.23E+09
ZNF559	8	1.86E-04	2.15E+09	2.21E-02	3.78E-01	0.0224499	0.028012	1.11E+05	NA	3.55E+08	4.87E+05
TMEM50B	8	1.87E-04	2.39E-04	1.59E-01	0.2529064	0.0169497	3.88E-03	1.73E+06	0.0203431	2.69E+07	6.78E-04
NUP85	8	1.89E-04	1.74E+08	1.11E-02	0.0528933	0.0410756	0.0470238	2.94E+08	0.3367634	0.0001037	8.77E+08
CHIC2	7	1.92E-04	1.02E-01	3.84E-03	0.000108	1.70E-02	0.9652809	2.53E+07	0.5128476	7.02E+00	3.32E+03
METAP1	7	0.0001944	3.29E+08	0.022107	0.0016887	0.801543	0.7475885	4.47E+03	0.3741736	4.70E-03	5.42E+04
AKR1B1	8	0.0001978	7.91E+04	0.0053939	4.54E+07	0.0287406	0.7351674	4.13E+03	0.8136926	1.80E-03	1.95E-04
GGA2	7	0.0001998	2.54E-04	0.0635704	0.0192078	0.076931	0.0823579	1.82E+05	0.0246103	4.18E+03	2.06E-04
MYL6	7	0.0002035	0.0009856	0.0008471	6.97E-02	0.7235795	0.5334058	3.53E-08	0.0014427	4.13E-01	1.41E-16
PLEKHO2	8	0.000211	1.65E-01	0.0004949	NA	0.029148	0.0096075	6.53E-04	0.0145941	7.83E+04	1.08E+09
TAF4	7	2.20E-04	5.55E-01	2.18E+08	0.0270435	0.2429331	1.81E-02	1.88E-01	0.0958226	7.86E-02	1.84E+02
SET	7	2.23E-04	1.72E+08	9.63E-03	0.0670632	0.0140415	0.5618594	4.26E+07	0.012988	5.04E-02	1.71E+02
DNAJA3	7	0.0002259	1.73E+08	3.03E+09	0.0210973	0.4438176	3.91E-01	6.55E+00	0.3188626	4.74E+07	1.10E+01
EMILIN2	7	0.0002265	1.80E+05	0.0019397	0.1630761	1.14E-02	0.2732134	NA	0.0008917	3.06E+02	1.26E+02
TBC1D14	8	2.29E-04	8.41E-03	0.0264956	0.2828363	1.24E+09	0.0239644	4.23E-02	0.058949	5.11E+09	2.48E+06
C14orf169	7	2.32E-04	0.00042882	4.35E+09	0.0050282	0.2479308	3.80E-01	1.09E+00	0.0315936	NA	4.87E-04
PIK3C2B	7	2.36E-04	1.87E+06	0.000587	0.4182952	0.014045	0.3697511	3.90E-06	0.1956959	5.76E-06	3.34E-04
PROK2	8	2.39E-04	6.27E+08	0.0015245	0.0398767	0.0010132	0.1158584	1.04E+08	NA	2.87E-05	1.09E+09
RPL32	7	2.43E-04	3.43E+08	0.9971519	0.1202588	0.0426562	0.9328377	3.13E+09	0.0057851	4.31E+08	2.49E-03
DNMT1	7	2.45E-04	4.65E+07	0.0021411	0.0050472	0.5994953	0.8516394	3.31E-03	0.2495846	3.74E-10	2.37E-01

CCND3	7	2.57E-04	0.94966176	4.97E-03	0.017539	7.37E+06	0.5414142	1.18E-03	0.8474469	1.40E-02	1.34E+04
SMYD3	7	2.59E-04	4.62E+09	0.0002693	5.42E-01	NA	0.2722733	7.72E+08	0.0037287	6.18E-04	3.36E+09
DDX56	8	2.65E-04	3.98E+08	0.0092068	0.0202924	0.2168527	0.0405669	3.52E+01	0.9097472	3.39E+07	9.58E+04
CCDC115	8	0.0002785	2.78E+08	1.72E-02	0.0118046	0.1538382	0.2221998	1.45E+01	0.0170548	1.47E+07	3.92E+07
DENND3	7	2.79E-04	1.73E-01	0.0177434	0.0002245	5.84E-02	0.0023498	1.39E-03	NA	5.90E+05	1.71E+07
FAM53C	7	2.87E-04	4.60E-03	0.0623335	0.2875489	0.0130916	0.0147941	5.35E+07	0.2583155	8.21E+06	1.65E+06
ACTR1B	8	2.88E-04	6.82E-04	0.0517406	0.0048121	0.0047325	0.0194396	5.00E+02	0.0650366	6.32E-04	1.29E+03
EDF1	7	2.89E-04	7.73E+09	NA	0.1963414	0.0020596	0.0013862	1.10E-01	0.021701	5.29E+09	2.23E+05
PHB	7	2.89E-04	8.24E+09	0.0003641	7.95E+09	0.9615794	0.9236872	2.31E+05	0.1845831	3.48E+09	2.42E+01
KIAA0141	7	0.0002997	4.88E+08	0.8843868	0.0287038	0.6107379	0.0012885	1.59E+05	0.0142754	NA	2.48E+09
POLE3	7	0.0003046	1.34E+08	0.0014363	2.94E-02	0.3468788	0.5334058	9.41E-04	0.2726939	2.36E-04	7.47E+09
PIK3IP1	7	0.0003052	9.70E+09	0.0275321	NA	0.0025956	9.88E-01	2.91E-02	NA	1.60E+03	7.35E+08
QPCT	7	0.0003132	0.00027024	0.2700683	0.0014368	8.96E+09	0.2922412	1.91E-03	NA	7.35E-01	1.90E+07
FGFR1OP2	7	0.0003175	3.17E-04	0.2039736	0.1425974	4.42E-02	8.05E+05	1.17E-03	NA	9.15E+06	5.94E+01
C16orf72	7	0.0003195	1.15E+09	2.27E+09	0.9619619	0.0071193	0.3919289	4.27E+03	0.1408373	7.90E-01	2.49E+06
B3GALT6	7	0.0003202	2.15E+07	4.00E-02	3.08E-02	0.2589771	0.0001126	NA	0.1678854	6.82E-04	1.73E+00
NDUFAF1	7	3.24E-04	5.30E+09	0.9098053	0.0719135	0.0078776	0.4492813	7.09E-02	0.0406159	2.12E+04	3.46E-10
LANCL2	7	3.27E-04	9.20E-04	9.92E-04	0.024985	NA	0.2656477	1.58E-02	NA	1.38E-03	4.27E+09
TPD52L2	8	3.27E-04	1.87E-02	NA	0.0176398	0.0057799	0.0392747	4.34E+08	0.9171391	9.10E+04	9.09E+03
ARHGEF1	7	0.0003504	1.36E+06	0.2186348	0.7328127	0.0457951	0.5046133	8.93E-07	0.049705	2.54E-08	2.19E-08
P2RY8	7	0.0003518	2.52E+07	0.0001697	0.00246	0.0667727	0.2146965	9.36E+03	0.8871512	6.88E-03	7.33E-08
MRPL54	7	0.0003554	3.63E-03	0.5143839	2.15E-02	0.0002748	0.0016304	3.85E-01	0.0024331	2.47E-01	2.69E-02
EXOSC5	8	3.66E-04	5.13E+08	3.52E+09	0.0006401	NA	0.0159727	1.86E+07	0.344958	2.92E+00	9.28E-03
ICAM2	8	3.68E-04	2.89E+05	0.0001853	0.0263953	0.0047705	0.2063059	NA	0.0186669	1.24E+01	6.30E+01
PWP1	7	0.0003732	4.07E+08	2.26E-02	0.02329	0.9892076	0.1375687	1.77E+05	0.1160815	2.82E-03	4.48E-03
ERCC1	8	0.0003803	6.71E-04	0.1238733	0.0140916	0.1951695	0.0478649	4.41E-02	0.0336098	7.47E+08	5.11E-09
NOL11	7	3.85E-04	2.27E-04	3.78E-04	0.4514261	0.5905453	0.188496	1.23E+06	0.0177996	6.32E+02	6.10E-04
TIMM9	7	3.88E-04	6.53E+08	0.0001496	0.0497106	0.3505921	0.2860538	2.31E-04	0.526	2.35E-04	5.79E+07
TMEM14A	7	3.92E-04	4.37E-04	2.59E+09	0.0107232	NA	0.6559403	2.55E+07	0.1767364	7.99E+05	1.30E+05
CD27	7	0.000396	5.64E+05	1.28E-03	3.60E-02	NA	0.9374238	7.47E+00	NA	3.21E-01	6.98E-01
POLR2I	7	0.0004013	0.00624884	0.0426398	0.0453183	0.0037616	0.0116946	0.4700522	0.0252021	0.089924	3.70E-01

NCOR2	7	0.0004189	0.63627768	0.481772	0.0009375	0.0014127	0.004059	2.90E+02	0.1229775	1.68E+04	8.38E-04
FURIN	7	0.000422	5.44E+09	0.0811369	0.8596459	0.009068	0.011173	8.58E-04	NA	8.86E+02	4.16E+09
COX10	7	0.0004333	2.34E-03	4.64E-04	0.0001373	NA	0.4380519	1.56E+06	NA	1.55E+06	1.07E+05
EXOSC8	7	4.34E-04	1.02E-03	0.0305776	0.475038	0.4736234	1.05E-01	3.15E-02	0.0049622	3.28E+05	4.12E+07
BZW2	8	0.0004404	1.72E+09	2.64E+09	0.0051562	0.0488067	0.6638025	4.07E+08	0.4199638	4.75E+06	1.34E+04
HACL1	7	4.48E-04	6.40E+08	0.0058549	5.44E-01	0.6901014	0.6808844	4.71E+06	0.0449196	8.39E+00	1.20E-04
DHPS	7	4.57E-04	9.05E+09	NA	0.0135746	0.8839534	0.0008253	8.85E+09	0.0265027	2.69E-01	7.21E+08
RPL37A	7	0.0004734	4.81E+08	5.18E-03	0.0275568	0.2976432	7.55E-01	2.46E+03	0.0090814	NA	4.94E+04
CCR7	7	0.0004876	5.22E+04	0.0149983	4.10E+09	0.6024989	3.99E-01	5.67E+01	0.1167534	4.79E+04	2.13E+02
PBXIP1	7	4.97E-04	1.60E+07	0.8574509	0.0998763	0.5688516	0.0119808	4.68E-02	0.0185813	9.61E+01	1.12E-20
UBE2W	7	0.0005196	4.56E+08	0.9744361	0.4121951	0.0243482	0.0036341	1.30E+05	0.0162115	1.49E-06	NA
PRKRA	7	0.0005206	NA	0.000462	0.4457996	0.0056979	0.003211	1.24E+03	0.2149268	4.48E+02	4.07E+08
MRPS27	7	5.46E-04	4.02E+07	0.0002399	0.0145662	NA	0.2655978	3.93E+03	0.9886692	9.26E+00	2.43E-02
BLOC1S1	7	0.0005492	6.92E+05	0.0091536	0.3315372	0.4024405	0.0215414	1.64E-01	0.1146411	4.77E-05	2.36E-15
TRIT1	7	0.0005572	0.00011397	4.34E+08	7.51E-01	0.3288496	0.0336023	1.32E+03	0.9559138	2.52E+01	1.58E-01
LHFPL2	7	5.62E-04	7.35E+09	0.2087427	0.4355009	0.0301166	0.0268904	6.99E+08	0.5579025	1.26E+06	4.16E+08
HIST1H2A	7	0.000568	0.04565732	0.0475873	4.50E+09	0.7773395	0.028648	0.0001621	NA	2.64E-01	4.27E-01
SCRN1	7	0.0005712	3.72E+07	0.8363756	0.0005714	NA	0.0872742	5.57E-04	0.0116845	3.65E+07	1.14E+01
ARPC1B	7	0.00058	0.00317464	8.24E+09	NA	0.0471208	0.2427621	1.95E+09	0.2963411	4.50E+06	1.60E+04
TOLLIP	7	0.0005898	0.000834	0.0105882	7.51E-03	0.7312066	0.1225692	3.92E-03	0.8229906	4.02E+07	3.33E+06
SEPHS2	7	0.0006245	2.35E-03	0.076833	0.4671225	0.6989646	0.0010471	1.92E+04	0.0022867	8.40E-07	2.17E-07
GSR	7	0.0006365	3.24E+03	NA	0.0038541	0.0330619	0.8043537	1.47E+04	NA	2.99E+09	2.89E+01
E2F5	7	0.0006424	5.04E-04	0.0072602	0.0183101	0.5291633	0.0608877	8.94E+08	NA	2.32E-04	8.38E+05
PHKA2	8	6.46E-04	7.08E-03	0.0018085	0.0100889	0.1200755	0.0759325	4.90E+07	0.0055634	6.07E+02	2.28E+00
NUBP1	8	6.61E-04	5.65E+09	1.00E-02	0.0061966	NA	0.12175	7.40E-03	0.0308956	1.40E-04	3.04E-04
RNASE6	7	0.0007031	0.00599778	0.0047337	0.853355	0.0116527	0.9094038	3.16E-02	NA	6.54E-04	7.23E-03
CYBB	7	0.0007135	0.52494997	3.10E+09	0.0289373	1.83E+09	0.0295466	NA	0.1198768	0.0250162	4.70E+06
ARL2BP	7	7.18E-04	2.14E-03	0.0414998	0.7822871	0.4015107	0.0223089	3.32E+06	0.0095448	9.97E-02	2.83E-04
SUPT16H	9	7.38E-04	1.90E+09	0.0003728	0.0006801	0.0248591	0.0012027	1.99E-02	0.3120948	2.71E+00	3.22E+06
UROS	7	0.0007408	0.00043201	0.0062624	0.0002245	0.7231776	0.881229	5.60E-03	0.0182198	4.78E-03	6.39E-02
RAB8B	7	0.0007449	3.83E+07	0.0031402	0.0692076	0.0343621	0.2156254	4.69E+09	0.1232854	1.83E+04	1.44E-06

ALKBH2	8	0.0007553	2.13E-04	0.0005278	0.0018947	NA	0.0013486	4.37E-04	0.2832495	2.01E+08	4.06E-04
NCL	9	0.000758	2.45E+06	0.0129925	0.0001007	0.0031027	0.7340383	1.29E+00	0.0200659	7.52E-07	4.96E-10
C16orf80	7	7.59E-04	3.56E+05	0.048211	0.5053816	8.07E+09	0.2045924	6.55E-02	0.0302612	NA	8.83E+04
CD19	7	0.0007898	3.06E-04	0.6002332	0.0023133	0.3022816	0.0067988	9.61E+08	NA	3.51E+09	8.97E+09
GTF2H4	7	0.0008028	0.00567447	0.0155765	0.0118046	0.6019106	0.0359911	3.49E+05	0.9385555	2.47E-02	4.78E-01
CLC	7	8.06E-04	2.72E-01	0.0073291	0.0057436	6.49E-03	0.4465294	3.33E-02	0.0006548	1.24E-03	6.34E-02
TNFRSF25	7	0.0008061	2.19E+06	0.2509092	0.0079597	0.041234	0.9487446	2.34E-02	0.0817867	1.24E-05	7.68E+06
SRP68	9	0.0008061	9.56E+09	0.0332586	0.0322615	0.0058354	0.0020042	9.48E+05	0.1119369	4.01E+01	2.72E+09
MFN2	7	8.21E-04	6.41E-03	0.8594255	0.0018127	0.7413191	0.027017	NA	0.0372174	3.73E-03	1.36E-03
HSPA1B	8	0.0008359	0.00036519	0.1853399	0.0013185	0.030955	0.6471958	0.0047081	0.025842	5.87E+07	0.0124598
MAP3K5	7	0.0008411	0.00720803	1.22E-03	0.0006282	0.3349057	0.3125527	0.0013853	0.0574175	1.17E-02	2.20E-04
RPUSD4	7	0.0008452	9.87E+07	0.0041002	0.0374634	0.3770319	0.8475938	1.26E+05	0.7820267	1.91E+09	1.84E+00
UTP14A	7	0.0008513	6.76E+09	0.023983	0.0121747	NA	2.79E+08	2.23E-01	0.7016622	1.15E+08	1.77E-04
ZBTB9	7	0.0008579	1.42E+08	0.0002431	0.0128518	NA	0.1975392	3.52E+01	NA	1.60E+09	2.49E+03
PRPF19	7	0.0008666	3.33E+09	2.06E+09	0.0034264	NA	0.1713313	3.29E+04	0.1974132	3.22E-02	2.13E-03
RPS13	7	8.72E-04	1.71E-04	0.0191021	0.0292441	0.0977171	7.51E-01	3.73E+09	0.0298951	9.89E-01	2.98E-02
CTDSPL2	7	8.74E-04	0.03884494	0.8412742	0.4043025	0.0073979	0.0173647	NA	0.0029501	2.39E-01	6.27E+04
MSRA	7	0.0008841	6.79E+08	6.27E-02	0.0001141	0.0499066	0.5137503	7.32E+06	0.9368583	3.38E+06	6.79E+07
PIH1D1	7	0.0008914	3.85E-04	0.545938	0.037399	0.9897717	8.04E-03	1.19E-03	0.5940958	4.21E+07	1.52E-02
ADK	7	9.06E-04	8.06E+08	2.29E-03	0.0012131	0.3928115	0.9036557	NA	0.0039337	3.38E+07	2.57E+08
NOSIP	8	0.0009229	4.45E+05	0.3869899	0.0251614	0.1750442	0.0049022	2.73E+04	0.0260786	7.04E-03	1.44E+07
RAB33B	7	0.0009256	0.001423	9.45E-01	0.0401137	0.0831206	0.0019531	0.0099165	NA	2.05E-11	9.49E+01
SH2B2	7	0.0009268	0.10641211	3.11E+09	0.5170336	0.0439904	2.52E-02	3.48E+09	0.9780591	9.70E+04	0.0397772
HSPA8	7	0.0009304	9.06E+08	NA	0.0001171	0.6117465	NA	3.57E+05	0.0172761	7.97E+09	2.07E+08
CDK4	7	0.0009403	6.02E+06	0.0002871	0.0003248	0.3349305	0.7506074	7.75E+07	0.2416739	2.20E+04	5.40E+04
TARBP2	8	9.47E-04	1.09E-04	5.97E+09	0.000357	0.4218748	0.0318463	7.41E-03	0.928764	4.22E-02	2.19E-04
PQLC1	8	0.0009532	0.0020009	0.0355223	0.0105708	0.013561	0.9358355	5.05E+05	NA	4.02E+06	8.24E+03
TBC1D10C	8	0.0009714	6.40E+08	4.66E+09	0.0168982	0.0188444	0.0863107	2.16E+09	0.007092	1.51E-01	3.12E+08
PARP1	7	9.74E-04	3.23E+07	9.59E+09	0.0374634	0.1816033	3.09E-01	9.66E-07	0.6194673	1.53E-09	1.24E-03
CBY1	7	0.0009797	1.77E-03	0.0009985	0.0494058	NA	0.1493274	4.67E+05	NA	3.97E+07	6.09E+07
WDR82	7	0.0009926	4.81E+08	0.0004973	NA	0.1040052	0.017374	2.32E-01	NA	2.59E-05	5.77E-05

PRPF31	8	0.0009964	8.49E+07	0.0647935	0.0177484	0.0011704	8.58E+08	2.34E+05	0.2451592	6.06E+03	3.04E+09
TMEM106	7	0.0009981	1.51E-04	0.7059062	0.8337719	0.0004225	1.96E+06	3.97E-03	0.8805002	2.59E-04	1.55E+05
YWHAQ	8	1.02E-03	4.85E-02	0.0230523	0.0280284	0.9891956	4.82E+09	8.57E+06	0.8266547	8.68E+09	1.30E-03
GOT2	8	1.05E-03	7.74E+07	0.000429	0.0481847	0.4924575	0.0215414	5.58E+03	0.7007722	6.19E+07	1.88E-03
TRIM28	7	1.06E-03	1.13E+07	0.1894061	7.98E-01	5.78E-03	2.22E-03	3.19E+00	0.6703891	2.14E+02	2.48E+09
PDHB	7	0.0010576	0.00126403	0.0098585	0.0258853	1.65E-01	0.2333651	0.0431757	0.03675	4.34E+03	0.3835109
HIF1A	7	1.06E-03	0.00562424	0.3771382	3.87E+09	0.2020099	0.0067156	1.96E-03	NA	6.51E+04	1.29E+02
CARD6	7	1.11E-03	3.23E+06	0.1336161	0.0030878	NA	0.1069144	3.15E-08	0.0366093	3.61E-07	2.08E-07
PAAF1	7	0.0011131	2.51E+08	0.0002091	NA	NA	0.1171437	6.77E-03	0.0412577	1.52E+04	1.78E+05
TIGD2	7	0.0011381	0.0041123	0.0106025	0.0065158	NA	0.012468	1.60E-03	NA	5.94E-01	1.03E-03
NARF	7	0.0011905	0.00056656	0.0042129	0.0172832	0.6031753	0.1313413	5.34E-01	0.9433159	2.03E-05	1.41E+02
PPRC1	7	0.0012097	1.94E+07	1.63E+08	0.0115968	0.1281304	0.5305794	3.97E-03	0.0696887	7.33E+02	6.21E-03
SLC41A1	7	0.0012101	8.34E+04	4.07E+09	0.0152718	NA	0.3588119	5.71E+04	NA	1.10E+03	4.79E+00
ENDOG	7	0.0012391	3.60E+09	3.03E+09	0.0232464	NA	0.0162799	1.85E-03	0.4227606	1.32E-01	5.21E+08
RPS19	7	0.0012414	1.59E+04	0.5265167	0.9030775	0.0421287	0.9077987	2.57E+08	0.0203921	1.32E+04	8.11E+05
RAB10	7	1.26E-03	4.13E+04	0.882993	0.1083605	0.2182309	0.039883	2.06E-03	0.0346032	4.13E+01	4.03E-06
ZDHHC12	7	0.0012891	0.00190027	0.0251945	0.6971196	0.1650998	0.0113684	2.34E+09	NA	7.31E-01	5.58E+00
RANBP9	7	0.0013172	NA	0.0298899	0.2626446	0.931048	0.006556	0.0100067	0.0021367	2.84E+05	1.46E-01
GSS	8	1.35E-03	0.0011176	0.0023703	0.0043773	NA	0.0031951	5.69E+07	0.384348	8.27E+05	1.47E+05
PTPN12	7	0.0013968	1.28E-01	NA	0.0111704	0.6669761	0.0001536	0.0029974	0.0254585	1.68E-01	4.35E+04
ACTR5	7	0.0014167	7.44E+08	0.0007156	0.0024142	NA	0.1631895	2.34E+01	NA	4.86E+00	6.38E+00
TPM3	7	0.0014229	1.97E-02	0.2365478	0.0006145	0.1758783	0.6806768	2.37E-02	0.0197019	1.12E-02	2.43E-03
HADH	8	0.0014306	0.00147611	8.08E+09	0.0113428	NA	0.032607	0.0329765	0.7298264	2.02E-04	6.12E+09
CCDC17	7	1.44E-03	7.11E-04	0.7163056	0.1397215	0.0140415	0.0036509	2.57E+07	NA	2.29E+06	9.15E+03
RBM4B	8	0.0014539	9.40E+07	0.0113018	0.5618216	0.0022418	0.1298421	8.75E+01	0.0430896	7.06E+04	3.53E-06
CHD9	8	1.45E-03	5.37E-04	2.56E-04	0.86733	0.0029684	0.0021044	7.06E-03	0.3923868	5.77E-02	5.22E+09
NADK	7	0.0014623	0.03414925	0.0019248	0.0088806	0.006157	9.59E+08	0.2242458	0.0151379	9.08E-01	1.20E-01
CS	7	0.0014703	1.80E+09	0.511303	0.0399752	0.0011262	0.7001781	1.14E+01	0.4313936	1.85E+04	3.20E+01
CD44	7	1.49E-03	1.57E-04	0.0316992	0.0044244	0.122811	0.9661207	2.76E-03	0.0114467	1.73E+02	1.17E-01
LRPAP1	8	0.0014934	9.16E+09	0.9700792	0.0322473	0.0213981	0.0342763	4.68E+02	0.3714581	8.15E+02	1.33E-03
UBTD1	7	1.63E-03	8.20E+09	2.35E+08	5.29E-02	6.23E-01	0.0172011	1.70E+08	0.8881511	8.33E-01	2.73E+04

MCM3	7	0.0016366	2.00E-04	NA	0.7783423	0.0002767	0.0467945	2.41E+01	0.1402754	1.22E-09	1.04E-01
THOC1	7	0.0016863	1.02E-04	0.0003028	0.0701548	0.0010737	0.6764056	2.17E+04	NA	3.83E-03	2.03E+04
FEM1C	8	1.74E-03	9.80E+08	0.0069393	0.6177274	0.0132101	0.7457734	4.19E+04	0.0345304	5.39E-12	1.40E-02
RAB11A	7	0.001743	0.00330977	7.71E-01	0.836636	0.2508196	2.92E+07	5.97E+06	0.0261384	1.34E+06	7.66E-05
RCC2	7	0.0017479	1.13E+09	0.0006097	3.72E+09	0.0581508	0.992366	8.73E+02	0.3680563	2.63E+04	3.45E-06
SDF2	7	0.0017485	4.06E+09	1.38E-01	0.0254638	0.0014853	0.9284584	1.12E+02	0.1687736	1.23E-02	9.15E-14
FBXO34	7	0.0017739	0.07238696	3.67E-02	0.0378953	0.6554923	0.0031496	2.13E-01	0.0178077	2.47E+07	3.87E+08
GSTP1	7	0.0018018	4.09E-04	0.0022613	0.3629031	0.8396182	0.8987174	3.70E+08	0.0203431	2.42E-04	5.17E+01
NOL8	8	1.80E-03	0.00863705	0.000478	6.09E-03	0.0173768	0.6213577	4.45E+08	0.9288148	2.59E+07	1.11E-03
RSAD1	7	1.82E-03	1.04E+07	0.0023654	0.0012097	NA	0.7750827	6.56E-06	0.07756	2.23E+03	4.76E-05
ST3GAL2	8	0.0018204	0.03262168	0.0143601	0.0003432	0.0140415	0.8468034	1.29E+08	0.0832333	3.66E+04	0.0011624
DOLK	7	0.0018262	0.00996106	2.54E+09	0.0108903	NA	0.1579712	1.14E+05	0.9329876	3.49E+08	0.0020324
AARSD1	7	0.0018315	0.04299893	4.02E-04	0.0003975	NA	0.0274482	8.06E-04	0.3879974	NA	6.92E+03
MICAL1	8	1.83E-03	1.82E-04	0.0001374	0.0035726	0.3657954	0.0345997	1.53E+08	0.192527	3.85E+04	2.74E+03
PTBP1	8	0.0018341	0.00018889	0.0016864	0.0352153	0.5307413	0.0001922	3.49E+01	0.7669588	1.75E-08	2.54E-06
UBE2A	7	1.91E-03	2.34E-03	NA	0.010035	0.047979	0.4010825	1.26E+06	0.2026539	4.95E-04	3.25E-01
TYROBP	7	0.0019129	0.03879047	3.01E+09	0.9247775	1.04E-01	0.098449	2.95E-04	0.0022042	4.32E-02	7.64E+08
TMEM120	7	1.92E-03	2.13E-04	0.0020394	NA	0.0802358	0.6338543	9.00E+01	0.0445212	9.49E-07	4.67E-07
DDX55	7	0.002005	6.28E-03	0.0398813	1.02E-02	0.5321216	0.7075736	9.81E-04	0.3912647	3.46E-01	5.44E+09
LAGE3	7	2.01E-03	1.25E+08	0.0112395	6.62E-04	0.4988178	0.0396888	3.87E+09	0.8820996	1.50E-01	1.16E-02
MYCBP2	7	0.0021017	6.89E+08	0.9946005	0.0092733	0.0823935	8.96E+09	1.28E-02	NA	3.45E-06	2.87E-05
TNFAIP3	7	2.14E-03	2.02E-01	0.0077829	0.0069584	0.0080497	0.8548702	1.94E-01	0.0078943	5.34E+09	4.58E-04
SURF6	7	0.0021394	3.99E+08	3.03E+09	0.2009427	0.0107842	0.0614447	5.33E+08	0.0348253	8.37E+08	0.8632793
COX4I1	7	2.16E-03	9.10E-04	0.7539451	0.0079975	0.0242729	0.7193201	3.43E-01	0.007026	1.92E-02	5.67E+06
NSUN4	7	0.0021658	7.00E-01	0.0054098	0.0298608	0.0130916	0.7659216	NA	0.0276233	1.03E+04	6.13E-03
DDX46	7	0.0021759	0.5734213	0.0001439	0.0411195	0.0423606	0.2253736	1.06E-03	0.0352969	7.67E-01	1.55E-01
CCDC6	7	0.0021864	2.97E-02	0.0011777	0.0019153	0.0978758	0.4546328	NA	0.0176588	1.13E+04	2.11E+03
CARS2	8	0.002196	0.00030618	0.5271995	3.62E-03	0.1318997	0.0336559	0.0062908	0.0251744	2.16E+05	3.67E+02
GBGT1	9	0.0022064	0.02083179	0.0283007	0.0478951	0.0171305	0.4469633	1.37E-03	0.0443797	2.69E+03	1.20E+01
LSM4	9	0.0022291	4.16E+09	0.0100892	0.0050341	0.0446659	0.7604717	2.90E-04	0.0216357	0.0008496	1.26E+05
PRDX5	7	0.0022291	1.71E-03	NA	8.08E-01	0.0004127	0.0343637	3.42E+03	0.2223051	5.91E+09	1.97E+04

NFKB1	7	0.002439	0.85601324	0.0246696	0.0001014	3.80E+08	0.0114592	0.4882046	0.0041616	9.39E-03	2.77E-01
TSFM	7	0.0024855	1.82E-02	1.73E-04	0.0010433	NA	0.6414581	1.35E+07	0.2150861	8.73E+06	2.31E+08
RNASEH1	7	0.002489	0.0145255	0.2975354	0.001213	0.0436476	0.595233	2.85E-03	0.1593827	3.40E+00	6.82E-02
PIK3CD	9	0.002505	2.57E-02	0.0012647	0.0029872	0.0256382	0.0053707	6.74E+08	0.0175706	0.2759606	3.25E+05
FASN	7	0.0025719	1.34E-03	7.73E+09	0.0061966	NA	0.6415948	8.83E+09	0.0286707	1.72E-02	7.17E-01
BCAT2	7	0.0025881	1.71E+09	3.59E+09	3.10E+09	NA	0.4759076	0.0001046	0.9084857	1.85E+09	1.16E+07
LRP10	7	0.0026062	0.24441708	0.0419356	5.51E+09	0.0191893	0.5605405	1.05E+09	0.0930108	1.50E+04	0.0011385
TMC8	7	0.0026072	3.42E+04	0.0003672	0.4048133	0.0958872	0.8312158	1.24E-03	0.0369473	3.03E-04	2.07E-02
SLC39A10	7	2.61E-03	6.58E-04	6.19E+09	0.0016043	NA	0.9806286	1.94E+05	NA	2.53E+01	5.37E+06
C9orf91	8	0.0026203	5.96E+07	1.96E-03	0.5554388	0.0002866	0.0284927	2.20E+00	0.0037851	NA	2.01E+02
MGMT	7	0.0026726	6.47E+07	0.000324	0.0505586	NA	0.3321439	4.74E+08	0.0309993	7.30E+04	2.40E+08
PRDX6	7	2.70E-03	3.45E-02	0.0358963	0.571823	0.0738546	2.38E+09	5.18E+08	0.004955	8.40E-01	1.83E+07
ZNF281	7	2.73E-03	8.68E+08	0.0046635	0.0004724	9.84E+09	0.3093088	5.50E+05	0.19486	6.85E-04	NA
SRFBP1	7	0.002824	4.58E-02	0.0031521	0.0003248	NA	1.58E-01	3.39E-02	0.2140339	0.0009355	4.98E-03
CSE1L	8	0.0028741	0.01924003	2.19E+09	0.9417573	3.53E+09	0.5137503	0.0004139	0.01895	7.58E+08	0.0007521
RBM14	7	0.0029517	8.94E-04	4.89E-03	0.0076891	0.5901792	0.937386	1.50E+03	0.6048313	1.20E+03	3.10E+04
AFG3L2	7	0.0030083	0.00052831	0.0003458	0.0006622	0.2730455	0.1637384	1.43E+05	NA	1.44E+02	6.94E+05
FBXW2	7	0.0030126	1.39E+09	0.907862	0.0218204	0.3622989	0.4575553	7.97E+06	0.008088	2.57E-04	1.12E+00
EDEM2	7	0.0030999	0.00486456	0.0077706	0.1768467	0.150668	5.44E-01	1.07E+09	0.014266	6.37E-02	4.53E-01
UBE2E2	7	0.0032278	0.00356668	0.0092281	0.0064084	0.7639407	0.368363	1.13E+07	NA	3.48E-03	4.05E+07
ABCC2	7	0.0032338	0.0010473	3.10E+09	0.9280242	NA	0.1601013	9.52E+04	0.0054925	1.98E-04	1.44E+06
POLR1C	7	0.003283	9.81E+08	NA	0.0214141	0.6846714	0.0463517	2.12E+04	0.2746018	5.23E+01	1.35E+05
RBBP7	7	0.0034598	5.69E+07	6.31E+09	0.2106201	0.8767307	0.0074259	2.01E+05	0.0817867	7.45E-01	3.56E+03
RFX5	7	0.003465	2.15E+07	NA	0.0010433	5.09E+09	0.4762249	1.03E-01	0.1791192	1.30E+02	2.34E-01
EARS2	7	0.0034943	5.37E-03	0.0028208	4.54E+07	NA	4.48E-01	1.45E+08	NA	1.43E-04	1.80E+04
TBC1D9	7	0.0035193	0.02935476	2.05E-01	0.0001411	NA	0.3148252	3.98E+07	0.0099275	4.79E+04	8.23E-03
XPO5	7	3.56E-03	6.17E-04	1.03E+09	0.0069508	NA	0.6256112	2.43E+04	0.3907414	2.29E+01	1.05E+03
NAT9	7	0.0036074	0.03099943	0.3249465	0.0189978	0.0209286	0.2886824	2.11E+05	0.0832333	1.91E+05	0.010257
BBS2	7	0.0036119	3.68E+09	0.0017715	0.0004034	NA	0.4650891	1.92E+01	0.3886903	8.21E+00	1.89E+02
GORASP2	7	0.0036326	1.57E-04	0.007107	0.0008719	0.1583954	0.8468034	1.17E+03	0.7952907	5.24E+06	1.78E-02
POGK	7	3.71E-03	6.70E-04	0.0455991	2.00E-02	0.9034187	0.8502587	5.68E+00	0.7055613	2.08E+09	2.41E-02

LEPROT	8	0.0037788	7.85E+08	1.54E+09	0.0309717	0.0162393	0.7313119	4.33E+05	0.7917434	2.81E-02	1.61E-04
MYO1F	7	0.0038101	0.17150288	2.36E+08	0.4901048	0.0450553	0.0048347	5.11E-01	0.0013114	1.09E-03	4.76E-02
ABHD12	7	0.0038356	0.00018946	0.0008906	0.0017891	NA	0.5867884	2.30E-03	NA	1.48E+09	4.87E-04
GTF3C1	8	0.0039522	1.29E+09	1.82E-02	6.13E-01	0.0125957	0.011173	1.05E+02	NA	1.36E+05	3.32E-03
LARS	7	0.0040252	1.76E-04	0.0004851	0.0030811	0.3825761	0.4358792	2.86E+04	0.7010862	5.46E-05	1.96E-02
PPP2R5A	7	0.0040409	0.01316239	0.0034775	0.0013691	0.710239	0.8603317	0.015714	0.9959223	4.66E+04	7.68E-04
CD300LB	7	4.12E-03	5.10E+09	0.0027511	0.0001373	0.0228342	0.2750589	1.34E+05	NA	2.66E+06	NA
CNNM3	7	0.0043236	1.46E+06	0.0006912	0.0186471	0.4477292	0.0579345	4.75E+00	0.0625259	1.78E+01	2.14E-03
PTMA	7	0.0043381	3.25E+07	0.0323706	0.5326829	0.1206564	0.0001384	6.24E+04	0.0117981	NA	2.28E-04
ODF2	7	4.44E-03	1.07E-03	0.0022159	0.0268102	0.0553685	0.0008453	NA	0.0982528	1.02E-02	1.33E+00
KIF20A	7	0.0045264	2.59E+09	0.0002907	0.1976546	NA	0.0071848	2.91E+08	0.0856782	3.94E-03	2.39E-04
CWF19L2	7	0.0045622	2.91E-01	0.0038876	0.0020543	0.0072559	0.7539763	NA	0.0182809	1.04E+07	2.17E+09
NUP107	7	0.0045936	0.04805921	0.0005593	0.8255531	0.4065808	5.35E-01	2.05E-03	0.0168094	3.95E+03	5.53E-04
FXYD5	7	4.67E-03	1.31E+07	0.583694	0.0039512	0.0330348	0.282374	4.96E+02	0.2941865	1.24E+07	8.94E+05
DUS1L	7	0.0047436	2.94E+09	0.0001665	0.0003339	NA	0.3938826	6.34E+06	0.5919174	1.29E-04	5.68E+08
COPS7B	8	4.76E-03	7.98E+09	0.0335453	0.0109498	0.322502	0.0423379	2.52E+02	NA	1.70E-04	1.80E-01
PPAN	7	0.0048242	0.00031148	5.57E+09	0.0066863	NA	0.020728	1.09E+05	0.1548057	NA	1.65E-03
DUSP2	8	0.0048336	1.91E+09	0.0006953	0.3171269	0.0002539	0.0431908	4.59E+02	0.1398056	4.80E-02	2.65E+08
SLC25A5	7	0.0049163	3.23E+08	0.0156749	0.0030005	0.3302459	0.9466687	1.73E-04	0.0841877	4.25E+09	5.41E+06
ZMYND19	7	0.0049943	0.00840085	4.15E+09	0.0115664	NA	0.1735517	0.0005085	NA	5.34E+07	6.88E-03
TRAP1	8	5.02E-03	2.92E+09	0.0002516	0.0023782	NA	0.0121165	2.88E+06	0.2676085	1.34E-05	1.27E+03
LMO2	7	0.005057	0.31613953	0.0009631	0.090847	0.0175618	0.014824	2.70E-02	NA	1.04E+06	0.0025808
IMP4	7	0.0051711	3.39E+08	1.51E-02	0.0280284	0.7825479	0.2216389	6.46E-04	0.1788555	2.05E-02	2.24E+04
FOXN2	8	0.0052765	NA	0.0481057	0.0004724	0.0195294	0.0044308	4.25E+07	NA	2.02E+02	1.17E-03
PPP1R2	8	0.0053587	1.34E+07	0.0323826	0.0003975	0.0791299	7.86E+08	1.90E+05	NA	0.0060093	2.40E+01
DDX21	7	0.0054307	0.00590989	0.0007776	0.0079582	0.9742436	0.5043689	NA	0.0241577	2.15E+09	5.55E+04
GRWD1	7	0.0056807	5.09E-03	3.04E+09	0.0078552	NA	0.226815	1.57E+07	0.8040569	2.73E+04	1.64E-02
PLEKHG4	7	0.0058117	1.88E+07	0.0025156	0.0012246	NA	0.3339857	8.09E+05	0.0155305	1.57E-01	1.09E+08
SLC35A5	8	0.0058362	1.39E-02	0.0046361	5.80E-04	0.0880424	0.0236911	4.48E-04	0.8332102	7.84E+04	8.07E+04
HSPA9	7	5.88E-03	1.91E-03	1.42E-03	0.0004441	0.7423731	0.278255	3.93E+05	0.8771672	4.93E-01	2.34E+02
CTCF	7	0.006002	0.00324298	0.8723497	0.0472563	0.0213437	0.3475078	3.13E+04	0.1056899	1.31E-09	7.55E-02

TK1	8	6.07E-03	1.44E-04	0.0052984	7.09E-03	NA	0.0012192	5.81E+05	0.0981791	5.55E+06	2.48E+08
LEPROTL	8	0.0060923	4.05E+07	0.9619442	0.0261847	0.9627751	8.25E+07	3.41E-02	0.0223758	4.08E+05	4.88E+07
SMARCC1	7	0.0061202	1.35E-04	0.0002398	0.0002066	6.63E-01	0.5710636	1.43E-03	0.3419245	8.06E-02	2.13E+04
DPEP2	7	6.24E-03	7.78E+06	3.17E-04	0.0618423	0.8760581	0.7819534	6.91E+09	0.0301818	1.79E+04	1.66E+05
SSRP1	7	0.0062847	1.18E+08	2.05E-02	0.0286795	0.9822867	0.884188	3.83E+00	0.2653852	2.38E-05	5.88E-02
PUS7	7	6.35E-03	0.0263875	0.0001077	0.0003449	0.0695101	0.3420365	6.25E+00	0.3089563	1.67E-04	5.66E+06
CEBPA	8	0.0066107	2.45E+09	0.000396	4.64E+09	0.3581055	0.063416	2.17E-04	0.008088	1.40E-04	1.73E+01
FARSA	8	0.0066536	0.00026648	0.0001962	0.0001428	NA	0.0003579	3.65E-04	0.3719171	0.0001123	3.28E+04
DDX17	7	0.0066633	7.52E-03	NA	0.0041723	0.0785457	0.7304515	5.31E+08	0.008088	2.96E+05	2.26E+08
EIF3A	7	0.0067506	1.32E-04	2.73E-03	NA	0.3899194	0.0013878	1.32E+06	0.4264615	2.13E-08	1.98E-08
CDCA5	8	0.0068243	0.00010183	0.0053146	0.0039341	NA	0.0162691	5.76E+07	0.1615626	0.0033023	6.25E+07
SFXN5	7	0.0068989	0.00020738	0.1183021	0.001408	NA	0.0052079	3.37E+05	NA	1.83E+03	1.58E-05
HSH2D	7	0.0069178	6.96E+07	0.0002986	0.0177019	0.2394455	0.7173625	2.77E+03	NA	3.76E+04	1.31E+03
ENO2	7	0.0069178	4.36E+08	0.0174058	8.04E-01	0.000152	0.1940586	1.95E+04	0.1501201	1.83E+04	5.41E+03
CECR5	7	6.94E-03	3.45E+09	0.0001094	2.66E+08	0.0094076	0.2367432	1.57E-03	0.2651776	NA	6.57E-04
RUSC1	7	0.0071904	1.94E-03	6.09E+09	0.1466421	0.8631239	0.016761	1.28E+06	0.0987922	1.23E-02	1.06E-03
INTS9	7	7.34E-03	7.81E+08	0.0986362	NA	2.66E+06	0.0139969	1.31E-06	0.0558355	8.94E-05	1.21E+06
TMEM55A	7	0.0074317	0.02228509	0.0789931	0.9305457	0.0219169	0.0039734	1.79E+09	0.0261384	NA	3.38E+00
CCDC107	7	0.0076125	2.26E-04	0.9571429	0.0102052	NA	0.7191168	7.35E+08	0.0295859	5.58E+06	6.06E+02
PRMT7	7	7.63E-03	3.94E+06	8.13E+09	0.0472767	NA	0.1600231	2.49E+07	0.5464907	3.54E-09	2.67E+04
NPM3	7	0.0077051	5.29E-03	0.0008786	0.6146775	0.3682811	0.047827	7.25E-04	0.008088	0.0821285	2.91E-02
RHOT2	8	7.89E-03	1.77E-02	0.8283208	0.013666	0.0282545	0.003177	7.35E+09	0.0773922	2.41E-04	4.01E+05
SLC5A6	8	0.008109	0.00209893	0.002066	0.0001536	0.8546134	2.05E+08	3.54E-04	0.3535909	0.0001923	4.08E+04
PIP5K1C	7	8.16E-03	2.93E-03	0.4563357	0.0164384	0.368221	0.0015859	9.24E+03	0.8102036	6.83E+04	1.43E-03
CCT4	7	0.0081911	4.33E+08	3.26E+09	0.0094173	NA	0.8994252	1.88E-02	0.5272653	1.15E-03	9.21E-03
ADORA2A	7	0.0083392	2.42E-01	5.31E+07	5.60E+08	0.0350681	0.0002358	4.08E+08	NA	1.41E-01	1.39E+00
PTDSS1	7	0.0084217	0.00012018	0.844657	0.0019236	0.3657382	0.0059856	1.01E+04	0.2177864	3.36E+05	2.51E+08
SRPRB	7	0.0084962	1.04E+09	0.0038024	4.31E+09	NA	0.2745079	6.70E+09	0.0828236	7.23E+05	6.72E+01
ALDH16A	7	0.0085624	1.06E+09	6.82E-01	0.0170972	0.3571114	0.0220044	6.75E+04	0.2434794	5.68E+08	5.47E+09
EPRS	8	0.0085996	1.79E+08	1.56E-02	0.0008023	0.0202503	0.5161478	1.96E-04	0.7487954	6.67E+00	5.56E+03
LIG1	7	0.0086115	9.19E+08	0.0524414	0.135698	0.8663518	0.0235063	5.88E+06	0.0242079	1.32E+05	1.83E+04

ALDOC	8	0.0086733	1.26E+07	9.27E-04	0.000105	0.0001206	0.9229901	7.59E+06	0.7160378	1.49E+09	0.0064356
PRPSAP2	7	8.90E-03	9.25E-04	NA	0.9512233	0.0004046	0.4961573	1.93E+09	0.0171418	5.09E-03	1.89E-02
TATDN2	7	0.0089771	1.26E-03	0.0114236	0.6557993	0.1521832	0.0062141	3.18E+03	0.7282503	7.82E-07	2.84E-01
RING1	7	8.99E-03	1.35E+08	1.11E-01	0.6289034	0.0423566	0.0410992	2.50E+02	0.7285289	1.25E+09	7.66E-05
ABHD5	7	8.99E-03	2.79E-02	4.92E-01	6.75E-03	1.52E+09	0.3269215	NA	0.0470116	3.33E-04	4.78E+08
FUNDC1	8	9.01E-03	9.51E+07	0.1578683	0.0120159	0.0163526	1.86E-02	5.53E-03	0.0073939	6.61E-03	8.35E-01
IDH3B	8	0.0093988	7.23E+08	0.1174893	0.0092989	0.1171759	0.0249545	7.17E+03	0.0349599	1.05E+07	8.08E+02
RAVER1	7	9.89E-03	0.0012486	0.0141812	0.0540446	0.0408086	0.0026393	1.13E+08	0.0703384	3.21E-01	2.77E-02
RHOF	7	0.0102768	5.20E+05	0.0004759	0.4349036	0.00047	0.6574653	2.14E-03	NA	2.75E+02	4.42E-03
LCP2	7	0.0103533	0.06215867	0.0003745	0.0338269	0.1367795	0.0756583	9.97E+06	0.0254585	6.99E-04	2.82E+07
IVD	7	1.04E-02	3.88E+08	6.84E-03	0.0104937	NA	0.1243257	1.12E+00	0.7483644	1.05E+05	6.65E+06
WDR77	8	1.06E-02	0.00010991	0.0001269	7.35E-04	0.9629907	0.0001832	3.08E+07	0.9908898	2.40E-02	1.09E-07
GLT1D1	7	0.0106396	0.00037484	0.0033203	0.0778575	0.9977795	0.307125	1.67E+00	0.0052952	6.70E+06	4.89E+03
DDX1	8	0.0107986	0.01326797	0.0029415	0.0068378	0.767847	0.0057117	3.42E-02	0.2256107	4.39E+06	2.24E-02
ABCB7	8	1.10E-02	1.22E-04	1.91E+09	0.3233582	0.0178302	0.0295475	1.07E-04	0.2822361	4.26E+08	4.19E-03
DEXI	7	0.011352	2.41E+09	0.0065817	0.0455614	0.6541187	0.530399	1.90E+07	0.3047053	9.72E+09	2.31E+04
ERLIN1	7	1.16E-02	8.51E+07	0.3804214	0.0068927	0.0248795	0.5618594	4.18E+01	0.0874354	1.02E-04	4.40E+02
CDC20	8	0.0117351	4.74E+09	0.0037194	0.0479669	NA	0.0326884	9.96E+07	0.1563661	3.95E-04	7.35E+07
MCM5	7	0.0120452	2.51E+09	4.04E-02	0.0830463	0.6920728	0.0017672	2.31E-02	0.0141744	1.01E-06	NA
AKR7A2	8	1.21E-02	3.34E+09	0.0267159	0.0058653	0.0002217	0.6515954	1.15E-03	0.0509099	7.73E+09	3.51E-04
ADAM17	7	1.22E-02	0.00281836	0.5538763	0.9341569	0.0123143	0.5852355	2.35E+06	0.0057495	1.89E+09	6.42E-04
AP3S1	7	1.24E-02	0.00283578	0.4207531	0.0043442	0.7650497	0.0176458	1.64E+08	NA	2.00E+02	3.55E-09
LTB	8	0.0123775	1.25E+08	NA	0.0028198	0.0002539	NA	0.0010243	0.0057495	1.13E+04	4.05E+03
LIPA	7	1.27E-02	2.51E-02	0.6691865	7.13E+09	0.5788307	0.7335856	2.21E-03	0.0311048	2.41E-03	1.80E-04
PPM1G	7	0.0128278	7.76E-04	0.7901197	0.0034325	2.55E-01	0.0434189	6.87E+04	0.1996689	3.46E+09	6.72E+06
IDH2	7	1.28E-02	4.89E+09	0.4607163	6.46E-02	0.001737	2.71E+08	5.83E-02	0.0047422	6.20E+07	1.20E-03
PALB2	7	0.0130294	0.00431592	3.80E+09	0.0473959	NA	0.6788864	3.23E+02	NA	8.74E+08	3.78E-03
NUDC	7	0.0131636	9.94E+08	0.0014366	0.00388	0.0199262	0.3143812	3.31E+09	0.8972046	8.63E-01	2.60E+07
RBM15B	7	0.0133442	0.03206425	0.0040017	0.0093679	NA	0.6995826	9.23E-04	NA	2.50E-04	1.28E+05
CCNDBP1	7	0.0134301	1.23E-03	0.7896663	5.33E+09	0.6815895	0.0558544	2.61E+07	0.0243635	1.45E-04	2.67E-03
PFAS	7	0.0134938	0.00012947	1.19E+09	0.0003105	NA	0.0980124	4.52E-01	0.9751866	1.69E-05	3.68E-04

FMNL1	7	0.0148173	2.47E-01	4.46E-02	0.2205856	0.70747	3.74E+06	1.80E+08	0.0086692	2.68E-02	2.43E-04
STAM2	7	0.0151531	0.04057959	0.1104321	0.0007893	0.4279945	3.25E-03	0.0411301	NA	3.30E+02	6.37E+06
CHST11	7	1.53E-02	3.05E-04	0.768447	0.4408453	0.0039623	NA	1.51E+08	0.0174405	3.21E+06	3.08E+04
PRPF4	7	0.0155732	0.00139214	9.38E+09	0.0071569	0.1229324	0.1217857	4.28E+04	0.7195546	5.14E+04	3.53E+08
LAS1L	7	0.0156082	1.62E+07	3.04E+09	0.0321274	NA	0.7200889	1.67E+00	0.416886	2.13E-07	9.94E-04
ACN9	7	0.0157078	3.45E+09	NA	0.0019459	0.0278272	0.1500869	6.09E+02	0.044759	NA	1.43E-05
DISP1	7	0.0163047	0.00023733	0.0238305	0.0008407	NA	0.4325339	3.26E+08	0.2720638	1.36E+07	7.13E+03
ASB13	7	1.63E-02	1.42E+08	2.99E+09	0.0040894	NA	1.19E-03	0.4088424	0.9162535	2.49E-03	1.38E-03
HEBP2	7	1.65E-02	1.07E+07	0.1595372	0.5386038	0.0081763	0.0007563	1.88E-03	0.7350165	1.31E-05	8.94E-13
REV1	8	1.70E-02	0.01062536	0.0011874	0.5726132	0.0217711	0.0256546	9.00E+07	0.9057605	3.03E+02	4.05E+05
PGM1	7	1.73E-02	9.16E-03	0.3382047	0.8633511	7.16E+09	0.1124919	1.37E+04	0.0348837	1.54E+02	8.64E+04
STARD7	7	1.73E-02	4.67E-02	0.2974412	5.36E+09	1.31E-01	0.0135572	3.50E+08	0.2231169	8.48E+04	4.65E+00
PRR7	7	0.017412	0.02686517	0.0251945	0.6984985	0.0003681	0.0494782	0.2151036	0.7263211	1.93E+08	0.0013746
CAD	7	1.77E-02	0.00021509	0.0001237	2.83E+09	NA	0.169923	4.44E+03	0.2593351	2.46E-02	1.73E+08
VAMP2	7	0.0177656	7.72E+07	0.0014505	0.357275	0.9552138	0.0341427	7.03E-06	NA	2.24E-02	8.55E-01
CCT8	7	0.0178825	3.91E-04	0.0167753	0.0485075	0.6097383	0.2917332	5.57E-04	0.9986063	1.44E-04	3.51E-02
PRTN3	7	0.0178964	2.72E+09	0.0020587	0.2938534	NA	0.0250421	6.01E+08	NA	4.56E-04	0.0002742
NCAPD3	7	0.0180738	1.68E-03	3.95E+09	4.25E-04	NA	0.2668423	9.95E+05	0.2676985	8.73E-07	4.26E-04
CLTC	7	0.0183078	0.00024922	0.0009568	0.9053937	0.3624576	0.0101761	1.67E-04	NA	4.37E-02	4.73E+04
SNRPG	7	0.0184828	2.48E-03	0.1135396	0.0081303	0.014045	0.3091759	6.76E+07	0.0166365	NA	4.12E-05
BCS1L	7	0.0184828	0.00103736	5.12E+09	0.0078921	NA	0.0280009	1.60E-01	0.8507533	1.84E+08	0.0029771
JARID2	7	0.0185775	3.94E+08	0.5752203	8.67E+05	0.166937	0.2986334	1.96E+03	0.0175706	3.88E-05	1.07E+00
SRRM1	7	1.86E-02	0.00015098	0.0011665	0.881237	0.1463679	0.4368136	1.50E-08	0.0415427	1.88E+02	1.02E-10
LARP1	7	0.0187268	0.90724163	0.7652056	0.0012641	0.4987447	0.0035908	0.0201093	0.007647	1.31E+07	3.38E-02
TNFRSF1E	8	0.018795	0.02390495	0.0002816	6.13E-03	0.0077751	0.2092376	7.49E-03	0.3207634	2.71E+07	9.41E+07
TNNI2	7	1.89E-02	4.84E-03	0.0831398	1.80E+08	0.0038211	0.9505798	6.37E+07	0.4892286	1.20E+08	4.35E+04
PLEKHO1	7	1.97E-02	7.60E+07	0.3622956	4.64E+09	0.000217	0.6107801	3.30E+01	NA	5.43E+02	2.46E+06
GADD45G	7	0.0196694	0.02200593	0.0059014	0.9936222	0.005544	0.3097536	6.78E+06	0.0595653	4.93E+07	6.85E+03
DGCR8	7	0.0198157	1.71E-04	0.9815256	3.80E+09	0.3341716	0.0318131	2.16E-04	0.3691756	1.40E+02	4.89E+02
RRN3	7	1.99E-02	0.05189696	3.04E+09	0.3570981	0.2995514	0.0059307	2.04E+08	0.0138638	5.76E+01	2.49E+03
INSIG2	7	0.0204137	5.34E-03	9.79E-01	0.001412	0.0156198	0.1556741	2.03E-02	0.4860161	6.42E+08	1.44E+05

ALG1	7	0.0206189	2.16E-02	3.59E+09	0.1340753	NA	0.0077642	1.77E+09	0.0500676	1.29E+09	5.05E-03
MRPS17	8	0.021038	0.01806754	9.78E+09	0.0070739	0.0093308	0.9678575	4.59E-02	0.7678429	2.81E+06	4.27E+09
ELP4	7	0.0211794	0.00100512	3.01E+09	0.0028959	NA	0.2472511	0.0402862	0.1669135	3.81E+08	3.52E+07
BCORL1	7	0.0214299	0.0019791	0.2955384	0.2938331	0.0057578	0.0182786	9.04E-01	0.0279051	1.51E-02	1.86E-04
GIMAP1	7	0.0217091	1.86E+09	0.1841848	0.0007638	NA	0.0067455	2.74E+00	NA	1.09E+01	8.14E+02
MRPS23	8	0.0218292	1.45E-02	1.13E-04	0.0236165	NA	0.8523028	2.58E-03	0.0185813	3.46E+09	1.36E+09
ISOC1	8	0.022242	0.00357635	1.85E+09	0.1426622	4.25E-02	0.0002209	1.00E+08	0.8190393	1.23E+07	1.51E-03
TBL3	8	0.0224452	9.16E+09	0.0399849	0.0289743	NA	0.0104431	7.60E+07	0.2779508	3.42E+08	1.54E+09
RRS1	7	2.25E-02	2.70E+09	8.26E+07	0.0044244	NA	0.2274657	2.78E-03	0.6685096	5.69E-04	3.46E+02
SRP72	7	0.0229546	4.43E-04	0.0219841	0.0265689	0.3214696	0.2966169	8.18E+09	0.9146105	7.34E+04	9.60E-03
ANKRD54	7	0.0230848	4.27E-02	0.0046378	0.7868357	0.0286492	0.4098823	7.12E+08	NA	1.65E-03	9.54E+04
SLC35B2	9	0.0233842	5.33E+09	0.0265002	0.0388157	0.0003681	0.0020373	4.95E+09	0.0861953	3.36E-03	1.25E+09
CD300LF	8	0.0234679	0.0153253	0.0025216	0.0268401	0.0212391	0.0184808	0.0621015	NA	0.0001991	1.65E+06
INPP5E	7	0.0235661	0.00010419	0.0002248	0.0381381	0.503419	0.0742387	2.86E-02	0.8190393	1.17E+05	8.02E+02
ACSS1	7	0.0245125	5.96E+08	0.0006359	0.1736687	0.3647528	0.0033752	1.04E-02	0.021964	1.21E-02	4.75E-01
DNTTIP1	7	0.0248825	0.01208085	0.7257565	0.0006332	0.011675	0.4494389	1.00E+08	0.0567915	4.65E+01	3.93E-02
TSPYL1	8	2.52E-02	0.00168691	0.545584	7.29E-04	3.38E-02	0.0178827	2.34E+03	0.0101996	1.76E-01	1.77E-02
RBMX	7	2.54E-02	4.71E+09	1.25E-02	0.0115571	0.8040321	0.9698	8.61E+04	0.1911352	2.79E+06	3.43E+00
RNF4	8	0.0259982	1.63E+09	0.0584869	0.5286159	0.0311679	0.0182786	1.55E+01	0.0365812	9.96E-03	2.45E+02
LILRB3	7	0.026194	1.63E+09	0.0002884	0.7971133	0.9626561	0.4951365	6.22E+04	0.003324	7.05E-06	2.37E+02
POP7	7	0.0262323	0.89770111	0.0403651	0.0004889	NA	8.62E-01	0.03307	0.0308753	0.0135041	2.48E-02
RNH1	7	2.82E-02	1.46E-02	0.8855946	8.18E+08	NA	0.0120684	7.73E-04	0.7187354	2.35E-02	1.60E+08
CNOT10	7	0.0288523	0.00014034	0.0252542	0.5157115	0.013809	0.0216819	5.86E+09	0.5041988	1.32E+06	1.13E-01
TSPAN14	7	0.0289811	0.00908008	3.42E-03	0.0038617	0.0049371	0.3071229	1.70E-01	NA	6.11E+06	1.73E+08
TMBIM4	7	2.91E-02	0.00918531	0.1027867	0.3410665	0.0107111	0.0336559	7.04E+03	NA	1.00E+05	1.18E-03
C7orf26	8	0.0292653	1.22E+09	0.0358242	0.1865825	0.0056979	0.0002325	4.56E+08	0.684558	5.59E+07	6.34E-03
NAP1L1	9	0.0298608	2.91E+07	0.0176492	0.0419907	0.0188444	0.011013	3.25E+02	0.0534836	1.14E+08	1.35E+07
PILRA	7	0.0309283	0.00534155	NA	3.06E+08	0.3131216	0.1528675	0.0442818	0.0045165	3.88E-03	1.83E+09
ECHS1	7	0.0309641	2.38E+07	6.09E+09	5.30E+08	0.0533326	0.5062695	2.19E+05	0.3397137	2.13E+08	9.18E+02
PNPO	8	0.0311207	7.81E+08	5.85E+09	0.0004046	0.3981321	0.1653637	1.17E+00	0.0336018	6.57E-03	2.33E-01
EIF5B	7	0.0311503	0.00035675	6.40E+08	3.15E-03	0.3022816	0.3835723	1.30E+02	0.1050788	2.73E-04	1.24E-02

PFKP	7	0.0311666	0.00061725	0.0054598	0.0008417	0.0027329	0.0641038	4.92E+08	0.3610686	7.42E-01	2.72E+00
TIMM44	7	0.0312239	0.00178873	0.00013	0.0005821	NA	0.0080385	3.09E-02	0.937763	8.03E+04	6.40E-01
MAN2A2	7	0.032008	0.00012677	0.3182364	0.0289743	0.0085791	0.1440332	3.47E+07	0.2180355	1.00E+09	1.88E+06
PTGES	7	3.21E-02	2.48E-02	3.41E+09	3.53E+06	0.0061329	0.3272702	NA	NA	1.99E+07	1.82E+07
HBD	7	0.0323055	8.34E-04	0.0007623	0.7822325	NA	0.7267084	3.39E-03	0.0308956	9.63E+08	7.05E-02
ANGEL2	7	0.0323055	2.03E-02	0.2925077	0.0098918	0.0277049	0.9878389	3.33E+09	0.0565929	1.47E-04	3.24E+06
NSUN2	7	3.35E-02	0.00066982	0.0001056	0.4897773	0.0452719	0.582382	1.83E+00	0.9788398	8.94E-04	1.44E+06
IRF9	8	0.0340708	2.36E-02	0.0019839	NA	0.9803579	0.0181109	3.30E-04	0.0106341	8.60E-03	1.69E-02
RPS9	7	0.0341995	0.03247494	9.04E-01	0.4090761	0.0207502	0.0240089	8.07E-01	0.0040418	6.40E+09	2.91E-04
CKAP2L	7	0.0342835	0.18766997	0.0007553	0.3605366	0.0043538	0.0272466	0.0002624	NA	1.26E+07	6.58E+09
RPL26L1	7	0.0347766	0.00625783	0.0007553	0.0057794	0.011653	0.4478728	1.11E+08	0.1330692	2.09E-01	1.68E-05
RBM28	7	0.0351271	0.00068072	0.3458319	0.0002749	0.3258619	0.0255886	0.0485488	0.9275481	7.29E-05	2.48E-04
SIPA1	7	0.0354631	0.11421652	2.44E+09	0.0070739	0.0011523	0.0033739	5.13E-02	0.2150152	0.0163554	1.83E-02
MYBBP1A	8	0.0355395	0.00194201	9.76E+09	0.0096748	NA	NA	2.32E+09	0.0156019	2.40E-05	4.79E+04
PEX11B	7	0.0355571	0.00860031	0.6476059	0.6436606	0.0205405	0.0334004	1.06E-04	0.0154908	1.42E-02	2.89E-01
LRMP	7	3.60E-02	3.11E-02	0.0011654	0.006072	0.1651372	0.2375833	4.12E-02	0.0122768	4.24E+05	7.73E-01
ITPR1	7	0.036006	0.28340532	0.0002531	0.0081686	0.0141768	0.1160671	2.15E+07	0.550144	2.08E-11	2.14E+03
ADCK1	7	0.0362607	2.86E+09	0.172495	0.000886	NA	2.29E+09	6.11E+01	NA	2.04E+00	9.70E+07
UBA3	7	3.64E-02	0.01460022	0.2235747	NA	0.0249762	0.1895442	5.76E+09	0.0286707	1.89E+08	2.21E+04
RABAC1	8	0.0367454	6.75E-03	0.0001984	0.4823973	0.0424962	0.0001858	2.97E+06	0.5837683	1.79E+01	1.37E+09
SENP5	7	0.0379027	4.44E-02	3.12E-01	0.0170164	0.0529868	0.0240989	4.25E+01	0.644961	1.53E-04	1.22E-03
NMI	7	3.79E-02	1.97E-03	0.2826258	0.0502619	0.7683119	0.0337998	1.44E+08	0.0058659	1.09E+08	4.93E-01
SUMF1	8	3.80E-02	2.81E-04	0.487972	0.003252	0.0157423	0.0167254	0.000334	0.0298247	6.81E-01	1.02E+05
ARHGEF3	8	3.97E-02	0.02485253	2.78E-01	0.001396	0.0072229	0.032432	7.44E+04	0.1521749	5.92E+06	3.51E+04
GOLGA1	8	0.0400042	3.60E+08	0.1669867	0.039888	0.018172	0.0640179	1.11E+07	0.0303045	0.0108154	2.31E+08
HIST1H2B	7	4.05E-02	0.0029663	0.4063944	0.0125129	0.3453087	0.0047946	1.54E+03	NA	1.89E+07	6.56E+07
DRG1	7	0.0412144	7.34E-01	0.061238	0.0394086	0.0102695	1.53E-04	0.2960441	0.0257248	5.86E-03	0.0001657
ARL6IP5	7	4.14E-02	1.32E-01	0.0540416	0.0022016	0.0023625	0.0001684	0.0010551	0.9853273	0.0370893	3.39E+09
SDHC	7	0.0414478	1.06E-02	NA	0.0003639	0.9402274	0.6770575	9.25E+09	0.0168743	2.47E+03	2.24E+07
ARF5	7	0.0420068	0.80773858	0.0085375	0.8072396	0.0296401	0.0383867	8.95E-01	0.004328	1.25E-03	1.21E+08
TBC1D10	8	0.0422537	1.18E+09	0.2252337	0.0087159	0.0003248	0.7217739	7.63E-07	0.0119753	0.0040121	9.69E-03

PRKAR2A	7	0.0433978	6.68E-04	0.0135749	0.0005138	0.5393006	0.6330365	6.00E+06	NA	1.82E+06	1.45E+08
SNRPA	8	4.35E-02	4.04E+07	0.0013372	0.0037584	NA	0.0035904	4.80E+08	0.9338959	2.15E-02	1.73E+09
TAF15	7	0.0437026	1.56E+09	NA	0.3528553	3.76E-03	0.4223212	1.07E-04	0.0363995	1.17E-08	1.12E-12
E4F1	8	0.0440076	0.06476062	0.0305668	0.902524	0.0033531	0.00021	2.04E-03	0.0458894	4.20E-04	1.44E-02
VAMP7	7	4.43E-02	3.17E-04	0.9424389	NA	0.0120646	0.3761755	2.71E+08	0.0428997	1.49E-03	1.10E-05
TROAP	7	4.51E-02	1.45E-03	0.0010399	0.0118738	NA	0.0039734	NA	0.0784694	2.38E+09	5.91E-04
FGD3	7	0.0452058	0.00011178	0.0019845	0.0125404	0.4653815	0.6927148	3.24E-02	0.0054925	7.33E-04	6.73E-02
SRM	7	0.0462092	8.97E+07	0.0016475	0.0026654	0.960895	0.0677023	1.82E-02	0.201155	3.01E+09	7.20E+09
GALNT11	7	0.0462893	0.0022267	7.63E-01	0.0087514	0.4128694	0.0135692	1.86E-04	0.9181791	5.35E+09	2.17E-04
GOLPH3	7	4.74E-02	0.00561201	0.0112327	0.1075127	7.75E-03	0.0021938	0.5742693	0.1857909	1.53E+09	0.0031466
GOLGA3	7	4.75E-02	2.34E-01	0.764169	0.0001441	0.0082616	0.0003736	4.73E-02	0.0964337	3.46E+03	4.13E-02
VDAC1	8	0.0477544	0.16295857	0.0118505	0.0051402	0.0002275	2.23E-04	3.87E-04	0.2153577	4.64E-02	4.38E+04
OSBPL9	8	4.78E-02	2.86E-02	0.6767647	0.0179245	0.0001226	0.8041918	1.04E+07	0.0293606	4.87E+09	1.40E+01
DIABLO	7	0.0482989	4.16E+09	0.293421	0.0021435	0.0284875	0.9414031	3.05E-02	0.0171794	4.99E-04	4.06E-01
POLR3A	7	4.84E-02	0.00014596	6.40E-01	0.0093232	0.3746744	0.0126259	1.36E-04	0.2501416	7.52E+02	2.00E-02
PAXIP1	7	0.0492425	0.01386775	9.83E+09	0.0260925	0.9119945	0.7242999	5.13E+07	0.1940629	9.72E+03	2.10E+08
CHD4	8	4.94E-02	1.87E-03	0.6286792	0.0437357	0.0268373	5.80E+04	3.29E+03	0.6769342	8.77E+03	6.69E-03
NLK	7	0.0495227	0.00022064	1.46E-02	0.5285804	NA	0.0131814	9.89E+03	0.1047872	1.08E+06	2.37E+08
RNASE2	7	0.8864361	1.83E+05	7.34E+07	0.0399752	8.84E-01	0.0003764	6.40E-12	NA	1.82E-01	2.90E-06
TGIF2	7	6.30E-02	4.49E+05	0.0060623	0.0255467	0.0001309	0.5788392	1.97E+00	NA	6.19E+06	2.51E+03
ST6GAL1	7	NA	5.84E+06	0.9898646	0.0179458	0.0058448	0.4285558	1.16E-05	0.0053223	3.01E-04	3.55E-09
LGALS1	7	0.9731509	1.86E+07	0.0358228	0.0544142	0.000316	0.0457559	2.64E+03	0.3819302	4.84E+06	1.21E+07
TMCC1	7	NA	1.87E+07	0.7855399	0.0130355	0.0297043	0.0061192	0.9317516	0.0037287	4.56E+07	0.0147968
RPL29	8	NA	4.59E+07	7.93E+09	0.0107551	NA	0.0139579	9.89E+09	0.0281342	0.0117551	2.41E+07
DRAM1	7	NA	6.85E+07	0.0490294	NA	0.0008359	NA	1.23E-03	0.0212071	7.72E-07	4.87E-08
EPHX2	8	0.0890416	7.31E+07	0.0306233	0.0231848	NA	0.0004228	2.73E-02	0.0159368	5.00E-03	1.39E+00
SLC22A4	7	NA	8.89E+07	NA	0.0110169	0.036787	NA	4.12E-08	0.0319752	6.47E-12	2.52E-05
PHF1	8	0.1278604	1.40E+08	0.0085511	0.0312277	0.0090081	0.3041274	7.11E+00	0.0307843	0.0350463	2.21E+06
PRKD2	7	NA	2.37E+08	0.0103541	0.000256	0.9286354	0.0013394	1.67E+06	0.0514606	0.0012017	2.85E+03
TOR1AIP1	7	0.0792484	4.36E+08	0.0022149	0.0013341	0.0288125	0.0147173	0.4334746	NA	1.77E+04	1.09E+02
BBX	7	0.9928077	6.40E+08	0.0378561	0.0014912	0.0526852	0.0030428	9.60E+04	NA	0.0043328	1.98E+06

NDE1	7	0.1942169	7.50E+07	0.0029179	5.39E+08	0.1080802	0.7313119	0.0009757	0.0097067	2.04E+00	1.00E+03
YY1	7	0.836863	8.68E+08	NA	0.0396598	0.0169086	7.35E+09	0.0004468	0.0201498	0.0693827	2.51E+07
MDH2	7	0.1177303	1.06E+09	0.0106369	0.0006873	0.3793957	0.0483325	0.0002817	0.9120891	6.94E+09	3.63E+07
SLC11A1	7	NA	1.56E+09	NA	0.0001997	0.0020193	0.1402463	3.75E+06	0.0184558	9.28E+08	0.0025493
HCP5	7	0.5140667	1.91E+09	0.0023297	1.83E+09	0.0041424	0.1616613	5.02E+08	NA	0.0026093	1.68E+07
MRPL4	7	NA	2.64E+09	0.0317338	0.0077191	NA	0.0020042	0.0181214	0.9815366	0.0012805	0.0010555
SDHAF1	7	NA	3.36E+09	0.0014703	NA	0.0020848	NA	3.99E+08	0.0352966	0.0126562	0.0022417
AKNA	7	0.2477872	3.84E+09	0.0001977	0.3214327	0.0006759	0.0005562	5.55E+04	NA	7.22E+09	1.02E-04
LYSMD2	7	0.5929564	4.42E+09	0.3058923	0.001015	0.0050457	0.0258213	2.78E+07	0.0026794	0.4432121	0.0004803
SMAD4	7	0.6890318	4.58E+09	0.2204249	0.0006331	0.4300489	1.48E+08	0.0010614	0.0137122	3.49E+06	1.30E-03
SND1	7	0.1466842	9.57E+09	0.0041903	0.0001544	0.6557181	0.0049853	6.66E+06	0.9810432	2.63E+00	7.15E+03
UBE2C	7	NA	0.00011008	5.86E+09	0.0302673	NA	0.5640609	6.57E+03	0.0165344	1.59E-01	2.50E+05
FAM49B	7	NA	0.00013107	NA	0.0187959	0.2818231	8.01E+07	3.54E+06	0.0028435	1.78E-09	1.20E-02
MBP	7	0.7027868	0.00013294	NA	0.0007383	0.0084178	0.0129755	1.06E+05	NA	0.0007447	5.21E-01
TNFAIP2	8	0.4924032	0.00014417	0.0199356	0.0189112	5.09E+09	0.0165832	7.57E+08	0.0022735	0.0002528	NA
SIN3B	7	0.1789076	0.00019334	0.8345948	0.0104814	0.0058837	0.0010177	2.94E+03	0.0786356	7.75E+02	2.61E+09
TRPM2	7	NA	0.00022693	0.3303496	0.0148085	0.0090174	0.5462315	5.17E+07	0.0173477	7.43E-07	1.65E+01
ASF1B	7	0.2640969	0.00022809	0.0001016	0.0007454	0.0555841	0.0443938	0.0265767	0.0092749	3.74E+07	0.9362616
APEH	7	0.3475274	0.0003072	0.0404639	3.63E+09	0.4074117	0.000274	8.32E+08	0.7380168	7.51E+07	3.07E+08
ARPC3	7	0.2409001	0.00031316	0.0382309	0.02519	0.1800138	0.6448115	7.11E+00	0.0066184	2.58E-06	7.20E-05
IDS	7	0.5395781	0.00039792	NA	0.0007653	0.057547	9.93E+08	1.43E+09	0.0091023	2.30E+07	3.31E+05
C1orf174	7	NA	0.00043488	0.0122451	0.0377976	0.0192454	NA	NA	0.0154908	0.0001595	0.0001756
CSTA	7	0.0561166	0.00049465	0.0006563	0.00334	0.0311679	0.6255742	5.19E+03	NA	1.20E-05	6.02E-14
TXNIP	8	0.7997172	0.00056277	0.0116124	0.0204912	7.52E+09	0.0512813	2.99E+09	0.0159368	4.55E+02	3.31E+03
UTP6	7	0.1297585	0.00073076	0.0465535	0.1623174	0.033091	0.0215423	0.0514644	0.0029669	1.12E-01	0.0001226
CDC42SE2	8	0.8062787	0.00081783	0.9027235	0.0001515	0.022717	3.74E+06	3.44E+03	0.0082882	1.38E+07	1.49E+00
MAZ	7	NA	0.00117175	0.8830925	0.0365093	0.0249081	0.0103897	8.02E+08	0.0805562	0.0013592	1.90E+09
PPP2R1A	8	0.0675065	0.00130026	0.0491982	0.0385807	0.0001236	0.0305361	6.60E-02	0.0433196	5.01E+07	0.1975175
PSMC6	7	0.6571336	0.00146231	NA	0.0071955	0.0025401	0.0016874	2.11E+08	0.3222284	2.20E+03	8.28E-02
SUCLG1	7	0.3954805	0.00150103	0.4426105	0.0060255	0.0021735	0.0114394	2.72E+08	0.3127465	6.67E+01	2.21E-06
DDX27	7	0.7469697	0.00192191	0.1242479	0.7958963	0.0014695	0.0006192	1.72E+01	0.0134479	1.05E+02	5.37E+06

MYO1G	8	0.1672012	0.00197081	0.022525	0.0001619	0.7005796	0.0084369	0.0094954	0.0188719	5.31E+07	0.0044376
SMAD7	7	NA	0.00241778	0.3857268	0.0115571	0.0004341	0.0380761	5.34E+01	0.1443635	0.0052084	3.25E+07
UPF1	7	0.9875105	0.00255933	0.2891657	0.0161003	0.0105366	0.0026976	3.28E+09	0.5902908	0.0026837	0.0039361
DOCK8	7	0.5281093	0.00286923	0.0051369	0.0023327	0.1175102	0.9926893	0.0068881	0.036274	8.55E+06	5.65E-01
G6PC3	7	0.1130012	0.00304172	0.0001271	0.0175103	NA	0.003963	0.3562696	0.0092749	2.52E+06	0.0062531
STK10	7	0.3032873	0.00398309	0.0004966	0.8845251	0.05867	0.0027407	1.88E+09	0.0250045	5.26E-03	4.61E+05
RCSD1	9	0.687014	0.00422287	0.0012398	0.0011896	0.024307	0.0189329	2.06E+00	0.0053993	3.36E+08	7.49E+09
MAN2B1	7	0.9602841	0.00644797	0.0003892	0.1506133	0.0020802	0.0004765	0.0001192	0.8866679	5.09E+08	1.32E+09
UBA52	8	0.0806127	0.00772447	0.0001331	0.044934	0.7771609	0.0266463	2.07E+07	0.0040533	0.0194983	0.0020038
ENO1	8	0.6770404	0.00820519	0.0059875	8.71E+08	0.0001751	0.1351093	7.52E+08	0.0005796	0.0002702	3.33E+06
INPP5D	7	0.4558717	0.00850124	0.0011754	0.5547451	0.3135321	4.06E+09	1.64E+09	0.0379114	2.36E+02	2.39E+05
TRAM2	7	0.2627268	0.00965255	0.0007124	0.0009821	NA	0.0291551	0.0032031	0.7949641	0.0007607	9.41E+08
STK40	7	0.0776918	0.00983291	0.0321821	0.0029296	0.044483	0.4481687	3.49E+08	0.0260786	0.5112443	0.0061559
UQCRQ	7	0.0975129	0.01056233	0.1328163	0.0112819	0.2441294	0.0001861	1.71E+07	0.0027604	0.020813	1.03E-10
ST3GAL1	7	0.9370911	0.01190993	0.0414998	4.16E+08	0.0017534	0.9772386	2.46E+02	0.5368939	0.0002939	1.42E+04
COX8A	7	0.6404474	0.01220859	0.7623483	0.0001218	0.6751449	0.0041932	0.0051805	0.0425217	3.16E+06	4.96E+07
ITGAL	8	0.1118919	0.01274695	0.0001718	0.0099255	0.0011103	0.0011663	5.37E+09	NA	1.49E+05	1.15E-02
HDDC3	7	0.0990879	0.01334205	0.0084625	0.0089756	0.0124643	0.0407256	0.7301674	0.040203	0.128888	2.08E+08
DCTN6	8	0.9491837	0.01463163	0.0069105	0.7934295	0.0016779	0.0013394	2.39E+09	0.0211151	8.04E+01	2.06E-09
FAM96A	7	0.145592	0.01493441	NA	0.0072507	0.105334	0.0280013	0.0035054	0.0059291	3.55E+05	1.10E+01
SMCHD1	7	0.9929217	0.01533345	0.0102792	NA	0.0234634	0.9148397	6.66E+09	0.0089048	8.20E+08	6.11E+08
IKZF1	7	0.9533651	0.01692517	0.003926	0.0286046	0.1955932	0.0072348	5.33E+04	0.5306669	5.47E+01	1.00E-08
PPHLN1	8	0.0898357	0.01955167	0.0119243	0.5732247	0.0064307	0.0050901	1.01E+07	0.0106093	9.76E+05	8.32E+09
RPL36A	7	NA	0.02250399	1.31E+09	0.0588424	NA	0.0021026	0.000219	0.007092	0.0007354	5.60E+06
EVI2A	7	0.8431753	0.02299479	0.6462614	0.006167	0.0236857	0.267353	0.0320377	0.0027268	1.64E+08	1.34E+06
CYB5D1	7	0.9912981	0.02455805	8.69E+08	0.002528	0.0068094	0.0043678	0.2128026	0.0383156	6.55E+08	0.1559
PAK1	8	0.8020561	0.02634703	0.0071967	0.0646735	0.0005019	0.0086035	1.37E+09	0.0022517	0.0007354	4.41E+09
RNF175	7	0.7029387	0.0295331	0.8290993	0.0308137	0.0238467	0.047036	0.0041412	NA	9.14E+06	5.27E+00
BMP6	7	0.9700235	0.03199051	1.63E+08	5.45E+09	1.32E+07	0.0404307	0.0035907	0.7432529	0.0008171	0.4835455
KDELR1	7	0.911642	0.03285944	0.0014969	0.0190258	0.6669131	0.0299692	0.0030469	0.0491812	0.1016001	0.0028226
RGS18	9	0.7568575	0.04078208	0.0075218	0.0176425	0.0014853	0.0001278	0.0001084	0.0024331	1.42E+08	4.86E-03

KIF3B	7	0.531234	0.0428803	0.0003601	0.131851	0.00034	0.710044	6.71E+04	0.0091296	0.0125272	0.0394159
SPATA5L1	7	0.7965108	0.04289941	0.0001961	0.0149466	0.0012754	0.7874399	0.0020828	0.6105431	6.47E+09	6.59E-04
ZBTB2	7	0.0778656	0.04611249	0.0232685	0.0181465	0.10301	5.16E+09	6.09E+03	0.4962739	0.0010285	5E-04
RDH11	7	0.4615358	0.15033588	0.0002549	0.000357	0.2656855	0.0002358	8.51E+07	0.0170724	3.77E+05	0.0412389
PLCB2	7	0.4045452	0.15372052	0.000678	7.28E+09	0.0026183	0.0004098	0.0169201	0.0073939	2.78E+01	0.2392025
TRIP6	7	0.3850632	0.78922682	0.0011916	0.0005726	0.5188254	0.0028911	0.0001095	0.0090814	8.75E+01	6.91E+08
CREB1	7	0.4481084	0.06908904	0.0017516	0.0374529	0.8135645	9.44E+06	9.70E+04	0.0093906	2.56E+03	9.15E+00
CFDP1	7	0.7107272	0.10832324	0.0035793	0.0005244	0.0130113	0.0325186	0.0054639	0.5757147	3.56E+08	1.24E+06
IKBKE	7	0.3951883	0.39469856	0.0047471	0.011471	0.0013469	0.0003102	0.0017634	NA	8.21E+09	2.08E-03
NDUFS5	7	0.4798981	0.14028178	0.0395779	0.0023839	0.0329314	0.1528028	5.60E+06	0.0278275	0.0357634	1.96E-09
IMPA1	7	0.8265722	0.13300845	0.9868604	0.0001366	0.0010268	0.0002224	0.03689	0.0097239	1.18E+04	1.83E+03
BUD31	7	0.8330695	0.71965227	0.7736367	0.0048713	0.0027887	0.0426212	1.47E+06	0.0244423	0.0005437	3.55E-09

Supplementary table 5. Serum cytokine measurement of sham and CLP animals.

Inflammatory mediator	Mean cytokine ± s.d (pg/µl)	
	Sham	**CLP**
G-CSF	21.89 ± 5.90	29.07 ± 2.25
IL-10	232.41 ± 16.98	261.24 ± 9.46
IL-1β	22.91 ± 8.19	36.14 ± 8.01
IL-2	9.03 ± 1.47	16.09 ± 3.05
IL-4	4.67 ± 0.30	5.63 ± 0.25
IFN-ɣ	10.4 ± 0.55	15.53 ± 1.28
IL-5	7.3 ± 0.18	9.53 ± 0.17
IL-13	5.05 ± 0.81	9.66 ± 0.97
IL-12p70	22.35 ± 5.78	48.22 ± 0.87
TNF-α	2.98 ± 0.46	4.8 ± 0.12

PARTE III

DISCUSSÃO

A EAS caracteriza-se por uma disfunção cerebral, ainda pouco compreendida, que ocorre com frequência devido à grave inflamação sistêmica desencadeada durante a fase aguda da sepse. De maneira geral, um acometimento cerebral em pacientes com sepse é considerado um fator independente de mal prognóstico. Diversos estudos já foram realizados na clínica a fim de identificar possíveis biomarcadores para diagnosticar de maneira precoce essa complicação que ocorre durante a sepse, permitindo antecipar o início do tratamento, diminuindo a sua taxa de mortalidade e os danos a longo prazo. Nesse sentido, um desbalanço no perfil sorológico de aminoácidos foi observado em pacientes com EAS, sendo esse perfil distinto entre paciente sobreviventes e não-sobreviventes (Mizock, Sabelli et al. 1990, Sprung, Cerra et al. 1991, Basler, Meier-Hellmann et al. 2002). Assim, a avaliação desse parâmetro emerge como um promissor biomarcador de dano cerebral de potencial uso clínico. Nessa tese nós observamos que animais submetidos à LCP possuem alterações sorológicas no perfil de aminoácidos semelhante ao observado em pacientes com EAS.

A diminuição nos níveis de glutamato e também da proporção de glutamato/glutamina observada no modelo de LCP possui valor preditivo de mortalidade em pacientes com sepse, como descrito por Poeze e colaboradores. Além disso, parecem ser mais precisos do que os parâmetros utilizados rotineiramente na prática clínica (Poeze, Luiking et al. 2008). O mecanismo exato que leva a diminuição na concentração plasmática de glutamato durante a sepse ainda não está esclarecido. Alguns autores atribuem essa redução ao seu consumo como substrato energético (Kantrow, Taylor et al. 1997), enquanto outros indicam que durante a sepse o glutamato é utilizado para a síntese *de novo* de glutamina e alanina (Bruins, Deutz et al. 2003). De fato, em nosso estudo não observamos alterações significativas nos

níveis sanguíneos desses aminoácidos, que provavelmente estão sendo mantidos às custas da utilização de glutamato. Além dos níveis de glutamato, a proporção de aminoácidos de cadeia lateral ramificada (BCAA, do inglês *branched-chain amino acid*) e dos aminoácidos aromáticos (AA) também já foi demonstrada estar alterada precocemente em pacientes acometidos por EAS (Basler, Meier-Hellmann et al. 2002). Corroborando, nosso modelo animal também apresenta uma diminuição da proporção BCAA/AA no soro, às custas de aumentados níveis de fenilalanina e triptofano. Assim, um elevado influxo de fenilalanina da corrente sanguínea para o cérebro contribuiria para acelerar a síntese de serotonina. Já a fenilalanina seria capaz de promover a síntese de catecolaminas e de falsos neurotransmissores, contribuindo para o dano cerebral observado durante a EAS (Fernstrom and Fernstrom 2007).

A avaliação do perfil de aminoácidos no LCR realizada nesse trabalho nos permitiu investigar a associação entre o perfil de aminoácidos observado no soro com àquele presente no SNC. Observamos, assim, que os níveis de BCAAs no LCR e no soro se correlacionam de maneira robusta (correlação forte). Enquanto os dos AAs e os de alanina, lisina e ornitina apresentaram uma correlação moderada. Adicionalmente, uma abordagem utilizando uma análise de redes de aminoácidos foi conduzida para identificar a associação entre os aminoácidos em cada fluido analisado. De modo geral, tanto no soro quanto no LCR de animais induzidos à sepse foi observada uma hiperassociação entre os aminoácidos analisados, fenômeno evidenciado pela formação de *clusters*. No soro dos animais submetidos à LCP, observamos a presença de dois grandes *clusters*: o primeiro com os BCAAs e o glutamato, e o segundo com alanina e metionina como principais nodos. Em relação à nossa análise no LCR, demonstramos uma alteração mais organizada, com a identificação de um grande *cluster* contendo 9 aminoácidos, sendo a metionina o

principal nodo. Essas alterações observadas evidenciam um orquestrado e homogêneo fenômeno no SNC e que não está presente no soro de animais cirurgicamente submetidos à LCP. De maneira surpreendente, apesar não ter sido observada qualquer correlação entre os níveis de metionina nos fluidos analisados, esse aminoácido foi encontrado como o principal nodo nos *clusters* observados tanto no SNC como no soro. De fato, já foi demonstrado que metabólitos da metionina, como a S-adenosilmetionina e a cisteína, encontram-se alterados tanto em pacientes (Wexler, Gough et al. 2018) como em modelos animais de sepse (Semmler, Smulders et al. 2008). Contudo, a importância do desbalanço do metabolismo da metionina e suas consequências fisiopatológicas no contexto da EAS ainda precisam ser melhor investigados.

Os resultados encontrados nesse trabalho refletem o perfil de aminoácidos de animais 24 horas após a indução cirúrgica de sepse, tempo escolhido a fim de refletir a fase aguda da doença a qual ainda não é observado o óbito dos animais. Contudo, a partir desses resultados se torna de grande interesse uma avaliação mais completa, incluindo fases ainda mais iniciais do processo de sepse. Assim, uma conduta clínica poderia ser iniciada de maneira ainda mais precoce caso se encontrem alterações nos níveis de aminoácidos. Em geral, esses resultados demonstram que o modelo de LCP reproduz as alterações no perfil de aminoácidos observada em paciente acometidos por EAS. Desse modo, o uso desse modelo animal demonstra, em mais um aspecto, seu alto valor translacional, podendo ser aplicado para o desenvolvimento de terapias visando o restabelecimento dos níveis de determinados aminoácidos durante a fase aguda da sepse.

Em casos graves, a inflamação sistêmica atinge majoritária e irreversivelmente funções associadas a região hipocampal de maneira a conduzir um dano cognitivo a

longo prazo (Chou, Lee et al. 2017). Corroborando, Semmler e colaboradores demonstraram uma acentuada atrofia hipocampal em pacientes sobreviventes à sepse (Semmler, Widmann et al. 2013). Recentemente, alguns estudos vêm sendo conduzidos com o intuito de investigar como a inflamação sistêmica impacta diferentes funções cerebrais, porém na maioria dos casos com foco neuronal ou microglial, enquanto que, o papel dos astrócitos nesses mecanismos de interação periférico/central permanece pouco elucidado. Nesse sentido, o uso de modelos de estudos apropriados para entender a participação dessas células em disfunções cerebrais decorrentes de episódios sistêmicos torna-se bastante importante.

A utilização da cultura primária de astrócitos representa uma alternativa ao estudo utilizando o tecido cerebral como um todo, pois nos permite elucidar o exato papel dessas células em diversas situações, sem a interferência de outros tipos celulares que podem mascarar a resposta astrocitária. Porém, cabe ressaltar que as condições de cultivo podem afetar a expressão gênica e o funcionamento de receptores, influenciando a interpretação dos dados obtidos (Lange, Bak et al. 2012). Esse fator é particularmente importante quando utilizamos como ferramenta de investigação a cultura de astrócitos provenientes de animais adultos submetidos a um insulto prévio, visto que a capacidade desses astrócitos manterem o fenótipo obtido durante a situação de injúria ainda permanece elusivo. Por esse motivo, nós desenvolvemos um estudo onde verificamos a resposta da cultura de astrócitos hipocampais provenientes de animais que sofreram um episódio de inflamação sistêmica severa e aguda, induzido por LCP, paralelamente a análise do tecido hipocampal total desses mesmos animais. Primeiramente, conforme esperado, observamos que os astrócitos provenientes de animais submetidos à LCP apresentaram um fenótipo pró-inflamatório, com aumento de expressão gênica e liberação de importantes citocinas pró-inflamatórias, como TNF-α e IL-1β.

Concomitante, observamos o aumento da expressão do fator de transcrição NFκB e da enzima iNOS tanto em culturas de astrócitos quando no tecido hipocampal total de animais sépticos, evidenciando que esses astrócitos carregam uma assinatura gênica que se mantém mesmo após o longo tempo de cultivo (3 a 4 semanas). Esses dados reforçam estudos prévios do nosso grupo que demonstraram que astrócitos provenientes de cérebro envelhecido possuem características distintas daqueles cultivados a partir de neonatos, conservando de certa forma as características do sistema a qual elas são provenientes (Bellaver, Souza et al. 2016, Souza, Bellaver et al. 2016).

Por outro lado, observamos algumas divergências importantes nas análises entre os dois tipos de amostras (tecido total e cultura de astrócitos). Em relação ao fator de crescimento endotelial vascular (VEGF, do inglês *vascular endothelial growth factor*), um fator expresso por astrócitos, microglia e oligodendrócitos que é capaz de controlar a permeabilidade da BSC, constatamos um aumento na sua expressão apenas em amostras de tecido hipocampal total de animais submetidos à LCP, enquanto que em culturas de astrócitos seus níveis de RNAm permaneceram inalterados. O aumento observado na expressão gênica de VEGF apenas em tecido total pode ser explicado pelo fato de diversos tipos celulares do SNC serem capazes de expressar esse fator, e portanto, os astrócitos não serem os principais responsáveis pelo aumento da sua expressão em resposta ao estímulo inflamatório (Ma, Zechariah et al. 2012, Wang, Kang et al. 2016). Além disso, o microambiente ao qual os astrócitos estão inseridos são grande determinantes da sua funcionalidade. Assim, o momento em que essas células são isoladas, perdendo o contato com a células endoteliais e outros tipos celulares do SNC, parece ser determinante para a perda das suas características como componentes da BSC (Jensen, Massie et al. 2013).

A interação entre diferentes tipos celulares também parece ter sido um fator determinante para alterações na expressão de TLRs nesse estudo. Enquanto os níveis de RNAm de TLR2 aumentaram apenas na cultura de astrócitos provenientes de animais submetidos à LCP, a expressão gênica de TLR4 aumentou apenas no tecido total, permanecendo inalterada na cultura de astrócitos. Sabe-se que as células microgliais são as células cerebrais que possuem maiores quantidades de TLR4 e que, além disso, respondem a ligantes de TLR mais rapidamente do que os astrócitos, sendo assim provável que a ativação dessas células seja capaz de mascarar a resposta astrocitária quando se trata de uma análise de tecido total (Carpentier, Begolka et al. 2005, Kielian 2006). Além disso, a microglia parece ter uma resposta a ligantes Gram-positivos que não envolva a ativação de TLR2, corroborando com os níveis inalterados de TLR2 observados na análise do tecido hipocampal total (Kielian 2006).

Apesar de observarmos essa clara resposta astrocitária frente a um quadro de sepse aguda, os mecanismos pelos quais essa inflamação sistêmica severa impacta tão fortemente a habilidade dos astrócitos manterem a homeostasia celular permanece pouco entendida. A compreensão desses mecanismos é particularmente desafiadora no contexto dessa patologia devido a grande heterogeneidade observada em relação a expressão gênica, a análise de citocinas alteradas e também aos desfechos observados entre os estudos (Tang, Huang et al. 2010, Iskander, Osuchowski et al. 2013). Ainda, devido às acentuadas diferenças entre a resposta imune na fase aguda e tardia da sepse, se faz necessária a avaliação e identificação dos mecanismos relacionados ao dano em cada uma das fases de maneira isolada. Baseado nisso, com o intuito de identificar as características em comum entre pacientes acometidos por sepse na sua fase aguda, nesse trabalho nós realizamos uma análise de transcriptoma sanguíneo de pacientes sépticos em comparação com indivíduos saudáveis, utilizando banco de dados disponíveis

online. De maneira interessante, apesar de nesse estudo terem sido encontrados diversos genes diferencialmente expressos (DEGs) e também processos biológicos infra e/ou suprarregulados relacionados à resposta imune e inflamatória, nossa análise visando identificar vias de sinalização acometidas durante a sepse não apontou alterações em vias diretamente relacionadas à inflamação. Contudo, nossa análise, que incluiu 10 estudos independentes, evidenciou alterações em vias de sinalização relacionadas ao metabolismo energético dentre os processos com mais DEGs durante a fase aguda de sepse. Assim, genes chave envolvidos no metabolismo de carbono, no TCA e nos processos de glicólise e gliconeogênese encontram-se suprarregulados em pacientes acometidos por sepse. Corroborando, Escobar e colaboradores demonstraram previamente, em modelo animal, que a estimulação de vias de regulação energética, como a da proteína cinase ativada por AMP (AMPK), é capaz de proteger contra a falência de órgãos e conferir uma maior taxa de sobrevivência após a indução de sepse (Escobar, Botero-Quintero et al. 2015). Adicionalmente, crescentes evidências sugerem que o desenvolvimento de disfunção cardíaca durante a sepse possa estar associado com uma deficiência no metabolismo energético e redução na produção de energia nos cardiomiócitos (Drosatos, Lymperopoulos et al. 2015). Já a extensão e o impacto dessas alterações energéticas no cérebro durante a EAS sobre a funcionalidade astrocitária permanecem ainda muito pouco explorados.

Com o intuito de transpor os achados encontrados nas análises de transcriptoma em células sanguíneas humanas para o nosso modelo experimental em roedores, e ainda verificar a sua influência no quadro de EAS, nós realizamos uma análise de metabolismo energético cerebral em animais submetidos à LCP. Assim, nós demonstramos, através da utilização de [^{18}F]FDG PET em modelo animal, um robusto hipometabolismo de glicose cerebral *in vivo* em ratos sépticos. Recentemente, uma

redução no metabolismo global de [^{18}F]FDG também foi demonstrada em modelo de sepse induzido por *Escherichia coli* em camundongos (Catarina, Luft et al. 2018). Atualmente o hipometabolismo indexado por [^{18}F]FDG PET é considerado um importante biomarcador de disfunção sináptica, com seus valores associados com déficit cognitivo na doença de Alzheimer (Pagani, De Carli et al. 2015, Gardener, Sohrabi et al. 2016, Weise, Chen et al. 2018). Assim, corroborando com os nossos resultados de hipometabolismo cerebral em modelo animal, sabe-se que indivíduos que experienciaram um episódio de sepse possuem um aumentado risco de desenvolverem demência à longo prazo (Cunningham and Hennessy 2015, Chou, Lee et al. 2017). A análise de metabolismo de glicose cerebral realizada nesse estudo demonstrou um hipometabolismo em diversas áreas, incluindo o hipocampo. De maneira controversa, Semmler e colaboradores, utilizando um modelo de injeção de LPS, não observaram alterações na captação hipocampal de [^{18}F]FDG (Semmler, Hermann et al. 2008). Como mencionado previamente, o hipocampo é uma das regiões cerebrais mais vulneráveis à sepse em humanos, e essa discrepância evidência a importância do cuidado ao utilizar diferentes modelos para indução de sepse. Assim, visando um estudo translacional, o modelo de LCP é visto na literatura especializada como o que melhor se correlaciona com a condição clínica observada em humanos (Lee and Huttemann 2014).

Nosso grupo recentemente demonstrou que a captação de glutamato pelos astrócitos está acoplada com o sinal de [^{18}F]FDG, sugerindo que a captação de [^{18}F]FDG reflete o metabolismo astrocitário (Zimmer, Parent et al. 2017). Consistentemente, nesse estudo nós observamos uma diminuição da captação de glutamato astrocitária em animais submetidos à LCP. Essa disfunção a captação de glutamato pelos astrócitos pode levar a hiperestimulação do sistema glutamatérgico decorrente dos níveis aumentados de glutamato na fenda sináptica, um fenômeno

extremamente prejudicial a homeostasia cerebral. Nesse sentido, a ocorrência de excitotoxicidade glutamatérgica está implicada na patologia de diversas doenças que acometem o SNC, incluindo no quadro de EAS (Gardoni and Di Luca 2006, Michels, Steckert et al. 2015). Contudo, apesar da redução na captação de glutamato astrocitária observada nesse trabalho, os níveis de glutamato no LCR dos animais induzidos à sepse não se alteraram em relação ao controle. Algumas hipóteses podem ser levantadas a partir desse achado. Primeiramente, nossas análises foram realizadas em um período de 24 h após a indução cirúrgica da sepse, e apesar de ter sido observada uma captação de glutamato astrocitária prejudicada, esse curto período pode não ser o suficiente para que haja acúmulo de glutamato cerebral. Segundo, já foi demonstrado na literatura que em situações de baixa disponibilidade de glicose os neurônios são capazes de oxidar eficientemente glutamato para suprir suas demandas energéticas e manter a produção de metabólitos mitocondriais, sendo assim, um quantidade reduzida de glutamato estaria disponível para liberação como neurotransmissor (Divakaruni, Wallace et al. 2017, Fendt and Verstreken 2017). Nesse sentido, a escassa disponibilidade de glicose observada durante a fase aguda da sepse impulsionaria os neurônios a utilizarem glutamato como substrato energético, fazendo com que haja uma liberação diminuída de glutamato após estimulação neuronal, prevenindo que ocorra seu acúmulo. Outro ponto importante a ser ressaltado é que apesar da quantificação de glutamato no LCR ser amplamente utilizada como representativa do ambiente extracelular *in vivo*, ela pode não captar pequenas flutuações decorrentes da sua liberação sináptica ou da sua captação astrocitária localizada em certas regiões (Featherstone and Shippy 2008).

Sabendo-se que a captação de glutamato do espaço extracelular é realizada primariamente por dois transportadores de glutamato exclusivamente astrocitários, GLAST e GLT-1, aqui nós observamos uma diminuição na expressão gênica de

GLAST que é contrabalanceada por um significativo aumento de GLT-1 em astrócitos provenientes de animais submetidos a um episódio de inflamação sistêmica severa. Uma vez que, aproximadamente 95% da captação de glutamato no cérebro adulto é realizada por GLT-1 (Holmseth, Dehnes et al. 2012), esse aumento importante na sua expressão pode indicar uma tentativa por parte dos astrócitos de reciclar os transportadores que estão com a sua atividade prejudicada. Contudo, esse aumento a nível de RNAm não se refletiu em uma efetiva tradução proteica. Nesse sentido, nossa análise de transcriptoma evidenciou uma suprarregulação de processos biológicos relacionados à tradução proteica ribossomal em pacientes acometidos por sepse, nos permitindo assim extrapolar que esses processos também estejam alterados em nosso modelo animal. Corroborando, um estudo recente demonstrou que um prejuízo na translação proteica está diretamente relacionado com dano renal durante a sepse, e que a reversão desse bloqueio atenua os sintomas promovidos nessa patologia (Hato, Maier et al. 2019). Em conjunto, esses achados apontam para a importância da realização de uma análise muito mais elaborada de translatoma, que vai além do transcriptoma e da proteômica, para que tenhamos um melhor entendimento dos processos deletérios envolvidos na sepse (Brar and Weissman 2015).

O processo de reatividade glial é característico da resposta astrocitária mediante alguma ameaça, e pode exercer tanto efeitos benéficos, quando ocorrer de maneira transitória, quanto deletérios, quando se torna um processo crônico (Filous and Silver 2016). Já vem sendo bem caracterizado na literatura que os astrócitos são ativados durante um processo inflamatório, aumentando a expressão de GFAP e liberando uma gama de citocinas e quimicionas pro-inflamatórias (Brahmachari, Fung et al. 2006, Gorina, Santalucia et al. 2009). Nesse sentido, nós observamos que os astrócitos hipocampais cultivados de animais que sofreram um insulto inflamatório severo e agudo

apresentam níveis aumentados de GFAP, indicando um fenótipo reativo dessas células gliais. Além disso, em relação ao citoesqueleto de actina nós observamos um rearranjo das fibras de estresse em astrócitos provenientes de animais LCP quando comparado ao grupo *sham*. O citoesqueleto astrocitário é uma estrutura altamente dinâmica que se reorganiza continuamente sempre que a célula altera a sua forma, se divide ou responde ao ambiente. As mudanças no citoesqueleto de actina são chave para a transmissão de sinal que levam à uma resposta celular apropriada, exercendo influência em funções críticas dos astrócitos, como sinalização de cálcio, homeostase iônica e transporte de glutamato (Alberts, Johnson et al. 2002).

Devido ao fato de o cérebro não ser uma estrutura imunologicamente privilegiada, as PBMCs estão constantemente patrulhando o SNC (Kleine and Benes 2006). Contudo, no contexto da sepse existe uma alta taxa de infiltração dessas células que podem resultar em prejuízo das funções cerebrais. Nesse sentido, a interação dinâmica entre PBMCs e astrócitos já foi previamente demonstrada no contexto da neuroAIDS (Richards, Narasipura et al. 2015), entretanto o seu papel na sepse permanece indefinido. Assim, visando analisar um possível envolvimento das PBMCs na ativação astrocitária nós expusemos culturas de astrócitos ao meio condicionado de culturas de PBMC (PBMC CM) obtidas a partir de animais sépticos. De forma interessante, enquanto no soro de animais sépticos nós observamos um aumento na liberação de diversas citocinas pró-inflamatórias (como IL-1β, IL-12p70, IFN-ɣ e TNF-α), no PBMC CM só foi observado um aumento nos níveis de TNF-α e IL-10, acompanhado de uma diminuição de do fator estimulante de colônia de granulócito (G-CSF, do inglês *granulocyte-colony stimulating factor*). Assim, a presença desses fatores foi capaz de promover uma ativação astrocitária direta, independente da presença de microglia, acompanhada de uma diminuição nas atividade de captação de glicose e

glutamato astrocitárias. Nesse sentido, estudos prévios demonstraram que mesmo um sutil aumento de níveis de TNF-α cerebrais é capaz de promover uma diminuição da atividade dos transportadores de glutamato astrocitários (Clark and Vissel 2016). Além disso, ratos com deleção de receptor de TNF-α tipo 1 não demonstraram perda cognitiva após indução de sepse por CLP (Calsavara, Soriani et al. 2015). Esses achados sugerem que importantes mediadores inflamatórios, como IL-1β, são dispensáveis para ativação astrocitária e consequente para a promoção do déficit energético durante a sepse. Baseado nesse contexto e nos achados presentes nesse trabalho, o TNF-α emerge como um crucial e independente fator de ativação astrocitária. É importante ressaltar que nesse estudo nós analisamos uma quantidade restrita de citocinas liberadas pelas PBMCs, dessa maneira, outros mediadores não avaliados podem estar também envolvidos no processo de ativação astrocitária aqui observado.

O mecanismo envolvido na regulação do metabolismo energético cerebral durante a sepse é muito pouco compreendido. Aqui nós demonstramos que o tratamento das células com PBMC CM provenientes de animais sépticos provoca uma diminuição nos processos de captação de glicose e glutamato astrocitários concomitante à diminuição da fosforilação de fosfatidilinositol 3-quinase (PI3K, do inglês *phosphoinositide 3-kinase*). Corroborando, nossa análise de transcriptoma apontou o gene de PI3K com um dos DEGs suprarregulados em pacientes com sepse, acompanhando por um aumento na expressão de seu regulador negativo, a PTEN. A via da PI3K contribui para uma variedade de processos que são críticos na mediação de muitos aspectos da função celular, incluindo captação de nutrientes, reações anabólicas e crescimento celular. Além disso, a via PI3K/Akt/mTOR é considerada reguladora-chave do metabolismo glicolítico aeróbio, modulando a captação de glicose celular através do controle da expressão dos transportadores de glicose de superfície (Ward and

Thompson 2012). Além disso, estudos prévios demonstram que essa via está envolvida na modulação da expressão de transportadores de glutamato, especificamente de GLT-1 (Zhang, Shi et al. 2013). No que diz respeito à sepse, já foi demonstrado que a inibição de PI3K diminui a taxa de sobrevivência em animais submetidos à LCP, além de promover um início mais rápido e severo dos sintomas (Wrann, Tabriz et al. 2007). A inibição da sinalização de PI3K/Akt ainda demonstrou aumentar a resposta inflamatória induzida por LPS em diferentes tipos celulares (Guha and Mackman 2002). Nesse sentido, aqui nós observamos que a inibição farmacológica de PI3K em culturas de astrócitos tratados com PBMC CM de animais sépticos produziu uma redução ainda mais acentuada na atividade de captação de glutamato. De maneira controversa, a inibição de PI3K não afetou a captação de glicose astrocitária em astrócitos tratados com PBMC CM de animais sépticos. Assim, o acoplamento entre captação de glutamato e captação de glicose astrocítico previamente reportado na literatura parece ser interrompido a nível de PI3K. Esses resultados sugerem que outras vias envolvidas no metabolismo energético podem estar atuando em paralelo na regulação da captação de glicose. Ainda, outras proteínas do eixo PI3K/Akt/mTOR necessitam ser avaliadas com o intuito de melhor compreender essa complexa regulação.

CONCLUSÃO

Os resultados obtidos nessa tese indicam que alterações sorológicas no perfil de aminoácidos refletem o desbalanço que ocorre no SNC, sugerindo a avaliação do perfil sorológico de aminoácidos como um potencial biomarcador na detecção precoce de EAS. Além disso, eles demonstram o grande potencial translacional do modelo animal de LCP para esse campo de pesquisa. Adicionalmente, aqui fornecemos novas evidências da participação direta dos astrócitos nos mecanismos pelos quais a inflamação sistêmica impacta negativamente a homeostase cerebral. Destacamos a

cultura de astrócitos provenientes de animais adultos como uma importante ferramenta de estudo das funções astrocitárias nessa condição patológica. Evidenciamos ainda o papel das PBMCs como importantes promotores da reatividade astrocitária e indutores ativos do hipometabolismo energético cerebral. Por fim, foi sugerido um papel regulatório para a via da PI3K no metabolismo astrocitário durante a sepse aguda. Com isso, nós avançamos na compreensão dos mecanismos pelo qual a inflamação sistêmica impacta na funcionalidade cerebral, indicando potenciais alvos para futuras modulações terapêuticas.

REFERÊNCIAS BIBLIOGRÁFICAS

Abbott, N. J., L. Ronnback and E. Hansson (2006). "Astrocyte-endothelial interactions at the blood-brain barrier." Nat Rev Neurosci **7**(1): 41-53.

Adrie, C., M. Bachelet, M. Vayssier-Taussat, F. Russo-Marie, I. Bouchaert, M. Adib-Conquy, J. M. Cavaillon, M. R. Pinsky, J. F. Dhainaut and B. S. Polla (2001). "Mitochondrial membrane potential and apoptosis peripheral blood monocytes in severe human sepsis." Am J Respir Crit Care Med **164**(3): 389-395.

Alberts, B., A. Johnson, J. Lewis, M. Raff, K. Roberts and P. Walter (2002). Molecular Biology of the Cell.

Anderson, C. M. and R. A. Swanson (2000). "Astrocyte glutamate transport: review of properties, regulation, and physiological functions." Glia **32**(1): 1-14.

Annane, D. (2009). "Hippocampus: a future target for sepsis treatment!" Intensive Care Med **35**(4): 585-586.

Attwell, D. and S. B. Laughlin (2001). "An energy budget for signaling in the grey matter of the brain." J Cereb Blood Flow Metab **21**(10): 1133-1145.

Basler, T., A. Meier-Hellmann, D. Bredle and K. Reinhart (2002). "Amino acid imbalance early in septic encephalopathy." Intensive Care Med **28**(3): 293-298.

Belanger, M., I. Allaman and P. J. Magistretti (2011). "Brain energy metabolism: focus on astrocyte-neuron metabolic cooperation." Cell Metab **14**(6): 724-738.

Bellaver, B., J. P. Dos Santos, D. T. Leffa, L. D. Bobermin, P. H. A. Roppa, I. L. da Silva Torres, C. A. Goncalves, D. O. Souza and A. Quincozes-Santos (2017). "Systemic Inflammation as a Driver of Brain Injury: the Astrocyte as an Emerging Player." Mol Neurobiol.

Bellaver, B., D. G. Souza, D. O. Souza and A. Quincozes-Santos (2014). "Resveratrol increases antioxidant defenses and deceases proinflammatory cytokines in hippocampal astocyte cultures from newborn, adult and aged Wistar rats." Toxicology in vitro **28**: 479-484.

Bellaver, B., D. G. Souza, D. O. Souza and A. Quincozes-Santos (2016). "Hippocampal Astrocyte Cultures from Adult and Aged Rats Reproduce Changes in Glial Functionality Observed in the Aging Brain." Mol Neurobiol.

Biron, B. M., A. Ayala and J. L. Lomas-Neira (2015). "Biomarkers for Sepsis: What Is and What Might Be?" Biomark Insights **10**(Suppl 4): 7-17.

Boomer, J. S., J. M. Green and R. S. Hotchkiss (2014). "The changing immune system in sepsis: is individualized immuno-modulatory therapy the answer?" Virulence **5**(1): 45-56.

Booth, H. D. E., W. D. Hirst and R. Wade-Martins (2017). "The Role of Astrocyte Dysfunction in Parkinson's Disease Pathogenesis." Trends Neurosci **40**(6): 358-370.

Brahmachari, S., Y. K. Fung and K. Pahan (2006). "Induction of glial fibrillary acidic protein expression in astrocytes by nitric oxide." J Neurosci **26**(18): 4930-4939.

Bramanti, V., D. Tomassoni, M. Avitabile, F. Amenta and R. Avola (2010). "Biomarkers of glial cell proliferation and differentiation in culture." Front Biosci (Schol Ed) **2**: 558-570.

Brar, G. A. and J. S. Weissman (2015). "Ribosome profiling reveals the what, when, where and how of protein synthesis." Nat Rev Mol Cell Biol **16**(11): 651-664.

Bruins, M. J., N. E. Deutz and P. B. Soeters (2003). "Aspects of organ protein, amino acid and glucose metabolism in a porcine model of hypermetabolic sepsis." Clin Sci (Lond) **104**(2): 127-141.

Calandra, T. and J. Cohen (2005). "The international sepsis forum consensus conference on definitions of infection in the intensive care unit." Crit Care Med **33**(7): 1538-1548.

Calsavara, A. C., F. M. Soriani, L. Q. Vieira, P. A. Costa, M. A. Rachid and A. L. Teixeira (2015). "TNFR1 absence protects against memory deficit induced by sepsis possibly through over-expression of hippocampal BDNF." Metab Brain Dis **30**(3): 669-678.

Cannon, J. G. (2000). "Inflammatory Cytokines in Nonpathological States." News Physiol Sci **15**: 298-303.

Carpentier, P. A., W. S. Begolka, J. K. Olson, A. Elhofy, W. J. Karpus and S. D. Miller (2005). "Differential activation of astrocytes by innate and adaptive immune stimuli." Glia **49**(3): 360-374.

Carter, S. F., K. Herholz, P. Rosa-Neto, L. Pellerin, A. Nordberg and E. R. Zimmer (2019). "Astrocyte Biomarkers in Alzheimer's Disease." Trends Mol Med.
Casey, L. C. (2000). "Immunologic response to infection and its role in septic shock." Crit Care Clin **16**(2): 193-213.
Catarina, A. V., C. Luft, S. Greggio, G. T. Venturin, F. Ferreira, E. P. Marques, L. Rodrigues, K. Wartchow, M. C. Leite, C. A. Goncalves, A. T. S. Wyse, J. C. Da Costa, J. R. De Oliveira, G. Branchini and F. B. Nunes (2018). "Fructose-1,6-bisphosphate preserves glucose metabolism integrity and reduces reactive oxygen species in the brain during experimental sepsis." Brain Res **1698**: 54-61.
Chen, L. F. and W. C. Greene (2004). "Shaping the nuclear action of NF-kappaB." Nat Rev Mol Cell Biol **5**(5): 392-401.
Chou, C. H., J. T. Lee, C. C. Lin, Y. F. Sung, C. C. Lin, C. H. Muo, F. C. Yang, C. P. Wen, I. K. Wang, C. H. Kao, C. Y. Hsu and C. H. Tseng (2017). "Septicemia is associated with increased risk for dementia: a population-based longitudinal study." Oncotarget **8**(48): 84300-84308.
Cinel, I. and S. M. Opal (2009). "Molecular biology of inflammation and sepsis: a primer." Crit Care Med **37**(1): 291-304.
Clark, I. A. and B. Vissel (2016). "Excess cerebral TNF causing glutamate excitotoxicity rationalizes treatment of neurodegenerative diseases and neurogenic pain by anti-TNF agents." J Neuroinflammation **13**(1): 236.
Clarke, L. E. and B. A. Barres (2013). "Emerging roles of astrocytes in neural circuit development." Nat Rev Neurosci **14**(5): 311-321.
Comim, C. M., V. Freiberger, L. Ventura, F. Mina, G. K. Ferreira, M. Michels, J. S. Generoso, E. L. Streck, J. Quevedo, T. Barichello and F. Dal-Pizzol (2017). "Inhibition of indoleamine 2,3-dioxygenase 1/2 prevented cognitive impairment and energetic metabolism changes in the hippocampus of adult rats subjected to polymicrobial sepsis." J Neuroimmunol **305**: 167-171.
Cotena, S. and O. Piazza (2012). "Sepsis-associated encephalopathy." Transl Med UniSa **2**: 20-27.
Cunningham, C. and E. Hennessy (2015). "Co-morbidity and systemic inflammation as drivers of cognitive decline: new experimental models adopting a broader paradigm in dementia research." Alzheimers Res Ther **7**(1): 33.
Danbolt, N. C. (2001). "Glutamate uptake." Prog Neurobiol **65**(1): 1-105.
Divakaruni, A. S., M. Wallace, C. Buren, K. Martyniuk, A. Y. Andreyev, E. Li, J. A. Fields, T. Cordes, I. J. Reynolds, B. L. Bloodgood and L. A. Raymond (2017). "Inhibition of the mitochondrial pyruvate carrier protects from excitotoxic neuronal death." **216**(4): 1091-1105.
Dringen, R. (2000). "Metabolism and functions of glutathione in brain." Prog Neurobiol **62**(6): 649-671.
Drosatos, K., A. Lymperopoulos, P. J. Kennel, N. Pollak, P. C. Schulze and I. J. Goldberg (2015). "Pathophysiology of sepsis-related cardiac dysfunction: driven by inflammation, energy mismanagement, or both?" Curr Heart Fail Rep **12**(2): 130-140.
Ebersoldt, M., T. Sharshar and D. Annane (2007). "Sepsis-associated delirium." Intensive Care Med **33**(6): 941-950.
Eng, L. F., R. S. Ghirnikar and Y. L. Lee (2000). "Glial fibrillary acidic protein: GFAP-thirty-one years (1969-2000)." Neurochem Res **25**(9-10): 1439-1451.
Escobar, D. A., A. M. Botero-Quintero, B. C. Kautza, J. Luciano, P. Loughran, S. Darwiche, M. R. Rosengart, B. S. Zuckerbraun and H. Gomez (2015). "Adenosine monophosphate-activated protein kinase activation protects against sepsis-induced organ injury and inflammation." J Surg Res **194**(1): 262-272.
Failli, V., M. A. Kopp, C. Gericke, P. Martus, S. Klingbeil, B. Brommer, I. Laginha, Y. Chen, M. J. DeVivo, U. Dirnagl and J. M. Schwab (2012). "Functional neurological recovery after spinal cord injury is impaired in patients with infections." Brain **135**(Pt 11): 3238-3250.
Faix, J. D. (2013). "Biomarkers of sepsis." Crit Rev Clin Lab Sci **50**(1): 23-36.
Farina, C., F. Aloisi and E. Meinl (2007). "Astrocytes are active players in cerebral innate immunity." Trends Immunol **28**(3): 138-145.

Featherstone, D. E. and S. A. Shippy (2008). "Regulation of synaptic transmission by ambient extracellular glutamate." Neuroscientist **14**(2): 171-181.
Fendt, S. M. and P. Verstreken (2017). "Neurons eat glutamate to stay alive." **216**(4): 863-865.
Fernstrom, J. D. and M. H. Fernstrom (2007). "Tyrosine, phenylalanine, and catecholamine synthesis and function in the brain." J Nutr **137**(6 Suppl 1): 1539S-1547S; discussion 1548S.
Filous, A. R. and J. Silver (2016). ""Targeting astrocytes in CNS injury and disease: A translational research approach"." Prog Neurobiol **144**: 173-187.
Friberg, D., J. Bryant, W. Shannon and T. L. Whiteside (1994). "In vitro cytokine production by normal human peripheral blood mononuclear cells as a measure of immunocompetence or the state of activation." Clin Diagn Lab Immunol **1**(3): 261-268.
Garcia-Caceres, C., C. Quarta, L. Varela, Y. Gao, T. Gruber, B. Legutko, M. Jastroch, P. Johansson, J. Ninkovic, C. X. Yi, O. Le Thuc, K. Szigeti-Buck, W. Cai, C. W. Meyer, P. T. Pfluger, A. M. Fernandez, S. Luquet, S. C. Woods, I. Torres-Aleman, C. R. Kahn, M. Gotz, T. L. Horvath and M. H. Tschop (2016). "Astrocytic Insulin Signaling Couples Brain Glucose Uptake with Nutrient Availability." Cell **166**(4): 867-880.
Gardener, S. L., H. R. Sohrabi, K. K. Shen, S. R. Rainey-Smith, M. Weinborn, K. A. Bates, T. Shah, J. K. Foster, N. Lenzo, O. Salvado, C. Laske, S. M. Laws, K. Taddei, G. Verdile and R. N. Martins (2016). "Cerebral Glucose Metabolism is Associated with Verbal but not Visual Memory Performance in Community-Dwelling Older Adults." J Alzheimers Dis **52**(2): 661-672.
Gardoni, F. and M. Di Luca (2006). "New targets for pharmacological intervention in the glutamatergic synapse." Eur J Pharmacol **545**(1): 2-10.
Gasparotto, J., C. S. Girardi, N. Somensi, C. T. Ribeiro, J. C. F. Moreira, M. Michels, B. Sonai, M. Rocha, A. V. Steckert, T. Barichello, J. Quevedo, F. Dal-Pizzol and D. P. Gelain (2018). "Receptor for advanced glycation end products mediates sepsis-triggered amyloid-beta accumulation, Tau phosphorylation, and cognitive impairment." J Biol Chem **293**(1): 226-244.
Godini, R. and H. Fallahi (2018). "Network analysis of inflammatory responses to sepsis by neutrophils and peripheral blood mononuclear cells." **13**(8): e0201674.
Gorina, R., T. Santalucia, V. Petegnief, A. Ejarque-Ortiz, J. Saura and A. M. Planas (2009). "Astrocytes are very sensitive to develop innate immune responses to lipid-carried short interfering RNA." Glia **57**(1): 93-107.
Gorshkov, K., F. Aguisanda, N. Thorne and W. Zheng (2018). "Astrocytes as targets for drug discovery." Drug Discov Today **23**(3): 673-680.
Gotts, J. E. and M. A. Matthay (2016). "Sepsis: pathophysiology and clinical management." Bmj **353**: i1585.
Guha, M. and N. Mackman (2002). "The phosphatidylinositol 3-kinase-Akt pathway limits lipopolysaccharide activation of signaling pathways and expression of inflammatory mediators in human monocytic cells." J Biol Chem **277**(35): 32124-32132.
Gupta, S. C., C. Sundaram, S. Reuter and B. B. Aggarwal (2010). "Inhibiting NF-kappaB activation by small molecules as a therapeutic strategy." Biochim Biophys Acta **1799**(10-12): 775-787.
Hamby, M. E., G. Coppola, Y. Ao, D. H. Geschwind, B. S. Khakh and M. V. Sofroniew (2012). "Inflammatory mediators alter the astrocyte transcriptome and calcium signaling elicited by multiple G-protein-coupled receptors." J Neurosci **32**(42): 14489-14510.
Hato, T., B. Maier, F. Syed, J. Myslinski, A. Zollman, Z. Plotkin, M. T. Eadon and P. C. Dagher (2019). "Bacterial sepsis triggers an antiviral response that causes translation shutdown." J Clin Invest **129**(1): 296-309.
Hayward, J. H. and S. J. Lee (2014). "A Decade of Research on TLR2 Discovering Its Pivotal Role in Glial Activation and Neuroinflammation in Neurodegenerative Diseases." Exp Neurobiol **23**(2): 138-147.
Heo, K., Y. J. Cho, K. J. Cho, H. W. Kim, H. J. Kim, H. Y. Shin, B. I. Lee and G. W. Kim (2006). "Minocycline inhibits caspase-dependent and -independent cell death pathways and is neuroprotective against hippocampal damage after treatment with kainic acid in mice." Neurosci Lett **398**(3): 195-200.

Herculano-Houzel, S. (2014). "The glia/neuron ratio: how it varies uniformly across brain structures and species and what that means for brain physiology and evolution." Glia **62**(9): 1377-1391.
Holmseth, S., Y. Dehnes, Y. H. Huang, V. V. Follin-Arbelet, N. J. Grutle, M. N. Mylonakou, C. Plachez, Y. Zhou, D. N. Furness, D. E. Bergles, K. P. Lehre and N. C. Danbolt (2012). "The density of EAAC1 (EAAT3) glutamate transporters expressed by neurons in the mammalian CNS." J Neurosci **32**(17): 6000-6013.
Hotchkiss, R. S., G. Monneret and D. Payen (2013). "Immunosuppression in sepsis: a novel understanding of the disorder and a new therapeutic approach." Lancet Infect Dis **13**(3): 260-268.
Iskander, K. N., M. F. Osuchowski, D. J. Stearns-Kurosawa, S. Kurosawa, D. Stepien, C. Valentine and D. G. Remick (2013). "Sepsis: multiple abnormalities, heterogeneous responses, and evolving understanding." Physiol Rev **93**(3): 1247-1288.
Jensen, C. J., A. Massie and J. De Keyser (2013). "Immune players in the CNS: the astrocyte." J Neuroimmune Pharmacol **8**(4): 824-839.
Kang, W. and J. M. Hebert (2011). "Signaling pathways in reactive astrocytes, a genetic perspective." Mol Neurobiol **43**(3): 147-154.
Kantrow, S. P., D. E. Taylor, M. S. Carraway and C. A. Piantadosi (1997). "Oxidative metabolism in rat hepatocytes and mitochondria during sepsis." Arch Biochem Biophys **345**(2): 278-288.
Katafuchi, T., M. Ifuku, S. Mawatari, M. Noda, K. Miake, M. Sugiyama and T. Fujino (2012). "Effects of plasmalogens on systemic lipopolysaccharide-induced glial activation and b-amyloid accumulation in adult mice." ANNALS of THE NEW YORK ACADEMY OF SCIENCES **1262**: 85-92.
Katial, R. K., D. Sachanandani, C. Pinney and M. M. Lieberman (1998). "Cytokine production in cell culture by peripheral blood mononuclear cells from immunocompetent hosts." Clin Diagn Lab Immunol **5**(1): 78-81.
Khakh, B. S., V. Beaumont, R. Cachope, I. Munoz-Sanjuan, S. A. Goldman and R. Grantyn (2017). "Unravelling and Exploiting Astrocyte Dysfunction in Huntington's Disease." Trends Neurosci **40**(7): 422-437.
Kielian, T. (2006). "Toll-like receptors in central nervous system glial inflammation and homeostasis." J Neurosci Res **83**(5): 711-730.
Kleine, T. O. and L. Benes (2006). "Immune surveillance of the human central nervous system (CNS): different migration pathways of immune cells through the blood-brain barrier and blood-cerebrospinal fluid barrier in healthy persons." Cytometry A **69**(3): 147-151.
Kopitar-Jerala, N. (2015). "Innate Immune Response in Brain, NF-Kappa B Signaling and Cystatins." Front Mol Neurosci **8**: 73.
Lange, S. C., L. K. Bak, H. S. Waagepetersen, A. Schousboe and M. D. Norenberg (2012). "Primary cultures of astrocytes: their value in understanding astrocytes in health and disease." Neurochem Res **37**(11): 2569-2588.
Lee, I. and M. Huttemann (2014). "Energy crisis: the role of oxidative phosphorylation in acute inflammation and sepsis." Biochim Biophys Acta **1842**(9): 1579-1586.
Lee, S. M. and W. S. An (2016). "New clinical criteria for septic shock: serum lactate level as new emerging vital sign." J Thorac Dis **8**(7): 1388-1390.
Lim, C., M. P. Alexander, G. LaFleche, D. M. Schnyer and M. Verfaellie (2004). "The neurological and cognitive sequelae of cardiac arrest." Neurology **63**(10): 1774-1778.
Liu, Z., Y. Li, Y. Cui, C. Roberts, M. Lu, U. Wilhelmsson, M. Pekny and M. Chopp (2014). "Beneficial effects of gfap/vimentin reactive astrocytes for axonal remodeling and motor behavioral recovery in mice after stroke." Glia **62**(12): 2022-2033.
Lovatt, D., U. Sonnewald, H. S. Waagepetersen, A. Schousboe, W. He, J. H. Lin, X. Han, T. Takano, S. Wang, F. J. Sim, S. A. Goldman and M. Nedergaard (2007). "The transcriptome and metabolic gene signature of protoplasmic astrocytes in the adult murine cortex." J Neurosci **27**(45): 12255-12266.
Ma, Y., A. Zechariah, Y. Qu and D. M. Hermann (2012). "Effects of vascular endothelial growth factor in ischemic stroke." J Neurosci Res **90**(10): 1873-1882.

McAfoose, J., H. Koerner and B. T. Baune (2009). "The effects of TNF deficiency on age-related cognitive performance." Psychoneuroendocrinology **34**(4): 615-619.
McKenna, M. C. (2007). "The glutamate-glutamine cycle is not stoichiometric: fates of glutamate in brain." J Neurosci Res **85**(15): 3347-3358.
Michels, M., A. V. Steckert, J. Quevedo, T. Barichello and F. Dal-Pizzol (2015). "Mechanisms of long-term cognitive dysfunction of sepsis: from blood-borne leukocytes to glial cells." Intensive Care Med Exp **3**(1): 30.
Miller, R. H. and M. C. Raff (1984). "Fibrous and protoplasmic astrocytes are biochemically and developmentally distinct." J Neurosci **4**(2): 585-592.
Mincheva-Tasheva, S. and R. M. Soler (2013). "NF-kappaB signaling pathways: role in nervous system physiology and pathology." Neuroscientist **19**(2): 175-194.
Mizock, B. A., H. C. Sabelli, A. Dubin, J. I. Javaid, A. Poulos and E. C. Rackow (1990). "Septic encephalopathy. Evidence for altered phenylalanine metabolism and comparison with hepatic encephalopathy." Arch Intern Med **150**(2): 443-449.
Monje, M. L., H. Toda and T. D. Palmer (2003). "Inflammatory blockade restores adult hippocampal neurogenesis." Science **302**(5651): 1760-1765.
Neves, F. S., P. T. Marques, F. Barros-Aragao, J. B. Nunes, A. M. Venancio, D. Cozachenco, R. L. Frozza, G. F. Passos, R. Costa, J. de Oliveira, D. F. Engel, A. F. De Bem, C. F. Benjamim, F. G. De Felice, S. T. Ferreira, J. R. Clarke and C. P. Figueiredo (2016). "Brain-Defective Insulin Signaling Is Associated to Late Cognitive Impairment in Post-Septic Mice." Mol Neurobiol.
Nolan, Y., V. A. Campbell, A. E. Bolton and M. A. Lynch (2005). "Evidence of an anti-inflammatory role for Vasogen's immune modulation therapy." Neuroimmunomodulation **12**(2): 113-116.
Nolan, Y., E. Vereker, A. M. Lynch and M. A. Lynch (2003). "Evidence that lipopolysaccharide-induced cell death is mediated by accumulation of reactive oxygen species and activation of p38 in rat cortex and hippocampus." Exp Neurol **184**(2): 794-804.
Nortley, R. and D. Attwell (2017). "Control of brain energy supply by astrocytes." Curr Opin Neurobiol **47**: 80-85.
Pagani, M., F. De Carli, S. Morbelli, J. Oberg, A. Chincarini, G. B. Frisoni, S. Galluzzi, R. Perneczky, A. Drzezga, B. N. van Berckel, R. Ossenkoppele, M. Didic, E. Guedj, A. Brugnolo, A. Picco, D. Arnaldi, M. Ferrara, A. Buschiazzo, G. Sambuceti and F. Nobili (2015). "Volume of interest-based [18F]fluorodeoxyglucose PET discriminates MCI converting to Alzheimer's disease from healthy controls. A European Alzheimer's Disease Consortium (EADC) study." Neuroimage Clin **7**: 34-42.
Pehar, M., B. A. Harlan, K. M. Killoy and M. R. Vargas (2017). "Role and Therapeutic Potential of Astrocytes in Amyotrophic Lateral Sclerosis." Curr Pharm Des **23**(33): 5010-5021.
Pekny, M., U. Wilhelmsson and M. Pekna (2014). "The dual role of astrocyte activation and reactive gliosis." Neurosci Lett **565**: 30-38.
Poeze, M., Y. C. Luiking, P. Breedveld, S. Manders and N. E. Deutz (2008). "Decreased plasma glutamate in early phases of septic shock with acute liver dysfunction is an independent predictor of survival." Clin Nutr **27**(4): 523-530.
Ransohoff, R. M. and M. A. Brown (2012). "Innate immunity in the central nervous system." J Clin Invest **122**(4): 1164-1171.
Ransohoff, R. M., D. Schafer, A. Vincent, N. E. Blachere and A. Bar-Or (2015). "Neuroinflammation: Ways in Which the Immune System Affects the Brain." Neurotherapeutics **12**(4): 896-909.
Reinhart, K., R. Daniels, N. Kissoon, F. R. Machado, R. D. Schachter and S. Finfer (2017). "Recognizing Sepsis as a Global Health Priority - A WHO Resolution." N Engl J Med **377**(5): 414-417.
Richards, M. H., S. D. Narasipura, S. Kim, M. S. Seaton, V. Lutgen and L. Al-Harthi (2015). "Dynamic interaction between astrocytes and infiltrating PBMCs in context of neuroAIDS." Glia **63**(3): 441-451.
Rivers, E., B. Nguyen, S. Havstad, J. Ressler, A. Muzzin, B. Knoblich, E. Peterson and M. Tomlanovich (2001). "Early goal-directed therapy in the treatment of severe sepsis and septic shock." N Engl J Med **345**(19): 1368-1377.

Rossi, D. (2015). "Astrocyte physiopathology: At the crossroads of intercellular networking, inflammation and cell death." Prog Neurobiol **130**: 86-120.
Rossi, D. J., J. D. Brady and C. Mohr (2007). "Astrocyte metabolism and signaling during brain ischemia." Nat Neurosci **10**(11): 1377-1386.
Russo, M. V. and D. B. McGavern (2015). "Immune Surveillance of the CNS following Infection and Injury." Trends Immunol **36**(10): 637-650.
Saha, R. N. and K. Pahan (2006). "Signals for the induction of nitric oxide synthase in astrocytes." Neurochem Int **49**(2): 154-163.
Santello, M., P. Bezzi and A. Volterra (2011). "TNFalpha controls glutamatergic gliotransmission in the hippocampal dentate gyrus." Neuron **69**(5): 988-1001.
Schousboe, A., L. K. Bak and H. S. Waagepetersen (2013). "Astrocytic Control of Biosynthesis and Turnover of the Neurotransmitters Glutamate and GABA." Front Endocrinol (Lausanne) **4**: 102.
Semmler, A., S. Hermann, F. Mormann, M. Weberpals, S. A. Paxian, T. Okulla, M. Schafers, M. P. Kummer, T. Klockgether and M. T. Heneka (2008). "Sepsis causes neuroinflammation and concomitant decrease of cerebral metabolism." J Neuroinflammation **5**: 38.
Semmler, A., Y. Smulders, E. Struys, D. Smith, S. Moskau, H. Blom and M. Linnebank (2008). "Methionine metabolism in an animal model of sepsis." Clin Chem Lab Med **46**(10): 1398-1402.
Semmler, A., C. N. Widmann, T. Okulla, H. Urbach, M. Kaiser, G. Widman, F. Mormann, J. Weide, K. Fliessbach, A. Hoeft, F. Jessen, C. Putensen and M. T. Heneka (2013). "Persistent cognitive impairment, hippocampal atrophy and EEG changes in sepsis survivors." J Neurol Neurosurg Psychiatry **84**(1): 62-69.
Shao, Y. and K. D. McCarthy (1994). "Plasticity of astrocytes." Glia **11**(2): 147-155.
Singer, M. (2014). "The role of mitochondrial dysfunction in sepsis-induced multi-organ failure." Virulence **5**(1): 66-72.
Singer, M., C. S. Deutschman, C. W. Seymour, M. Shankar-Hari, D. Annane, M. Bauer, R. Bellomo, G. R. Bernard, J. D. Chiche, C. M. Coopersmith, R. S. Hotchkiss, M. M. Levy, J. C. Marshall, G. S. Martin, S. M. Opal, G. D. Rubenfeld, T. van der Poll, J. L. Vincent and D. C. Angus (2016). "The Third International Consensus Definitions for Sepsis and Septic Shock (Sepsis-3)." Jama **315**(8): 801-810.
Sjovall, F., S. Morota, J. Persson, M. J. Hansson and E. Elmer (2013). "Patients with sepsis exhibit increased mitochondrial respiratory capacity in peripheral blood immune cells." Crit Care **17**(4): R152.
Skytt, D. M., K. K. Madsen, K. Pajecka, A. Schousboe and H. S. Waagepetersen (2010). "Characterization of primary and secondary cultures of astrocytes prepared from mouse cerebral cortex." Neurochem Res **35**(12): 2043-2052.
Sofroniew, M. V. (2014). "Astrogliosis." Cold Spring Harb Perspect Biol **7**(2): a020420.
Souza, D. G., B. Bellaver, L. D. Bobermin, D. O. Souza and A. Quincozes-Santos (2016). "Anti-aging effects of guanosine in glial cells." Purinergic Signal.
Souza, D. G., B. Bellaver, D. O. Souza and A. Quincozes-Santos (2013). "Characterization of adult rat astrocyte cutures." PLoS One **8**: E60282.
Souza, D. G., B. Bellaver, S. R. Terra, F. C. Guma, D. O. Souza and A. Quincozes-Santos (2017). "In Vitro Adult Astrocytes Are Derived from Mature Cells and Reproduce In Vivo Redox Profile." J Cell Biochem.
Sprung, C. L., F. B. Cerra, H. R. Freund, R. M. Schein, F. N. Konstantinides, E. H. Marcial and M. Pena (1991). "Amino acid alterations and encephalopathy in the sepsis syndrome." Crit Care Med **19**(6): 753-757.
Steckert, A. V., D. Dominguini, M. Michels, H. M. Abelaira, D. B. Tomaz, B. Sonai, A. B. de Moura, D. Matos, J. B. I. da Silva, G. Z. Reus, T. Barichello, J. Quevedo and F. Dal-Pizzol (2017). "The impact of chronic mild stress on long-term depressive behavior in rats which have survived sepsis." J Psychiatr Res **94**: 47-53.
Stobart, J. L. and C. M. Anderson (2013). "Multifunctional role of astrocytes as gatekeepers of neuronal energy supply." Front Cell Neurosci **7**: 38.

Tang, B. M., S. J. Huang and A. S. McLean (2010). "Genome-wide transcription profiling of human sepsis: a systematic review." Crit Care **14**(6): R237.
Tang, B. M., A. S. McLean, I. W. Dawes, S. J. Huang and R. C. Lin (2009). "Gene-expression profiling of peripheral blood mononuclear cells in sepsis." Crit Care Med **37**(3): 882-888.
Waisman, A., R. S. Liblau and B. Becher (2015). "Innate and adaptive immune responses in the CNS." Lancet Neurol **14**(9): 945-955.
Wang, D. D. and A. Bordey (2008). "The astrocyte odyssey." Prog Neurobiol **86**(4): 342-367.
Wang, X., K. Kang, S. Wang, J. Yao and X. Zhang (2016). "Focal cerebral ischemic tolerance and change in blood-brain barrier permeability after repetitive pure oxygen exposure preconditioning in a rodent model." J Neurosurg **125**(4): 943-952.
Ward, P. S. and C. B. Thompson (2012). "Signaling in control of cell growth and metabolism." Cold Spring Harb Perspect Biol **4**(7): a006783.
Weise, C. M., K. Chen, Y. Chen, X. Kuang, C. R. Savage and E. M. Reiman (2018). "Left lateralized cerebral glucose metabolism declines in amyloid-beta positive persons with mild cognitive impairment." Neuroimage Clin **20**: 286-296.
Wexler, O., M. S. Gough, M. A. M. Morgan, C. M. Mack, M. J. Apostolakos, K. P. Doolin, R. A. Mooney, E. Arning, T. Bottiglieri and A. P. Pietropaoli (2018). "Methionine Metabolites in Patients With Sepsis." J Intensive Care Med **33**(1): 37-47.
Wichterman, K. A., A. E. Baue and I. H. Chaudry (1980). "Sepsis and septic shock--a review of laboratory models and a proposal." J Surg Res **29**(2): 189-201.
Wilhelmsson, U., L. Li, M. Pekna, C. H. Berthold, S. Blom, C. Eliasson, O. Renner, E. Bushong, M. Ellisman, T. E. Morgan and M. Pekny (2004). "Absence of glial fibrillary acidic protein and vimentin prevents hypertrophy of astrocytic processes and improves post-traumatic regeneration." J Neurosci **24**(21): 5016-5021.
Wilson, J. X. and G. B. Young (2003). "Progress in clinical neurosciences: sepsis-associated encephalopathy: evolving concepts." Can J Neurol Sci **30**(2): 98-105.
Wrann, C. D., N. A. Tabriz, T. Barkhausen, A. Klos, M. van Griensven, H. C. Pape, D. O. Kendoff, R. Guo, P. A. Ward, C. Krettek and N. C. Riedemann (2007). "The phosphatidylinositol 3-kinase signaling pathway exerts protective effects during sepsis by controlling C5a-mediated activation of innate immune functions." J Immunol **178**(9): 5940-5948.
Yokoo, H., S. Chiba, K. Tomita, M. Takashina, H. Sagara, S. Yagisita, Y. Takano and Y. Hattori (2012). "Neurodegenerative evidence in mice brains with cecal ligation and puncture-induced sepsis: preventive effect of the free radical scavenger edaravone." PLoS One **7**(12): e51539.
Young, G. B. (2010). "Sparing brain damage in severe sepsis: a beginning." Crit Care **14**(3): 159.
Zhang, S., X. Wang, S. Ai, W. Ouyang, Y. Le and J. Tong (2017). "Sepsis-induced selective loss of NMDA receptors modulates hippocampal neuropathology in surviving septic mice." **12**(11): e0188273.
Zhang, X., M. Shi, M. Bjoras, W. Wang, G. Zhang, J. Han, Z. Liu, Y. Zhang, B. Wang, J. Chen, Y. Zhu, L. Xiong and G. Zhao (2013). "Ginsenoside Rd promotes glutamate clearance by up-regulating glial glutamate transporter GLT-1 via PI3K/AKT and ERK1/2 pathways." Front Pharmacol **4**: 152.
Ziaja, M. (2013). "Septic encephalopathy." Curr Neurol Neurosci Rep **13**(10): 383.
Zimmer, E. R., M. J. Parent, D. G. Souza, A. Leuzy, C. Lecrux, H. I. Kim, S. Gauthier, L. Pellerin and E. Hamel (2017). "[18F]FDG PET signal is driven by astroglial glutamate transport."

ANEXOS

ANEXO I: Artigos publicados durante o período de doutoramento cujos temas se relacionam a esta tese, mas não foram incluídos no corpo principal da tese

ANEXO I-A: Resveratrol Protects Hippocampal Astrocytes Against LPS-Induced Neurotoxicity Through HO-1, p38 and ERK Pathways.

Publicado no periódico Neurochemical Research

Neurochem Res (2015) 40:1600–1608
DOI 10.1007/s11064-015-1636-8

ORIGINAL PAPER

Resveratrol Protects Hippocampal Astrocytes Against LPS-Induced Neurotoxicity Through HO-1, p38 and ERK Pathways

Bruna Bellaver[1] · Débora Guerini Souza[1] · Larissa Daniele Bobermin[1] · Diogo Onofre Souza[1] · Carlos-Alberto Gonçalves[1] · André Quincozes-Santos[1]

Received: 25 January 2015 / Revised: 3 June 2015 / Accepted: 6 June 2015 / Published online: 19 June 2015

Abstract Resveratrol, a phytoalexin found in grapes and wine, exhibits antioxidant, anti-inflammatory, anti-aging and antitumor activities. Resveratrol also protects neurons and astrocytes in several neurological disease models. Astrocytes are responsible for modulating neurotransmitter systems, synaptic information, ionic homeostasis, energy metabolism, antioxidant defense and inflammatory response. In previous work, we showed that resveratrol modulates important glial functions, including glutamate uptake, glutamine synthetase activity, glutathione (GSH) levels and inflammatory response. Furthermore, astrocytes express toll-like receptors that specifically recognize lipopolysaccharide (LPS), which has been widely used to study experimentally inflammatory response. In this sense, LPS may stimulate pro-inflammatory cytokines release and oxidative stress. Moreover, there is interplay between these signals through signaling pathways such as NFκB, HO-1 and MAPK. Thus, here, we evaluated the effects of resveratrol on LPS-stimulated inflammatory response in hippocampal primary astrocyte cultures and the putative role of HO-1, p38 and ERK pathways in the protective effect of resveratrol. LPS increased the levels of TNF-α, IL-1β, IL-6 and IL-18 and resveratrol prevented these effects. Resveratrol also prevented the oxidative and nitrosative stress induced by LPS as well as the decrease in GSH content. Additionally, we demonstrated the involvement of NFκB, HO-1, p38 and ERK signaling pathways in the protective effect of resveratrol, providing the first mechanistic explanation for these effects in hippocampal astrocytes. Our findings reinforce the neuroprotective effects of resveratrol, which are mainly associated with anti-inflammatory and antioxidant activities.

Keywords Astrocytes · Resveratrol · LPS · Cytokines · NFκB · HO-1

✉ André Quincozes-Santos
andrequincozes@ufrgs.br; andrequincozes@yahoo.com.br

[1] Departamento de Bioquímica, Programa de Pós-Graduação em Ciências Biológicas: Bioquímica, Instituto de Ciências Básicas da Saúde, Universidade Federal do Rio Grande do Sul, Rua Ramiro Barcelos, 2600 – Anexo, Bairro Santa Cecília, Porto Alegre, RS 90035-003, Brazil

Introduction

Astrocytes, the more versatile cells in the central nervous system (CNS), have a fundamental role in normal brain development and function [1, 2]. Astrocytes contribute to maintenance of synaptic information processing and ionic homeostasis; regulate energy metabolism and release of neurotrophic factors; modulate the biosynthesis and release of antioxidant defenses and the main anti- and proinflammatory cytokines [2–8]. Although immune responses in the CNS are mainly attributed to microglia, due to the capacity of these cells to present antigens, astrocytes express toll-like receptors (TLR) and build up responses to immune triggers by releasing proinflammatory molecules [9, 10].

Lipopolysaccharide (LPS) is the main component of outer membrane of gran-negative bacteria and has been widely used to study experimentally inflammatory response, including in the CNS [11, 12]. In this sense, astrocytes have TLR4, which belongs to TLR family receptors, and specifically recognizes LPS [12, 13]. The exposure to LPS can lead to release of proinflammatory cytokines and it in turn activate the transcription factor NFκB, nitric oxide (NO) release and overproduction of reactive oxygen species (ROS) [11, 14]. Furthermore, there is a close relationship between oxidative stress and

ANEXO I-B: Guanosine inhibits LPS-induced pro-inflammatory response and oxidative stress in hippocampal astrocytes through the heme oxygenase-1 pathway.

Publicado no periódico Purinergic Signaling

Purinergic Signalling
DOI 10.1007/s11302-015-9475-2

ORIGINAL ARTICLE

Guanosine inhibits LPS-induced pro-inflammatory response and oxidative stress in hippocampal astrocytes through the heme oxygenase-1 pathway

Bruna Bellaver[1] · **Débora Guerini Souza**[1] · **Larissa Daniele Bobermin**[1] · **Carlos-Alberto Gonçalves**[1] · **Diogo Onofre Souza**[1] · **André Quincozes-Santos**[1]

Received: 23 June 2015 / Accepted: 24 September 2015

Abstract Guanosine, a guanine-based purine, is an extracellular signaling molecule that is released from astrocytes and has been shown to promote central nervous system defenses in several in vivo and in vitro injury models. Our group recently demonstrated that guanosine exhibits glioprotective effects in the C6 astroglial cell line by associating the heme oxygenase-1 (HO-1) signaling pathway with protection against azide-induced oxidative stress. Astrocyte overactivation contributes to the triggering of brain inflammation, a condition that is closely related to the development of many neurological disorders. These cells sense and amplify inflammatory signals from microglia and/or initiate the release of inflammatory mediators that are strictly related to transcriptional factors, such as nuclear factor kappa B (NFκB), that are modulated by HO-1. Astrocytes also express toll-like receptors (TLRs); TLRs specifically recognize lipopolysaccharide (LPS), which has been widely used to experimentally study inflammatory response. This study was designed to understand the glioprotective mechanism of guanosine against the inflammatory and oxidative damage induced by LPS exposure in primary cultures of hippocampal astrocytes. Treatment of astrocytes with LPS resulted in deleterious effects, including the augmentation of pro-inflammatory cytokine levels, NFκB activation, mitochondrial dysfunction, increased levels of oxygen/nitrogen species, and decreased levels of antioxidative defenses. Guanosine was able to prevent these effects, protecting the hippocampal astrocytes against LPS-induced cytotoxicity through activation of the HO-1 pathway. Additionally, the anti-inflammatory effects of guanosine were independent of the adenosinergic system. These results highlight the potential role of guanosine against neuroinflammatory-related diseases.

Keywords Guanosine · Astrocytes · Neuroinflammation · Glioprotection · HO-1 · NFκB

Introduction

Neuroinflammation, well-marked by activation of the innate immune system of the brain, plays a role in the early mechanisms involved in the pathology of many neurodegenerative and acute illnesses, such as Alzheimer's disease, Parkinson's disease, and stroke [1–3]. Brain inflammation is triggered by the activation of glial cells, which can promote an increase in the infiltration of peripheral immune cells, the production of inflammatory mediators, and the generation of reactive oxygen/nitrogen species (ROS/RNS) [4]. Thus, proper regulation of inflammation by glial cell management could be of vital importance to delay disease progression in several neurological disorders.

Astrocytes are the most abundant glial cell type in the central nervous system (CNS), and under physiological conditions, they play key housekeeping roles offering structural, metabolic, and trophic support to neuronal survivor [5–7]. However, astrocyte overactivation promotes the release of a broad array of cytokines, such as interleukin-1β (IL-1β) and tumor necrosis factor α (TNF-α), chemokines, and ROS. Secondary waves of immune cell infiltration into the CNS are also a result, and all of these processes may lead to cognitive

✉ Bruna Bellaver
brunabellaver90@gmail.com

[1] Departamento de Bioquímica, Programa de Pós-Graduação em Ciências Biológicas: Bioquímica, Instituto de Ciências Básicas da Saúde, Universidade Federal do Rio Grande do Sul, Rua Ramiro Barcelos, 2600, Anexo, Bairro Santa Cecília, Porto Alegre, RS 90035-003, Brazil

Published online: 02 October 2015

ANEXO II: Artigos publicados durante o período de doutoramento cujos temas não se relacionam diretamente a esta tese.

ANEXO II-A: Astrocytes from adult Wistar rats aged in vitro show changes in glial functions.

Publicado no periódico Neurochemistry International

Neurochemistry International xxx (2015) 1–5

Contents lists available at ScienceDirect

Neurochemistry International

journal homepage: www.elsevier.com/locate/nci

Astrocytes from adult Wistar rats aged *in vitro* show changes in glial functions

Débora Guerini Souza*, Bruna Bellaver, Gustavo Santos Raupp, Diogo Onofre Souza, André Quincozes-Santos

Biochemistry Department, Basic Health Sciences Institute, Federal University of Rio Grande do Sul, Porto Alegre, RS, Brazil

ARTICLE INFO

Article history:
Received 16 March 2015
Received in revised form
25 June 2015
Accepted 21 July 2015
Available online xxx

Keywords:
Adult astrocytes
Astrocytes aged *in vitro*
Brain aging
Glucose uptake
Glutamine synthetase activity
Glutathione

ABSTRACT

Astrocytes, the most versatile cells of the central nervous system, play an important role in the regulation of neurotransmitter homeostasis, energy metabolism, antioxidant defenses and the anti-inflammatory response. Recently, our group characterized cortical astrocyte cultures from adult Wistar rats. In line with that work, we studied glial function using an experimental *in vitro* model of aging astrocytes (30 days *in vitro* after reaching confluence) from newborn (NB), adult (AD) and aged (AG) Wistar rats. We evaluated metabolic parameters, such as the glucose uptake, glutamine synthetase (GS) activity, and glutathione (GSH) content, as well as the GFAP, GLUT-1 and xCT expression. AD and AG astrocytes take up less glucose than NB astrocytes and had decreased GLUT1 expression levels. Furthermore, AD and AG astrocytes exhibited decreased GS activity compared to NB cells. Simultaneously, AD and AG astrocytes showed an increase in GSH levels, along with an increase in xCT expression. NB, AD and AG astrocytes presented similar morphology; however, differences in GFAP levels were observed. Taken together, these results improve the knowledge of cerebral senescence and represent an innovative tool for brain studies of aging.

1. Introduction

Astrocytes are robust glial cells that play several roles in central nervous system (CNS) homeostasis. They are responsible for neurotransmitter management, synaptic processing, ionic homeostasis, antioxidant defenses and the anti-inflammatory response as well as energy metabolism (Jiang and Cadenas, 2014; Maragakis and Rothstein, 2006; Parpura et al., 2012; Perea et al., 2014; Wang and Bordey, 2008). Their strategically positioned processes are able to reach both blood capillaries and other cells, allowing them to carry energy substrates that provide metabolic fuel for brain activity (Belanger et al., 2011; Schousboe et al., 2011). These functions can likely be attributed to an organized cytoskeleton, which implicates the presence of characteristic intermediate filaments, such as glial fibrillary acidic protein (GFAP), a classical cytoskeletal marker of astrocytes. GFAP is thought to contribute to a broad number of functions, such as mechanical strength and astrocytic shape (Menet et al., 2001; Middeldorp and Hol, 2011).

Astrocytes are also known to be both highly oxidative and glycolytic, and through glucose transporter 1 (GLUT 1), they are able to transport glucose from the blood to the inside of the cell and thereby provide metabolic fuel for the CNS (Benarroch, 2014; Nedergaard et al., 2003). Moreover, astrocytes are critical cells in glutamatergic transmission homeostasis. They take up glutamate through their high-affinity glutamate transporters GLT-1 and GLAST (Anderson and Swanson, 2000; Benarroch, 2010; Danbolt, 2001; Ye and Sontheimer, 2002), which may then be used as a substrate for oxidation in the tricarboxylic acids cycle, to synthesize either the tripeptide glutathione (GSH), the major antioxidant of the brain, or glutamine through glutamine synthetase (EC 6.3.1.2) (Dringen, 2000; Uwechue et al., 2012; Mates et al., 2002; Lee et al., 2010). Astrocytes are not only able to take up glutamate but also able to release it in a non-vesicular manner through a cystine-glutamate antiporter (system x_c^-), allowing it to activate extrasynaptic receptors and shape synaptic activity. System x_c^- is an important source of cystine, which is intracellularly converted to cysteine, the rate-limiting substrate in GSH biosynthesis (Lewerenz et al., 2006; Sato et al., 1999).

Previous studies from our group have shown that adult and aged

* Corresponding author. Biochemistry Department, Basic Health Sciences Institute, Federal University of Rio Grande do Sul, Porto Alegre, Ramiro Barcelos, 2600, Anexo, PO Box: 90035-003, RS, Brazil.
E-mail address: debsrs@gmail.com (D.G. Souza).

http://dx.doi.org/10.1016/j.neuint.2015.07.016
0197-0186/

ANEXO II-B: Characterization of Amino Acid Profile and Enzymatic Activity in Adult Rat Astrocyte Cultures.

Publicado no periódico Neurochemical Research

Neurochem Res
DOI 10.1007/s11064-016-1871-7

ORIGINAL PAPER

Characterization of Amino Acid Profile and Enzymatic Activity in Adult Rat Astrocyte Cultures

Débora Guerini Souza[1] · Bruna Bellaver[1] · Gisele Hansel[1] · Bernardo Assein Arús[1] · Gabriela Bellaver[1] · Aline Longoni[1] · Janaina Kolling[1] · Angela T. S. Wyse[1] · Diogo Onofre Souza[1] · André Quincozes-Santos[1]

Received: 24 November 2015 / Revised: 1 February 2016 / Accepted: 11 February 2016

Abstract Astrocytes are multitasking players in brain complexity, possessing several receptors and mechanisms to detect, participate and modulate neuronal communication. The functionality of astrocytes has been mainly unraveled through the study of primary astrocyte cultures, and recently our research group characterized a model of astrocyte cultures derived from adult Wistar rats. We, herein, aim to characterize other basal functions of these cells to explore the potential of this model for studying the adult brain. To characterize the astrocytic phenotype, we determined the presence of GFAP, GLAST and GLT 1 proteins in cells by immunofluorescence. Next, we determined the concentrations of thirteen amino acids, ATP, ADP, adenosine and calcium in astrocyte cultures, as well as the activities of Na^+/K^+-ATPase and acetylcholine esterase. Furthermore, we assessed the presence of the GABA transporter 1 (GAT 1) and cannabinoid receptor 1 (CB 1) in the astrocytes. Cells demonstrated the presence of glutamine, consistent with their role in the glutamate–glutamine cycle, as well as glutamate and D-serine, amino acids classically known to act as gliotransmitters. ATP was produced and released by the cells and ADP was consumed. Calcium levels were in agreement with those reported in the literature, as were the enzymatic activities measured. The presence of GAT 1 was detected, but the presence of CB 1 was not, suggesting a decreased neuroprotective capacity in adult astrocytes under in vitro conditions. Taken together, our results show cellular functionality regarding the astrocytic role in gliotransmission and neurotransmitter management since they are able to produce and release gliotransmitters and to modulate the cholinergic and GABAergic systems.

Keywords Adult astrocytes · Gliotransmitters · Amino acids · Na^+/K^+-ATPase · AChE

Introduction

Astrocytes are multitasking players in brain complexity, acting as secretory cells of the central nervous system (CNS) releasing neurotransmitters, neuromodulators and trophic factors [1–3]. They sense neural communication, as is evident by the expression of numerous neurotransmitter receptors, transporters and enzymes on their membranes [4]. These cells also release gliotransmitters, such as glutamate, D-serine and ATP, which interact with pre- and post-synaptic receptors in the tripartite synapse [5–7]. Astrocytes are also primary homeostatic cells of the brain, and most of their functionality has been unraveled through the study of primary astrocyte cultures, especially those related to glutamate and GABA metabolism, their antioxidant defense and energy capabilities [8–11].

Recent studies have employed astrocyte cultures derived from adult rats, which are unsurprisingly different to those derived from newborn animals, since their connections on the tissue that they are inserted in are far more complex. As such, we previously published a routine astrocyte culture protocol from adult Wistar rats; these cells present classical astrocytic markers, take up glutamate, and actively participate in antioxidant and inflammatory responses [12]. Additionally, these cells presented age-related glial

✉ Débora Guerini Souza
debsrs@gmail.com

[1] Departamento de Bioquímica, Instituto de Ciências Básicas da Saúde, Universidade Federal do Rio Grande do Sul, Ramiro Barcelos, 2600, Anexo, PO Box: 90035-003, Porto Alegre, RS, Brazil

Published online: 25 February 2016

ANEXO II-C: Signaling mechanisms underlying the glioprotective effects of resveratrol against mitochondrial dysfunction.

Publicado no periódico BBA - Molecular Basis of Disease

Biochimica et Biophysica Acta 1862 (2016) 1827–1838

Contents lists available at ScienceDirect

Biochimica et Biophysica Acta

journal homepage: www.elsevier.com/locate/bbadis

Signaling mechanisms underlying the glioprotective effects of resveratrol against mitochondrial dysfunction

Bruna Bellaver *, Larissa Daniele Bobermin, Débora Guerini Souza, Marília Danielly Nunes Rodrigues, Adriano Martimbianco de Assis, Moacir Wajner, Carlos-Alberto Gonçalves, Diogo Onofre Souza, André Quincozes-Santos *

Departamento de Bioquímica, Programa de Pós-Graduação em Ciências Biológicas: Bioquímica, Instituto de Ciências Básicas da Saúde, Universidade Federal do Rio Grande do Sul, Porto Alegre, RS, Brazil

ARTICLE INFO

Article history:
Received 17 February 2016
Received in revised form 2 June 2016
Accepted 29 June 2016
Available online 01 July 2016

Keywords:
Resveratrol
Mitochondrial dysfunction
Heme oxygenase-1 (HO-1)
Hippocampal astrocytes
Nuclear factor kappa B (NFκB)

ABSTRACT

Resveratrol, a polyphenol found in grapes and red wine, exhibits antioxidant, anti-inflammatory, anti-aging and, neuroprotective effects. Resveratrol also plays a significant role modulating glial functionality, protecting the health of neuroglial cells against several neuropsychiatric in vivo and in vitro experimental models. Mitochondrial impairment strongly affected astrocyte functions and consequently brain homeostasis. Molecules that promote astrocyte mitochondrial protection are fundamental to maintain brain energy balance and cellular redox state, contributing to brain healthy. Thus, the present study was designed to evaluate some glioprotective mechanisms of resveratrol against mitochondrial damage promoted by azide exposure in hippocampal primary astrocyte cultures. Azide treatment provoked deleterious effects, including the dysfunction of mitochondria, the deterioration of redox homeostasis, the augmentation of pro-inflammatory cytokines and impairment of glutamate uptake activity. However, resveratrol prevented these effects, protecting hippocampal astrocytes against azide-induced cytotoxicity through the heme-oxygenase-1 (HO-1) pathway and inhibiting p38 mitogen-activated protein kinase (p38 MAPK) and nuclear factor kappa B (NFκB) activation. Resveratrol also protected astrocytes via phosphatidylinositide 3-kinase (PI3K)/Akt. These results contribute to the comprehension of the mechanisms by which resveratrol mediates hippocampal astrocyte protection against mitochondrial failure and implicate resveratrol as an important glioprotective molecule.

1. Introduction

Mitochondrial failure is recognized as a common feature encountered in brain aging and many neurological diseases, particularly in the pathogenesis of neurodegenerative disorders [1–3]. The dysfunction of mitochondrial energy metabolism reduces ATP production, followed by the generation of reactive oxygen species (ROS). The decreased activity of complex IV in the electron transport chain has been detected in the brains of patients with ischemia, epilepsy, and Alzheimer's and Huntington's diseases [2,4,5]. Accordingly, sodium azide is a rapid inhibitor of cytochrome *c* oxidase, reflecting the frequent use of this molecule to induce acute oxidative stress.

Resveratrol (3,5,4′-trihidroxy-*trans*-stilbene) is a polyphenol commonly detected in a variety of dietary sources, including grapes, peanuts and wine. The neuroprotective effects of resveratrol might reflect the antioxidant, anti-inflammatory and anti-aging properties of this compound [6–11]. This phytoalexin has been implicated in the protection of astrocytes and neurons against in vivo and in vitro experimental models [12–16]. Recently, we demonstrated that the protective effects of resveratrol against an inflammatory challenge in astrocytes might be associated with heme oxygenase-1 (HO-1), p38 mitogen-activated protein kinase (p38 MAPK) and extracellular signal–regulated kinase (ERK) pathways [17]. Although the protective role of resveratrol in the central nervous system (CNS) has been well established, the mechanisms of the effects mediated by astrocytes have not been fully clarified.

Astrocytes are the most abundant glial cell type in the CNS, and these cells participate in a wide range of functions to maintain brain homeostasis [18–20]. Following brain damage, these cells become reactive, triggering a cascade of events, which play a key role in the recruitment of other glial cells, strongly affecting neuronal survival [21–23]. In conditions of oxidative injury and inflammation, the astrocytic synthesis

* Corresponding authors at: Departamento de Bioquímica, Programa de Pós-Graduação em Ciências Biológicas: Bioquímica, Instituto de Ciências Básicas da Saúde, Universidade, Federal do Rio Grande do Sul, Rua Ramiro Barcelos, 2600 — Anexo, Bairro Santa Cecília, 90035-003, Porto Alegre, RS, Brazil.
E-mail addresses: brunabellaver90@gmail.com (B. Bellaver), andrequincozes@ufrgs.br (A. Quincozes-Santos).

http://dx.doi.org/10.1016/j.bbadis.2016.06.018
0925-4439/

ANEXO II-D: Higher Vulnerability of Menadione-Exposed Cortical Astrocytes of Glutaryl-CoA Dehydrogenase Deficient Mice to Oxidative Stress, Mitochondrial Dysfunction, and Cell Death: Implications for the Neurodegeneration in Glutaric Aciduria Type I.

Publicado no periódico Molecular Neurobiology

Mol Neurobiol
DOI 10.1007/s12035-016-0023-z

Higher Vulnerability of Menadione-Exposed Cortical Astrocytes of Glutaryl-CoA Dehydrogenase Deficient Mice to Oxidative Stress, Mitochondrial Dysfunction, and Cell Death: Implications for the Neurodegeneration in Glutaric Aciduria Type I

Marília Danyelle Nunes Rodrigues[1] · Bianca Seminotti[1] · Ângela Zanatta[1] · Aline de Mello Gonçalves[1] · Bruna Bellaver[1] · Alexandre Umpierrez Amaral[1] · André Quincozes-Santos[1] · Stephen Irwin Goodman[2] · Michael Woontner[2] · Diogo Onofre Souza[1] · Moacir Wajner[1,3]

Received: 1 March 2016 / Accepted: 1 August 2016

Abstract Patients affected by glutaric aciduria type I (GA-I) show progressive cortical leukoencephalopathy whose pathogenesis is poorly known. In the present work, we exposed cortical astrocytes of wild-type ($Gcdh^{+/+}$) and glutaryl-CoA dehydrogenase knockout ($Gcdh^{-/-}$) mice to the oxidative stress inducer menadione and measured mitochondrial bioenergetics, redox homeostasis, and cell viability. Mitochondrial function (MTT and JC1-mitochondrial membrane potential assays), redox homeostasis (DCFH oxidation, nitrate and nitrite production, GSH concentrations and activities of the antioxidant enzymes SOD and GPx), and cell death (propidium iodide incorporation) were evaluated in primary cortical astrocyte cultures of $Gcdh^{+/+}$ and $Gcdh^{-/-}$ mice unstimulated and stimulated by menadione. We also measured the pro-inflammatory response (TNFα levels, IL1-β and NF- B) in unstimulated astrocytes obtained from these mice. $Gcdh^{-/-}$ mice astrocytes were more vulnerable to menadione-induced oxidative stress (decreased GSH concentrations and altered activities of the antioxidant enzymes), mitochondrial dysfunction (decrease of MTT reduction and JC1 values), and cell death as compared with $Gcdh^{+/+}$ astrocytes. A higher inflammatory response (TNFα, IL1-β and NF- B) was also observed in $Gcdh^{-/-}$ mice astrocytes. These data indicate a higher susceptibility of $Gcdh^{-/-}$ cortical astrocytes to oxidative stress and mitochondrial dysfunction, probably leading to cell death. It is presumed that these pathomechanisms may contribute to the cortical leukodystrophy observed in GA-I patients.

Keywords Glutaric aciduria type I · $Gcdh^{-/-}$ mice astrocytes · Oxidative stress · Mitochondrial dysfunction · Pro-inflammatory response

Introduction

Glutaric aciduria type I (GA-I, McKusick 23,167, OMIM #231,670) is a disorder of organic acid metabolism caused by mutations in the gene that codes glutaryl-CoA dehydrogenase (GCDH) that is involved in the degradation of the amino acids lysine, hydroxylysine, and tryptophan [1]. GCDH deficiency leads to predominant accumulation of glutaric acid (GA) and 3-hydroxyglutaric acid (3-HGA) in tissues and body fluids [2, 3].

Patients usually present at birth macrocephaly with frontotemporal atrophy, as well as progressive leukodystrophy with cortical atrophy and marked dystonia and dyskinesia following encephalopathic episodes during or following infections that are accompanied by destruction of striatal neurons [4, 5].

A knockout mice model of GA-I ($Gcdh^{-/-}$) with complete loss of GCDH activity accompanied by high levels of GA-I metabolites in tissues and body fluids was established and

✉ Moacir Wajner
mwajner@ufrgs.br

[1] Departamento e PPG Bioquímica, ICBS/Universidade Federal do Rio Grande do Sul (UFRGS), Rua Ramiro Barcelos N° 2600, Anexo, Porto Alegre, RS CEP90035-003, Brazil

[2] Department of Pediatrics, University of Colorado Denver, Aurora, CO, USA

[3] Serviço de Genética Médica, Hospital de Clínicas de Porto Alegre, Porto Alegre, RS, Brazil

Published online: 10 August 2016

ANEXO II-E: Anti-aging effects of guanosine in glial cells.

Publicado no periódico Purinegic Signalling

Purinergic Signalling
DOI 10.1007/s11302-016-9533-4

ORIGINAL ARTICLE

Anti-aging effects of guanosine in glial cells

Débora Guerini Souza[1] · **Bruna Bellaver**[1] · **Larissa Daniele Bobermin**[1] · **Diogo Onofre Souza**[1,2] · **André Quincozes-Santos**[1,2]

Received: 13 April 2016 / Accepted: 24 August 2016

Abstract Guanosine, a guanine-based purine, has been shown to exert beneficial roles in in vitro and in vivo injury models of neural cells. Guanosine is released from astrocytes and modulates important astroglial functions, including glutamatergic metabolism, antioxidant, and anti-inflammatory activities. Astrocytes are crucial for regulating the neurotransmitter system and synaptic information processes, ionic homeostasis, energy metabolism, antioxidant defenses, and the inflammatory response. Aging is a natural process that induces numerous changes in the astrocyte functionality. Thus, the search for molecules able to reduce the glial dysfunction associated with aging may represent an approach for avoiding the onset of age-related neurological diseases. Hence, the aim of this study was to evaluate the anti-aging effects of guanosine, using primary astrocyte cultures from newborn, adult, and aged Wistar rats. Concomitantly, we evaluated the role of heme oxygenase 1 (HO-1) in guanosine-mediated glioprotection. We observed age-dependent changes in glutamate uptake, glutamine synthetase (GS) activity, the glutathione (GSH) system, pro-inflammatory cytokine (tumor necrosis factor α (TNF-α) and interleukin 1β (IL-1β)) release, and the transcriptional activity of nuclear factor kB (NFkB), which were prevented by guanosine in an HO-1-dependent manner. Our findings suggest guanosine to be a promising therapeutic agent able to provide glioprotection during the aging process. Thus, this study contributes to the understanding of the cellular and molecular mechanisms of guanosine in the aging process.

Keywords Aging · Adult/aged astrocytes · Guanosine · Heme oxygenase 1

✉ André Quincozes-Santos
andrequincozes@ufrgs.br

[1] Programa de Pós-Graduação em Ciências Biológicas: Bioquímica, Instituto de Ciências Básicas da Saúde, Universidade Federal do Rio Grande do Sul, Rio Grande do Sul, RS, Brazil

[2] Departamento de Bioquímica, Instituto de Ciências Básicas da Saúde, Universidade Federal do Rio Grande do Sul, Rio Grande do Sul, RS, Brazil

Introduction

Guanine-based purines are known to act as extracellular signaling molecules, exerting trophic and neuroprotective roles in in vitro and in vivo experimental models [1–5]. Guanosine, more specifically, has been shown to induce numerous beneficial cellular responses in several brain injuries, such as seizures, hypoxia, anxiety-like behavior, ischemia, and glucose deprivation [1, 6–9]. In addition to demonstrating the ability to modulate glutamatergic metabolism, avoiding the overactivation of glutamate receptors, and exerting antioxidant and anti-inflammatory activities [10–12], guanosine can also modulate several signaling pathways to provide neuroprotection [1, 13, 14]. However, despite the increasing evidence of the protective effects of guanosine in neural cells, its mechanism of action is not fully understood.

Our group has previously demonstrated the interplay between guanosine and the enzyme heme oxygenase 1 (HO-1) [12, 14], which is the major enzyme responsible for the conversion of heme into CO and the antioxidant products biliverdin and bilirubin [15, 16]. It has been reported that HO-1 may be a therapeutic target in the aging process and/or neurodegenerative diseases. Increased HO-1 activity correlates with protection against stressful conditions, such as hypoxia/

Published online: 01 September 2016

ANEXO II-F: Resveratrol modulates GSH system in C6 astroglial cells through heme oxygenase 1 pathway.

Publicado no periódico Molecular and Cellular Biochemistry

Mol Cell Biochem
DOI 10.1007/s11010-016-2917-5

Resveratrol modulates GSH system in C6 astroglial cells through heme oxygenase 1 pathway

Bernardo Assein Arús[1] · Débora Guerini Souza[1] · Bruna Bellaver[1] · Diogo Onofre Souza[1] · Carlos-Alberto Gonçalves[1] · André Quincozes-Santos[1] · Larissa Daniele Bobermin[1]

Received: 23 October 2016 / Accepted: 21 December 2016

Abstract Resveratrol is a dietary polyphenol that displays neuroprotective properties in several in vivo and in vitro experimental models, by modulating oxidative and inflammatory responses. Glutathione (GSH) is a key antioxidant in the central nervous system (CNS) that modulates several cellular processes, and its depletion is associated with oxidative stress and inflammation. Therefore, this study sought to investigate the protective effects of resveratrol against GSH depletion pharmacologically induced by buthionine sulfoximine (BSO) in C6 astroglial cells, as well as its underlying cellular mechanisms. BSO exposure resulted in several detrimental effects, decreasing glutamate-cysteine ligase (GCL) activity, cystine uptake, GSH intracellular content and the activities of the antioxidant enzymes glutathione peroxidase (GPx) and glutathione reductase (GR). Moreover, BSO increased reactive oxygen/nitrogen species (ROS/RNS) levels and pro-inflammatory cytokine release. Resveratrol prevented these effects by protecting astroglial cells against BSO-induced cytotoxicity, by modulating oxidative and inflammatory responses. Additionally, we observed that pharmacological inhibition of heme oxygenase 1 (HO-1), an essential cellular defense against oxidative and inflammatory injuries, abolished all the protective effects of resveratrol. These observations suggest HO-1 pathway as a cellular effector in the mechanism by which resveratrol protects astroglial cells against GSH depletion, a condition that may be associated to neurodegenerative diseases.

✉ Larissa Daniele Bobermin
larissabobermin@gmail.com

[1] Departamento de Bioquímica, Programa de Pós-Graduação em Ciências Biológicas: Bioquímica, Instituto de Ciências Básicas da Saúde, Universidade Federal do Rio Grande do Sul, Porto Alegre, Brazil

Keywords Astroglial cells · Glutathione · Buthionine sulfoximine · Oxidative stress · Inflammatory response · Heme oxygenase 1

Introduction

The dietary polyphenol resveratrol (3,5,4′-*trans*-trihydroxystilbene), primarily available in peanuts, berries, grapes, and red wine, has been broadly studied due to its protective properties, such as antioxidant, anti-inflammatory, anti-aging, and cardioprotective activities [1–4]. Additionally, resveratrol is associated with neuroprotection, exhibiting beneficial effects in several in vitro and in vivo models of brain diseases, including Alzheimer's, Parkinson's, and stroke [5–8]. Although the mechanisms underlying the protective action of resveratrol are not fully understood, there is increasing evidence indicating that its potent antioxidant properties play an important role in neuroprotection. Such properties derive from resveratrol's ability to directly scavenge oxidative species and/or from the activation of pathways involved in antioxidant defenses [9–11].

Among these pathways, resveratrol is able to activate heme oxygenase 1 (HO-1), a fundamental defense mechanism for cells exposed to oxidant challenges [6, 12]. HO-1 (EC 1.14.14.18) is the inducible rate-limiting enzyme in the pathway through which pro-oxidant heme is degraded into antioxidants biliverdin and bilirubin [13–15]. Increase in HO-1 activity is associated with protection against stressful conditions, such as oxidative stress and inflammation. Among other effects, HO-1 is able to counteract the activation of nuclear factor κB (NFκB), the major inflammatory and oxidative regulator factor in the central nervous system (CNS) [16].

ANEXO II-G: Homocysteine Induces Glial Reactivity in Adult Rat Astrocyte Cultures.

Publicado no periódico Molecular Neurobiology

Mol Neurobiol
DOI 10.1007/s12035-017-0463-0

Homocysteine Induces Glial Reactivity in Adult Rat Astrocyte Cultures

Aline Longoni[1] · Bruna Bellaver[1] · Larissa Daniele Bobermin[1] · Camila Leite Santos[1] · Yasmine Nonose[1] · Janaina Kolling[1] · Tiago M. dos Santos[1] · Adriano M. de Assis[1] · André Quincozes-Santos[1,2] · Angela T. S. Wyse[1,2]

Received: 12 December 2016 / Accepted: 16 February 2017

Abstract Astrocytes are dynamic glial cells associated to neurotransmitter systems, metabolic functions, antioxidant defense, and inflammatory response, maintaining the brain homeostasis. Elevated concentrations of homocysteine (Hcy) are involved in the pathogenesis of age-related neurodegenerative disorders, such as Parkinson and Alzheimer diseases. In line with this, our hypothesis was that Hcy could promote glial reactivity in a model of cortical primary astrocyte cultures from adult Wistar rats. Thus, cortical astrocytes were incubated with different concentrations of Hcy (10, 30, and 100 μM) during 24 h. After the treatment, we analyzed cell viability, morphological parameters, antioxidant defenses, and inflammatory response. Hcy did not induce any alteration in cell viability; however, it was able to induce cytoskeleton rearrangement. The treatment with Hcy also promoted a significant decrease in the activities of Na^+, K^+ ATPase, superoxide dismutase (SOD), and glutathione peroxidase (GPx), as well as in the glutathione (GSH) content. Additionally, Hcy induced an increase in the pro-inflammatory cytokine release. In an attempt to elucidate the putative mechanisms involved in the Hcy-induced glial reactivity, we measured the nuclear factor kappa B (NFκB) transcriptional activity and heme oxygenase 1 (HO-1) expression, which were activated and inhibited by Hcy, respectively. In summary, our findings provide important evidences that Hcy modulates critical astrocyte parameters from adult rats, which might be associated to the aging process.

Keywords Homocysteine · Cortical adult astrocytes · Oxidative stress · Inflammatory response · NFκB · Heme oxygenase 1

Introduction

Homocysteine (Hcy) is an amino acid sulfur and non-proteinogenic that is formed in unequal quantities in the metabolism of methionine, an essential amino acid. Hcy levels are controlled through two regulatory mechanisms: (a) remethylation, forming methionine and getting a methyl group from 5-methyltetrahydrofolate or betaine, and (b) transsulfuration, when it undergoes condensation with serine, producing cystathionine, via reaction catalyzed by cystathionine-β-synthase, this product after being cleaved to cysteine [1]. Moreover, Hcy metabolism requires coenzymes such as vitamins B_6 and B_{12} and folic acid. Deficiencies in these cofactors are associated with hyperhomocysteinemia (HHcy) that is an abnormal high level of Hcy in the blood, commonly associated to cytotoxicity. In addition, mild levels of Hcy (>30 μM) have been reported as an independent risk factor for cognitive dysfunction [2] and neurodegenerative disorders [3]. According to previous studies from our group, mild HHcy induces oxidative stress and neuroinflammation in the cerebral cortex of rats [4, 5]. Recently, we have also demonstrated that Hcy (30 μM) altered mitochondrial functionality and induced oxidative stress and neuronal death in slices from the cerebral cortex of rats [6].

Astrocytes correspond to 50% of the total number of cells in the central nervous system (CNS), being the most versatile

✉ André Quincozes-Santos
andrequincozes@ufrgs.br

[1] Programa de Pós-graduação em Ciências Biológicas: Bioquímica, ICBS, Instituto de Ciências Básicas da Saúde, Universidade Federal do Rio Grande do Sul, Rua Ramiro Barcelos, 2600 Anexo, Bairro Santa Cecília, Porto Alegre, RS 90035–003, Brazil

[2] Departamento de Bioquímica, ICBS, Universidade Federal do Rio Grande do Sul, Porto Alegre, Brazil

Published online: 02 March 2017

ANEXO II-H: Cortical Bilateral Adaptations in Rats Submitted to Focal Cerebral Ischemia: Emphasis on Glial Metabolism.

Publicado no periódico Molecular Neurobiology

Mol Neurobiol
DOI 10.1007/s12035-017-0458-x

Cortical Bilateral Adaptations in Rats Submitted to Focal Cerebral Ischemia: Emphasis on Glial Metabolism

Yasmine Nonose[1] · Pedro E. Gewehr[1] · Roberto F. Almeida[1] · Jussemara S. da Silva[1] · Bruna Bellaver[1] · Leo A. M. Martins[1] · Eduardo R. Zimmer[1,2] · Samuel Greggio[2] · Gianina T. Venturin[2] · Jaderson C. Da Costa[2] · André Quincozes-Santos[1,3] · Luc Pellerin[4] · Diogo O. de Souza[1,3] · Adriano M. de Assis[1]

Received: 11 December 2016 / Accepted: 13 February 2017

Abstract This study was performed to evaluate the bilateral effects of focal permanent ischemia (FPI) on glial metabolism in the cerebral cortex. Two and 9 days after FPI induction, we analyze [^{18}F]FDG metabolism by micro-PET, astrocyte morphology and reactivity by immunohistochemistry, cytokines and trophic factors by ELISA, glutamate transporters by RT-PCR, monocarboxylate transporters (MCTs) by western blot, and substrate uptake and oxidation by ex vivo slices model. The FPI was induced surgically by thermocoagulation of the blood in the pial vessels of the motor and sensorimotor cortices in adult (90 days old) male Wistar rats. Neurochemical analyses were performed separately on both ipsilateral and contralateral cortical hemispheres. In both cortical hemispheres, we observed an increase in tumor necrosis factor alpha (TNF-α), interleukin-1β (IL-1β), and glutamate transporter 1 (GLT-1) mRNA levels; lactate oxidation; and glutamate uptake and a decrease in brain-derived neurotrophic factor (BDNF) after 2 days of FPI. Nine days after FPI, we observed an increase in TNF-α levels and a decrease in BDNF, GLT-1, and glutamate aspartate transporter (GLAST) mRNA levels in both hemispheres. Additionally, most of the unilateral alterations were found only in the ipsilateral hemisphere and persisted until 9 days post-FPI. They include diminished in vivo glucose uptake and GLAST expression, followed by increased glial fibrillary acidic protein (GFAP) gray values, astrocyte reactivity, and glutamate oxidation. Astrocytes presented signs of long-lasting reactivity, showing a radial morphology. In the intact hemisphere, there was a decrease in MCT2 levels, which did not persist. Our study shows the bilateralism of glial modifications following FPI, highlighting the role of energy metabolism adaptations on brain recovery post-ischemia.

Keywords Astrocytes · Energy metabolism · Stroke · Contralateral hemisphere · Glial reactivity

Introduction

Stroke is responsible for significant mortality and long-term disability worldwide [1, 2]. In the USA, more than 140,000 people die each year from stroke (www.strokecenter.org), while most survivors need to receive continuous care due to sequelae [3, 4]. In acute ischemic stroke, the brain regions with severely impaired blood flow become rapidly and irreversibly injured and are referred to as ischemic *core* [5]. Surrounding the *core*, there is an area of constrained blood flow called ischemic *penumbra*, which presents a partially preserved energy metabolism and structural pattern. Salvage of this penumbral region is associated with neurological improvement and recovery [6, 7].

In addition to the ischemic penumbra, other brain areas might be relevant to improve outcome after stroke. Some

Electronic supplementary material The online version of this article (doi:10.1007/s12035-017-0458-x) contains supplementary material, which is available to authorized users.

✉ Adriano M. de Assis
adriano.assis@ufrgs.br

[1] Postgraduate Program in Biological Sciences: Biochemistry, ICBS, Universidade Federal do Rio Grande do Sul (UFRGS), Rua Ramiro Barcelos, 2600 – Anexo Santa Cecília, Porto Alegre, RS 90035-003, Brazil

[2] Brain Institute of Rio Grande do Sul, Pontifícia Universidade Católica do Rio Grande do Sul (PUCRS), Porto Alegre, RS 90619-900, Brazil

[3] Department of Biochemistry, Universidade Federal do Rio Grande do Sul (UFRGS), Porto Alegre, RS 90035-003, Brazil

[4] Department of Physiology, University of Lausanne, 1005 Lausanne, Switzerland

Published online: 07 March 2017

ANEXO II-I: N-acetylcysteine Prevents Alcohol Related Neuroinflammation in Rats.

Publicado no periódico Neurochemical Research

Neurochem Res
DOI 10.1007/s11064-017-2218-8

ORIGINAL PAPER

N-acetylcysteine Prevents Alcohol Related Neuroinflammation in Rats

Ricardo Schneider Jr[1] · Solange Bandiera[2] · Débora Guerini Souza[3] · Bruna Bellaver[3] · Greice Caletti[2] · André Quincozes-Santos[3] · Elaine Elisabetsky[2,3] · Rosane Gomez[1,2]

Received: 26 October 2016 / Revised: 17 January 2017 / Accepted: 25 February 2017

Abstract Alcoholism has been characterized as a systemic pro-inflammatory condition and alcohol withdrawal has been linked to various changes in the brain homeostasis, including oxidative stress and glutamate hyperactivity. *N*-acetylcysteine (NAC) is an anti-inflammatory and antioxidant multi-target drug with promising results in psychiatry, including drug addiction. We assessed the effects of NAC on the serum and brain inflammatory cytokines after cessation of chronic alcohol treatment in rats. Male Wistar rats received 2 g/kg alcohol or vehicle twice a day by oral gavage for 30 days. Rats were treated, from day 31 to 34, with NAC (60 or 90 mg/kg) or saline, intraperitoneally, once daily. Rats were sacrificed at day 35, trunk blood was collected and the frontal cortex and hippocampus dissected for assessment of TNF-α, IL-1β, IL-6, IL-18, IL-10. NAC prevented the increase of pro-inflammatory cytokines and the decrease of anti-inflammatory cytokine in the frontal cortex and hippocampus. No changes were observed on serum cytokines. We conclude that NAC protects against inflammation induced by chronic (30 days) alcohol ingestion followed by 5 days cessation in two rat brain areas. Because inflammation has been documented and associated with craving and relapse in alcoholics, the data revealed by this study points to the validity of NAC clinical evaluation in the context of alcohol detoxification and withdrawal.

Keywords Cytokines · Drug abuse · Ethanol · Frontal cortex · Hippocampus · NAC

Introduction

Alcohol use disorder is the cause of 3.3 million deaths every year [1] adding to the number of alcohol-impaired driving fatalities. Alcohol and its metabolites induce organ injury by inducing oxidative stress and increasing systemic endotoxins [1, 2]. These processes trigger inflammatory responses, affecting end organs such as the liver, blood vessels, heart, pancreas, brain, and others [2, 3]. Accordingly, alcoholism is now viewed as a systemic inflammatory condition and cytokines as biomarkers of alcohol abuse [4, 5].

In the central nervous system (CNS), alcohol-induced neuroinflammation activates microglia and astrocytes, contributing to neurodegeneration and impaired neuronal regeneration in alcoholics [2, 6]. The serum levels of interleukins as IL-6 and IL-10 are elevated after a single alcohol intake in alcoholics compared with non-alcoholic volunteers [5]. Postmortem study showed that the levels of the key pro-inflammatory cytokine MCP-1 (monocyte chemoattractant protein 1), as well as microglial activity are higher in alcoholic than non-alcoholic subjects [7]. Studies also suggest that cytokines regulate voluntary alcohol intake in rodents [8, 9]. The pro-inflammatory cytokines IL-1β, TNF-α, and NFkB are elevated after chronic alcohol administration or voluntary consumption in the rodents hippocampus and in the cortex [10, 11]. Studies evaluating CNS cytokine levels after alcohol cessation are scarce. In humans, IL-10, IL-12, and interferon (IFNγ) plasma levels

✉ Rosane Gomez
rosane.gomez@ufrgs.br

[1] Programa de Pós-Graduação em Neurociências, Universidade Federal do Rio Grande do Sul (UFRGS), Rua Sarmento Leite, 500/305, Porto Alegre, RS 90050170, Brazil

[2] Programa de Pós-Graduação em Farmacologia e Terapêutica, Universidade Federal do Rio Grande do Sul (UFRGS), Rua Sarmento Leite, 500/313, Porto Alegre, RS 90050170, Brazil

[3] Programa de Pós-Graduação em Bioquímica, UFRGS, Rua Ramiro Barcelos, 2600, Porto Alegre, RS 90035003, Brazil

Published online: 16 March 2017

ANEXO II-J: In Vitro Adult Astrocytes are Derived From Mature Cells and Reproduce in Vivo Redox Profile.

Publicado no periódico Journal of Cellular Biochemistry

FASTTRACK
Journal of Cellular Biochemistry 118:3111–3118 (2017)

Journal of Cellular Biochemistry

In Vitro Adult Astrocytes are Derived From Mature Cells and Reproduce in Vivo Redox Profile

Débora Guerini Souza,[1]* Bruna Bellaver,[1] Silvia Resende Terra,[1] Fatima Costa Rodrigues Guma,[1,2] Diogo Onofre Souza,[1,2] and André Quincozes-Santos[1,2]*

[1]*Programa de Pós-Graduação em Ciências Biológicas: Bioquímica, Instituto de Ciências Básicas da Saúde, Universidade Federal do Rio Grande do Sul, Rio Grande do Sul, Brazil*

[2]*Departamento de Bioquímica, Instituto de Ciências Básicas da Saúde, Universidade Federal do Rio Grande do Sul, Rio Grande do Sul, Brazil*

ABSTRACT

Astrocytes are versatile cells involved in synaptic information processing, energy metabolism, redox homeostasis, inflammatory response, and structural support of the brain. Recently, we established a routine protocol of cultured astrocytes derived from adult and aged Wistar rats, which present several different responses compared to newborn astrocytes, commonly used to characterize the role of the astrocytes in the central nervous system. Previous studies hypothesized that astrocyte cultures prepared from adult animals derive from immature precursors present in the adult tissue throughout life. Since our group has already demonstrated that the glial functionality of adult astrocytes differs from newborn cultures, the aim of this study was to confirm that our in vitro astrocytes were derived from mature cells. Therefore, we evaluated cytoskeleton proteins, such as glial fibrillary acidic protein and vimentin, as well as Sox10, an essential marker of immature glial cells, in ex vivo tissue and in in vitro astrocytes from the same animals (1, 90, and 180 days old). In addition, we examined the mitochondrial functionality and the cellular redox homeostasis. Our results suggest that adult and aged astrocytes are derived from mature cells and that changes in mitochondrial parameters in ex vivo tissue were reproduced in in vitro astrocytes. J. Cell. Biochem. 118: 3111–3118, 2017.

KEY WORDS: ADULT/AGED ASTROCYTES; Sox10; MITOCHONDRIAL FUNCTIONALITY

Astrocytes, the most versatile cells of the central nervous system (CNS), are crucial for the metabolic and redox homeostasis, inflammatory response and structural support of the brain [Hertz and Zielke, 2004; Khakh and Sofroniew, 2015; Bolanos, 2016]. Much of the understanding of astrocytes has been obtained from studies conducted in cultured primary astrocytes in physiological and pathological conditions [Lange et al., 2012]. In this sense, cultured astrocytes are most often derived from newborn mice or rats, however, at this stage, gliogenesis is not complete [Hertz et al., 1998; Lange et al., 2012]. Once astrocytes are mature, the classical cytoskeleton astrocytic marker glial fibrillary acidic protein (GFAP) is present, and along with vimentin, plays an essential role in mechanical strength, intracellular transport, and astrocytic shape [Hol and Pekny, 2015; Yang and Wang, 2015].

There are important differences between the immature and the mature brain, with significant implications in brain functionality [Sun et al., 2013; Herculano-Houzel, 2014]. Astrocytes derived from mature animals contain well-established connections, more organized than immature tissue, which is more plastic and labile to stimuli. Thus, mature astrocytes may respond more reliably and help to elucidate the role of astrocytes in the aging brain [Souza et al., 2013; Bellaver et al., 2016]. In line with this, we have recently established a routine protocol of cultured mature astrocytes derived from adult and aged Wistar rats to study biochemical, pharmacological and morphological properties of the CNS associated to aging and/or age-related neurological diseases [Souza et al., 2013, 2016b]. A previous report has, however, suggested that preparing astrocyte cultures from adult animals does not result in mature astrocytes

Conflict of interest: The authors declare there are no conflicts of interest.

Grant sponsor: Conselho Nacional de Desenvolvimento Científico e Tecnológico; Grant sponsor: Coordenação de Aperfeiçoamento de Pessoal de Nível Superior; Grant sponsor: Fundação de Amparo à Pesquisa do Estado do Rio Grande do Sul; Grant sponsor: Federal University of Rio Grande do Sul; Grant sponsor: Instituto Nacional de Ciência e Tecnologia para Excitotoxicidade e Neuroproteção.

*Correspondence to: Débora Guerini de Souza, PhD, and André Quincozes-Santos, PhD, Departamento de Bioquímica, Universidade Federal do Rio Grande do Sul, Rua Ramiro Barcelos, 2600-Anexo, Bairro Santa Cecília, 90035-003 Porto Alegre, RS, Brazil. E-mail: debsrs@gmail.com, andrequincozes@ufrgs.br

Manuscript Received: 11 December 2016; Manuscript Accepted: 3 April 2017

Accepted manuscript online in Wiley Online Library (wileyonlinelibrary.com): 4 April 2017

DOI 10.1002/jcb.26028 • © 2017 Wiley Periodicals, Inc.

ANEXO II-K: Increased Oxidative Parameters and Decreased Cytokine Levels in an Animal Model of Attention-Deficit/Hyperactivity Disorder.

Publicado no periódico Neurochemical Research

Neurochem Res (2017) 42:3084–3092
DOI 10.1007/s11064-017-2341-6

ORIGINAL PAPER

Increased Oxidative Parameters and Decreased Cytokine Levels in an Animal Model of Attention-Deficit/Hyperactivity Disorder

Douglas Teixeira Leffa[1,2,3] · Bruna Bellaver[4] · Carla de Oliveira[1,2,3] · Isabel Cristina de Macedo[2,3] · Joice Soares de Freitas[2,3] · Eugenio Horacio Grevet[5,6] · Wolnei Caumo[1] · Luis Augusto Rohde[5,6,7] · André Quincozes-Santos[4] · Iraci L. S. Torres[1,2,3]

Received: 29 March 2017 / Revised: 25 May 2017 / Accepted: 22 June 2017 / Published online: 29 June 2017

Abstract Attention-deficit/hyperactivity disorder (ADHD) is a highly heterogeneous disorder characterized by impairing levels of hyperactivity, impulsivity and inattention. Oxidative and inflammatory parameters have been recognized among its multiple predisposing pathways, and clinical studies indicate that ADHD patients have increased oxidative stress. In this study, we aimed to evaluate oxidative (DCFH oxidation, glutathione levels, glutathione peroxidase, catalase and superoxide dismutase activities) and inflammatory (TNF-α, IL-1β and IL-10) parameters in the most widely accepted animal model of ADHD, the spontaneously hypertensive rats (SHR). Prefrontal cortex, cortex (remaining regions), striatum and hippocampus of adult male SHR and Wistar Kyoto rats were studied. SHR presented increased reactive oxygen species (ROS) production in the cortex, striatum and hippocampus. In SHR, glutathione peroxidase activity was decreased in the prefrontal cortex and hippocampus. TNF-α levels were reduced in the prefrontal cortex, cortex (remaining regions), hippocampus and striatum of SHR. Besides, IL-1β and IL-10 levels were decreased in the cortex of the ADHD model. Results indicate that SHR presented an oxidative profile that is characterized by an increase in ROS production without an effective antioxidant counterbalance. In addition, this strain showed a decrease in cytokine levels, mainly TNF-α, indicating a basal deficit. These results may present a new approach to the cognitive disturbances seen in the SHR.

Keywords ADHD · SHR · Oxidative stress · Cytokines

✉ Iraci L. S. Torres
iltorres@hcpa.edu.br

1 Post-Graduate Program in Medicine: Medical Sciences, School of Medicine, Universidade Federal do Rio Grande do Sul, Porto Alegre, Brazil

2 Animal Experimentation Unit and Graduate Research Group, Hospital de Clínicas de Porto Alegre, Porto Alegre, Brazil

3 Laboratory of Pain Pharmacology and Neuromodulation: Pre clinical studies - Pharmacology Department, Institute of Basic Health Sciences, Universidade Federal do Rio Grande do Sul, Porto Alegre, Brazil

4 Biochemistry Department, Institute of Basic Health Sciences, Universidade Federal do Rio Grande do Sul, Porto Alegre, Brazil

5 Psychiatry Department, Universidade Federal do Rio Grande do Sul, Porto Alegre, Brazil

6 ADHD Outpatient Program, Hospital de Clínicas de Porto Alegre, Porto Alegre, Brazil

7 National Institute of Developmental Psychiatry for Children and Adolescents, Porto Alegre, Brazil

Introduction

Attention-deficit/hyperactivity disorder (ADHD) is characterized by impairing levels of hyperactivity, impulsivity and inattention [1]. Its prevalence is estimated to be 5.3% in children and adolescents [2] and 2.5% in adults [3]. Although a common disorder, its pathophysiology is not completely understood. Studies on neuroimaging, cognition and biochemical assessment have been delineating ADHD as a heterogeneous disorder with a multifactorial causation [1].

Among the multiple pathways predisposing to ADHD phenotype, oxidative parameters have been increasingly investigated. There is a growing body of literature indicating that an increase in oxidative markers might be related with the pathophysiology of psychiatric disorders as cause and/or consequence of abnormal brain signaling [4]. In ADHD, a recent meta-analysis including six studies with

ANEXO II-L: Transcranial direct current stimulation improves long-term memory deficits in an animal model of attention-deficit/hyperactivity disorder and modulates oxidative and inflammatory parameters.

Publicado no peródico Brain Stimulation

Brain Stimulation 11 (2018) 743–751

Contents lists available at ScienceDirect

Brain Stimulation

journal homepage: http://www.journals.elsevier.com/brain-stimulation

Transcranial direct current stimulation improves long-term memory deficits in an animal model of attention-deficit/hyperactivity disorder and modulates oxidative and inflammatory parameters

Douglas Teixeira Leffa [a, b, c], Bruna Bellaver [d], Artur Alban Salvi [b, c], Carla de Oliveira [a, b, c], Wolnei Caumo [a, e], Eugenio Horacio Grevet [g, h], Felipe Fregni [f], André Quincozes-Santos [d], Luis Augusto Rohde [g, h, i], Iraci L.S. Torres [a, b, c, *]

[a] Post-Graduate Program in Medicine: Medical Sciences, School of Medicine, Universidade Federal do Rio Grande do Sul, Porto Alegre, Brazil
[b] Animal Experimentation Unit and Graduate Research Group, Hospital de Clínicas de Porto Alegre, Porto Alegre, Brazil
[c] Laboratory of Pain Pharmacology and Neuromodulation: Pre Clinical Studies - Pharmacology Department, Institute of Basic Health Sciences, Universidade Federal do Rio Grande do Sul, Porto Alegre, Brazil
[d] Biochemistry Department, Institute of Basic Health Sciences, Universidade Federal do Rio Grande do Sul, Porto Alegre, Brazil
[e] Pain and Palliative Care Service, Laboratory of Pain & Neuromodulation, Hospital de Clínicas de Porto Alegre, Universidade Federal do Rio Grande do Sul, Porto Alegre, Rio Grande do Sul, Brazil
[f] Laboratory of Neuromodulation, Department of Physical Medicine & Rehabilitation, Spaulding Rehabilitation Hospital and Massachusetts General Hospital, Harvard University, Boston, United States
[g] Psychiatry Department, Universidade Federal do Rio Grande do Sul, Porto Alegre, Brazil
[h] ADHD Outpatient Program, Hospital de Clínicas de Porto Alegre, Brazil
[i] National Institute of Developmental Psychiatry for Children and Adolescents, Brazil

ARTICLE INFO

Article history:
Received 27 July 2017
Received in revised form
26 March 2018
Accepted 2 April 2018
Available online 5 April 2018

Keywords:
ADHD
tDCS
SHR

ABSTRACT

Background: Transcranial direct current stimulation (tDCS) is a technique that modulates neuronal activity and has been proposed as a potential therapeutic tool for attention-deficit/hyperactivity disorder (ADHD) symptoms. Although pilot studies have shown evidence of efficacy, its mechanism of action remains unclear.

Objective/Hypothesis: We evaluated the effects of tDCS on behavioral (working and long-term memory) and neurochemical (oxidative and inflammatory parameters) outcomes related to ADHD pathophysiology. We used the most widely accepted animal model of ADHD: spontaneously hypertensive rats (SHR). The selected behavioral outcomes have been shown to be altered in both ADHD patients and animal models, and were chosen for their relation to the proposed mechanistic action of tDCS.

Methods: Adult male SHR and their control, the Wistar Kyoto rats (WKY), were subjected to 20 min of bicephalic tDCS or sham stimulation for 8 consecutive days. Working memory, long-term memory, and neurochemical outcomes were evaluated.

Results: TDCS improved long-term memory deficits presented by the SHR. No change in working memory performance was observed. In the hippocampus, tDCS increased both the production of reactive oxygen species in SHR and the levels of the antioxidant molecule glutathione in both strains. TDCS also modulated inflammatory response in the brains of WKY by downregulating pro-inflammatory cytokines.

Conclusion: TDCS had significant effects that were specific for strain, type of behavioral and neurochemical outcomes. The long-term memory improvement in the SHR may point to a possible therapeutic role of tDCS in ADHD that does not seem to be mediated by inflammatory markers. Additionally, the anti-inflammatory effects observed in the brain of WKY after tDCS needs to be further explored.

* Corresponding author. Departamento de Farmacologia - ICBS, UFRGS; Rua Sarmento Leite, 500 sala 305, 90050-170, Porto Alegre, RS, Brazil.
E-mail address: iltorres@hcpa.edu.br (I.L.S. Torres).

https://doi.org/10.1016/j.brs.2018.04.001
1935-861X/

ANEXO II-M: Combined use of alcohol and tobacco smoke change oxidative, inflammatory, and neurotrophic parameters in different brain areas of rats.

Publicado no periódico ACS Chemical Neuroscience

ACS Chemical Neuroscience
Cite This: ACS Chem. Neurosci. 2019, 10, 1336−1346
Research Article
pubs.acs.org/chemneuro

Combined Exposure to Alcohol and Tobacco Smoke Changes Oxidative, Inflammatory, and Neurotrophic Parameters in Different Areas of the Brains of Rats

Dayane A. Quinteros,[†] Alana Witt Hansen,[*,†] Bruna Bellaver,[‡] Larissa D. Bobermin,[‡] Rianne R. Pulcinelli,[†] Solange Bandiera,[†] Greice Caletti,[†] Paula E. R. Bitencourt,[†] André Quincozes-Santos,[‡] and Rosane Gomez[†]

[†]Programa de Pós-Graduação em Ciência Biológicas: Farmacologia e Terapêutica (PPGFT), Universidade Federal do Rio Grande do Sul (UFRGS), Porto Alegre 90040-060, Brazil

[‡]Programa de Pós-Graduação em Ciência Biológicas: Bioquímica, UFRGS, Porto Alegre 90050-170, Brazil

Supporting Information

ABSTRACT: Devastating effects of exposure to alcohol and tobacco smoke on health are extensively reported in the literature. However, few studies have attempted to elucidate the consequences of their combined use on the central nervous system. Here we studied the effect of this combined use on some oxidative, inflammatory, and neurotrophic parameters in the hippocampus, striatum, and frontal cortex of rats. Adult Wistar rats were allocated into control (CT), alcohol (AL), tobacco smoke (TB), or combined (ALTB) groups. Rats were exposed to environmental air (CT and AL groups) or to the smoke from six cigarettes (TB and ALTB groups) immediately after tap water (CT and TB) or 2 g of alcohol/kg (AL and ALTB) oral gavage administration, twice a day, for 4 weeks. On day 28, rats were euthanized and areas of the brain were dissected to evaluate some cellular redox parameters, pro-inflammatory cytokine levels, and brain-derived neurotrophic factor (BDNF) levels. A one-way analysis of variance showed that the ALTB combined treatment significantly increased oxidative stress levels in the hippocampus. ALTB also increased interleukin-1β levels in the striatum and frontal cortex and tumoral necrosis factor-α levels in the frontal cortex compared with those of AL, TB, and CT rats. Combined treatment also decreased the BDNF levels in the frontal cortex of rats. Oxidative damage was found, more importantly, in the hippocampus, and inflammatory parameters were extended to all areas of the brain that were studied. Our results showed an interaction between alcohol and tobacco smoke according to the area of the brain, suggesting an additional risk of neural damage in alcoholics who smoke.

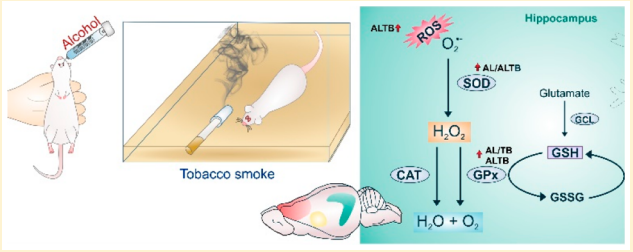

KEYWORDS: *Cytokines, cigarette, ethanol, neurotrophine, neurotoxicity, oxidative stress*

INTRODUCTION

According to the World Health Organization, the harmful use of alcohol causes great disease, social, and economic burdens. Alcohol use disorder causes more than 60 diseases and is associated with violence and road traffic accidents related to more than 3 million death per year.[1] Similarly, tobacco consumption is an epidemic and one of the greatest public health problems.[1,2] Active or passive tobacco smoking is associated with more than 6 million deaths per year, related to pulmonary, cardiac, and vascular diseases and different forms of cancer.[2] Although these alarming numbers are related to alcohol use and tobacco smoke, few studies have attempted to elucidate the biological and functional consequences of their combined use on the central nervous system (CNS). This is a relevant problem because studies have shown that almost 80% of alcoholics smoke regularly and smokers consume more alcohol per occasion than nonsmokers.[3,4] Additionally, smokers consume alcohol in a larger quantity per occasion and more frequently than nonsmokers.[4] There is no evident reason for the prevalence of the combined use, and as mentioned above, few studies have explored the consequences of this association.

In vitro and *in vivo* studies showed that alcohol and its metabolite, acetaldehyde, changed the cellular redox status in the brain, generating oxidative and nitrosative stress and decreasing antioxidant enzyme levelss, with biomolecule damage being a consequence.[5,6] Moreover, chronic alcohol use has been recognized as a systemic inflammatory disease.[7−9] Indeed, alcohol use increases plasma levels of pro-inflammatory cytokines in humans and rodents.[7,8,10] In the brain, levels of cytokines such as tumor necrosis factor α (TNF-α) and

Received: August 11, 2018
Accepted: January 17, 2019
Published: January 17, 2019

DOI: 10.1021/acschemneuro.8b00412
ACS Chem. Neurosci. 2019, 10, 1336−1346